Australian National University

Cellular reprogramming for brain repair

Negar Mahmoudi

March 2024

A thesis submitted for the degree of Doctor of Philosophy of

The Australian National University

The research described in this thesis is my original work, except where otherwise acknowledged.

Negar Mahmoudi

March 2024

I would like to dedicate my thesis to my family. I love you with all my heart.

To my husband Hossein, you have been always a supporter of all my endeavours.

&

To many friends.

Acknowledgments

I would like to express my sincere gratitude to my supervisors. I have been extremely lucky to have a supervisory panel with multi-disciplinary backgrounds and have their valuable guidance and feedback from different points of view. I would like to express my deepest appreciation to my primary supervisor, Prof. David Nisbet, for his guidance and constant support throughout the research process. His expertise and encouragement have been instrumental in the successful completion of this thesis.

I would like to show my gratitude to my co-supervisors, for their guidance through my PhD journey. To Prof. Alan Harvey, the master of cell reprogramming, Prof. Clare Parish, an expert in cell biology, and A/Prof. Richard Williams, master of bioengineered self-assembling peptide hydrogel. I would also like to acknowledge that this research was supported by an Australian Government Research Training Program (RTP) Scholarship. I would also like to thank my friends and colleagues at the John Curtin School of Medical Research.

Of course, thanks to everyone in the LΛB group for listening to my presentations and providing supportive and constructive comments.

Access to the facilities and technical support of the Centre for Advanced Microscopy (CAM) with funding through the Australian Microscopy and Microanalysis Research Facility (AMMRF) is gratefully acknowledged. I also want to especially thank Dr. Melanie Rug, Daryl Webb, and Joanne Lee for inducting me to visualise the outcome of my experiment with a fluorescent microscope, TEM, and SEM. Moreover, I want to thank Dr Nathalie Dehorter for performing whole-cell electrophysiological recording and analysis.

My biggest gratitude to my parents, brother, and sisters, who always supported me from childhood and encouraged me to pursue my higher education.

Above all, I would like to thank Hossein, my husband and best friend who has always been there for me not only in life but also during my PhD journey.

Abstract

The inability of the central nervous system (CNS) to regenerate effectively is a barrier to the successful treatment of traumatic injuries and neurodegenerative diseases. As with other cells in the body, neurons are sensitive to injury and degenerative/inflammatory conditions that often result in cell death. While neurons are frequently lost in response to injury or degeneration, astrocytes on the other hand become activated, proliferative, and assemble to enclose a necrotic region and form glial scars. The astrocyte response to injury presents a valuable therapeutic target as they perform both cytotrophic and cytotoxic functions, sometimes concomitantly, after injury. An adeno-associated virus (AAV) vector encoded with specific transcription factors (TFs) that targets astrocytes and potentially converts/reprograms them to functional neurons is of interest in developing novel therapeutic solutions for traumatic brain injury (TBI). Viral vectors such as lentivirus and retrovirus integrate with host-cell genome and pose a series of risks including insertional mutagenesis, transgene integration, and strong immunogenicity[1,2]. However, AAV does not have the problem associated with the integration of host-cell genome as it forms circular concatemers that persist as episomes in the nucleus of transduced cells and does not integrate into host genomes[3].

This project aims to reprogram reactive astrocytes to neurons using TFs both *in vitro* and *in vivo*. Furthermore, a bio-inspired self-assembling peptide (SAP) hydrogel is used to provide spatiotemporal release of AAVs *in vivo* to address multiple difficulties with viral vector delivery by shielding and confining the vectors to the site of therapeutic need. Additionally, these SAP hydrogels have been functionalised to provide relevant biologically active motifs. These motifs can mimic the native cellular microenvironment of the brain. To further drive the survival, differentiation, and maturation of reprogrammed cells, we have developed a hybrid

composite biomaterial, incorporating electrospun short fibres (SFs) loaded with valproic acid (VPA) small molecule within our novel SAP hydrogel matrix.

We found that NeuroD1/ and SOX2 TFs can trans-differentiate and dedifferentiate reactive astrocytes to neurons *in vitro*, respectively. More importantly, both SOX2 and NeuroD1-mediated reprogramming resulted in neural replenishment *in vivo*. Furthermore, NeuroD1 encoded AAV could significantly reduce the glial scar intensity 28 days post-implantation *in vivo* in a brain injury model. The presentation of SAP+AAV-NeuroD1 also altered the morphology of astrocytes far away from the lesion site due to the alleviation of inflammatory cells (astrocytes and microglia) in the injury site. This demonstrates the ability of NeuroD1 to reprogram reactive astrocytes to functional neurons and potentially alter the phenotype of reactive astrocytes near the injury site. Thus, this SAP hydrogel is promising as a 3D biomimetic cell culture environment (high water content, stiffness within the range of soft tissue, presenting laminin-derived IKVAV peptide as a bio-functional epitope to encourage cell infiltration into the scaffold for neural tissue engineering) and payload delivery platform for future studies of tissue engineering strategies that can manipulate the inflammatory response to improve functional recovery outcomes.

To summarise, the research reported here demonstrates i) functionalisation and materials characterisation, ii) the effect of AAV encoded with SOX2 and NeuroD1 TFs on reprogramming reactive astrocytes to functional neurons, iii) the impact of VPA in neural differentiation and maturation, iv) the effect of SAP hydrogels in AAV distribution in brain injury model *in vivo.*

Achievements

Journal publications

- **Negar Mahmoudi**, Yi Wang, Niamh Moriarty, Noorya Y. Ahmed, Nathalie Dehorter, Leszek Lisowski, Alan R Harvey, Clare L. Parish, Richard J. Williams, and David R. Nisbet, “"Neuronal Replenishment via Hydrogel-Rationed Delivery of Reprogramming Factors." ***ACS nano*** (2024).
- Kevin C. L. Law*, **Negar Mahmoudi*,** Zahra E. Zadeh, Richard. J. Williams, Cameron P. J. Hunt, Andras Nagy, Lachlan H. Thompson, David R. Nisbet, Clare L. Parish, “A Selective, Hydrogel-Based Prodrug Delivery System Efficiently Activates a Suicide Gene to Remove Undifferentiated Human Stem Cells Within Neural Grafts”. **Advanced Functional Materials** (2023): 2305771
- **Negar Mahmoudi,** Elmira Mohamed, Shiva Soltani Dehnavi, Lilith M Caballero Aguilar, Alan R Harvey, Clare L. Parish, Richard J. Williams, and David R. Nisbet, "Calming the Nerves via the Immune Instructive Physiochemical Properties of Self-Assembling Peptide Hydrogels." **Advanced Science** (2023): 2303707.
- Shiva Soltani Dehnavi*, Arianna Cembran*, **Negar Mahmoudi**, Stephanie Franks, Nicolo Malagutti, Benjamin Long, Leszek Lisowski, Alan R Harvey, Clare L. Parish, Richard J. Williams, David R. Nisbet, "Molecular camouflage by a context-specific hydrogel as the key to unlock the potential of viral vector gene therapy." **Chemical Engineering Journal** 477 (2023): 146857.
- Bram Servais, **Negar Mahmoudi,** Vini Gautam, Wei Tong, Michael Ibbotson, David R. Nisbet, and David Collins, “Engineering next generation brain-on-a-chip platforms” (**Nature Reviews Bioengineering, Major revision**)

- **Negar Mahmoudi**, Nathan Reynolds, Noorya Y. Ahmed, Nathalie Dehorter, Leszek Lisowski, Alan R Harvey, Clare L. Parish, Richard J. Williams, and David R. Nisbet, "In vivo generation of functional neurons with focally defined hydrogel factories that recruit, reprogram, and release" **(paper in preparation)**

(*Co-first authors)

Conferences

- 33rd Annual Conference of the European Society for Biomaterials (ESB), Davos, Switzerland, September 2023. Oral Presentation
- TERMIS World Congress. Jeju, South Korea, October 2022. Poster Presentation
- The 17th Pacific Polymer Conference (PPC17), December 2022, Brisbane, Australia; Poster Presentation.

Grants

- The Gretel and Gordon Bootes Medical Research Foundation (2022), (co-investigator). Self-assembled peptide hydrogels as scaffolds to promote haemostasis and tissue regeneration post brain insult.

Awards

- 1st prize winner of image competition in Centre for Advanced Microscopy (2022), Miniature Big Bang
- 2nd prize winner of image competition in Brain Teaser event in John Curtin School od Medical Research (JCSMR) (2022), Miniature Big Bang

- 2nd prize winner of image competition in Centre for Advanced Microscopy (2021)

  Fireworks

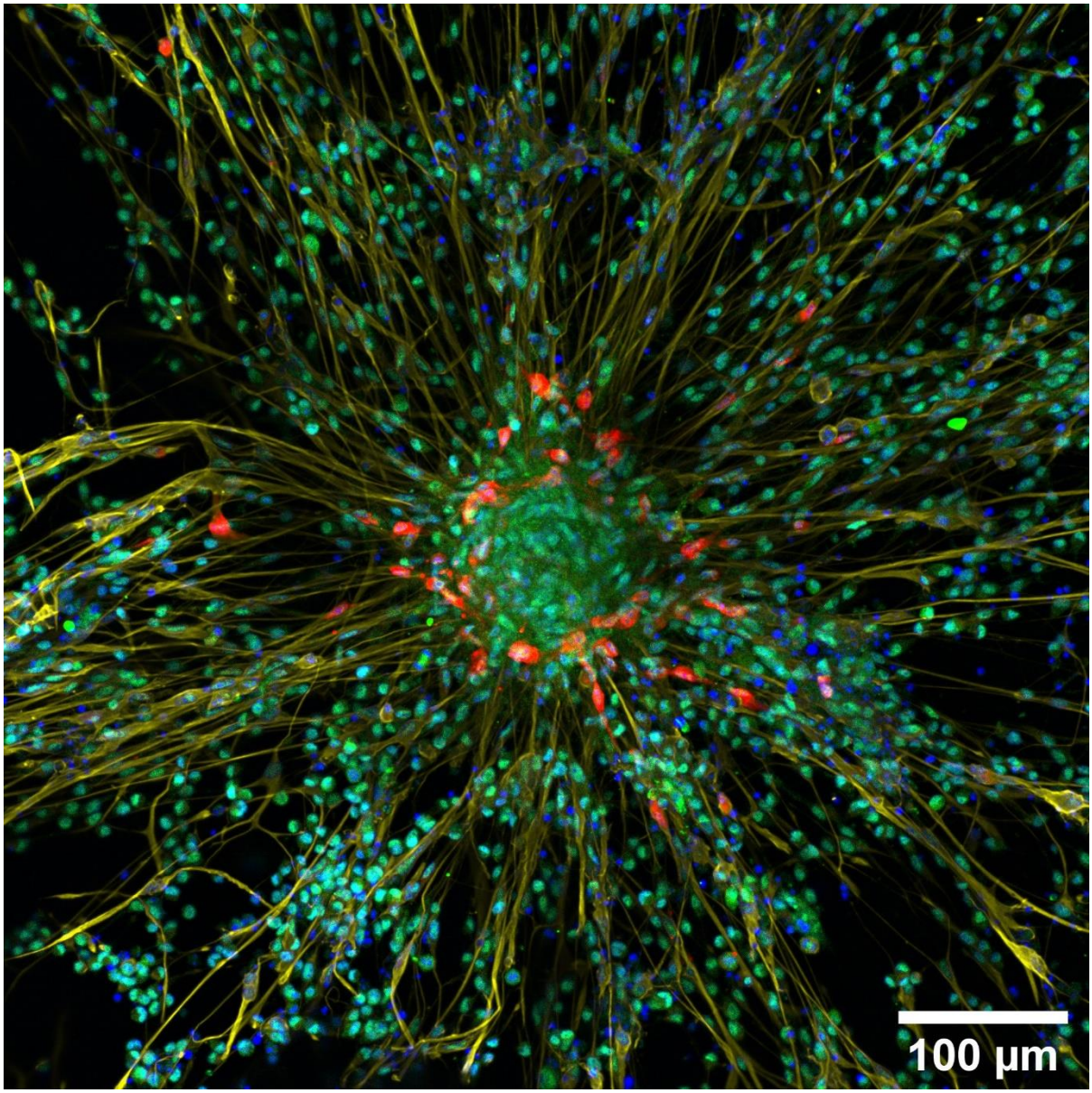

Miniature Big Bang

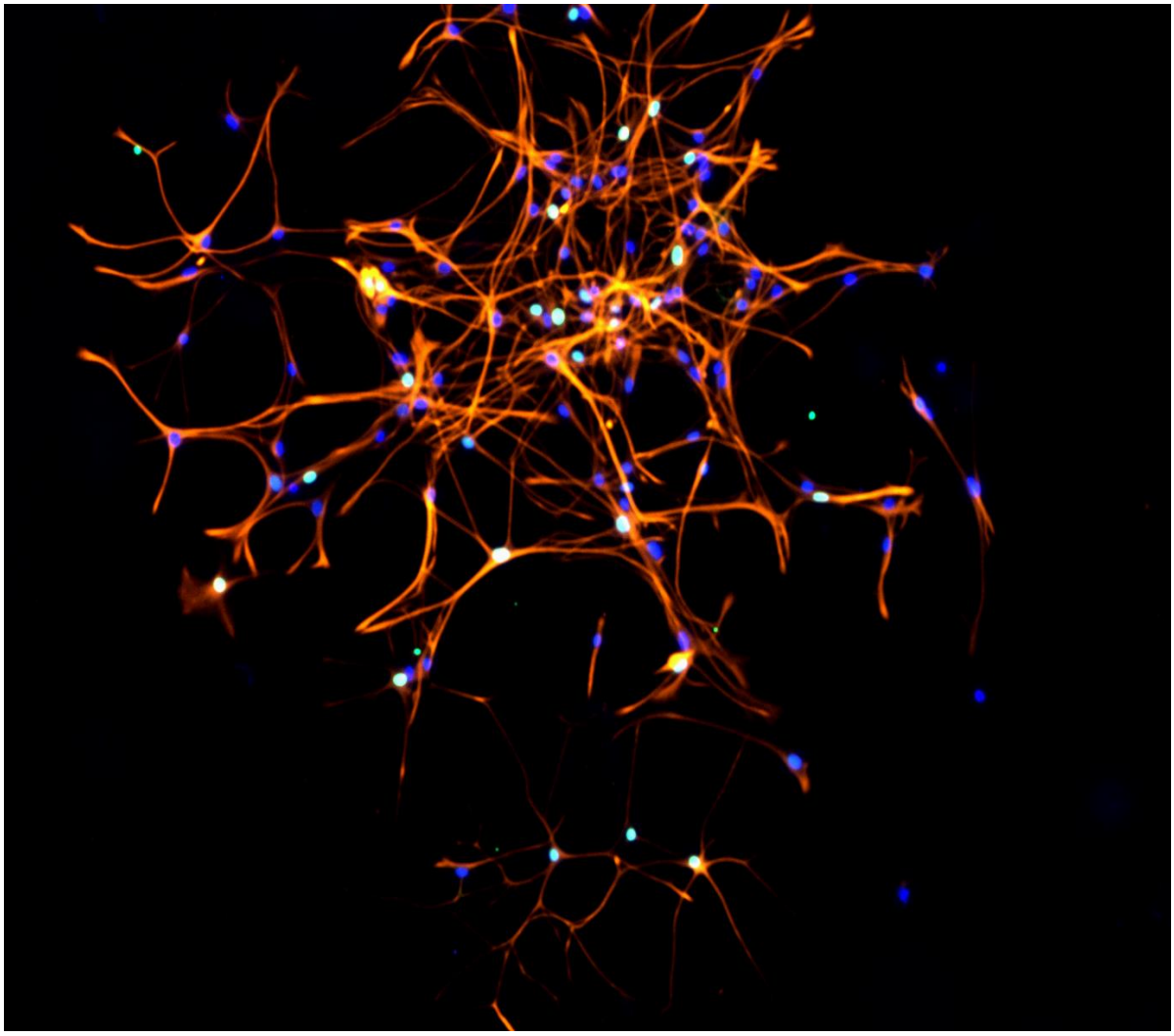

Fireworks

Table of contents

Acknowledgments....4

Abstract....6

Achievements....8

Journal publications....8

Conferences....9

Grants....9

Awards....9

Table of contents....13

List of tables....20

List of figures....21

List of Abbreviations....31

Chapter 1. Introduction....35

1.1 Background....36

1.2 Research gap....39

1.3 Aims....39

1.4 Thesis outline....40

1.4.1 Literature Review....41

1.4.2 Materials and methods....41

1.4.3 Synthesis and physiochemical characterisation 41

1.4.4 *In vitro* and *in vivo* trans-differentiation of reactive astrocytes to functional neurons 41

1.4.5 *In vitro* and *in vivo* dedifferentiation of astrocytes 42

1.4.6 Conclusion and future perspectives 42

1.4.7 Appendices 42

Chapter 2. Literature review 43

2.1 Preamble 43

2.2 Introduction 44

2.3 TBI pathology 45

2.4 The physiological and pathological functions of astrocytes 49

2.5 Extracellular matrix (ECM) mimics 51

2.6 Hydrogels as an *in situ* forming scaffolds for local CNS application 52

2.7 Self-assembling peptide (SAP) hydrogels as a biomimetic ECM 55

2.8 Astrocyte reprogramming through the ectopic expression of transcription factors (TFs) 58

2.8.1 NeuroD1 transcription factor 60

2.8.2 SOX2 transcription factor 61

2.9 Gene therapy using viral vector delivery 63

2.9.1 Adeno- associated viral vectors (AAVs) 64

Chapter 3. Materials and methods 71

3.1 Preamble 71

3.2 Solid phase peptide synthesis (SPPS) 72

3.3 Self-assembled peptide (SAP) hydrogel preparation 73

3.4 Polylactic acid (PLA) scaffold fabrication, valproic acid (VPA) immobilisation, and characterisation 73

3.5 Short fibreproduction 74

3.6 Physiochemical characterisation 75

3.6.1 Spectroscopy analysis 75

3.6.2 Rheology 75

3.6.3 Mesh size 76

3.6.4 Transmission electron microscopy (TEM) 76

3.6.5 Zeta potential 76

3.6.6 Scanning electron microscopy (SEM) 76

3.7 Hybrid composite biomaterial fabrication, and VPA degradation and release profile investigation 77

3.8 Degradation and release profile *in vitro* using high performance liquid chromatography (HPLC)-orbitrap 77

3.9 AAV vector production and purification 78

3.10 Cell and culture conditions 79

3.10.1 Primary astrocyte culture 79

3.10.2 Primary cortical neuron culture 80

3.10.3 Human astrocytes culture 80

3.10.4 Astrocyte *in vitro* cell transduction 81

3.10.5 Protocol for direct conversion of astrocytes into induced neurons 81

3.10.6 Protocol for dedifferentiation of astrocytes to neural progenitor and then induced neurons 82

3.10.7 Conversion efficiency and neuronal purity (*in vitro*) 82

3.10.8 Electrophysiological examination of NeuroD1 and SOX2 converted cells *in vitro* 82

3.10.9 MTT (3-[4,5-dimethylthiazol-2-yl]-2,5-iphenyltetrazoliumbromide) assay .. 83

3.11 In vivo 84

3.11.1 Stereotaxic surgery and viral vector delivery 84

3.11.2 AAV titration optimisation: 85

3.11.3 In vivo AAV transduction 85

3.12 Immunocytochemistry and immunohistochemical staining, imaging and analysis .. 85

3.13 Release profiles of AAV-NeuroD1/ or AAV-SOX2 from Fmoc-DDIKVAV SAP hydrogel 87

3.14 Quantitative PCR 87

3.15 Astroglia scar measurement 88

3.16 Statistical analysis 88

Chapter 4. Synthesis and physiochemical characterisation of SAP hydrogel/ fibre scaffold 89

4.1 Preamble 89

4.2 Results and discussion 90

4.2.1 Chemical structure of Fmoc-SAP hydrogels 90

4.2.2 Rheological behavior/mechanical properties of Fmoc-SAP hydrogels 92

4.2.3 Mesh size 93

4.2.4 Morphology of Fmoc-SAP hydrogel scaffolds 94

4.2.5 Zeta potential (Surface charge) 95

4.2.6 *In vitro* cytotoxicity of the fabricated hydrogels with astrocytes 96

4.2.7 Characterisation of polylactic acid (PLA)±valproic acid (VPA) electrospun nanofibreand PLA±VPA short fibres (SFs) 97

4.3 Summary 102

Chapter 5. *In vitro* and *in vivo* trans-differentiation of reactive astrocytes to neurons 104

5.1 Preamble 104

5.2 Abstract 105

5.3 Introduction 106

5.4 Results and discussion 110

5.4.1 *In vitro* conversion of primary astrocytes to neuronal cells 110

5.4.2 *In vitro* conversion of human astrocytes to neuronal cells 133

5.4.3 Reprogrammed primary astrocytes and human astrocytes were able to fire action potentials 141

5.4.4 SAP hydrogels prolongs AAV-NeuroD1 release 143

5.4.5 AAV dosage optimisation in a needle stick injury model 144

5.4.6 Incorporating AAV-NeuroD1 within a SAP hydrogel sustains and confines viral delivery within the needle track.....146

5.4.7 DJ gfaABC1D-mCherry preferentially transduces astrocytes.....148

5.4.8 Reprogramming of reactive astrocytes reduces the glial scar after injury.....150

5.4.9 Reprogrammed neurons transition through an immature stage 152

5.4.10 The overall number of neurons increased within the needle track.....153

Chapter 6. *In vitro* and *in vivo* dedifferentiation of reactive astrocytes 156

6.1 Preamble.....156

6.2 Abstract 157

6.3 Introduction 158

Results and Discussion 160

6.3.1 AAV-SOX2 dosage optimisation *in vitro*.....160

6.3.2 SOX2 transduced astrocytes pass through a proliferative state. 163

6.3.3 *In vitro* transduction of primary astrocytes with SOX2 leads to astrocyte to neuron conversion. 168

6.3.4 Cell cycle analysis and GFAP expression at 28 DPT 173

6.3.5 Reprogrammed primary astrocytes were able to initiate action potentials 176

6.3.6 Hybrid composite biomaterial prolongs delivery of VPA 181

6.3.7 Incorporating AAV-SOX2 within a SAP hydrogel sustains viral delivery while retains viral functional activity 181

6.3.8 SOX2 forced expression generates intermediate neuroblast cells *in vivo* 183

6.4 Summary 184

Chapter 7. Conclusion and future perspectives 186

7.1 Preamble 186

7.2 Conclusion 187

7.3 Future perspectives 190

References 192

Appendix A 236

List of tables

Table 2.1. Benefits and applications of biologically derived and synthetic hydrogels in neural applications. Hydrogels made of biologically derived materials such collagen, hyaluronic acid, alginate, fibrin, chitosan, xyloglucan and methylcellulose have been used in treatment of CNS injuries. pHPMA, pHEMA and PEG are also the most investigated synthetic hydrogels for CNS treatment. 53

Table 2.2. Characteristics of different AAV serotypes 66

List of figures

Figure 2.1. Schematic illustration showing the temporal cellular infiltration response after TBI. Created with BioRender.com. 48

Figure 2.2. A) Schematic of Fmoc-DDIKVAV and Fmoc-DIKVAVD peptide structure and B) peptide assembly driven by π–π stacking interactions and C) polar and non-polar, non-covalent intramolecular interactions to form a D) hollow nanofibre and E) hydrogel matrix formation through the entanglement of the nanofibres[145]. 56

Figure 2.3. AAV and its variant generation. (a) The single-stranded DNA genome of the wild type of AAV is shown. The rep open reading frames (ORF) encodes four non-structural proteins from the 5' ORF of wild-type (Rep40, Rep52, Rep68 and Rep78) that are essential for viral replication, transcription regulation, genome integration and virion assembly/packaging. The cap ORF encodes 3 structural proteins from the 3' ORF (VP1, VP2 and VP3) which form the 60-mer viral capsid at the ratio of 1:1:10 (VP1:VP2:VP3)[205]. (b) Crystal structure of the AAV capsid (c) Recombinant adeno-associated viral vectors (rAAVs) are originally constructed by deleting both rep and cap genes and replacing these with therapeutic gene sequences, along with adenoviral helper genes that are needed for replication. The ITRs are the only viral sequences retained in AAV vectors[189]. 66

Figure 2.4. Schematic overview of the AAV vector transduction pathway, A) trans-differentiation (with NeuroD1), and B) indirect reprogramming/dedifferentiation (with SOX2) proposed in this thesis. AAV bind to receptor on the surface of astrocyte (1) followed by trafficking to endosome (2) and endosome scape (3). Once in the nucleus, AAV capsids are uncoated and the AAV genome is released (single strand DNA (ssDNA)) (4). Then AAV ssDNA genome is converted into double-stranded DNA (5), followed by transcription (6) and

nuclear export of mRNA (7) for translation and expression of the therapeutic transgene (8). Then the astrocyte converts to induced neurons directly or indirectly based on the transgene NeuroD1, or SOX2, respectively as illustrated. Created with BioRender.com 68

Figure 3.1. Schematic illustration of LC-Mass sample preparation procedure. 78

Figure 4.1. FTIR and CD spectra of single, co-assembled, and mixed Fmoc-SAP hydrogels. A) FTIR spectroscopic analysis confirmed the antiparallel β-sheet at 1630 cm^{-1} and 1690 cm^{-1}. B) CD spectra of all assemblies show the transition in the region 180-220 nm indicating the presence of β-sheet. DDIKVAV (orange), DIKVAVD (violet), DDIKVAV+DIKVAVD (Co-assembly) (red), DDIKVAV+DIKVAVD (Mix) (black), DDIKVAVL (pink), DIKVAVD+DDIKVAVL (Co-assembly) (navy blue), DIKVAVD+DDIKVAVL (Mix) (green), DIKVAVHD (blue), and DIKVAVL+DIKVAVHD (yellow). 91

Figure 4.2. Rheological analysis for single, co-assembled, and mixed Fmoc-SAP hydrogels. Mechanical properties characterisation for single/ co-assembled/and mixed hydrogels. Rheological analysis confirms viscoelastic behaviour of all fabricated hydrogels confirmed with storage modulus (G′) greater than loss modulus (G″). 93

Figure 4.3. Mesh size (ξ) value of Fmoc-SAP hydrogels. Results showing the calculated mesh size values (based on the equation of the theory of rubber elasticity) 94

Figure 4.4. TEM images of some of the fabricated Fmoc-SAP hydrogels with different magnifications (scales= 200 nm, 100 nm and 0.5 μm). 95

Figure 4.5. (A) Surface ζ-potential values (mV) of Fmoc- SAP hydrogels. Fmoc-SAP hydrogels showing different surface zeta potential. 96

Figure 4.6. Primary astrocyte cells viability (%) in the presence of different diluted hydrogels. Cells were incubated in diluted hydrogels for 48 h. Then an MTT assay was performed to

measure cell viability. Cells cultured in DMEM were used as a positive control, and culture wells without cells but containing triplicate of just DMEM and dilutions of each hydrogel were used as a negative control. Mean values (n= 4) are shown with ±SE, standard one-way ANOVA was performed *(*p<0.05, **p<0.01).* The normal distribution of data is shown alongside the box plots as well. 97

Figure 4.7. SEM of electrospun nanofibres at different magnifications. A) PLA electrospun nanofibres B) PLA+VPA electrospun nanofibres C) The corresponding histograms of the PLA fibre diameter distribution, D) The corresponding histograms of the PLA+VPA fibre diameter distribution. Scale bars= 10 µm, and 2 µm.....100

Figure 4.8. SEM of short fibres (SFs). A) PLA SFs B) PLA+VPA SFs C) The corresponding histograms of the PLA SFs length distribution, D) The corresponding histograms of the PLA+VPA SFs length distribution. Scale bars: 10 µm. 101

Figure 4.9. Rheological analysis and CD spectra for pure Fmoc-DDIKVAV SAP hydrogel (orange) and hybrid composite biomaterial (SAP hydrogel + SFs) (pink). A) Mechanical properties characterisation for both pure hydrogel and hybrid composite biomaterial confirms their viscoelastic behaviour (storage modulus (G′) greater than loss modulus (G″)). B) CD spectra confirms the presence of β-sheet structure in both hydrogels suggesting the inclusion of SFs did not disrupt hydrogel's structure.....102

Figure 5.1. Graphical abstract of Chapter 5. Astrocyte A schematic diagram showing astrocyte from 1-2 days postnatal pups reprogramming/trans-differentiation to induced neurons (iN) *in vitro.* Created with BioRender.com.....105

Figure 5.2. Percentage of astrocytes in primary mouse astrocyte culture. (A) Quantification data based on FACS analysis demonstrates 91 ± 6.0% of cells were positive for astrocyte marker (GFAP). (n=7/per group).....110

Figure 5.3. *In vitro* direct reprogramming of astrocytes to induced neurons (iN) 10- and 28-days post transduction (DPT). (A-D) A representative image of astrocytes transduced with AAV-NeuroD1 or (E, F) empty vector control, AAV-mCherry and stained with transduction efficiency marker (red), astrocytic protein GFAP (yellow), neuronal markers β3 tubulin or MAP2 (green), and DAPI (blue). (A, B), After 10 DPT significant increase in the population of cells expressing the neural lineage marker β tubulin and MAP2 (green) was observed, further increasing by 28 DPT. (E, F) Representative images of control culture transduced with empty vector showing no altered morphology of the cultured astrocytes. (G, H) Representative FACS plots for DJ gfaABC1D-NeuroD1-mCherry and DJ gfaABC1D-mCherry transduced astrocyte cultures showing proportions of mCherry+, β3 tubulin+ or MAP2+ populations. n=3-5 independent cultures/group. (I, J) Quantification of mCherry+, β3 tubulin+ and MAP2+ cells in culture. Data represents Mean + SEM, *$p < 0.05$; ** $p < 0.01$; *** $p < 0.001$, **** $p < 0.0001$. Scale bar= 100µm.....133

Figure 5.4. *In vitro* trans-differentiation of human astrocytes to induced neurons (iN) at 10/ and28 DPT. (A-D) A representative image of human astrocytes transduced with AAV-NeuroD1 or (E, F) empty vector control, AAV-mCherry and stained with transduction efficiency marker mCherry (red), astrocytic protein GFAP (yellow), neuronal markers β3 tubulin or MAP2 (green), and DAPI (blue). (A, B), After 10 DPT a significant increase in the proportion of cells expressing β tubulin and MAP2 (green) was observed, further increasing by 28 DPT. (E, F) Representative images of control culture transduced with empty vector showing no altered morphology of the cultured astrocytes. (G, H) Representative FACS plots for DJ gfaABC1D-NeuroD1-mCherry and DJ gfaABC1D-mCherry transduced astrocyte cultures showing proportions of mCherry+, β3 tubulin+ or MAP2+ populations. n=3-5 independent cultures/group. (I, J) Quantification of mCherry+, β3 tubulin+ and MAP2+ cells

in culture. Data represents Mean + SEM, **p < 0.05; ** p < 0.01; *** p < 0.001, **** p < 0.0001*. Scale bar=100 µm. 141

Figure 5.5. The ND1-mediated Primary astrocytes (PA) and human astrocytes (HA) reprogramming was monitored *in vitro* and functionally characterised. (A, G) Resting membrane potential for PA and HA, respectively. (B, H) Representative examples of spontanous calcium activity in recorded cells. (C, I) Action potential and spikelet resulting from 25 pA current steps in cell. (D, J) Overlaid action potentials from all recorded cells. (E, K) Action potential threshold. (F, L) Amplitude of action potential (from threshold to peak). (M, N) A representative image of recorded cells visualized by the infusion of Neurobiotin (yellow) (positive for mCherry (red) and NeuN (green)). 143

Figure 5.6. Fmoc-DDIKVAV SAP hydrogel show sheat-thinning properties and prolongs AAV-NeuroD1 release. (A) Rheological analysis confirms viscoelastic behaviour of all fabricated hydrogels confirmed with storage modulus (G′) greater than loss modulus (G″). (B) shear thinning properties of the DDIKVAV confirms sol-gel transition upon injection and during AAV incorporation. (C) Mesh size (ξ) (nm) value of the Fmoc-DDIKVAV calculated based on the equation of the theory of rubber elasticity. (D) Release profile of the DJ gfaABC1D-NeuroD1-mCherry from SAP hydrogel showing the concentration of AAV released from hydrogel at any given timepoints. 144

Figure 5.7. Representative images at the AAV-mCherry injection site illustrating transduced cells (red) co-labeled with astrocytic marker GFAP (green) across different ratio of SAP:AAV. Arrowheads indicate double stained cells.....146

Figure 5.8. AAV distribution in the brain. A) Schematic overview of the designed experiment. B) AAV±SAP implantation. C) AAV distribution within the brain in AAV±SAP identified with mCherry positive cells (shown as red) in representative overview of different

sections of a brain. Left hemisphere (AAV+SAP), Right hemisphere (AAV+Saline). Scale bar= 400 µm.....147

Figure 5.9. AAV-NeuroD1 transduced GFAP-expressing cells preferentially. A representative image of the core section of AAV-mCherry (control empty vector) implantation in left hemisphere. (C) cortical neurons transduced with AAV-NeuroD1 and stained at 3DPT. The coronal sections/ cortical neurons stained with transduction efficiency marker (mCherry, red), astrocytic protein GFAP (yellow), neuronal marker NeuN (B, Bi)/ or MAP2 (C) (green), and DAPI (blue), scale bar= 400 µm (A, B), 100 µm (C). Some double stained cells with mCherry are indicated with arrowhead. 149

Figure 5.10. Direct reprogramming of astrocytes attenuated astrogliosis and microglial activation. Inflammatory activities including astrogliosis and microglia activation were examined within and adjacent to the needle track. (A-D) Representative overview of different sections of a brain. Astrocyte accumulation or glial scar thickness from different brain sections and Iba-1 expression were examined 4 weeks post NeuroD1 and empty vector transduction. GFAP positive astrocytes (yellow) and Iba-1 positive microglia (Green) were significantly less intense within the needle track in the NeuroD1 treated mice compared to control group. The quantification data in (E) demonstrates a significant reduction in GFAP positive astrogliosis and (F) demonstrates a significant decrease in active microglia after NeuroD1 treatment. Scale bar=400 µm. ***p < 0.01*, ****p < 0.001*, *****p < 0.0001*. Data are represented as mean ± SD. (n = 3-5/ per group).....152

Figure 5.11. Direct reprogramming of astrocytes give rise to DCX postive cells within the AAV-NeuroD1 injected brain. A) DCX staining in subventricular zone (SVZ) to confirm the DCX staining. B) Schematic brain coronal section showing area imaged relative to injection site. C) Representative image of DCX/mCherry, RHS (AAV-NeuroD1+Saline). D)

Representative image of DCX/mCherry, LHS (AAV-NeuroD1+SAP). E) High magnification images showing a DCX+ cell colocalized with mCherry validate that the mCherry expression silences as the cell reprograms to neuronal phenotype. Scale bar=500 µm. 153

Figure 5.12. Direct reprogramming of astrocytes increases the overal number of NeuN postive cells within the AAV-NeuroD1 injected region. Representative overview of LHS and RHS of the control AAV±SAP (A and B) and NeuroD1 ±SAP (C and D). NeuN positive cells (green) were dramatically less in empty vector injected brain sections compared to NeuroD1-AAV injected one. Interestingly, NeuroD1-AAV+SAP treated mice showed significantly higher NeuN replenishment compared to AAV-NeuroD1 without SAP. E) Data are represented as mean ± SD. (n = 6/per group). Scale bar= 400 µm. ***p < 0.01,* ****p < 0.001,* *****p < 0.0001*.....154

Figure 6.1. Graphical abstract of Chapter 6. Astrocyte culture from 1-2 days postnatal pups reprogramming/de-differentiation to induced neurons (iN) passes through neural progenitor cells (NPCs)/Neural stem cells (NSCs). Created with BioRender.com.....157

Figure 6.2. Transduction efficiency of DJ gfaABC1D-SOX2-mCherry. Cells were transduced with A) MOT=10^5 and B) MOT=10^6, fixed and stained with transduction efficiency marker (red), neuronal marker β3 tubulin (green), astrocytic protein GFAP (yellow), and DAPI (blue) at 10 DPT. C) Representative data of FACS plots for DJ gfaABC1D-SOX2-mCherry transduced astrocyte with MOT=10^5 and MOT=10^6. D) Quantification data for mCherry+, β tubulin+, and double positive cells (both mCherry+ and β tubulin+ cells shown in Q10 and Q2). Data represents Mean ± SEM, **** *p < 0.0001*. Scale bar=100µm.....163

Figure 6.3. Fluorescent/live microscopy and cell cycle analysis for AAV-SOX2 and AAV-mCherry transduced cells. A representative image of astrocytes transduced with A) AAV-mCherry and B) AAV-SOX2, and stained with nestin marker (green), anti-mCherry (red),

anti-GFAP (yellow), and DAPI (blue). C) Quantification data showing the population of nestin+, mCherry+, and double positive cells (both nestin+ and mCherry+) in culture. D) The percentage of confluence for AAV-SOX2 and AAV-mCherry transduced cells at any given time point acquired using IncuCyte live imaging. E, F) Cell cycle analysis on AAV-SOX2 and AAV-mCherry transduced astrocytes showing significant increase in S phase and G2/M phase of SOX2 transduced cells indicating the presence of iPNSCs. Data represents Mean ± SEM, * $p < 0.05$, ** $p < 0.01$, *** $p < 0.001$. n=3-5 independent cultures/group. Scale bar=100µm.....168

Figure 6.4. Non-transduced/ AAV-mCherry transduced/ or AAV-SOX2 transduced astrocytes supplemented/treated with either BDNF/or VPA *in vitro*. A representative image of A) non-transduced primary astrocytes, (B) empty vector (AAV-mCherry) transduced astrocytes, and (C) AAV-SOX2 transduced astrocytes treated with BDNF/or VPA for 28 days and stained with β3 tubulin/ MAP2/or NeuN (green), anti-mCherry (red), anti-GFAP (yellow), and DAPI (blue). D-F) Representative FACS plots for non-transduced/ AAV-mCherry/ and AAV-SOX2 transduced astrocytes reveal different population of positive cells for different markers. G-I) Quantified cell counts for different cell markers with different conditions at 28 DPT. Scale bar= 100µm. *** $p < 0.001$, **** $p < 0.0001$. n=3/group.....172

Figure 6.5. Cell cycle analysis on transduced cells at 28 DPT. A-C) Quantification of G1, S, and G2/M phases for primary astrocytes, primary cortical neurons, and AAV-SOX2 transduced astrocytes. D) Representative images of cell cycle plots acquired from flow cytometry for different cells. E) Quantification of GFAP+, mCherry+, and double positive cells (both GFAP+ and mCherry+), based on FACS data reveals a drastic reduction of mCherry+, GFAP+ and double positive cells after 28 DPT in AAV-SOX2 transduced astrocytes compared to AAV-mCherry transduced astrocytes. F) Representative FACS plot

for AAV-SOX2 transduced cells indication different population of GFAP+, mCherry+, and double positive cells. ** $p < 0.01$ *** $p < 0.001$, **** $p < 0.0001$. n=3/group.....175

Figure 6.6. The SOX2-mediated reprogramming in both VPA and BDNF supplemented media was monitored *in vitro* and functionally characterised. (A, I) Resting membrane potential for SOX2 transduced cells supplemented with VPA and BDNF, respectively. (B, J) Spikelet resulting from 25 pA current steps in cells. (C, K) Overlaid spikelet from all recorded cells. (D, L) Spikelet threshold. (E, M) Peak potential of spikelet. (F, N) Amplitude (G, O) Rise time of spikelet. (H, P) Decay time of spikelet. 177

Figure 6.7. The SOX2-mediated reprogramming in both VPA and BDNF supplemented media was monitored *in vitro* and functionally characterised. (A, J) Resting membrane potential for SOX2 transduced cells supplemented with VPA and BDNF, respectively. (B, K) Representative examples of spontanous calcium activity in recorded cells. (C, L) Action potential resulting from 25 pA current steps in cells. (D, M) Overlaid action potentials from all recorded cells. (E, N) Action potential threshold. (F, O) Peak potential of action potential. (G, P) Amplitude of action potential (from threshold to peak). (H, Q) Rise time of action potential (10%-90% of amplitude). (I, R) Decay time of action potential. 180

Figure 6.8. In vitro release profile of VPA from hybrid composite biomaterial. A) Schematic diagram of in vitro study design, B) Quantification of VPA release from hybrid composite biomaterial over 8 weeks. Data represent mean ± SEM. n=3/time point. Panel A is Created with BioRender.com. 181

Figure 6.9. Hydrogel encapsulated AAV-SOX2 prolonged viral release and retains its functional activity. A) Schematic diagram of *in vitro* study design, B) Quantification of AAV-SOX2 release from SAP hydrogel at defined time points. Representative images of (C)

AAV-SOX2 and (D) empty vector (AAV-mCherry) transduced cells. Scale bar= 100µm. Data represent mean ± SEM. n=3/time point. Panel A is Created with BioRender.com. 183

Figure 6.10. SOX2 ectopic expression induces doublecortin (DCX+) neuroblast cells. Representative images at the A) AAV-SOX2 and B) AAV-mCherry injection site sites illustrating DCX+ cells (green), mCherry transduced cells (red), and DAPI (Blue). Scale bar= 100µm. 184

List of Abbreviations

2D	two-dimensional
3D	three-dimensional
AA	amino acid
AAV	adeno-associated virus
AAVDJ	a synthetic serotype of adeno-associated virus with chimeric capsid of AAV2, 8 and 9
ABI	acquired brain injury
AP	action potential
BBB	blood brain barrier
BDNF	brain derived neurotrophic factor
CD	circular dichroism
CDMEM	complete DMEM
CNS	central nervous system
CSPGs	chondroitin sulfate proteoglycans
D	aspartate/aspartic acid
DDIKVAV	aspartic acid-aspartic acid-isoleucine-lysine-valine-alanine-valine
DI H2O	deionised water
DIKVAV	aspartic acid-isoleucine-lysine-valine-alanine-valine (laminin inspired peptide)
DIPEA	N,N-diisopropylethylamine
DIV	days *in vitro*
DMF	dimethylformamide
DMSO	dimethyl sulfoxide
DPT	days post transduction
DS	Donkey serum
DYIGSRF	aspartate-tyrosine-isoleucine-glycine-serine-arganine-phenylalanine

E14.5	embryonic day 14.5
ECM	extracellular matrix
EGF	epidermal growth factor
FA	formic acid
FACS	fluorescence-activated cell sorting
FBR	foreign body reaction
FBS	fetal bovine serum
FGF	fibroblast growth factor
Fmoc	Fluorenylmethyloxycarbonyl
FTIR	Fourier transform infrared spectroscopy
G'	storage modulus/young modulus
G"	loss modulus
GCV	ganciclovir
GFAP	glial fibrillary acidic protein
HBSS	Hank's buffered saline solution
HBTU	0-Benzotriazole-N,N,N',N'-tetramethyl-uronium-hexafluoro-phosphate
HCI	hydrochloric acid
HOBt	hydroxybenzotriazole
HPLC	high-performance liquid chromatography
ICC	immunocytochemistry
IHC	immunohistochemistry
IKVAV	isoleucine-lysine-valine-alanine-valine
IL	interleukin
iN	induced neurons
iPSCs	induced pluripotent stem cells
Iba-1	ionized calcium binding adaptor molecule 1

K	lysine
LAB	Laboratory of Advanced Biomaterials
MAP2	Microtubule-associated protein 2
MTT	(3-[4,5-dimethylthiazol-2-yl]-2,5-iphenyltetrazoliumbromide)
MOI/MOT	multiplicity of infection/multiplicity of transduction
NaOH	sodium hydroxide
NeuN	nuclear antigen marker for neurons
NeuroD1	Neurogenic differentiation 1
NPCs	neural precursor/progenitor cells
NSCs	neural stem cells
PBS	phosphate buffer saline
PBST	0.03% Tween20 in PBS
PDL	poly-D-lysine
PEG	polyethylene glycol
PFA	paraformaldehyde
PLA	poly (L-lactic acid)
PLS	polysaccharide
pKa	acid dissociation constant
RFP	red fluorescent protein
RGD	arginine-glycine-aspartate
SAP	self-assembling peptide
SEM	scanning electron microscopy
SFs	short fibres
SGZ	subgranular zone
SOX2	SRY-box 2
SPPS	solid-phase peptide synthesis

SVZ	subventricular zone
TBI	traumatic brain injury
TEM	transmission electron microscopy
TES	triethylsilane
TF	transcription factor
TFA	tritluoroacetic acid
Tuj1	β-tubulin III for neuron maker
UF	uranyl formate
UV	ultraviolet
VPA	Valproic acid

Chapter 1. Introduction

1.1 Background

Injury to the central nervous system (CNS) may occur due to a wide range of conditions including infections, stroke, neurodegenerative disease, and trauma. Of these, brain and spinal cord damage that is associated with trauma as a result of vascular insult, contusive or penetrating injuries, are considered particularly challenging cases because of their acute onset and the limited capacity of damaged neurons to regenerate within the mature CNS[4]. A key barrier to functional repair and regeneration following traumatic brain injury (TBI) is the unconducive environment within the injury site and harmful inflammatory responses. TBI is a dynamic condition where an initial primary injury is followed by a cascade of secondary injuries that often leads to further neural tissue loss, a loss can continue over hours, months, and even years[5]. If TBI remains untreated it may lead to the early development of several neurodegenerative diseases and other mental illnesses[6].

Targeting cells involved in the reactive and inflammatory response after TBI, in particular astrocytes, has previously been highlighted as a promising therapeutic option[7]. Astrocytes respond to TBI by pronounced morphological and biochemical changes such as altered gene expression, hypertrophy and proliferation that occurs in a graded fashion in relation to the severity of the injury[8]. It is well-understood that reactive astrocytes within the injured area have a double-faceted role by simultaneously imparting a protective as well as inhibitory role in neural regeneration[9]. Recent evidence indicates that the formed glial scar provides several important beneficial functions such as confining the lesion and preventing its spread, promoting repair of the blood-brain barrier (BBB), and limiting neuronal loss in ischemic stroke and neurotrauma[9]. Despite these beneficial effects, the resulting mature glial scars tend to persist for long periods and act as a barrier to axonal re-growth and extension beyond the site of the initial injury resulting in dystrophic end balls, and negatively affects the integration of neural grafts into the host tissue[10]. As such, the development of strategies to maximise the beneficial

cytotrophic and minimise the harmful cytotoxic outcomes of the reactive inflammatory response would contribute to the development of treatments to achieve improved functional recovery after injury. Yet, despite the numerous efforts focused on treatment strategies for neural loss, thus far no current intervention explicitly can promote spontaneous restoration of neurological function. Therefore, the clinical prognosis of TBI in both preclinical and clinical trials, due in part to the structural complexity of the tissue, is poor[11,12].

Post insult, astrocytes become reactive, meaning they are hypertrophied and proliferate, and ultimately form glial scars. Therefore, the accumulation of these cells around and within an injury site represents a significant opportunity if such cells can be reprogrammed, using gene therapy, into functional neurons that can support repair and reconstruction. This may constitute a novel therapeutic strategy for disease and injuries that are associated with damage to cell populations within the CNS[13].

However, even if this is possible the growth inhibitory environment induced by a glial scar still needs to be addressed. In part, the regenerative capacity of tissues is determined by the plasticity and robustness of the extracellular matrix (ECM), and disruption thereof can cause significant adverse effects[14]. Rapid changes to the ECM occurring during injury, or more gradual degradation due to neurodegenerative disease, means the natural ECM cannot effectively support cells within the affected volume of tissue. This lack of support hinders the infiltration and organisation of regenerative cellular elements in the local region[15]. The ECM performs many essential functions in the brain, and provides the three-dimensional (3D) space for the cells to orientate themselves within, and provides a complex framework to help influence cellular function once established[16].

Challenges associated with the reconstitution of a favorable environment for regeneration could partially be overcome using biomaterials. Biomaterials enhance immunomodulatory processes by improving drug and cell delivery to the injured tissue. Furthermore, the materials themselves

can support healing and may be designed to act as immunomodulators, thereby contributing to tissue regeneration and endogenous repair processes. Therefore, herein we aim to repair the brain, partially, using a combinatorial approach: 1) to address the primary insult through the reprograming of glia to generate replacement neurons and, 2) to reduce the secondary damage by protecting residual host neurons in the penumbra and attenuating the intensity of glial scar. This will be achieved by the structural support offered by the self-assembling peptide (SAP) hydrogel nanoscaffolds, their ability to rebuild the ECM, and the ability of these scaffolds to provide targeted gene therapy and sustain neurotrophic support.

This work provides evidence for *in vitro* and *in vivo* glia-to-neuron conversion by fate reprogramming transcription factors (TFs) (proneural genes). These TFs are delivered through adeno-associated viral vectors (AAVs) incorporated into the injury site. Such reprogramming approach through trans-differentiation and dedifferentiation allows us to generate induced neurons (iN) while simultaneously reducing reactive glial cells without complete depletion of astrocytes. Trans-differentiation, also known as lineage reprogramming, is the process by which one somatic cell is converted into another cell in a different lineage without passing through an intermediate multipotent state (herein, using NeuroD1 TF). However, dedifferentiation (herein, using SOX2 TF) implies that the differentiated cells lose phenotypic characteristics under certain conditions and are reversed into stem cells, which can further proliferate and differentiate into mature cells[17]. Astrocytes can be reversed to form neural spheres, which have the characteristics of neural stem cells (NSCs) and possess self-renewal ability and multi-directional differentiation potential, and thus can differentiate into neurons, astrocytes, or oligodendrocytes *in vitro*[18].

To summarise, this project aims to use bio-inspired SAP hydrogel to immobilise and embed AAVs encoded with SOX2 and NeuroD1 TFs, to convert astrocytes to neurons through dedifferentiation/ and trans-differentiation, respectively. These TFs have been selected because

of their role during normal neurogenesis in development[19]. These TFs bind and activate cis-regulatory elements that modulate transcription and thereby direct cell-type-specific gene expression programs[20].

1.2 Research gap

Several labs have recently been working on the reprogramming of astrocytes to neurons[19,21–27]. However, there are concerns about the leakage of AAV to preexisting neurons, neutralisation, off-target effects, and high dosage administration. Furthermore, even though, neural stem/progenitor cells (NSCs) can be generated as an intermediate cell type from astrocytes on their way to generate neurons both *in vivo* and *in vitro*, limitations including i) uncontrolled reactivation of transgenes, ii) potential tumorigenicity, and iii) probable tissue damage due to persistent of transgene hamper their use in clinical applications[18].

Therefore, the novelty of this proposal lies in the interdisciplinary combinations. This project will make a significant advance in the treatment of brain traumas through the merging of parallel technologies –nanofabrication, biofunctionalisation and gene delivery – to engineer multi-component adjuvant scaffolding that represent a rational therapeutic strategy for brain regeneration. Our sophisticated multicomponent SAP scaffolds offer protection to the AAVs from antibody neutralisation and enable improved delivery. In addition, these strategies aim to localise gene expression to the microenvironment in and surrounding the material specifically to reactive astrocytes to simultaneously remove their inhibitory capability and encourage new neuron formation.

1.3 Aims

We hypothesised that AAVs encoded with SOX2, or NeuroD1 TFs can re-specialise astrocytes and reprogram them to functional neurons *in vitro* and *in vivo* in a brain injury model. To confirm targeted reprogramming of glia to neurons, studies were initially carried out on

cultured primary postnatal day 1.5-2 murine astrocytes. In summary, the research plan was to investigate the following aims:

Aim 1: The ability of AAV-SOX2/ or AAV-NeuroD1 TFs to transduce and convert primary astrocytes to functional neurons *in vitro* was demonstrated.

Aim 2: The ability of the Fmoc-DDIKVAV hydrogel to embed AAV-SOX2 and AAV-NeuroD1 TFs and provide controlled and sustained release for these AAVs was demonstrated.

Aim 3: The optimised SAP scaffold was implanted into the brain to deliver TF encoded AAVs to the injured area to reprogram astrocytes into neurons *in vivo*, whilst additionally protecting the penumbra, to promote functional repair.

Aim 4: A hybrid composite biomaterial was developed through incorporation of VPA loaded short fibres within the Fmoc-DDIKVAV hydrogel. Then, the diffusion and release kinetics of VPA from the fabricated hybrid composite biomaterial was monitored and studied for 8 weeks' time.

1.4 Thesis outline

This thesis focuses on the reprogramming of reactive astrocytes to neurons as a potential therapy for TBI. The following chapters are either published articles, submitted manuscripts, or manuscripts in preparation. This thesis is divided into seven chapters, as outlined here. The thesis begins with a literature review to present the past and current research on the reprogramming of astrocytes, biomaterials used to facilitate the remodeling after TBI, different approaches for the delivery of TFs with a particular focus on attenuating the inflammatory cells specially astrocytes as the cells of interest in this project. Then, a biological assessment of the astrocyte in the presence of AAV encoded with and without TFs in vitro and in vivo is presented. The thesis concludes by presenting future directions for the development of

biomaterials to facilitate the delivery of TFs within the site of injury to provide a potential treatment approach for TBI.

1.4.1 Literature Review

Chapter 2 provides a review of the past and current literature on TBI pathology, the importance of targeting reactive astrocytes as a promising treatment option, extracellular matrix (ECM) mimicking biomaterials (specifically the focus of the project self-assembling peptide hydrogels), and pioneer TFs for reprogramming of astrocytes to neurons either directly or indirectly.

1.4.2 Materials and methods

Chapter 3 presents the materials and methods, including fabrication, characterisation of different library of self-assembling peptide (SAP) hydrogels and PLA±valproic acid (VPA) electrospun nanofibres, as well as cell cultures, *in vitro*, and *in vivo* protocols used for biological assessment.

1.4.3 Synthesis and physiochemical characterisation

Chapter 4 presents the physiochemical properties of the fabricated SAP hydrogels, and PLA±VPA electrospun nanofibres. Furthermore, the biocompatibility of the different library of the fabricated SAP hydrogels are investigated. The materials and experimental methodology used in this chapter were described in Chapter 3.

1.4.4 *In vitro* and *in vivo* trans-differentiation of reactive astrocytes to functional neurons

Chapter 5 presents the efficiency of AAV-NeuroD1 to trans-differentiate reactive astrocytes to functional neurons in both primary astrocytes and human astrocytes *in vitro*. Moreover, the ability of AAV-NeuroD1 to trans-differentiate reactive astrocytes within the glial scar, *in vivo*, are investigated.

1.4.5 *In vitro* and *in vivo* dedifferentiation of astrocytes

Chapter 6 presents the indirect reprogramming of primary astrocytes to neurons. Using AAV-SOX2, astrocytes are shown to dedifferentiate to a less specialised cell type, induced progenitor neural stem cells, and further differentiate to neurons.

1.4.6 Conclusion and future perspectives

Chapter 7 provides concluding remarks on the research presented in this thesis and its contributions and impact on the research field of gene therapy and biomaterials for TBI. Perspectives for the future directions of using these TFs and SAP hydrogels as a treatment strategy for traumatic injury and other neurodegenerative diseases are also presented.

1.4.7 Appendices

The appendices include full published works not discussed in this thesis (Appendix A)

Chapter 2. Literature review

2.1 Preamble

This chapter presents a critical review of the literature including traumatic brain (TBI) injury pathology, inflammatory response after TBI, astrocyte role in injury, gene therapy, reprogramming, and the use of self-assembling peptide (SAP) hydrogels as a promising biomaterial to treat TBI. Some parts of this chapter are published as a review paper entitled ‘Calming the nerves via the immune instructive physiochemical properties of self-assembling peptide hydrogels’, in Advanced Science journal in (2023).

2.2 Introduction

Due to a lack of effective treatments after TBI, it is one of the leading causes of long-term disability and death worldwide, resulting in an enormous socio-economic burden both to society and patients' families[28],[29]. TBI has a complex prognosis, as it includes any physical event resulting in insult - typically a primary (direct) mechanical injury and secondary (indirect) insult to the surrounding parenchyma[30]. In the longer term, complex secondary brain injury is difficult to treat, as it includes disturbance of ion homeostasis, excitatory toxicity, oxidative stress, inflammation, demyelination and cell death[31]. Given the irreversible tissue damage and cell death caused by primary injury, we only focus on the mechanism of secondary injury. So far, numerous factors in secondary injury have been investigated, such as excitotoxicity, oxidative stress, neuroinflammation, apoptosis, axonal degeneration, and formation of cavity and glial scar[32].

In severe tissue injuries, CNS shows very little tendency towards tissue regeneration due to formation of tissue lesions characterised by distinct non-neural and neural cellular compartments segregated from adjacent viable neural tissue by dense glial scars formed mainly by resident reactive astrocytes (expressing elevated levels of glial fibrillary acidic protein (GFAP)) [33],[34]. These reactive astrocytes also secrete a range of molecules that in turn restrict axon plasticity[35,36].

Therapeutic cell replacement strategies after neurotrauma or in the diseased, degenerate CNS include the transplantation of fetal neural tissue or adult stem cells, engraftment of neural stem cells (NSCs) that can be derived from various sources such as embryonic stem cells, and transplantation of induced pluripotent stem cells (iPSCs). Although the transplantation of exogenous cells is promising in certain ways, some approaches are the subject of ethical controversy, and there are issues regarding immunorejection, sustained viability of grafted cells, the inability of newly grafted cells to functionally integrate into neural circuits and

potential tumorigenesis[1,37,38]. Using patient's own cells was pursued in an attempt to resolve ethical controversies and immunological rejection[39] which is a very time-consuming process and the time required to prepare cells for autologous transplantation is longer than therapeutically optimal window. Additionally, there is still potential risk of tumorigenesis from residual undifferentiated stem cells in the injured environment[40]. Furthermore, transplantation may disrupt the internal environment at the graft location[1].

To overcome some disadvantages of cell transplantation, focus has shifted to repairing neural function through manipulating other resident cells in the adult central nervous system (CNS). Astrocytes are a promising cell source to replace lost neurons due to disease or trauma owing to their capacity for dedifferentiation and proliferation under pathological conditions. Therefore, reprogramming of reactive astrocytes adjacent to the insult into functional neurons may provide an alternative therapeutic approach in order to begin the reconstruction of the injured or diseased brain.

Understanding, evaluating, and designing strategies to manipulate reactive astrocytes after injury is an innovative approach, with the potential to improve brain repair using a patient's own intrinsic cell population. Recent reprogramming studies have confirmed that astrocytes within the mature CNS can be transformed to functional neurons in different disease models. Biomaterials can be used as an interesting platform to deliver the gene of interest to the site of therapeutic need, replace damaged or lost neurons, and provide functional motifs and physical support for newly generated and nearby cells. Therefore, to develop and design the combinatorial approach understanding CNS pathology is important.

2.3 TBI pathology

The CNS exhibits a severely limited capacity for the repair and reconstitution of neurons and axonal connections[41]. Upon acute brain injury, both neurons and glial cells may immediately die or degenerate, often leading to the formation of a cystic cavity[42][10,43]. Consequently,

tissue insult resulting from disease or TBI causes permanent death of neural cells while glial cells become activated by injury, alter their phenotype, then migrate to and proliferate at the injury site[42].

Substantial advances have been made in understanding CNS pathology in response to injury, important when designing effective biomaterial interventions[44]. Following a primary injury, secondary damage is provoked through a complex and ongoing cascade of cellular and molecular events, including further axonal degeneration, demyelination, neuroinflammation, oxidative stress, mitochondrial and synaptic damage, cerebral edema, and disruption of the blood–brain barrier (BBB)[45,46]. In response to injury, dynamic multicellular interactions (**Figure 2.1**) effectively isolate adjacent viable neural tissue and allow recruited inflammation to resolve potentially noxious elements[47–49]. Following TBI, microglia and astrocytes initiate a cascade of immune events directed by the release of damage-associated molecular patterns (DAMPs)[50,51]. Neutrophils are the first leukocytes infiltrating the lesion sites within 24h post injury. They appear to contribute to inflammation by further destabilising the BBB with the release of matrix metalloproteinase (MMPs) and generating cytotoxic amounts of reactive oxygen species (ROS) and reactive nitrogen species, such as inducible nitric oxide synthase (iNOS). The inflammatory cytokines produced by leukocytes, astrocytes, microglia, and neurons induce local and systemic immune responses[52]. This causes further neuronal cell death and attracts more immune cells into the lesion further exacerbating the inflammatory response. Post-injury changes in the characteristics of the extracellular space (ECS) are also critical and affect normal function[53].

Activation and polarization of microglia, the resident CNS macrophage, is integral to the response of brain injury[54]. Macrophages and microglia exist as (pro-inflammatory) M1 and (anti-inflammatory/pro-healing) M2 phenotypes[55–57]. The latest research indicates that the majority of microglia and recruited macrophages at the site of injury have mixed M1- and M2-

like activation profiles[58]. Also, there is a shift from a dominance of M2-like microglia toward M1-like microglia within one week of injury[59]. As a result, the ratio of M1:M2 microglia shifts from 1:5 (day 1) to 7.5:1 (day 7) following injury[60]. Several factors influence M1-/M2-like polarization in the injured brain, such as injury severity, location within grey or white matter, sex, or aging. For efficient tissue repair post-TBI, both M1-like and M2-like functional responses are required. Despite the essential role of microglia to the capacity of the nervous system to recover from injury, they can also contribute to sustained inflammation that can limit recovery and drive chronic disease processes.

Neuroinflammation as an important factor in TBI pathology is characterised by the migration of activated microglia and astrocytes to the injury site, resulting in the release of pro-inflammatory factors that mitigate recovery events and exacerbate neuronal cell death. It is considered possible to increase the longevity of implantable therapeutic devices in the CNS by reducing glial scarring, attenuating pro-inflammatory secretions from immune cells, and promoting a regenerative environment at the site of a lesion.

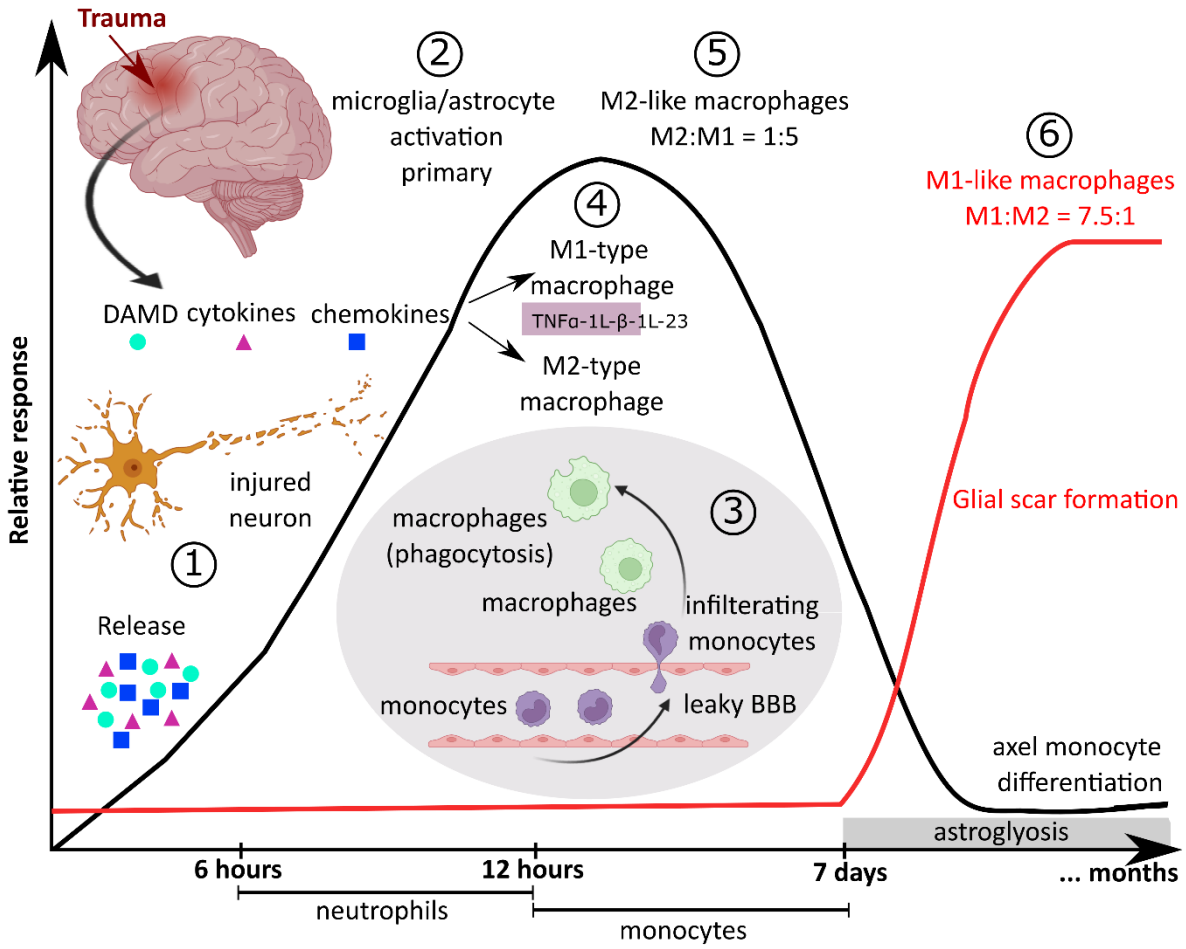

Figure 2.1. Schematic illustration showing the temporal cellular infiltration response after TBI. Created with BioRender.com.

Despite advances in uncovering mechanisms that underlie neuroinflammation in TBI and also in neurodegenerative disease, therapies that prevent neuronal loss are elusive. For example, targeting of disease-defining markers such as amyloid-β and tau in Alzheimer disease or α-synuclein in Parkinson disease has been met with limited success, suggesting that these proteins do not act in isolation but form part of a pathological network. This network could involve phenotypic alteration of multiple cell types in the CNS, including astrocytes, which have a major neurosupportive, homeostatic role in the healthy CNS but adopt reactive states under acute or chronic adverse conditions. Therefore, better understanding of astrocyte function is likely to assist in the development of new therapeutic strategies.

2.4 The physiological and pathological functions of astrocytes

Glial cells are the second-most abundant component of the mammalian nervous system after neurons. Astrocytes are the most specialised and abundant glial cell type and under normal conditions tile the entire CNS in a non-overlapping manner, playing a pivotal role in the physiology and homeostasis of the brain[43]. They secrete many neuroactive molecules that influence neuronal survival, synaptic activity and plasticity[61]. Astrocytes are well positioned in the CNS so that their processes contact blood vessels, axons (at nodes of Ranvier), neighboring astrocytes through gap junction, and synapses[43]. Thus, astrocytes regulate fluid and ion homeostasis[62], control blood flow[63], promote the generation of new blood vessels, protect neurons from excitotoxicity injury and cell death, promote the formation of synapses[64–66], provide nutrition and energy metabolites to neurons[67], and are involved in the construction and functional architecture of the BBB[68]. As their list of known functions has grown, their potential for repairing the nervous system has received increased attention[69–73].

Astrocytes are equipped with many receptors and intracellular signaling cascades to respond quickly to even small changes in their environment through a process referred to as reactive astrogliosis[74]. They become reactive in response to all pathological conditions in the CNS during progressive disease and acute injuries (e.g., stroke or trauma). Although reactive astrogliosis is used widely as a pathological hallmark of diseased CNS tissue, definitions of reactive astrogliosis can vary considerably among authors and there are no widely accepted categories of intensity or severity. Based on a large body of observations in experimental animals, a definition of reactive astrogliosis has recently been proposed [226] that encompasses four key features[43]: i) cellular and functional changes in astrocytes that occur in response to all forms and severity of CNS injury and disease including subtle perturbations, ii) changes in molecular expression, progressive cellular hypertrophy, and in severe cases, proliferation and

scar formation, iii) changes in inter- and intracellular signaling molecules[75], iv) altered astrocyte activities both through gain and loss of functions that can impact both beneficially and detrimentally on surrounding neural and non-neural cells. Reactivity of astrocytes affects the pattern of soluble and diffusible molecules, and results in alteration of neuron-astrocyte communication[61],[76,77].

Upregulation of GFAP expression can be regarded as a sensitive and reliable marker that labels most reactive astrocytes that are responding to CNS injuries and not immunohistochemically detectable in all non-reactive astrocytes in healthy tissue[43]. Following injury, reactive astrocytes demarcate injured area and act as a physical and chemical barrier and secrete neuroinhibitory factors to prevent neuronal growth, leading to distortion/regression of the brain parenchyma and scarring[9]. Different gradations of reactive astrogliosis depend on the nerve injury severity[43]. For mild to moderate reactive gliosis most astrocytes stay within their tiled domains; however, for severe reactive astrogliosis newly proliferated astrocytes, begin to disrupt astrocyte domains following a long-lasting reorganization of tissue architecture is observed. Severe reactive astrogliosis with compact glial scar formation have densely overlapping processes and include newly proliferated astrocytes as well as other cells such as fibromeningeal cells and other glia, together with deposition of dense collagenous extracellular matrix[9]. Apart from reactive astrocytes some other extracellular matrix molecules in the glial scar like chondroitin sulfate proteoglycan (CSPG) and some other myelin associated proteins (e.g., MAG and OMgp) have inhibitory effect and act as substantial barrier to regenerate and are largely responsible for the inability to repair damage[78],[79].

As the pathophysiology of acute injuries are immensely intricate, researchers have increasingly designed a combinatorial approach using biomaterial-based treatments to develop a platform approach that can replace the function of the regenerative extracellular matrix (ECM) for long enough for the innate processes to take over. These ECM mimicking biomaterials have the

ability to not only support those damaged cells but also deliver the payload (gene of interest, therapeutic drugs, neurotrophic factors, and anti-inflammatory molecules) to the zone of injury.

2.5 Extracellular matrix (ECM) mimics

ECM is a porous micro- /and nano-structured substrate made of different fibrillar proteins extensively crosslinked with each other and intertwined with a glycosaminoglycan network. This structure results in matrix that is resilient to tension, compression, and mechanical stress. The ECS refers to the space outside the cells occupied with fluid and various metabolites, ions, proteins, lipids, and other biomolecules framing the structure of the respective tissue like the extracellular matrix, affecting cellular function such as extracellular vesicles, cytokines, chemokines, hormones, etc. The interrelationship between the structure of ECS and ECM is still being explored[80].

ECM proteins may display cellular binding sites that affect cell adhesion, migration, proliferation, and differentiation. Therefore, ECM represents an intricate and dynamic system that modulates and influences various cellular functions at the organ and tissue level. Replicating these physiological structures can be advantageous for a scaffold's efficacy[81]. Therefore, the ECM mimicking materials must wholly or partially perform multiple functions: matching the structure and composition of healthy tissue, protecting degenerating neural cells, overcoming the BBB, replacing the lost neurons using endogenous/exogenous stem cells, promoting angiogenesis, and providing a conducive microenvironment for regenerated cells to survive and integrate into the neural circuits.

In nature, the ECM performs a wide range of functional roles. Biomaterials development has focused on synthetically reproducing one or more of these key aspects. The use of biocompatible materials acting as scaffolds capable of supporting damaged cells and providing sustained local release of exogenous therapeutics and anti-inflammatory molecules, may overcome some of the clinical deficiencies of the existing approaches, minimise systemic

exposure and associated side effects, and promote repair and reconstruction within an injured area of the brain.

2.6 Hydrogels as an *in situ* forming scaffolds for local CNS application

Among different biomaterials that have been developed for transplantation into soft tissue, such as the CNS, hydrogels (i.e., water-swollen materials) are considered the most promising because they can match the mechanical properties of the tissue, are non-cytotoxic, are suitable for payload delivery, fill odd-shaped (amorphous) insult sites[82], and allow both facile migration of cells and diffusion of biomolecules out of the scaffold while maintaining a physical structure[83],[82].

Hydrogels are crosslinked hydrophilic polymer networks that retain large amount of water, which are widely being used in the therapeutic of ischemic diseases and many other aspects experimentally and clinically[84]. Hydrogels can be formed with different gelators such as natural biological sourced materials (acellularized tissue and ECM-derived macromolecules such as collagen, hyaluronic acid (HA), chitosan, synthetic molecules (poly(ethylene glycol) (PEG), polyacrylamide, polymetharylamide), and synthetic supramolecular hydrogelators ((SAP), monosaccharide). The benefits and applications of biologically-derived and synthetic hydrogels are reviewed in Table 2.1. Both natural and synthetic polymers can be designed to be injectable using variety of crosslinking methods[85,86]. Among the biological sources, proteins and peptides are of special interest in the body because they serve as the foundation of the ECM components such as collagen, and the cell-membrane integrin that mediate molecular recognition between cells and ECM[87]. Biologically inspired proteins or polymers are the third class of materials with the aim of providing instructive cues, responding to the physiological environment, and degradation over time without any trace of toxic materials[88]. However, protein materials sourced from animals present batch-to-batch variability, carry a risk of immunogenicity, and also tuning their composition or material properties can be

challenging which limiting translation to clinical settings[89–91]. Additionally, naturally derived hydrogels such as collagen, gelatin, alginate, and HA have several major drawbacks including long-term instability, poor mechanical properties, presence of unwanted contamination, and fast degradation, especially *in vivo*[92]. While synthetic hydrogels, such as poly(lactic acid), poly(glycolic acid) and PEG, overcome these issues, with precise fabrication, purification, and control over properties to mimic specific target tissues, they are often limited in terms of biofunctionality/biological activity and biologically-mediated degradation without further modification[93,94]. However, there are still some key problems to solve when considering cell-directed hydrogels as a topical application for TBI. As such, these issues need to be addressed to develop an effective and robust hydrogel that can tolerate the ischaemic environment within the brain over the length of treatment, while simultaneously minimising harm to the patient. In this context, polypeptide hydrogels formed by peptide self-assembly exhibited advantages over other polymeric biomaterials for use in neural tissue engineering and preparation of advanced materials[95,96] owing to their tunability and the possibility to optimise their characteristics without any batch to batch differences.

Table 2.1. Benefits and applications of biologically derived and synthetic hydrogels in neural applications. Hydrogels made of biologically derived materials such collagen, hyaluronic acid, alginate, fibrin, chitosan, xyloglucan and methylcellulose have been used in treatment of CNS injuries. pHPMA, pHEMA and PEG are also the most investigated synthetic hydrogels for CNS treatment.

Hydrogel composition	Benefits	Applications	Ref
Biologically-derived hydrogels			
Collagen	• Loading and controlled-releasing of nerve growth factor and bone marrow-derived mesenchymal stem cells. • Supporting neural cell attachment and proliferation, thus enhancing reconstruction of neural networks. • Demonstrating recovery of motor function.	• Traumatic brain injury	[97–100]
Hyaluronic acid	• Constituent of the brain ECM.	• Diseases and injury in the central nervous system	[101–105]

	• Chemically and physically modified with brain regenerative factors and reactive oxygen species. • Promoting the motor, learning and memory ability.		
Alginate	• Maintaining neural cells in the undifferentiated state and retaining their pluripotent capabilities without any enzymatic treatment. • Proper mechanical properties for expansion or manipulation. • Localized drug release.	• Neural cell culture • Spinal cord injury • Drug delivery • Cell-based therapies	[106–108]
Fibrin	• Improving the survival and migration of the transplanted cells. • Loading with tumoral necrosis factor. • Accelerating nerve regeneration.	• Spinal cord injury • Peripheral nerve regeneration	[109,110]
Chitosan	• Proper 3D scaffold for neural tissue engineering. • Proper osmolarity for promoting cell survival. • Loading with Metformin, thus promoting the upregulation of neural regeneration–related proteins. • Loading with ferulic/succinic acid, thus increasing tissue regeneration and decreasing the inflammatory reactions.	• Neural tissue engineering • Stem–cell neural regeneration • Brain injury	[111–113]
Xyloglucan	• Thermoresponsive scaffold to assist the regeneration of the injured spinal cord.	• Spinal cord injury	[114]
Methylcellulose	• Functionalising and loading with biological moieties to promote neural regeneration. • Tunable mechanical properties. • Thermoresponsive properties.	• Central nervous system injuries	[115,116]
Synthetic hydrogels			
Poly(N-2-(hydroxypropyl)methacrylamide) (pHPMA) Poly(hydroxyethylmethacrylate) (pHEMA)	• Modified with biological moieties. • Promoting ingrowth of connective tissue.	• Parkinson's disease • Nervous tissue repair • Extensive spinal cord spinal cord injury	[117–122]
Polyethylene glycol (PEG)	• Promoting neural stem cell migration and differentiation. • Proper mechanical properties. • Delivery of hydrophobic drugs for site-specific delivery without systemic circulation.	• Injuries to and diseases of the CNS • Drug delivery against glioma recurrence	[123–125]

2.7 Self-assembling peptide (SAP) hydrogels as a biomimetic ECM

Internal architecture and mechanical properties are characteristics that must be defined when designing a hydrogel. For example, at the microscopic level: its biochemical signature, stiffness, pore size, porosity, swelling, and viscoelasticity, are all factors that will affect tissue regeneration properties at the lesion site[126]. Polypeptide hydrogels formed by peptide self-assembly are promising polymeric biomaterials owing to their sequence and structure relationship and the possibility to optimise their characteristics without significant batch to batch differences. Functionally designed SAPs have been increasingly investigated as tailorable biophysical and biomechanical materials for neural tissue engineering and preparation of advanced materials for CNS regenerative medicine[95,96]. These SAP gels are able to create a permissive 3D environment for cell migration, glial scar prevention, and axonal extension[127,128]. In addition, they have many inherent properties, including i) a minimal risk of carrying biological pathogens or contaminants[129], ii) a highly hydrated 3D environment for cell growth and migration, similar to the native ECM of host tissue[130],[131]; iii) excellent physiological tunability and compatibility as well as minimal cytotoxicity due to its composition of naturally occurring amino acids[132]; iv) ease of synthesis and customisation with bioactive moieties, v) capacity to flow and gelate in even hard-to-access brain lesions and fill the cavities, regardless of their size and shape[127]; vi) stable secondary structures (α-helix, β-sheet, or random coil) [130,133] and vii) long term biocompatibility and biodegradability (hydrolytic or enzymatic degradation)[134,135].

The shear-thinning properties of these designed SAPs is attributed to their noncovalent cross-linking bonds that can easily break and reform[136]. Self-assembly is driven by non-covalent binding and spontaneous organisation of peptides into different kinds of supramolecular structures, from nanotubes, nanosphere, nanofibres, vesicles, micelles, β-sheets to other novel morphologies based on the molecular self-assembly approach[137]. This organisation is

usually triggered by changes in temperature, pH, or by the presence of monovalent or divalent electrolyte ions[129,138,139]. Typically, SAPs are composed of alternating positive and negative amino acids (or alternating hydrophobic and hydrophilic amino acids) that assemble into nanofibrous networks capable of entrapping water. It may be possible to achieve biocompatibility and safe degradability without immunogenicity issues. These engineered biocompatible nanofibrescaffolds can serve as a permissive bridge for axonal regeneration or as cell/drug carriers[140,141].

It is well established that the inclusion of both the charged hydrophilic amino acid and hydrophobic sequences rapidly self-assembled into a β-sheet structure and the inclusion of aryl functionalities such as fluorenylmethoxycarbonyl (Fmoc) enhance peptide stability through π-π interactions by inducing the formation of highly ordered 3D fibrillar networks[142] **(Figure 2.2).** The process of peptide self-assembly is often guided by the combination of various polar and non-polar noncovalent intramolecular interactions like electrostatic interactions, hydrogen bonds, hydrophobic interactions, van der Waals forces, and well-known π-π stacking to maintain molecules at a stable low-energy state (thermodynamically stable structures determined by $\Delta G_{\text{self-assembly}}$)[143],[144].

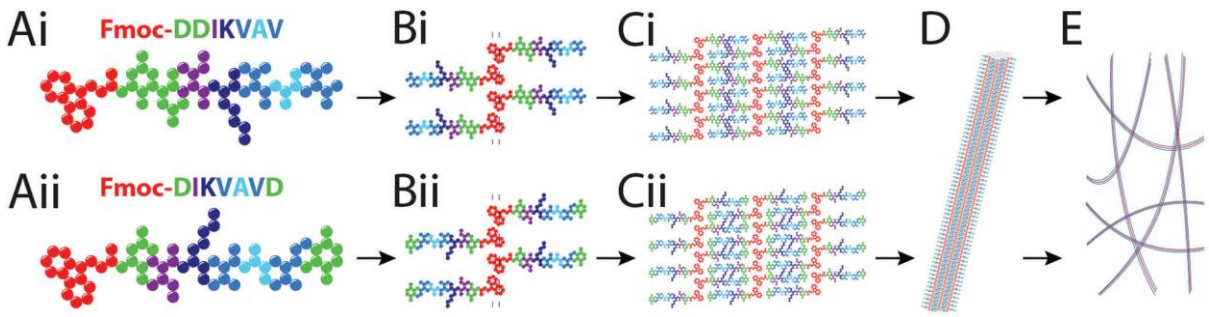

Figure 2.2. A) Schematic of Fmoc-DDIKVAV and Fmoc-DIKVAVD peptide structure and B) peptide assembly driven by π–π stacking interactions and C) polar and non-polar, non-covalent intramolecular interactions to form a D) hollow nanofibre and E) hydrogel matrix formation through the entanglement of the nanofibres[145].

These 3D SAP hydrogels should mimic the biomechanical, topographical, and biochemical properties of the ECM while concomitantly undergo optimal self-assembly under mild, physiological conditions (pH=7.4, 37◦C) and without the use of strong organic solvent[146]. To make a hydrogel free from any traces of organic solvents, a pH switch was applied resulting in a material that matches the mechanical and chemical properties of the brain. N-Fluorenylmethyloxycarbonyl self-assembling peptides (Fmoc-SAPs) have gained considerable interest in recent years mainly due to their ability to fill irregular insult sites, provide structural support to damaged tissue, attenuate inflammation, and to be modified for bio-functionalisation[147]. It is reported that Fmoc-DDIKVAV offers a suitable neural scaffold for brain repair since it contains IKVAV epitope and is capable of self-assembly at physiological pH (7.4)[146].

Defining the biological interactions of the polymeric scaffolds with cells is as important as the physical properties of the scaffold. Thus, the use of unique peptide sequences (functional motifs) plays an essential role in designing tissue engineering biomaterials since they interact with cells and have varying influences on intracellular processes such as adhesion, proliferation, differentiation, and migration. In this regard, scaffolds have often been modified with cell-adhesive ligands targeting the integrin family of cell-surface receptors to initiate cell pathways[148].

One way to provide cell attachment to the material is the incorporation of peptide that displays a specific binding sequence. The interactions between implanted hydrogel and endogenous brain cells have the potential to induce many different reparative and anti-inflammatory cellular pathways through binding of cell adhesive molecules/functional motifs. Thus, the use of unique peptide sequences/ functional motifs plays an essential role in hydrogels since they interact with cells and have varying influences on intracellular processes. In this regard, scaffolds have often been modified with cell-adhesive ligands targeting the integrin family of cell-surface

receptors to initiate cell pathways. Laminin is a pivotal substrate along which nerve axons will grow and incorporate into scaffolds to enhance cell adhesion and migration. Natural ECM proteins like fibronectin and laminin are the most important integrin proteins providing great cellular attachment and can be mimicked by short peptide motifs sequences namely (arginine-glycine-aspartic acid) RGD[149], isoleucine-lysine-valine-alanine-valine (IKVAV)[150], and tyrosine-isoleucine-glycine-serine-arginine (YIGSR). RGD is highly effective at promoting cell attachment[151], YIGSR sequence possess capability to promote not only neurite outgrowth but also facilitates the cell binding[152] and IKVAV peptide facilitates neurite extension[153],[121]. RGD is known to bind through integrins α5β1, α8β1, αVβ1, αIIbβ3, αVβ3, αVβ5, and αVβ6. IKVAV and YIGSR, laminin-derived motifs, are known to bind through integrins α1 chain and the β1 chain, respectively[154]. Among these short peptide motifs, IKVAV, the major protein in laminin, has become the epitome of CNS tissue engineering scaffolds as it increases the viability and maturation of neurons[155] and also inhibits the formation of the glial scar by attenuating astrogliosis and cell death at the core of the lesion site[6]. Recently, our group proved that Fmoc-DDIKVAV hydrogel is stable when formed in phosphate-buffered saline at pH 7.4 with no effect on the non-covalent interactions between individual SAPs responsible for self-assembly[146]. In this project, SAP hydrogels will be used as a platform for payload delivery (neurotrophic factor and viral gene delivery) and also scaffold to provide physiochemical support for newly generated cells and surrounding tissue.

2.8 Astrocyte reprogramming through the ectopic expression of transcription factors (TFs)

With regard to the CNS, resident glial cells have been directly or indirectly converted into functional neurons in the adult brain and spinal cord[149–156]. *In vivo* reprogramming holds great promise for future therapy and offer several advantages over fetal or stem cell

transplantation including i) using endogenous cells that avoid immunorejection caused by external cell transplantation, ii) the capacity to regenerate new cells at the injury sites using neighboring cells, iii) targeting proliferating cells and converting them to post-mitotic neurons, iv) the intrinsic lineage of the neighboring cells at a specific region may be a critical factor for the cell's identity after *in vivo* reprogramming[160]. Note here that astrocytes in the mouse cortex are different from their counterparts in the striatum in terms of reprogrammability and neuronal identity despite expressing the same transcription factors. Such subtle regional differences in intrinsic cell lineage may be too difficult to closely mimic in a petri dish[156].

TFs play a pivotal role in the modulation of cell fate. TFs are proteins that bind to specific DNA domain which may result in increased or decreased gene transcription, if binds to activation domain or repression domain, respectively. The TFs expression can force cell fate reprogramming either through trans-differentiation from one lineage to another, or through dedifferentiation. The process of regressing to a previous, less-specialised cell fate is known as "dedifferentiation". These cells can then differentiate back into a specialised cell, though not necessarily the same cell fate they previously occupied. In the process of trans-differentiation, cells regressing to a point where they can switch lineage, allowing them to differentiate into another cell type directly without becoming pluripotent stem cells[161].

Changing one cell to another requires changes in gene expression. Therefore, for reprogramming astrocytes to neurons, genes expressed in the astrocytes (as a starter cell) have to be shut down and those expressed specifically in neurons need to be activated. However, this process may not be as easy as it sounds because genes that are not expressed in neurons are often shut off (e.g., silenced by chromatin marks) and wrapped around the nucleosome, whereas the DNA that is transcribed is ‘‘open’’ between nucleosomes. Most transcription factors (TFs) cannot access this rather ‘‘inaccessible’’ DNA; however, some factors can bind DNA in closed conformation and start activating transcription. These special TFs are referred

to as ‘‘pioneer’’ TFs because they have the unique ability to engage silent, unmarked chromatin (open close chromatin[162]) and initiating the recruitment of other factors to activate specific gene expression to a new fate[163–165]. Pioneer TFs are mobile in the nucleus and interact transiently with chromatin[166], and recent *in vitro* studies[166] unraveled several ways in which pioneer factors engage nucleosomes and scan DNA to ultimately activate transcription at previously silenced sites. As master regulators of enhancer activation, pioneers are thus crucial for the implementation of correct cell fate decisions in development, and as such, they hold tremendous potential for therapy through cellular reprogramming. Pioneer TFs are not that different from most other TFs and that a gradient of properties could demarcate the behaviour of so- called pioneers, for example, a greater affinity of pioneers for DNA target sites, for closed- chromatin proteins or for nucleosomes[167].

To fulfill the aim of this project, conversion of astrocytes to neurons, we used two main approaches to direct the fate of reactive astrocytes into neurons: *in vitro/in vivo* trans-differentiation and *in vitro/in vivo* dedifferentiation using NeuroD1 and SOX2 TFs, respectively.

2.8.1 NeuroD1 transcription factor

Transcription regulation is essential for the correct functioning of cells during development and in postnatal life. The basic Helix-loop-Helix (bHLH) superfamily is well conserved throughout evolution and plays critical roles in development, maintenance, and function of the CNS[168]. At the transcription level, TFs control certain physiological or biochemical processes[169]. During the development of the nervous system, proneural bHLH transcription factors have pivotal roles in the regulation of cell proliferation, neuronal terminal differentiation, and specification[170,171]. Most of the bHLH factors are involved in the conversion of glial cells to neurons, including Achaete Scute Complex-like 1 (Ascl1), and Neuronal Differentiation 1 (NeuroD1), and Neurogenin2 (Ngn2)[172,173].

NeuroD1 is a neural differentiation factor that is widely expressed in developing CNS/ (the early stages of brain development) and can not only drive the differentiation of neural stem cells (NSCs) to neurons but also promotes neuronal maturation and survival [174]. Given its prominent function during embryonic neurogenesis, it has also recently been used to reprogram other somatic cell types into neurons. It has been reported that ectopic expression of NeuroD1 as a terminal differentiation factor, inhibits cell proliferation and directly reprograms the astrocytes into glutamatergic neurons without transition through the neuroprogenitor stage[175].

The neurons converted by highly and continuously expressed NeuroD1 are mostly glutamatergic (i.e., excitatory) subtype in the brain and spinal cord[176,177], which is consistent with the fact that NeuroD1 is a glutamatergic neuron-lineage determination factor during development[178,179]. So far, this trans-differentiation strategy has been promoted in stroke, AD, Parkinson's disease (PD), Huntington's disease, and other neurological diseases to increase neuronal regeneration and improve disease symptoms[177,180,181], suggesting that NeuroD1 as a highly potent factor that promotes neuronal fate.

One concern during neuronal reprogramming is cell death since the converting cells undergo dramatic metabolic changes. It has been revealed that during and after NeuroD1-mediated conversion apoptotic cells are rarely observed as determined by TUNEL assay[177]. This data suggests that NeuroD1 is not only a reprogramming factor but also a survival factor. This dual role of NeuroD1 during neuronal conversion may explain its higher conversion efficiency over other reprogramming factors. These TF-based trans-differentiation from glial cells into neurons provides a new path toward neural regeneration and repair.

2.8.2 SOX2 transcription factor

Reprogramming of astrocytes to induced pluripotent stem cells (iPSCs) can be achieved using the viral expression of four pluripotency TFs, so called 'Yamanaka' TFs (Oct4, Sox2, Klf4,

and c-Myc)[182]. Through a cooperative interaction these factors drive pluripotent-specific expression of the numerous genes and play key roles in determining the fate of embryonic stem cells (ESCs), regulating two distinct and opposing functions: indefinite self-renewal without signs of change and differentiation (form specialised cells). However, the combination of several TFs has been subsequently shown to induce tumorigenesis *in vivo*[183,184]. Moreover, directing differentiation from a pluripotent state typically involves lengthy, multistep protocols and is therefore inefficient, often producing heterogeneous populations of developmentally immature cells.

SOX2 TF has become widely known because of its functional connection to the stem cell state[185,186]. SOX TFs govern diverse cellular processes during development, such as maintaining the pluripotency of stem cells, cell proliferation, cell fate decisions/germ layer formation as well as terminal cell differentiation into tissues and organs. The overexpression of SOX2 single TF not only is sufficient to reprogram astrocytes to induced neural progenitor stem cells (iPNSCs) but also no histological signs of tumorigenesis in brains or spinal cords were observed when examined up to 1 year post virus injection[21,24]. The resulting iPNSCs can be directed to differentiate *in vitro* toward desired target populations by recapitulating the relevant embryonic programs[187], offering potential for regenerative therapy and permitting disease modeling, toxicology testing and drug discovery. Sox2 also converts astrocytes into mainly glutamatergic neurons[188].

Therapeutics based on TFs have the potential to revolutionise medicine. As TFs are made of proteins, they are susceptible to enzyme degradation. Moreover, TFs target cellular genome. Therefore, their use as transgene/therapeutic agent depends on the development of suitable delivery technologies that allow them to reach their action site inside the cells and control their expression in a spatiotemporal manner. Viral vectors are one of the most explored and used technologies for introducing TFs in the host cells, both *in vitro* and *in vivo.*

2.9 Gene therapy using viral vector delivery

Gene therapy (i.e., the delivery of new therapeutic genetic material) is a promising approach to treatment many complex disorders, including chronic conditions such as heart disease, neurodegenerative disorders, stroke, and diabetes mellitus[189],[190]. More specifically, gene therapy has been recognised as an attractive option for curing CNS diseases. Therefore, to facilitate delivery of gene therapies to the intracellular compartment of target cells, a vector must be employed.

A variety of methods have been developed to deliver TFs, most of which relied on biological, chemical- or physical based delivery system for transfection. Chemical-based delivery based on nanocarriers regarded as low risk of gene integration and insertional mutation but suffer from transfection efficiency and stability[191]. Biological-based delivery can be categorised as integrative vectors (retrovirus and lentivirus) and nonintegrative vectors. Integrative viruses have drawbacks of insertional mutagenesis, reactivation of transgenes and uncontrolled silencing[1,2], which prompted nonintegrating viruses to be a safer method. Moreover, in recent years, researchers have developed a DNAzyme-based gene delivery system that are responsive to MicroRNAs (miRNA) or mRNA to achieve targeted delivery[192]. MiRNAs are short, untranslated, regulatory RNA molecules that lead to the degradation of target mRNAs or the suppression of mRNA translation, thereby inhibiting the synthesis of proteins and achieving the regulation of genes[193,194]. To provide a tightly controlled gene expression of miRNAs, they are being combined with other targeting strategies such as capsid-modified viral vectors or surface-modified non-viral vectors. Viral vectors are regarded as the preferred option due to their ability to deliver therapeutic cargo to specific target cells with diagnostically measurable, persistent effects. Of all the reported vehicles for TF introduction to astrocytes, the non-pathogenic parvovirus adeno-associated virus (AAV) has emerged as a safe, robust, easy to prepare, and effective vector of choice for gene therapy in CNS[135].

2.9.1 Adeno- associated viral vectors (AAVs)

Gene therapy with derived AAVs have gained significant attention and will be the focus of this thesis because of their high infection rate, low pathogenicity in human, and haves been approved by the FDA in clinical trials[195]. Furthermore, they are mostly non-integrative and can transduce a wide variety of terminally differentiated tissues, dividing and non-dividing cells. Adenoviruses are icosahedral particles consisting of a large DNA genome, which remains in extrachromosomal form following infection[196].

Recombinant adeno-associated virus (rAAV) vectors are small (~25 nm), non-enveloped, cloning capacity of 4.7-kb of single-stranded DNA (ssDNA). They are classified as dependoviruses belonging to the parvovirus's family[197]. AAV is nonreplicating on its own and its life cycle is dependent on the presence of a helper virus to mediate a productive infection[198]. AAV expression vectors normally have limited room for recombining exogeneous genes, and thus they are not suitable for delivering several genes simultaneously which is a major limitation of this vector system[198]. However, on the other hand, the relatively small particle size of rAAV allows it to be delivered in higher titers to achieve greater expression levels of the packaged TF genes.

The viral genome consists of rep and cap genes required for viral genome replication and encoding structural protein (respectively). These two genes are flanked by two T-shaped (two hairpin) structures called inverted terminal repeats (ITRs) at either end of the viral genome comprising 145 nucleotides **(Figure 2.3)**[189] which are structural elements required for second strand synthesis, genome amplification, integration into the chromosome, and ssDNA packaging. The ITRs, only sequences of viral origin residing in rAAVs, largely serve as the viral origins of replication and the packaging signal[199],[189].

To generate rAAVs a therapeutic gene sequences (genes of interest) is inserted between the ITRs and replaces both rep and cap genes along with adenoviral helper genes that are needed

for replication[200]. Infection with AAV is initiated by binding to cell receptor, serotype-specific glycan 'primary' receptors, thus viral capsid determines the ability of the resulting rAAV vector to transduce cells. To date, *Twelve* naturally occurring serotypes and 108 variants of AAV have been isolated from different animal species, which differ in their amino acid sequence of the capsid[201]. Because the capsid interacts with different receptors on target cells and influences the post-entry transduction steps, AAV vectors bearing different capsids have different transduction abilities (i.e., cell tropism and kinetic of transgene expression), identifying an appropriate capsid for the targeted cell type and tissue is an integral part of successful gene delivery as they infect different cell types and tissue based on their capsid protein recognition by cell surface receptors[202,203].

AAV has appeared to be a vector of choice for *in vivo* cell conversion or reprogramming due to their episomal presence within the cells. However, efficient gene delivery has always been a challenge to the success of gene therapy include acute toxicity from the presenting foreign materials and viral vector neutralisation as a result of cellular immune response provoked by transduced cells[204],[190]. In order to create a safe viral vector, the viral particles must lose the ability to self-replicate while retaining their capacity to integrate in the host genome. For this reason, the coding regions of the virus must be replaced by the genetic information of the therapeutic gene of interest, while leaving the cis-acting sequences intact. As such, higher generation viral vectors contain more deletion to their viral genome to generate well-tolerated recombinant vectors and decrease the possibility of generating a severe immune response[190]. But, since the immune system is designed to fight against viruses, even heavily modified viruses can initiate the immune response[190]. Moreover, gene delivery to CNS has been largely neuron centric and as such, the application of AAV vectors to deliver transgenes to astrocytes is a relatively unexplored avenue.

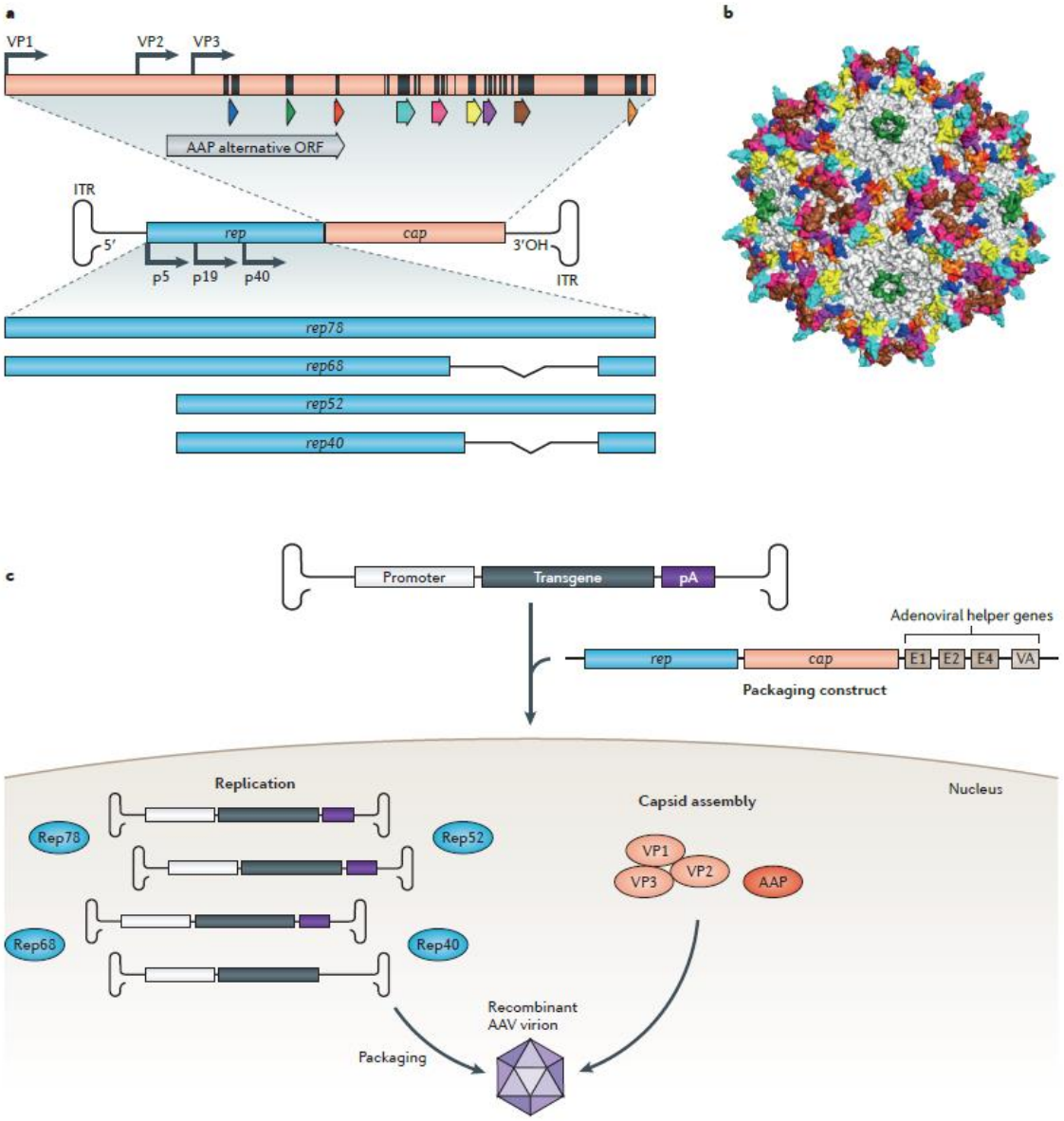

Figure 2.3. AAV and its variant generation. (a) The single-stranded DNA genome of the wild type of AAV is shown. The rep open reading frames (ORF) encodes four non-structural proteins from the 5' ORF of wild-type (Rep40, Rep52, Rep68 and Rep78) that are essential for viral replication, transcription regulation, genome integration and virion assembly/packaging. The cap ORF encodes 3 structural proteins from the 3' ORF (VP1, VP2 and VP3) which form the 60-mer viral capsid at the ratio of 1:1:10 (VP1:VP2:VP3)[205]. **(b)** Crystal structure of the AAV capsid (c) Recombinant adeno-associated viral vectors (rAAVs) are originally constructed by deleting both rep and cap genes and replacing these with therapeutic gene sequences, along with adenoviral helper genes that are needed for replication. The ITRs are the only viral sequences retained in AAV vectors[189].

Depending on the serotype, AAVs can have specific tropism for specific organs and tissues of the body. There are different AAV serotypes that vary in many aspects[203] (Table 2.2).

Table 2.2. Characteristics of different AAV serotypes

AAV serotype	Primary receptor	Tropism
AAV1	Sialic acid	Endothelial vascular smooth muscles, cardiomyocytes, skeletal muscle, CNS, retinal cells

AAV2	hepatocyte growth factor receptor (HSPG)	skeletal muscle, renal tissue, hepatocytes, CNS, retinal cells
AAV3	HSPG	Inner ear cells, hepatocytes, inner ear cells
AAV4	Sialic acid	Cardiomyocytes, renal tissue, airway epithelia, CNS, retinal cells
AAV5	Sialic acid	Endothelial vascular smooth muscles, hepatocytes, airway epithelia, CNS, retinal cells
AAV6	Sialic acid and HSPG	Cardiomyocytes, skeletal muscle, airway epithelia
AAV7	-	Endothelial vascular smooth muscles, cardiomyocytes, skeletal muscle, hepatocytes, CNS, retinal cells
AAV8	laminin receptor (LR)	Cardiomyocytes, skeletal muscle, renal tissue, pancreatic cells, hepatocytes, retinal cells
AAV9	terminal N-linked galactose	Cardiomyocytes, skeletal muscle, renal tissue, Leydig cells, pancreatic cells, hepatocytes, airway epithelia, CNS, retinal cells
AAV10	-	renal tissue, adrenal glands, lymph nodes, colon cells, small intestine cells, pancreatic cells, hepatocytes, airway epithelia, CNS, retinal cells
AAV11	-	renal tissue, adrenal glands, lymph nodes, small intestine cells, hepatocytes, CNS
AAV12	potential receptors (mannose and mannosamine)	skeletal muscle, salivary glands, airway epithelia
AAV13	-	

In the brain, combining vector serotypes that have a natural propensity toward astrocyte transduction with astrocyte-specific promoters can enhance transgene expression in astrocytes while reducing the expression in neuronal populations[206]. The current method to bypass off-targeting transduction is utilising tissue-specific promoters to drive the expression of the transduced gene and the modification of the surface recognition elements of recombinant viral particles to change their cell-recognition properties and improve cell-specific targeting[207],[208]. The multiple steps of AAV transduction that include receptor binding, cell entry, intracellular trafficking, uncoating, second-strand synthesis, vector genome stabilization, and trans-differentiation/ or dedifferentiation to neurons are illustrated in **Figure 2.4**.

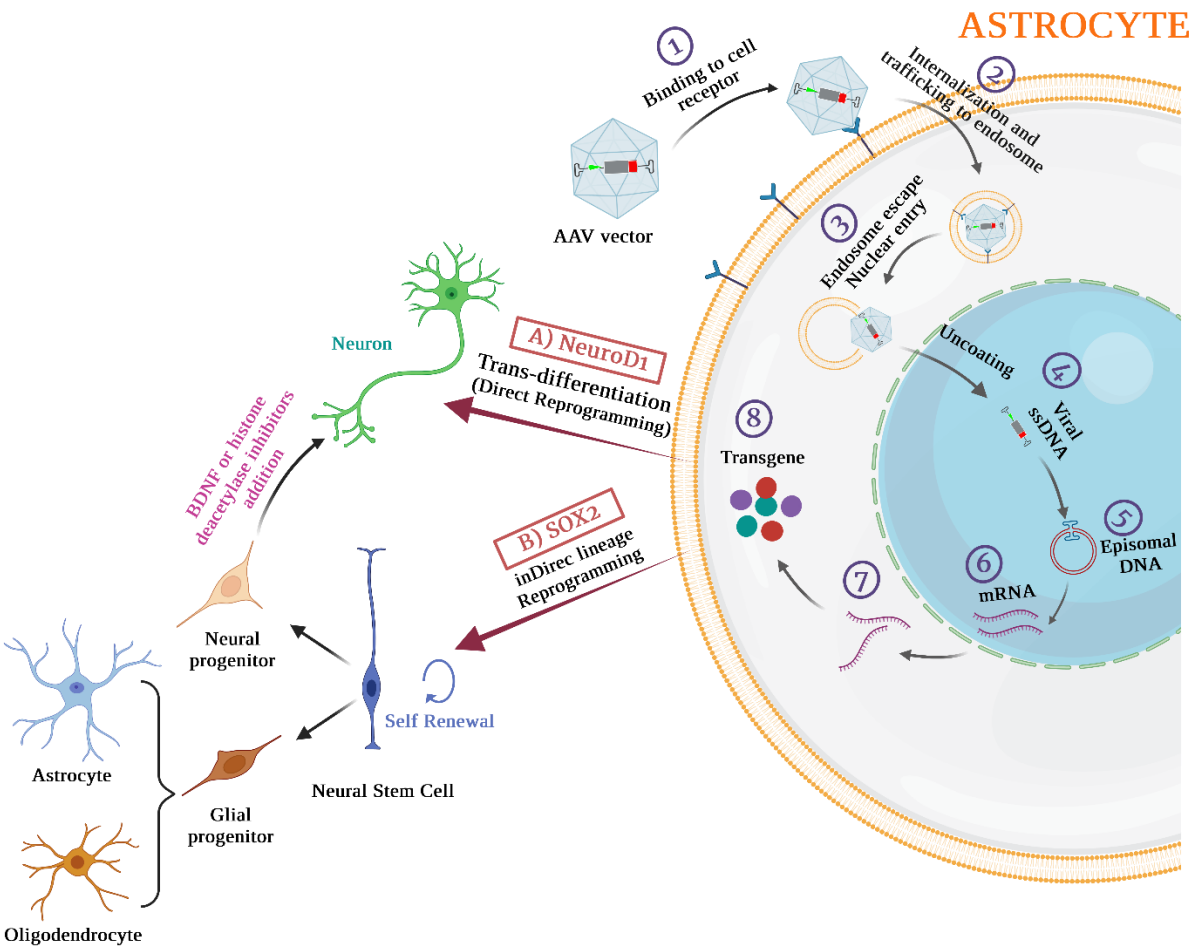

Figure 2.4. Schematic overview of the AAV vector transduction pathway, A) trans-differentiation (with NeuroD1), and **B)** indirect reprogramming/dedifferentiation (with SOX2) proposed in this thesis. AAV bind to receptor on the surface of astrocyte **(1)** followed by trafficking to endosome **(2)** and endosome scape **(3)**. Once in the nucleus, AAV capsids are uncoated and the AAV genome is released (single strand DNA (ssDNA)) **(4)**. Then AAV ssDNA genome is converted into double-stranded DNA **(5)**, followed by transcription **(6)** and nuclear export of mRNA **(7)** for translation and expression of the therapeutic transgene **(8)**. Then the astrocyte converts to induced neurons directly or indirectly based on the transgene NeuroD1, or SOX2, respectively as illustrated. **Created with BioRender.com**

Considering the role of astrocytes in the on-going secondary damage in TBI, an AAV vector that targets astrocytes could show benefit as a potential treatment for TBI. As such, in this project the AAV is equipped with gfaABC1D promoter to allow specific targeting to GFAP expressing reactive astrocytes to reduce the viral vector dose administered as well as the chance of off-target transduction. The gfaABC1D promoter is a new and truncated version of gfa2 GFAP promoter, and since it is only 681 bp in size[209], it allows for greater flexibility in

creating therapeutic AAV constructs with less transgene size restrictions. Therefore, it is possible to insert a relatively large transgene into the vector[210].

Rational design of AAV capsids is a simple method for enhancing AAV transduction efficiency. AAV-DJ is a highly recombinogenic hybrid vector created from DNA shuffling of eight AAV serotypes[211], which mediates efficient gene expression both *in vitro* and *in vivo*. AAV2 and AAV8 are the closest parental vectors of AAV-DJ. It has been reported that AAV-DJ capsid could lead to significant improvement for gene delivery both *in vitro* and *in vivo*[212]. In line with this, we have also shown that this serotype has the highest affinity to transduce astrocytes compared to AAV2 and AAV5 serotype. Therefore, this serotype is selected for this project.

However, even from the earliest studies, it was obvious that rAAV gene transfer elicited neutralising antibody responses to the AAV capsid, which limited the ability to re-dose rAAV vectors with the same serotype capsid[213]. AAV delivery into the brain or eye results in less immunogenicity due to immunological privilege, nonetheless the influence of neutralising antibodies against AAV capsids often leads to decreased vector transduction over time[214,215]. As such, in this project AAV will be delivered locally in the injury site to address the limitation of re-dosing of AAV. The use of hydrogels can significantly improve gene therapy due to their capacity for incorporation of viral vector payloads and concomitantly protecting them from clearance by the host immune system, degradation, and antibody neutralisation[216]. Moreover, viral vector encapsulation into hydrogels not only inhibits the spread of genetic material to off-target cells but also encourages their controlled release into preferred targets. It has been reported that affinity peptides, hydrogel modified with lysine-based repeats, can retain 25% more vectors compared to control peptides and subsequently enhance the transduction efficiency by 5-15-fold[217]. In another study, different libraries of

SAP hydrogels showed different capacities to retain AAVs based on the surface charge, peptide sequence, and mesh size[218].

To summarise, AAV vectors will be used in this project to deliver NeuroD1, SOX2 TFs to the reactive astrocytes. Furthermore, to enhance transduction efficiency *in vivo*, AAVs will be encapsulated in SAP hydrogels to help shield from neutralising antibodies and further minimize any host immune responses.

Chapter 3. Materials and methods

3.1 Preamble

This chapter provides a detailed description of the materials used and methods employed throughout this thesis. All material fabrication and characterisation, as well as the biological work was conducted in the Laboratory of Advanced Biomaterials (LΛB) at the Australian National University (ANU). *In vivo* work presented in Chapter 5 and Chapter 6 was conducted at the Florey Institute for Neuroscience and Mental Health. Scanning electron microscopy, transmission electron microscopy, and confocal microscopy were conducted at the Centre of Advanced Microscopy (CAM center), and the fluorescence activated cell sorting was conducted at the Imaging & Cytometry Facility in the John Curtin School of Medical Research, both at the ANU. The results obtained from these experiments are presented in Chapter 4Chapter 4, Chapter 5, and Chapter 6.

3.2 Solid phase peptide synthesis (SPPS)

Fmoc-SAPs were synthesised manually using solid-phase peptide synthesis (SPPS) as previously described[146]. In a rotating reactor vessel 0.4 mmol of resin was swelled in DMF for 15 min. In series, peptide synthesis was carried out by stepwise removal of protecting Fmoc groups of the N-terminal in 20% piperidine in DMF for 20 min at room temperature (RT), followed by a coupling step. The next amino acid in the sequence coupled by reaction with a 2 mmol solution of the amino acid in DMF with hydroxybenzotriazole (HOBt), O-benzotriazole-N,N,N',N'-tetramethyl-uronium-hexa-fluoro-phosphate (HBTU), and N,N-diisopropylethylamine (DIPEA) for 60 min. The deprotection and coupling processes were repeated until the desired sequence was obtained. The final Fmoc group was not removed.

After every deprotection and coupling step, the resin was washed with DMF to remove the reaction solution. Then, the resin was washed with dichloromethane (DCM) to perform a Kaiser test/ninhydrin reaction to confirm reaction progress based on the presence or absence of free amine groups. The final resin and Fmoc-protected peptide were washed with ethanol and stored under vacuum for at least 2 d before cleaving the peptide from the resin.

Cleavage was performed in trifluoroacetic acid (TFA) containing 2.5% triethylsilane (TES) and 2.5% deionized water for 2 hours. The peptide was recovered by filtration through glass wool, and excess TFA was removed under gently flowing nitrogen gas until 5 mL peptide solution remained. The remaining solution was precipitated in a solution of 10 mM hydrochloric acid (HCl) and washed in dry ice-cooled ether and separated by centrifugation (twice in HCl and then five times in cold diethyl ether). This product was dried under constant vacuum for at least 2 d before being ground into a fine white powder and dried for a further 7 d before use.

3.3 Self-assembled peptide (SAP) hydrogel preparation

Fmoc-SAP hydrogels were assembled to a final peptide concentration of 15 mg/ml. In brief, 10 mg of Fmoc-SAP powders were suspended/dissolved in deionized water (DI H_2O) and fully dissolved by minimal addition of sodium hydroxide (NaOH, 0.5 M) while vortexing. Next, the self-assembly was induced by a pH switching method using the dropwise addition of hydrochloric acid (HCl, 0.1 M) with continuous vortexing until physiological pH was reached, measured using a microprobe pH meter. Then Phosphate-buffered saline (PBS, pH 7.4) was added to make up the volume (666 µL) to achieve the desired final peptide concentration (15 mg/ml). Then the gel was exposed to ultraviolet (UV) light for 20 minutes.

Note: Fmoc-DDIKVAV (95-99% desalted) used in Chapter 5 and Chapter 6 was manufactured by Pepmic, China. The gel formation procedure was the same as above.

3.4 Polylactic acid (PLA) scaffold fabrication, valproic acid (VPA) immobilisation, and characterisation

Electrospinning is a technique that employs electrostatic forces to produce electrospun fibres with diameters ranging from micrometers to nanometers depending on the polymer types and processing conditions[219]. This is an appealing method for producing polymer biomaterials owing to its simplicity and capability to monitor morphology, porosity, and composition.

To create an electrospun scaffold material, first poly(lactic acid) (PLA) dissolved in Chloroform: Acetone volatile solvents to create the spinning solution. The volatility of the solvents is such that they are lost to the atmosphere between the spinneret and collection plate, so that only thin fibres of the scaffold material are collected. To fabricate valproic acid loaded fibres, as the polymer initially exists in solution, blending approach is the simplest approach compared to other approaches (e.g., coaxial electrospinning, surface immobilisation) but provides the highest loading rate[220]. As such, VPA was added directly into the PLA solution to produce a homogenously loaded scaffold material[220]. Then, electrospinning was

performed by applying a high voltage between a collection plate and PLA/ PLA+VPA polymer solution flowing through a metal needle. The competing forces result in a very thin fibreformation on the collection plate. A specific feature of the final electrospun fibreis that structural design parameters such as porosity, morphology, fibreconsistency, surface area, and final scaffold thickness could be tuned easily by modification of the environmental and processing conditions (applied voltage, working distance between spinneret and collector, solution flow rate) and solution properties (solvents, scaffold material concentration, additional surfactants or other additives)[221]. Fibrealignment can be controlled by changing the collector type. Randomly aligned fibres accumulate on a stationary collection plate, while a rapidly rotating collection drum forces fibre alignment because it collects fibres like winding a spool of thread.

Polymer solutions of 10% (w/v) were made with 3:1 chloroform and acetone and magnetically stirred at room temperature to dissolve completely. For Valproic acid (VPA) loaded fibres, VPA was mixed with the PLA solution at the ratio of 1/30 (v/v%). The prepared solution was then loaded into a plastic syringe with an 18G×1$_{1/2}$ gauge needle, and programmable syringe pump. The solution was dispensed at a rate of 2 mL/h while charged to 20 kV at a working distance of 15 cm. The fibres were collected on an aluminium collector, rotating at 1000 rpm during a 2.5-hour period. The collected scaffold was then stored in a desiccator.

3.5 Short fibreproduction

Electrospun nanofibres (PLA±VPA) were cut at the size of 20 μm on a Leica microtome (SM 2010R), using dry ice to freeze small pieces of the intact scaffolds in an upright position embedded in cryo-mounting media (TissueTek OCT, Fisher Scientific, USA). After cutting, the resultant short fibres (SFs) were collected and washed with DI water 3 times to remove the tissue mounting media, then the SFs were recovered by centrifugation at for 15 minutes at 4000 rpm.

3.6 Physiochemical characterisation

3.6.1 Spectroscopy analysis

Fourier transform infrared (FTIR) spectroscopy measurements were performed for SAP hydrogels using an Alpha Platinum Attenuated Total Reflectance FTIR (Bruker Optics, Germany), with ~ 20 µl undiluted hydrogel samples. The FTIR spectrum of all samples was recorded to be in the range of 1550–1750 cm^{-1}.

To determine the structures of the SAP hydrogels circular dichroism (CD) spectra analysis was performed using a Chirascan CD Spectrometer (Applied Photophisics Limited) in the wavelength range of 180 - 320 nm. Samples were prepared by diluting ~10 µl of the SAP hydrogel samples in DI H_2O with 1:100 ratio (Pathlength = 1 mm, step size = 0.5 nm, and bandwidth = 1 nm). For CD spectra measurements, samples were added to a quartz cuvette with a 1-mm path length (Hellma Standard Cuvette 110QS (Quartz Suprasil); Hellma Analytics). The data were averaged and smoothed post-acquisition utilizing Chirascan software. DI H2O was considered as a baseline and subtracted in both CD and FTIR spectra.

3.6.2 Rheology

A frequency sweep study was performed on SAP supramolecular hydrogel, and SAP+PLA composite biomaterial using a Kinexus Pro+ Rheometer (Malvern) to conduct the rheological analysis. A flat plate (20 mm with solvent trap, Upper Geometry: PU20 SR1351 SS, Lower Geometry: PLS55 C0177 SS) was used with a gap size fixed at 0.2 mm. 80 µL of the sample was placed on the clean sample holder and water was added to the solvent trap. Frequency sweeps were performed from 0.1-100 Hz at a constant oscillatory strain at 0.1% at 37°C.

Furthermore, mesh size can be calculated using storage modulus aquird from rheology experiment based on the following equation.

3.6.3 Mesh size

The average mesh size (ξ, nm) can be calculated based on the so-called rubber elastic theory (RET) from the following equation:

Equation (1) $\zeta = (G' N_A/RT)^{-1/3}$

where G′ is the storage modulus, N_A is the Avogadro constant (6.022×10^{23}), R is the gas constant (8.314 J/K mol) and T is the temperature (310 K)[145,222].

3.6.4 Transmission electron microscopy (TEM)

Negative stain TEM analysis was conducted using a Hitachi H7100FA using a tungsten filament fitting at 100 kV. Formvar-coated copper grids were glow-discharged at 15 mA for 30 s, then immersed in the hydrogel sample for approximately 30 s, followed by immersion in DI H2O to wash, with blotting in between. The grids were then briefly immersed in one drop of uranyl formate (UF, 0.75%, 25 µl) negative stain solution, stain and blotted, followed by immersion in a second drop of UF for 30 s. Before TEM imaging, the grids were left to dry for at least 2 hours.

3.6.5 Zeta potential

Zetasizer (Nano ZS (Redbadge), ZEN3600, Malvern Instrument, Malvern, UK) was used to compare the z-potential of different Fmoc-SAP hydrogels. Each hydrogel was resuspended in a total solution of 1 mL of DI H2O (dilution 1:100) and loaded into a capillary zeta cell with a syringe. Measurements were analysed with Zetasizer Marvel Software provided by the company.

3.6.6 Scanning electron microscopy (SEM)

Scanning electron microscopy (SEM) was performed on a Zeiss UltraPlus electron microscope using a 5.0 kV beam and an in-lens detector to visualise the morphology of electrospun nanofibres. Samples were affixed to double sided carbon tape and then were sputter coated

with platinum for 60 seconds at 20 mA. Electrospun nanofibres were cut to small pieces and placed on the carbon tape and coated with platinum. SF solution droplets (10 µL) were allowed to air dry on the carbon tape before being platinum coated. After imaging with SEM, nanofibre diameter and length were analysed using ImageJ.

3.7 Hybrid composite biomaterial fabrication, and VPA degradation and release profile investigation

The PLA+VPA SFs embedded in Fmoc-DDIKVAV (15mg/ml) hydrogel to fabricate a hybrid composite biomaterial. Then to investigate VPA release profile, 150 µl of the fabricated hybrid composite biomaterial cast in 96 well plates (n=3) and placed in incubator (37°C, 5% CO2) to equilibrate. After 1h, 100 µL of PBS was gently added on top of the composite hydrogel and at appropriate intervals of 1, 8, 24 h, and 1, 2, 3, 4, 5, 6, 7, 8 weeks the supernatant was removed and replenished with an identical volume of fresh PBS each time. For degradation analysis, triplicate 100 µL samples of 1 µg ml−1 solution of VPA in PBS was added to wells of a 96-well plate for each time point. The collected samples were stored at −20 °C until analyses with LC-MS.

3.8 Degradation and release profile *in vitro* using high performance liquid chromatography (HPLC)-orbitrap

The VPA concentrations were determined by LC-MS spectrometer (Thermo Scientific Q-Exactive Focus hybrid quadrupole-Orbitrap). 40 µL of collected supernatant from composite biomaterial, were transferred to HPLC vials and dried down using SpeedVac (ambient temperature/1 h), then dispersed in 100 µL of Milli Q water+0.1% Formic acid (FA), vortexed and sonicated. The resultant solution was then filtered through a 0.2-µm membrane filter followed by centrifugation at 1000 RPM for 5min. A total of 10 µL of each sample was injected (flow rate of 0.2 mL/min) into LC-MS spectrometer (Thermo Scientific Q-Exactive Focus hybrid quadrupole-Orbitrap). Chromatographic separation was achieved using an ACQuity

C18, LC column of 2.1×50 mm, 1.7 µm. The mobile phase was a 95:5 (v/v) mixture of 0.1% FA in water and acetonitrile (v/v).

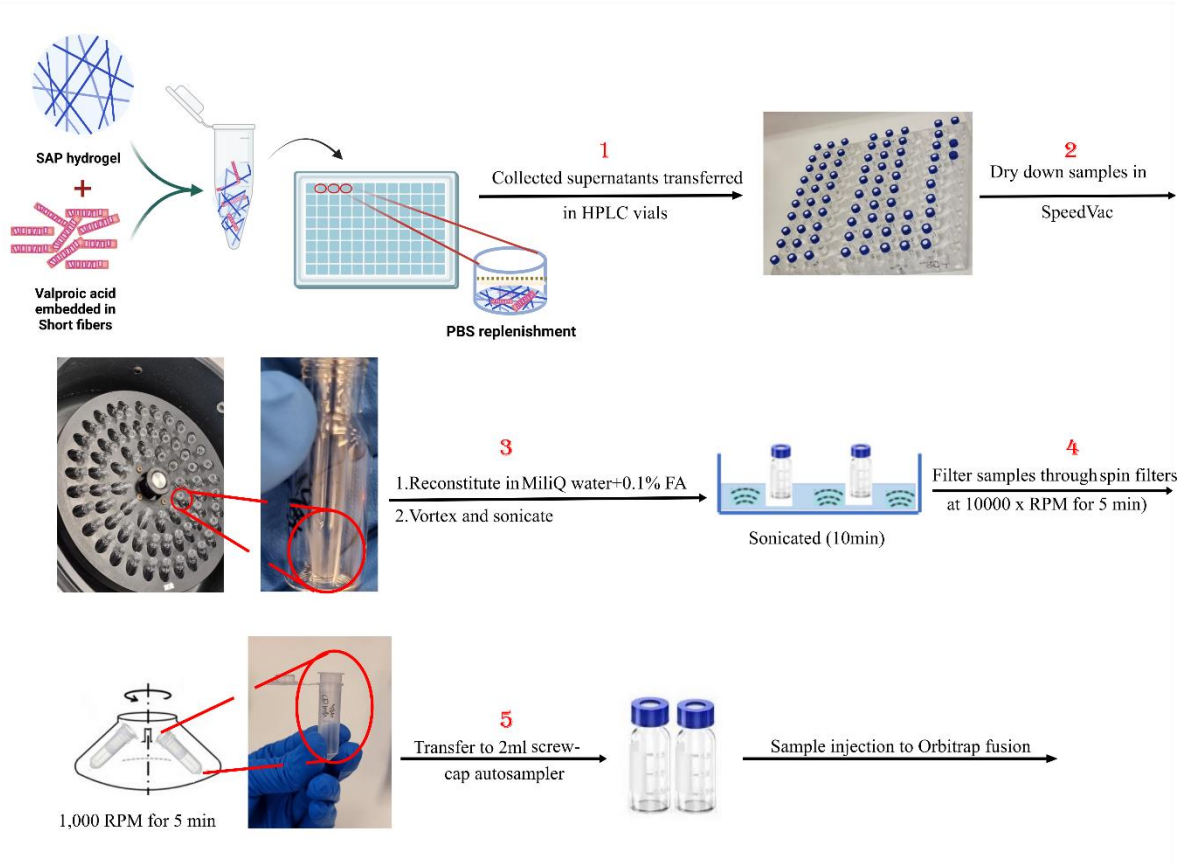

Figure 3.1. Schematic illustration of LC-Mass sample preparation procedure.

3.9 AAV vector production and purification

AAV production was performed at the Vector and Genome Engineering Facility (VEGF) at the Children's Medical Research Institute (CMRI), Sydney, Australia. Briefly, HEK293 cells (ATCC) were used as a substrate for AAV production using PEI (polyethylenimine MW 25000), with a 1:1:2 molar ratio of pCap:pTransgene:pAd5. Vector particles purification was performed using standard iodixanol gradients (4 different layers of gradient (15%, 25%, 40%, and 60%) containing PBS-MgKNa, Optiprep, and Phenol Red (just for 25% and 60% gradient)). Vector particles were collected from a thin layer between 40%-60% gradient buffer. Amicon Ultra-4 Centrifuge Filter Units with Ultracel-100 kDa membrane (EMD Millipore,

Cat# Z648043) were used for final buffer exchange (Phosphate-buffered saline [PBS, Gibco, Cat# 14190], 50 mM NaCl [Gibco, Cat#24740], 0.001 %, Pluronic F68 [v/v] [Gibco, Cat# 24040]). Vector particles were collected, precipitated, and concentrated by centrifugation and concentration step (volume 200-500 µl). Vector preparations were quantified using droplet digital PCR (ddPCR) (qPCR, Bio-Rad, Cat# 172-5125) using mCherry primers (F: 5'-CACTACGACGCTGAGGTCAA-3'; R: 5'-GTGGGAGGTGATGTCCAACT -3'. We achieved a viral titer of at least 9.44×10^{12} vg/ml, 1.02×10^{13} vg/ml, and 9.6×10^{12} for DJ gfaABC1D-NeuroD1-mCherry, DJ gfaABC1D-SOX2-mCherry, and DJ gfaABC1D-mCherry, respectively.

3.10 Cell and culture conditions

Ethics: All animal procedures and techniques were carried out in compliance with the Australian National Health and Medical Research Council's (NHMRC) published Code of Practice for the Use of Animals in Research and were confirmed by the Florey Institute of Neuroscience and Mental Health animal ethics committee or the ANU Animal Care and Use Committee (Animal Ethics Protocol Number: A2020/20).

3.10.1 Primary astrocyte culture

The cortices of the brains were carefully dissected from postnatal day (P) 1.5-2 Swiss mice pups in the cold DMEM High Glucose. Meninges were removed and the forebrain tissue dissociated mechanically to generate a single-cell suspension. Subsequently, cells were centrifuged for 10 min at 1000 rpm, resuspended in the CDMEM culture medium (DMEM 10:10:1, 10% fetal bovine serum (FBS) (Gibco), 10% horse serum (HS) (Gibco), and 1% penicillin/streptomycin (Hyclone)) at 37 °C (10 ml per forebrain). Cells were plated on a poly-d-lysine (PDL) coated 75 cm2 flask and maintained at 37 °C and 5% CO2.

The astrocytes were allowed to grow to confluency (14 days) with media changes every 3 to 5 days. Upon confluency, loosely attached microglia and oligodendrocyte precursor cells were

removed by shaking rigorously using an orbital shaker overnight (230 rpm at 37°C). Cells were then washed 3 times with PBS (1x) and digested with trypsin/EDTA for 10 min at 37 °C. Astrocytic cells were resuspended in the fresh astrocytic medium composed of DMEM 5:5:1 (5% FBS (Gibco), 5% HS (Gibco), and 1% pen/strep (Hyclone).

3.10.2 Primary cortical neuron culture

Swiss mice were time mated overnight, with a vaginal plug on the next morning (as the embryonic day E 0.5). Pregnant mice were sacrificed by cervical dislocation to collect embryonic day 14.5 (E14.5) fetuses, followed by cortex collection without hindbrain, olfactory bulb and meninges under sterile conditions. The cortices were trypsinised for digestion over 20 minutes in HBSS with 1x 0.25% trypsin (Gibco), 1x DNAase (Gibco) at 37°C, and then cells were washed three times with HBSS. Tissue was dissociated in serum-free minimum essential medium (MEM) solution with 10% fetal bovine serum (FBS) for cell suspension, and cell counting with the trypan blue staining using a haemocytometer was performed. Cells with desired cell density were loaded into culture plates. After 3 hours attachment, media are replaced with fresh primary neurobasal culture media (including neurobasal medium (Gibco) with 1% serum-free B27 supplement (Gibco), 5 mM glutamine (Gibco) and 10 μg/ml gentamicin (Sigma)) and cultured for 5 days.

3.10.3 Human astrocytes culture

Human astrocytes (Gibco), human brain progenitor-derived astrocytes, were cultured in Geltrex matrix-coated T-75 flasks in ‘astrocyte medium’ composed of 44 ml DMEM (AM, ScienCell), 0.5 ml N2 supplement, 5 ml FBS, and 0.5 ml 1x penicillin/streptomycin (HyClone) (1% pen/strep). Cells were incubated at 37 °C with 5% CO2 with medium changed every three days. Upon confluence, cells were rinsed in PBS, dissociated in Trypsin/EDTA solution 1X (Sigma-Aldrich), centrifuged and finally resuspended in fresh culture medium.

3.10.4 Astrocyte *in vitro* cell transduction

To evaluate transduction efficiency, astrocytes (primary murine astrocytes or human brain progenitor-derived astrocytes) were transduced with DJ gfaABC1D-NeuroD1-mCherry, DJ gfaABC1D-SOX2-mCherry, and DJ gfaABC1D-mCherry (empty vector) as control. Briefly, astrocytes were seeded in 24-well plates onto poly-D-lysine (PDL) coated glass coverslip (Thermo Fisher, Waltham, MA, USA). The cells were allowed to grow in this condition for 5–7 days. To transduce astrocytes, the viral vectors were thawed on ice, followed by the addition of an appropriate amount of vector into each well (multiplicity of transduction (MOT)=10^5 for AAV-NeuroD1 and MOT=10^6 for AAV-SOX2), plus negative control wells (MOT=0), and positive control DJ gfaABC1D-mCherry (MOT=5) and allowed to proceed for 24 h. One-day post transduction, media were completely replaced with fresh differentiation medium to minimize viral exposure. Cell medium was replenished every 3-4 days. After 10/ and 28 days post transduction (DPT), the transduced cells were fixed and immunostained to examine cell fate, the efficiency of transduction, and conversion.

3.10.5 Protocol for direct conversion of astrocytes into induced neurons

The cultured passaged astrocytes (primary murine astrocytes/ or human brain progenitor-derived astrocytes) were cultured on PDL coated glass coverslip (Thermo Fisher, Waltham, MA, USA). After 7 days, they were transduced with DJ gfaABC1D-NeuroD1-mCherry as described earlier. The next day, the medium was changed to the neuronal differentiation medium which contained DMEM/F12 (Gibco), 0.5% FBS (Gibco), 3.5 mM glucose (Sigma), penicillin/streptomycin (Gibco), and N2 supplement (Gibco). Brain-derived neurotrophic factor (BDNF, 20 ng/ml, Invitrogen) was added to the cultures every 3-4 days to promote synaptic maturation[223].

3.10.6 Protocol for dedifferentiation of astrocytes to neural progenitor and then induced neurons

Cell fate reprogramming relies not only on the roles of reprogramming genes but also on the influence of external microenvironment[224] (culture conditions). So, twenty-four hours after infection of astrocytes with DJ gfaABC1D-SOX2-mCherry, the medium was changed to the progenitor culture media: DMEM/F12 (Gibco) supplemented with 1× N2 and 1× B27, 20 ng/ml fibroblast growth factor (bFGF), 20 ng/ml epidermal growth factor (EGF), penicillin/streptomycin (Gibco). EGF and bFGF were used in culture conditions to enhance the emergence of progenitor/neural stem cells. For neuronal differentiation, media was supplemented with brain-derived neurotrophic factor (BDNF, 20 ng/ml, Invitrogen) to the cultured medium every 3-4 days to promote synaptic maturation during differentiation[223].

3.10.7 Conversion efficiency and neuronal purity (*in vitro*)

Conversion efficiency was analysed by Flow cytometry (Fusion, BD Bioscience) analysis. Briefly, the adherent immunostained cells were manually detached from well plates using scraper and suspended in PBS. Then the conversion efficiency was calculated as the percentage of β-tubulin, MAP2, or NeuN positive cells to quantify reprogrammed neurons and the percentage of mCherry positive cells as infection/transduction rate. Quantitative data are presented as the mean±SD.

3.10.8 Electrophysiological examination of NeuroD1 and SOX2 converted cells *in vitro*

After 28/42 days post AAV-NeuroD1/ and AAV-SOX2 transduction, cell activity analysis of converted cells, identified by the morphological phenotype of axonal outgrowth with neurite extension, were examined using whole-cell patch clamp recordings. Briefly, coverslips containing cells were transferred to a chamber and continuously superfused with ACSF at 21–23◦C (containing in mM: 124 NaCl, 3 KCl, 2 CaCl2, 1 MgCl2, 1.25 NaH2PO4, 26 NaHCO3 and 10 glucose saturated with 95% O2 and 5% CO2, pH 7.2-7.4, 275-285 mOsm). Recording

electrodes were pulled from borosilicate glass pipettes (Sutter Instrument) had a tip resistance between 5 and 8 MW. We used a potassium gluconate-based internal solution containing (in mM): 140 K gluconate, 10 HEPES, 2 NaCl, 4 KCl, 4 ATP, and 0.4 GTP at a pH of 7.4. Recordings were performed using a Multiclamp 700B (Axon Instruments) EPC9 amplifier, and using the WinWCP software (created by John Dempster, University of Strathclyde). Circuit capacitance was corrected following gigaseal formation. Series resistance and liquid junction potential were not corrected. Following break-in, the test pulse was monitored for a few seconds to ensure a stable, low access resistance (Ra <20MΩ). To measure postsynaptic currents, the cell was held in voltage clamp at -70 mV for excitatory glutamatergic currents. Action potentials were elicited and recorded under current-clamp mode via increasing steps of depolarising current. Electrophysiological data was analysed in Easy Electrophysiology. Action potential kinetics were determined using the automated detection modules, with the threshold calculated as the leading inflection (the minimum of the first derivative prior to the action potential peak). During recordings, patched cells were filled with Neurobiotin (2-5 mg/ml). Following the completion of recordings from a culture, coverslips were washed 3 times with PBS (1X) and placed into 4% PFA for 20 min at room temperature to fix cells, followed by PBS washes (pH 7.4, 3×5 min), then stored in the fridge until immunocytochemistry.

3.10.9 MTT (3-[4,5-dimethylthiazol-2-yl]-2,5-iphenyltetrazoliumbromide) assay

To evaluate the toxicity/biocompatibility of fabricated hydrogels MTT (3-[4,5-dimethylthiazol-2-yl]-2,5-iphenyltetrazoliumbromide) assays was conducted.

To this end, astrocyte cells were seeded at 10,000 cells per well in a 96-well plate and were maintained for two days prior to hydrogel exposure. Hydrogel solutions were prepared at 1:6 with CDMEM 5:5:1 (to yield a mixture of 20 μL hydrogel and 100 μL for each well), to avoid a hydrogel layer forming over the cells and interfering with the subsequent assay. Plates were incubated for a further 2 days before the MTT assay.

After 48h a CyQUANT MTT cell proliferation assay (invitrogen) was performed as per the manufacturer's instructions. Briefly, a mixture of 100 µl CDMEM 5:5:1 and 10 µl MTT dye was added to each well (with triplicate of negative (DMEM 5:5:1 alone, diluted of each hydrogel alone) and positive control (cell+DMEM 5:5:1)), covered with foil and incubated (37°C with 5% CO2) for 3 hours. After 3h, all the medium discarded but 25 µl and replace with 50 µL of sterile dimethyl sulfoxide (DMSO, Sigma Aldrich) and incubated (37°C with 5% CO2) for 10 minutes, covered in foil. Then each sample were mixed thoroughly by repeated pipetting to dissolve the purple crystals generated. The optical density (OD) of formazan in the solution was measured using a TECAN Infinite M200 Pro plate reader at 540 nm with 60 seconds orbital shaking prior to reading. Cell proliferation was calculated using **Equation 3.1**.

Cell percentage (%) = S-Csn/Cp-Cn

where S is the absorbance of wells with hydrogel in contact with cells. Csn is the absorbance obtained from the negative control of each corresponding hydrogel with media and without cells. Cp and Cn were the absorbance related to the positive (DMEM added to the cells) and negative control (DMEM added to the media without cells), respectively. Values were averaged and normalized, and plotted as mean ± SEM.

3.11 In vivo

3.11.1 Stereotaxic surgery and viral vector delivery

- **Needle stab injury:**

Mice (n=27 female Swiss) were anesthetised 2% Isoflurane inhalation. Mice were secured in a stereotaxic frame and an incision made to expose the skull. A small burr hold was drilled into the skull through which a needle stick injury was made using a Hamilton needle (external diameter 0.5 mm) into the right and left striatum at following coordinates: 1.0mm anterior and 2.0mm lateral from Bregma, and at a depth of 2.8mm below the surface of the dura.

3.11.2 AAV titration optimisation:

A high dose of AAVs often leads to toxic effects after injection into animal tissues[225,226], and is also accompanied by a significant leakage of expression of target genes to neural cells other than glial cells. So, it is imperative to determine the optimum dosage of AAV. To examine this, the mice were divided in 5 different groups and injected with AAV (DJ gfaABC1D-mCherry) in the absence or presence of SAP (Fmoc-DDIKVAV) at varying concentrations. All animals received a total volume of 1µL/injection. The groups included SAP alone, AAV (virus neat), AAV:SAP high dose (1:1), AAV:SAP medium dose (1:3), and SAP:AAV low dose (1:10).

3.11.3 In vivo AAV transduction

To evaluate *in vivo* reprogramming efficiency, stereotaxic injection of DJ gfaABC1D-NeuroD1-mCherry (AAV-NeuroD1), SOX2-mCherry (AAV-SOX2), and DJ gfaABC1D-mCherry (AAV-mCherry, control) was performed using a fine glass capillary (external diameter 100 µm) coupled to a 10 µl Hamilton syringe. Mice were again anaesthetized using 2% isoflurane. Mice (female,10 weeks, n=5-7/group) received bilateral microinjections of the different viral vector suspensions (1 µl/injection) diluted in sterile Saline (injected in right hemisphere) or diluted in SAP (injected in left hemisphere). Groups were as follows: i) Saline + AAV-NeuroD1 (1:1), ii) SAP + AAV-NeuroD1 (1:1), iii) Saline + AAV-SOX2 (1:1), iv) SAP + AAV-SOX2 (1:1), v) Saline + AAV-mCherry (empty vector) (1:1), vi) SAP + AAV-mCherry (empty vector) (1:1). Injections were made into the same site as the initial injury (AP-1.0mm, L-2.0mm, deep 2.8 mm below the surface of the dura).

3.12 Immunocytochemistry and immunohistochemical staining, imaging and analysis

For *in vitro* immunocytochemistry (ICC), upon the completion of the culture period, cells were washed 3 times with PBS (1X) and fixed in 4% PFA for 20 min at room temperature (RT),

followed by PBS washes (pH 7.4, 3×5 min). Plates were then sealed with parafilm and stored in the fridge until immunocytochemistry.

Cells were incubated with primary antibodies solution diluted in 5% donkey serum (DS) (Merck) and 0.3% Triton-X (Sigma Aldrich) in PBS (TPBS) for neural and astrocyte markers. Mouse monoclonal anti-β tubulin/TUJ1, (1:500, biolegend), goat monoclonal anti-glial fibrillary acidic protein (GFAP, 1:500, Abcam), and chicken polyclonal anti-mCherry (mCherry, 1:1000, Abcam), Rabbit monoclonal anti-Microtubule-associated protein 2 (MAP2, 1:1000, Abcam) were added at room temperature and incubated for overnight, followed by 3x 10 minute PBS washes and a 1 hour 10% donkey block (Merck). Secondary antibodies with Alexa Fluor-488/555/647 (1:500, abcam) in 2% DS and TPBS were then added for 2 hours, followed by a 10-minute Hoechst (1:5000, Life Technologies) incubation and three PBS (1X) washes. Plates were then sealed with parafilm and stored in the fridge until imaging.

For *in vivo* immunocytochemistry, at 28 days post AAV delivery, mice were killed by an overdose of sodium pentobarbitone (100 mg/kg) and transcardially perfused with Tyrode's buffer followed by 4% paraformaldehyde (PFA). Brains were post-fixed in 4% PFA for 2 hours and stored in 20% sucrose (in PBS) prior to cryosectioning on a freezing microtome Brain sections (40 μm) were serially collected (1:12) and stored in an anti-freezing solution at -20°C. Brain sections were rinsed in PBS three times for 5 min each. Then sections were blocked with a blocking solution containing 5% DS, 0.3% TPBS, and 0.02% Sodium Azide for 1 hour at RT while shaking. Primary antibodies diluted in 5% DS, 0.3% TPBS, and 0.02% Sodium Azide (overnight incubation at RT) used were: goat anti-Glial Fibrillary Acidic Protein (GFAP, 1:500, Abcam; astrocyte marker), chicken anti-mCherry (mCherry, 1:1000, Abcam), rabbit anti-NeuN (NeuN, 1:1000; neural marker), rabbit anti-iba1 (1:1000, WAKO, 019-19741, microglial marker), and mouse anti-doublecortin (1:50, Biotechnology). The next day, brain slices were washed 3 times with PBS and blocking solution containing 5% DS, 0.3% TPBS, and 0.02%

Sodium Azide was added for 1 hour left at RT. Then, a secondary antibody solution (5% DS, 0.3% TPBS, and 0.02% Sodium Azide) with Alexa fluor-488, 555 and 674 conjugated donkey anti-rabbit/goat/ck at a dilution of 1:200 was added, and brain slices were incubated for 2 hours at RT. After discarding the solution and PBS washes, 10-min incubation of Hoechst nuclear marker counter-staining (1:5000) in PBS/Sodium Azide occurred.

For both ICC and IHC, brain slices or cells were mounted on coverslip using DAKO Fluorescent mounting medium (Agilent) and imaged. Cells were visualised with either Zeiss 780 Confocal or Leica SP5 confocal microscope/Axioobserver. To precisely analyse the rate of transduction and conversion efficiency for ICC, fluorescence activated cell sorting (FACS) analysis was performed.

3.13 Release profiles of AAV-NeuroD1/ or AAV-SOX2 from Fmoc-DDIKVAV SAP hydrogel

To determine their release profiles, DJ gfaABC1D-NeuroD1-mCherry/ or DJ gfaABC1D-SOX2-mCherry, with titers at 9.44×10^{12} (NeuroD1) and 1.02×10^{13} (SOX2), was mixed at a set volume (0.3 µl NeuroD1, 8 µl of SOX2) with the Fmoc-DDIKVAV solutions prior to gelation. The SAP-AAV solutions were then self-assembled/gelated as described above. Then 150 µl of SAP+AAV gel transferred into a 96-well plate and 100 µl of PBS was gently added to the top of the hydrogels. Plates were incubated at 37 °C with 5% CO2 and PBS replenishment was conducted at specific time intervals (1 h, 3 h, 8 h, 24 h, 48 h, 72 h, 120 h). The PBS supernatants were collected and stored at -80 °C until the day of analysis. The released vectors were quantified using a qPCR Adeno-Associated Virus Titration (Titer) Kit (Abcam, Australia).

3.14 Quantitative PCR

To determine the AAV titer at different time points the qPCR Titration (Titer) was used. Briefly, the collected supernatants at each time points were mixed with Virus Lysis Buffer (1:1 ratio) and incubated for 10 min at 70°C to isolate viral DNA. Afterwards, 10 µl of 2X qPCR

MasterMix+High ROX reference Dye, 2 µl Primer Mix, and 6 µl Nuclease-free H2O were mixed with 2 µl of the lysed sample (extracted viral DNA/ or Standard Control DNA). The samples were prepared in 96-well plate on ice. Finally, the qPCR reactions were performed, consisting of enzyme activation (10 mins at 95 °C), denaturation (95 °C, 30 Cycle/15 secs duration each), and annealing/extension (60 °C, 30 Cycle/1 mins duration each). Standard calibration curve was performed using 10-fold serial dilutions of the Standard Control DNA in Nuclease-free H2O in triplicate.

3.15 Astroglia scar measurement

Glial scar measurements were performed using ImageJ analysis of the area of GFAP-positive fluorescence in the glial scar region adjacent to and within the injury area (needle track). The thickness of the glial scar/primary astrocytic scar and local astrocytic disturbance distances were measured perpendicular to the needle tract.

3.16 Statistical analysis

One-way analysis of variance (ANOVAs) tests was performed to compare significant statistical differences between groups. $*p < 0.05$; $** p < 0.01$; $*** p < 0.001$; $**** p < 0.0001$ was considered statistically significant. Data were reported as mean ± standard deviation of the mean (SD).

Chapter 4. Synthesis and physiochemical characterisation of SAP hydrogel/ fibre scaffold

4.1 Preamble

In this chapter, the synthesis physiochemical properties of the fabricated SAP hydrogels and hybrid composite biomaterial (SAP hydrogel+ electrospun short fibres) are investigated. SAP hydrogels have drawn significant attention due to their favorable properties, including their ability to provide a 3D microenvironment, biocompatibility, ease of synthesis, and tunability. In addition to SAP hydrogels, poly lactic acid (PLA), electrospun nanofibres are also considered promising materials due to their high surface area, biocompatibility, and broad flexibility. Therefore, due to hydrogel and electrospun nanofibre's unique properties, more and more attention has been paid to the composites of these polymers in various biological and biomedical fields. Here, SAP hydrogels and the hybrid composite biomaterial have been used as a platform for *the in situ* delivery of AAVs and small molecules. In this chapter, the physiochemical properties of the SAP hydrogel, electrospun nanofibres, and hybrid composite biomaterial were investigated. The materials and experimental methodology used in this chapter were described in Chapter 3.

4.2 Results and discussion

A library of peptide hydrogels contained a core biochemical peptide motif, IKVAV, presenting part of the α1 subunit of laminin. As discussed earlier, the peptide sequences were synthesised with an aromatic Fmoc moiety, protecting the N- terminus of the peptide and providing shared electrons for π– π stacking interactions. Herein, the π–π stacking embeds the N- terminus and the first two residues within the core of the assembly while only presenting the subsequent peptide sequence to the surface. Then, to ensure self-assembly of the peptides at physiological pH, the SAP system was functionalised via either an increased positive charge with additional –NH2 groups at the C-terminus, or negative –COOH groups at the C-terminus, or hydrophobic contribution of side chain at its C-terminus. These modifications resulted in alteration of pKa, the gelation time, and PH. However, all the fabricated hydrogels presented in this thesis were self-assembled in physiological pH with viscoelastic behaviour confirmed through Rheology. Depending on the peptide sequence the resultant hydrogels exhibited different crosslinking density, stiffness, surface charge, and mesh size.

Resulting hydrogels were characterised using several techniques such as Fourier-transform infrared spectroscopy **(**FTIR, **Figure 4.1A)**, circular dichroism **(**CD, **Figure 4.1B)**, Rheology **(Figure 4.2)**, mesh size **(Figure 4.3)**, transmission electron microscopy **(**TEM, **Figure 4.4)**, and zeta potential **(Figure 4.5)**, to confirm antiparallel beta-sheet structure, mechanical properties/viscoelastic behaviour, mesh size (porosity of hydrogels), nanofibreformation, and hydrogel's surface charge, respectively.

4.2.1 Chemical structure of Fmoc-SAP hydrogels

It is well established that the π-β assembly is the dominant structural mechanism in Fmoc-protected peptides which drives the assembly of the SAP hydrogels system. To confirm that the library of observed nanostructures was underpinned by π-β assembly motifs, FTIR and CD spectroscopy was carried out. The resulting FTIR spectra **(Figure 4.1A)** of the single, co-

assembled, and mixed hydrogels exhibited the distinct anti-parallel β-sheet signal (the major peak at approximately 1630 cm^{-1} and a minor peak at 1690 cm^{-1}). Complementary to FTIR, CD spectra were collected between the wavenumbers of 180 and 320 nm. CD results further confirmed the presence of β-sheet structure of the hydrogels with the amide regions of the system (between 180-220 nm) **(Figure 4.1B)**.

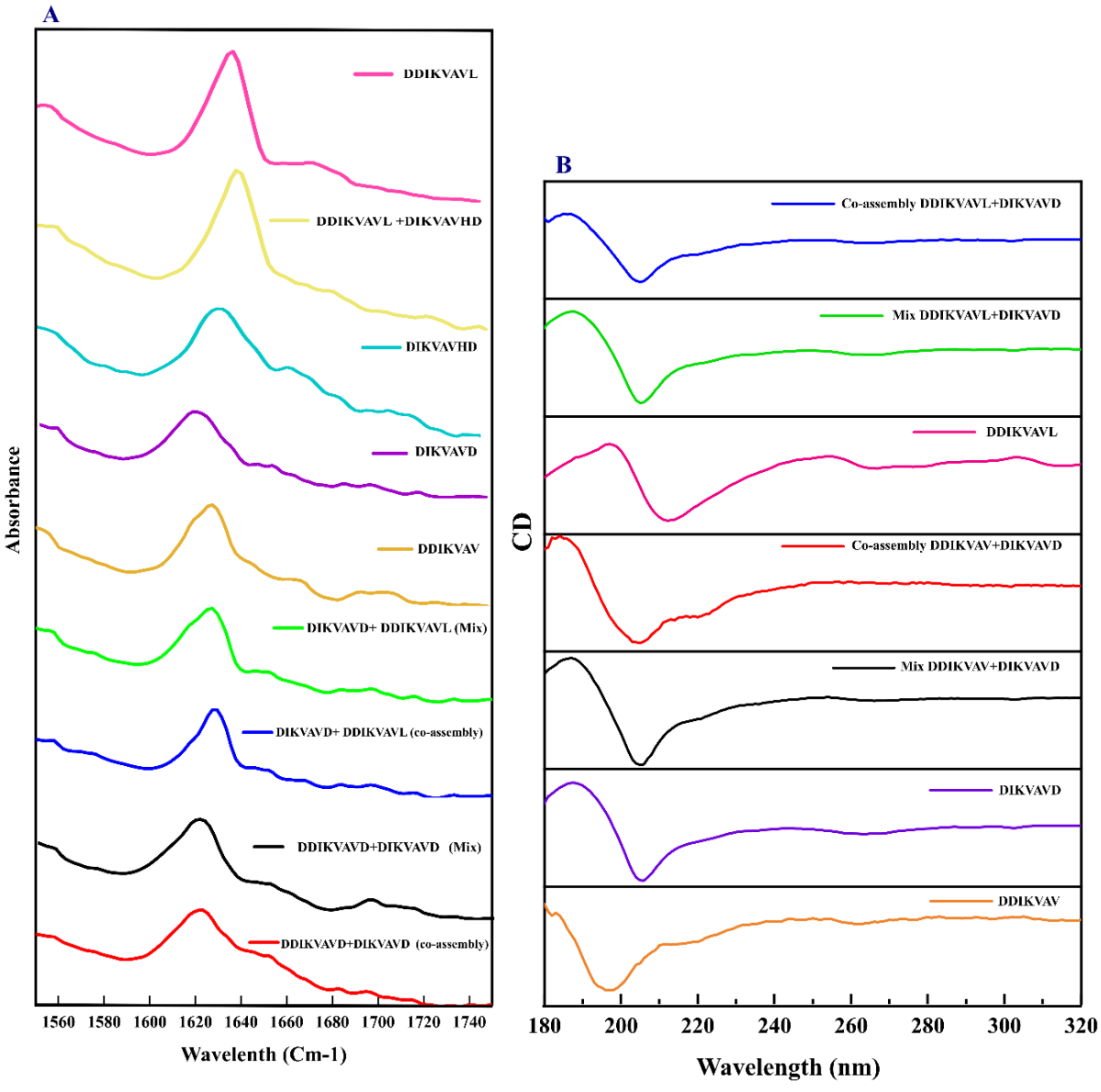

Figure 4.1. FTIR and CD spectra of single, co-assembled, and mixed Fmoc-SAP hydrogels. A) FTIR spectroscopic analysis confirmed the antiparallel β-sheet at 1630 cm^{-1} and 1690 cm^{-1}. **B)** CD spectra of all assemblies show the transition in the region 180-220 nm indicating the presence of β-sheet. DDIKVAV (orange), DIKVAVD (violet), DDIKVAV+DIKVAVD (Co-assembly) (red), DDIKVAV+DIKVAVD (Mix) (black), DDIKVAVL (pink), DIKVAVD+DDIKVAVL (Co-assembly) (navy blue), DIKVAVD+DDIKVAVL (Mix) (green), DIKVAVHD (blue), and DIKVAVL+DIKVAVHD (yellow).

4.2.2 Rheological behavior/mechanical properties of Fmoc-SAP hydrogels

The aim of tissue engineering is the creation of a scaffold structure that has the appropriate physical, chemical, and mechanical properties to facilitate cell penetration and tissue formation in three dimensions. It is well known that the mechanical properties of the scaffold can influence cell proliferation and differentiation and is as important as chemical properties. For brain tissue engineering the range of the elastic moduli of the scaffold should closely mimic native ECM of neural tissue ranging from 10^2 -10^3. As such, to monitor the mechanical properties of the fabricated SAP hydrogels and confirm whether they are really a hydrogel or not a rheology study was performed. As demonstrated in the rheology data **(Figure 4.2)**, all of the hydrogels show higher storage modulus (G') than loss modulus (G") and exhibit viscoelastic behaviour which is important in hydrogels with shear-thinning properties. Interestingly, the results show that stiffness of the co-assembled and mixed hydrogels for both DIKVAVD+DDIKVAV and DIKVAVD+DDIKVAVL hydrogels are different. These data indicate that the combination method plays an important role in determining the overall properties of hydrogel including mechanical properties and stiffness.

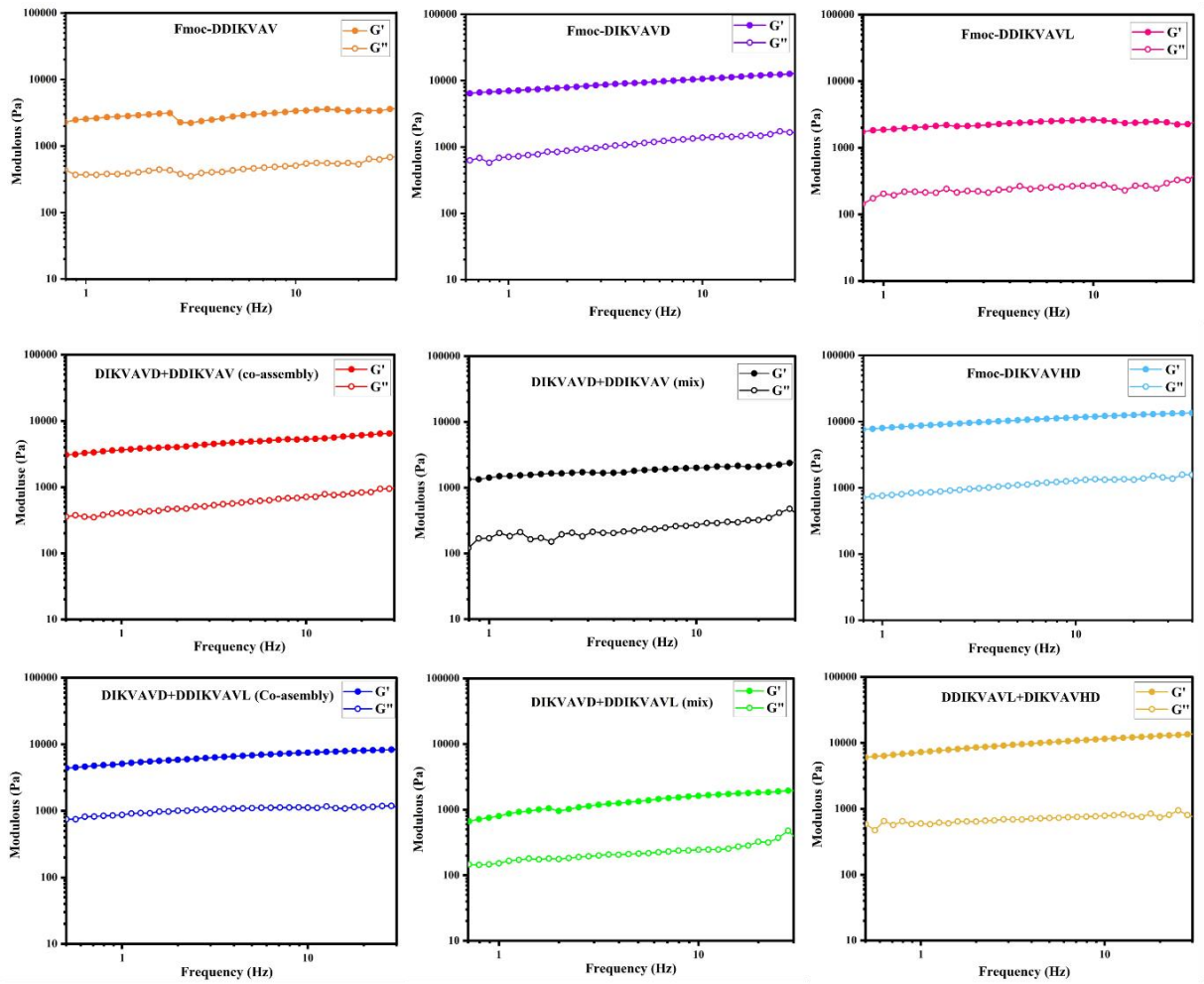

Figure 4.2. Rheological analysis for single, co-assembled, and mixed Fmoc-SAP hydrogels. Mechanical properties characterisation for single/ co-assembled/and mixed hydrogels. Rheological analysis confirms viscoelastic behaviour of all fabricated hydrogels confirmed with storage modulus (G′) greater than loss modulus (G″).

4.2.3 Mesh size

Hydrogels consist of a crosslinked polymer network, and open spaces are defined as the distance (Å) between the crosslinking points, called mesh size. The mesh size allows the liquid and small solute diffusion. As a scaffold and drug delivery systems it is of paramount importance to calculate/measure the mesh size of hydrogel because the mesh size determines how a drug diffuses through a hydrogel. To this end, here rheology was used to evaluate the average mesh size of the hydrogels **(Equation 1)**.

Results from comparison of the mesh size of different Fmoc-SAP hydrogels reported in **Figure 4.3**. As it can be seen, the mesh size can be controlled changing peptide sequences. The results

show that the mesh size of the fabricated hydrogels are within the typical range reported for hydrogels (5-100 nm)[227].

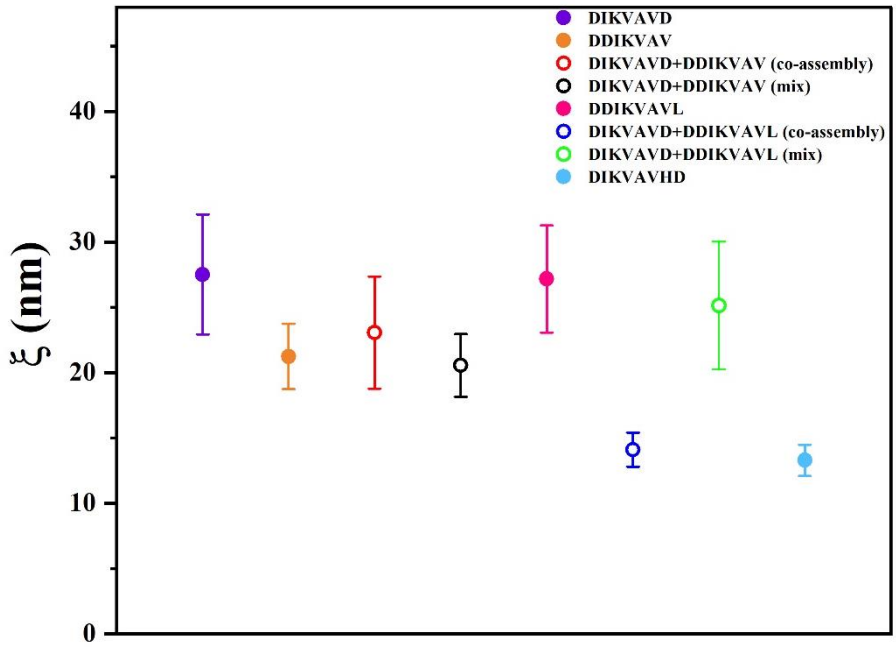

Figure 4.3. Mesh size (ξ) value of Fmoc-SAP hydrogels. Results showing the calculated mesh size values (based on the equation of the theory of rubber elasticity)

4.2.4 Morphology of Fmoc-SAP hydrogel scaffolds

The formation of the nanofibrous network of the different SAP hydrogels was confirmed with negatively stained TEM **(Figure 4.4)**. As it can be seen, a homogenous and interwoven nanofibrous network was achieved using pH switching method in all fabricated hydrogels. These images suggesting that the overall mechanism of assembly was broadly maintained and highlighting the non-destructive nature of the hydrogel.

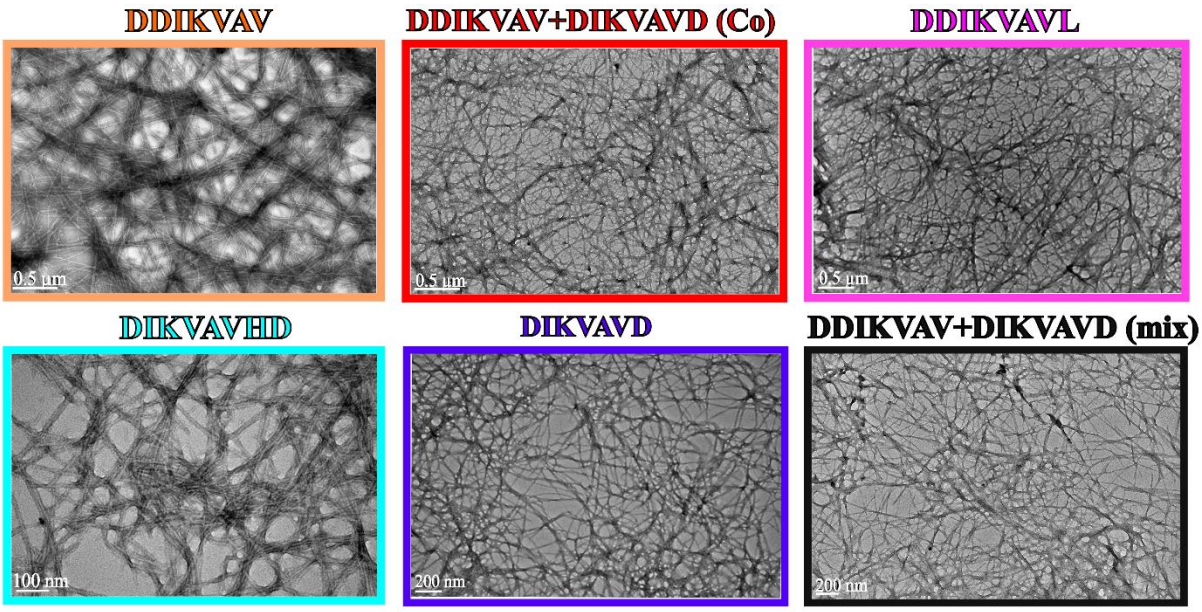

Figure 4.4. TEM images of some of the fabricated Fmoc-SAP hydrogels with different magnifications (scales= 200 nm, 100 nm and 0.5 µm).

4.2.5 Zeta potential (Surface charge)

Additionally, the surface charge of the different library of Fmoc-SAP hydrogels dispersed in DI water with a concentration of 0.01 v/v. The surface charges of hydrogels (ζ-potential values) were assessed using a Marvel Zetasizer **(Figure 4.5).** Among different hydrogels DDIKVAV+DIKVAVD (Co-assembly) and DIKVAVD+DDIKVAVL (Co-assembly) have the highest negative surface charge and DDIKVAV has the lowest negative charge. As mentioned before the combination method plays a role in determining the overall properties of hydrogel. As expected, the ζ-potential values of the co-assembled and mixed hydrogels for both DDIKVAVD+DIKVAVD and DIKVAVD+DDIKVAVL were different. The ζ-potential value for the mixed hydrogels was the average of both hydrogels but for co-assembly of these hydrogels and all other co-assembled hydrogels this pattern was not observed, and they exhibited more negative ζ-potential value than their individual constitute.

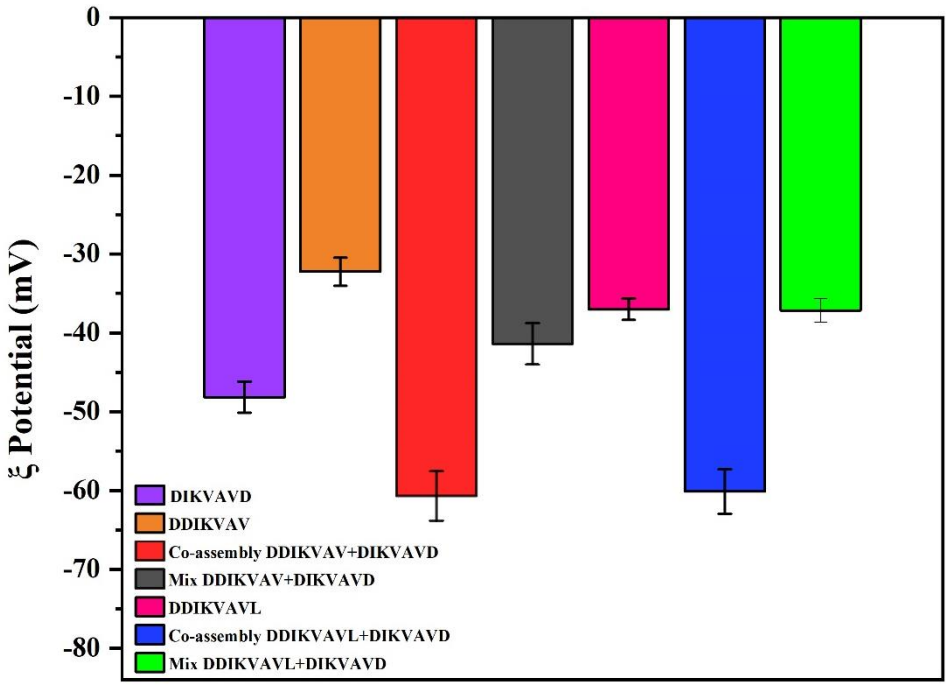

Figure 4.5. (A) Surface ζ-potential values (mV) of Fmoc- SAP hydrogels. Fmoc-SAP hydrogels showing different surface zeta potential.

4.2.6 *In vitro* cytotoxicity of the fabricated hydrogels with astrocytes

In order to demonstrate the cytotoxicity of the fabricated SAP hydrogels *in vitro*, astrocytes were incubated with different library of diluted hydrogel (1:6 ratio with DMEM) for 48 h after which the cytotoxicity studied using MTT assay.

As demonstrated in **(Figure 4.6),** only Fmoc-DDIKVAV and mix Fmoc-DDIKVAV+ Fmoc-DIKVAVD exhibited the acceptable viability range (70-80%) among all the fabricated hydrogels, with Fmoc-DDIKVAV demonstrate highest. Therefore, Fmoc-DDIKVAV hydrogel was chosen for the subsequent *in vitro/ in vivo* study.

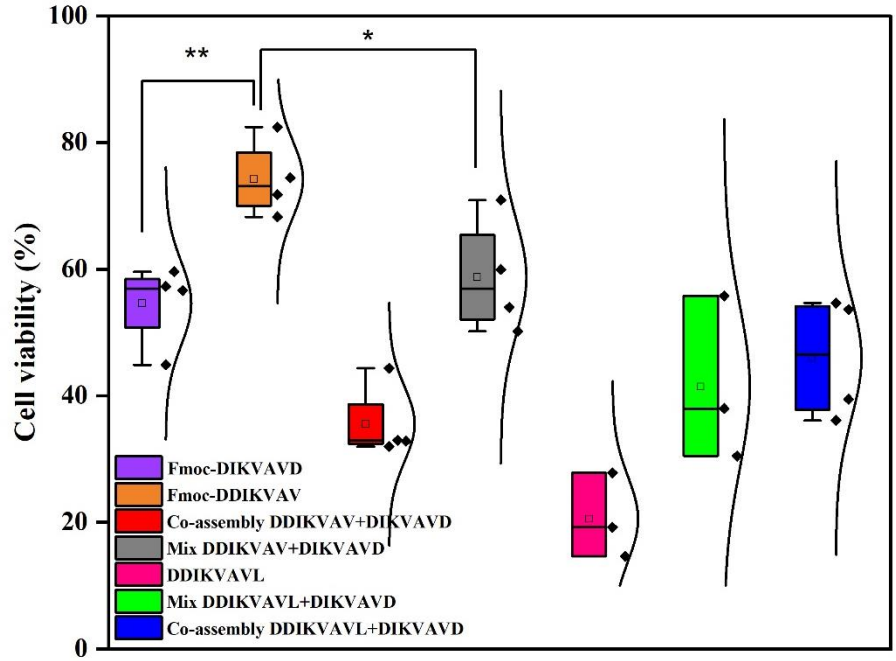

Figure 4.6. Primary astrocyte cells viability (%) in the presence of different diluted hydrogels. Cells were incubated in diluted hydrogels for 48 h. Then an MTT assay was performed to measure cell viability. Cells cultured in DMEM were used as a positive control, and culture wells without cells but containing triplicate of just DMEM and dilutions of each hydrogel were used as a negative control. Mean values (n= 4) are shown with ±SE, standard one-way ANOVA was performed *(*p<0.05, **p<0.01).* The normal distribution of data is shown alongside the box plots as well.

4.2.7 Characterisation of polylactic acid (PLA)±valproic acid (VPA) electrospun nanofibreand PLA±VPA short fibres (SFs)

Necessary for success in reprogramming and differentiation of neural progenitor cells to neurons is the presence of neurotrophic factor/ or small molecule such as VPA at the site of injury to drive differentiation and maturation of the reprogrammed cells. Due to hydrogel and electrospun nanofibre's unique properties, more and more attention has been paid to the composites of these polymers various biological and biomedical fields[228–231]. Electrospinning-fibres feature high surface area and broad flexibility. Hydrogels have highly controlled properties including 3D networks, biodegradation, mechanical strength, and so forth. The incorporation of active principles in hydrogel's nanofibrous meshes proved to be an efficient method for *in situ* delivery of a wide range of drugs, expanding the possibility and applicability of them[145]. Electrospinning can be used with natural or synthetic scaffold

materials and can accommodate many additives, including therapeutic agents, proteins, growth factors and provide a sustained, continuous release for 28 to 90 days with bioactivity unaffected by the harsh solvents confirmed by neurite outgrowth from PC12 cells *in vitro*[232–234]. As such, we loaded VPA into polylactic acid (PLA) electrospun nanofibres to provide a controlled and sustained release of the drug over time. Furthermore, to mimic brain's extracellular matrix (ECM) while providing further controlled release the VPA, the fabricated electrospun scaffold was cut into short loose fibres and mixed into a Fmoc-DDIKVAV SAP hydrogel, called hybrid composite biomaterial. The resultant hybrid composite biomaterial can integrate better into the cystic cavity of the brain, provide a good interface with the host tissue, and better mimic the ECM of the brain in terms of stiffness, laminin protein epitope, and 3D structure.

PLA electrospun nanofibres were formed under applying voltage as described in Chapter 3. SEM imaging was used to assess and confirm the resultant fibremorphology and its alignment. The fibremorphology is shown in

Figure 4.7**A, B.** Both groups of electrospun nanofibres (PLA±VPA) showed a smooth and bead-free fibres structure (indicating the optimal flow rate and polymer concentration (10%)[235]) with uniform diameters **(**

Figure 4.7**A, B)**. Inclusion of VPA in the electrospinning solution had no adverse effect on the resultant electrospun fibres' shape, morphology, and porosity. Image analysis showed that the average fibre diameters of fabricated electrospun nanofibres were 1.6 ± 0.9µm (**Figure 4.7C, D**). Then electrospun nanofibres were then to 20 µm lengths on a Leica microtome to make short fibres (SFs). The SEM images and image analysis on resultant SFs (PLASFs ± VPA)

displayed the homogenous fibredistribution with length of 22.4 ± 7.4 µm for PLA SFs and 28.4 ± 8.2µm for PLA+VPA SFs (**Figure 4.8A-D**).

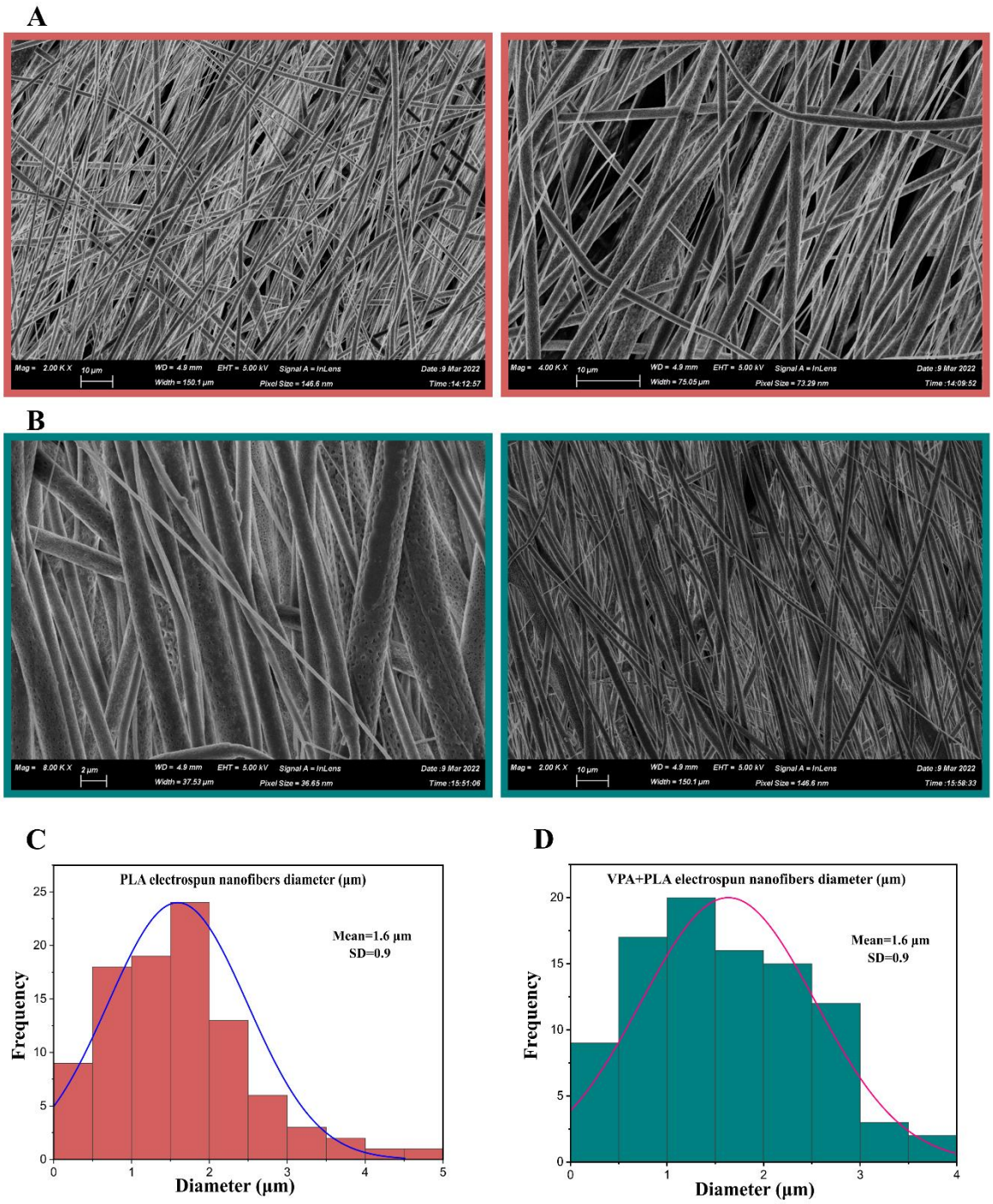

Figure 4.7. SEM of electrospun nanofibres at different magnifications. A) PLA electrospun nanofibres **B)** PLA+VPA electrospun nanofibres **C)** The corresponding histograms of the PLA fibre diameter distribution, **D)** The corresponding histograms of the PLA+VPA fibre diameter distribution. Scale bars= 10 µm, and 2 µm

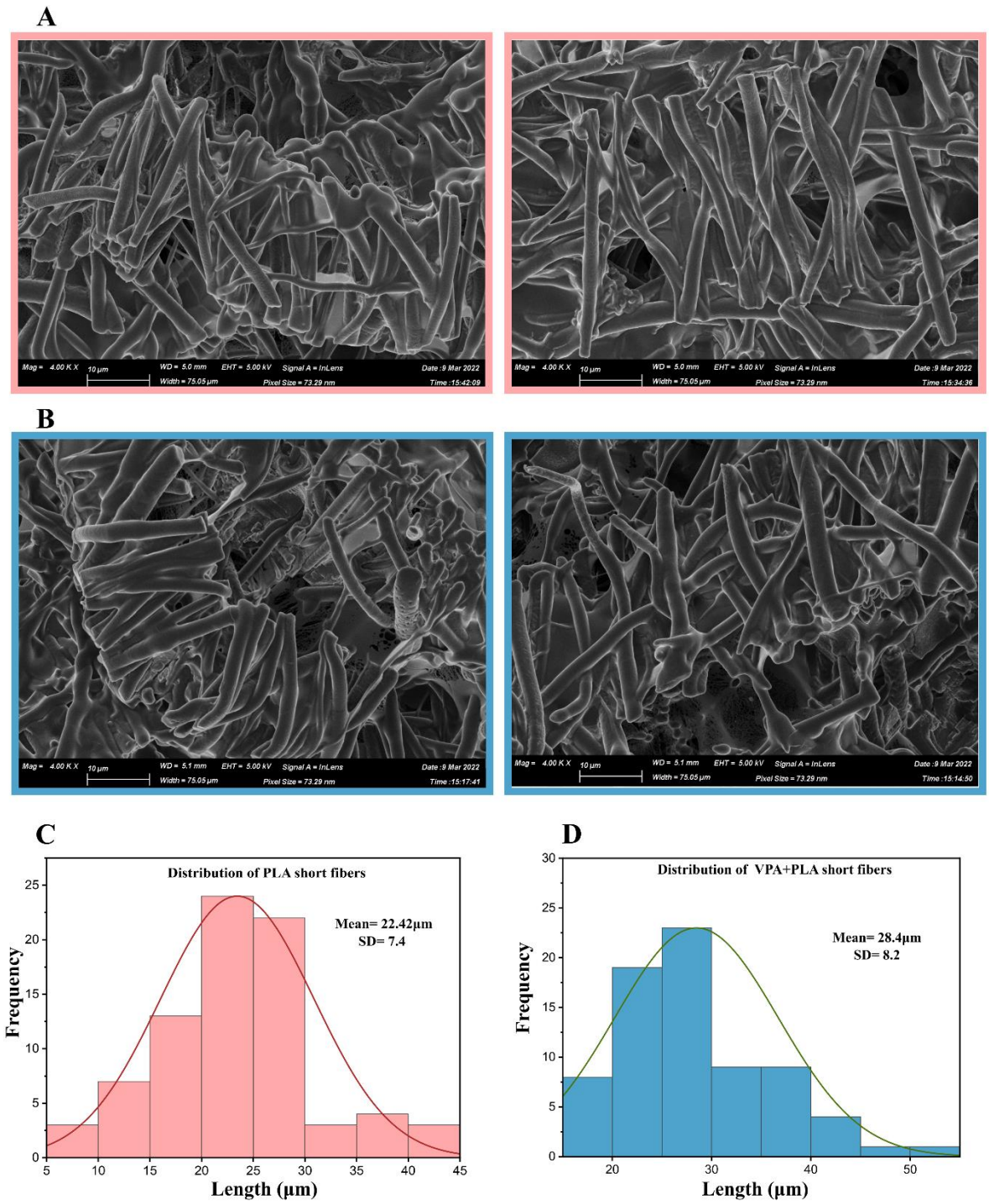

Figure 4.8. SEM of short fibres (SFs). A) PLA SFs **B)** PLA+VPA SFs **C)** The corresponding histograms of the PLA SFs length distribution, **D)** The corresponding histograms of the PLA+VPA SFs length distribution. Scale bars: 10 µm.

Then substrate stiffness/elasticity and CD spectra analysis of the Fmoc-DDIKVAV SAP hydrogel and hybrid composite biomaterial were studied to make sure structure and viscoelastic behaviour of hydrogels maintained after the incorporation of SFs. Both fabricated Fmoc-

DDIKVAV SAP hydrogel and hybrid composite biomaterial demonstrated viscoelastic behaviour (G'>G") and mechanical properties within the range of rodent brain stiffness **Figure 4.9A.** The inclusion of SFs in DDIKVAV SAP hydrogel did not disrupt the viscoelastic behaviour of the hydrogel and slightly improved the stiffness of the hydrogels which is completely in line with other studies showing the inclusion of electrospun nanofibres reinforce the mechanical properties (higher modulus) compared to pure hydrogel[236,237]. Moreover, the stable structure of SAP hydrogels driven by various polar and non-polar, non-covalent intramolecular interactions was conserved through the process of SFs incorporation as confirmed by CD spectra. CD results confirmed self-assembly of the peptide into β-sheet dominant structure (<220 nm) in both SAP hydrogel and hybrid composite biomaterial **Figure 4.9B**.

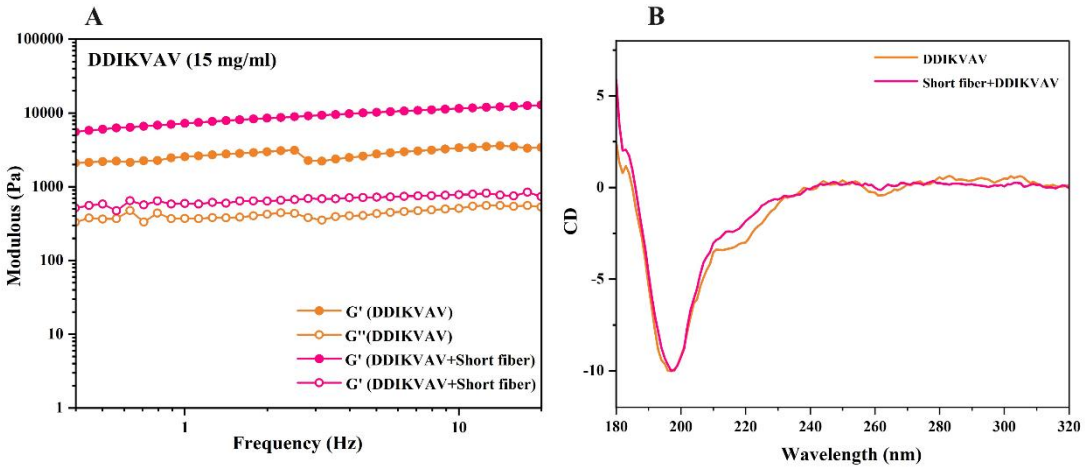

Figure 4.9. Rheological analysis and CD spectra for pure Fmoc-DDIKVAV SAP hydrogel (orange) and hybrid composite biomaterial (SAP hydrogel + SFs) (pink). A) Mechanical properties characterisation for both pure hydrogel and hybrid composite biomaterial confirms their viscoelastic behaviour (storage modulus (G′) greater than loss modulus (G″)). **B)** CD spectra confirms the presence of β-sheet structure in both hydrogels suggesting the inclusion of SFs did not disrupt hydrogel's structure.

4.3 Summary

In this chapter, the SPPS method was employed to produce the desired peptide sequences followed by the pH switching method to fabricate SAP hydrogel with nanofibres structure for tissue engineering and payload applications. The effects of different amino acid sequences on

the physicochemical properties of resultant SAP hydrogel were investigated. Moreover, the structure and morphology of PLA electrospun nanofibres with and without VPA small molecules and the hybrid composite biomaterial were investigated.

We have confirmed that the structure of PLA electrospun nanofibres was not altered after the inclusion of VPA in the polymeric solution. Moreover, the inclusion of the electrospun nanofibres in SAP hydrogel did not disrupt the assembly mechanism.

In conclusion, SAP hydrogels, PLA electrospun nanofibres, and hybrid composite biomaterials were obtained with desired physiochemical properties suitable for soft tissue (brain) application.

Chapter 5. *In vitro* and *in vivo* trans-differentiation of reactive astrocytes to neurons

5.1 Preamble

In this chapter, NeuroD1-AAV is used to trans-differentiate reactive astrocytes to functional neurons capable of initiating action potentials. The materials and experimental methodology used in this chapter are described in Chapter 3. A paper reporting subsequent *in vitro/in vivo* studies is entitled “Neuronal replenishment via hydrogel rationed delivery of reprogramming factors” and published in ACS nano journal.

Author contribution: Negar Mahmoudi performed the major experiments, analysed the data, made the figures and original draft. Niamh Moriarty and Clare Parish implanted animals. Nathalie Dehorter and Noorya Ahmed performed whole-cell electrophysiological recording and analysis. Leszek Lisowski provided expertise and guidance on viral constructs and packaging. Alan Harvey provided detailed feedback on all areas of the project and reviewed the manuscript. Clare Parish, Richard Williams, and David Nisbet reviewed the data interpretation and manuscript content and supervised the entire project. David Nisbet also supported this study financially.

5.2 Abstract

The limited regenerative capacity of the central nervous system (CNS) results in irreversible neuronal loss after insult. The ability to reprogram resident reactive astrocytes at the injury site into induced neurons (iNs) by direct lineage reprogramming holds significant potential for neural repair. Key challenges remain, including the stability and appropriate targeting of the viral vectors to ectopically express the reprograming transgene. Here we utilised a self-assembling peptide (SAP) hydrogel to provide targeted spatiotemporal release of an adeno-associated viral vector (AAV) carrying the neural reprograming transgene, NeuroD1. This approach prevents high viral dosage in the target tissue, limits off-target delivery, minimises immunogenic responses and thereby reduces neutralisation of the targeting vector. *In vitro* the vector induced new neuron formation, evidenced using morphological, histochemical and electrophysiological readouts. *In vivo*, we used ectopic expression of SAP-delivered AAV-NeuroD1 to induce trans-differentiation of reactive host astrocytes into iN and reduce glial scarring. These findings may open a new, safe, and efficient approach for the potential treatment of injuries in the brain and spinal cord.

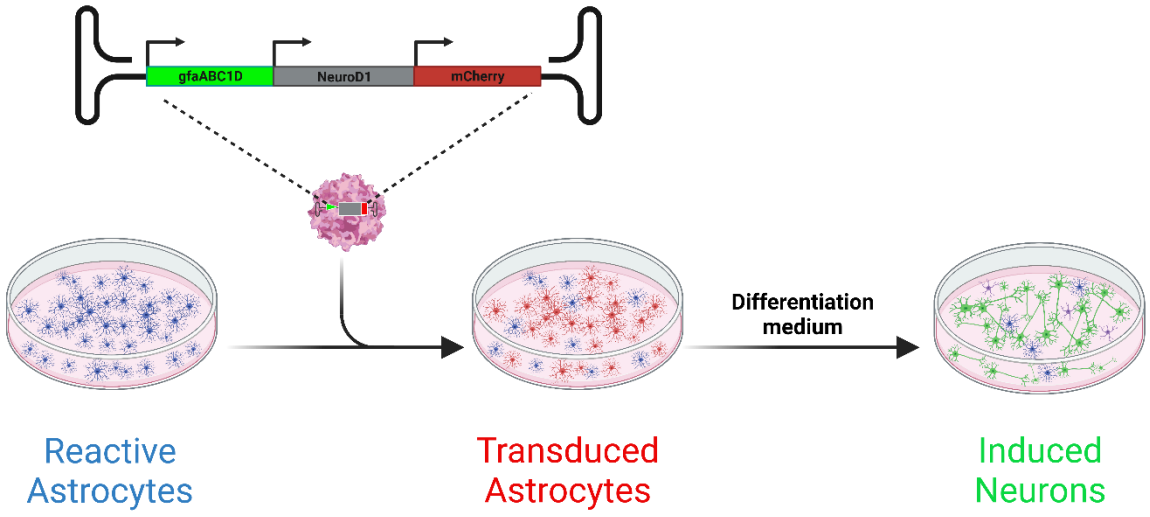

Figure 5.1. Graphical abstract of Chapter 5. Astrocyte A schematic diagram showing astrocyte from 1-2 days postnatal pups reprogramming/trans-differentiation to induced neurons (iN) *in vitro*. **Created with BioRender.com**

5.3 Introduction

Irreversible loss of neurons, disruption of fibretracts and the formation of a restrictive barrier of reactive astrocytes in response to central nervous system (CNS) injury are widely regarded causes of failed regeneration[49]. After decades of research there is increasing evidence that the adult mammalian brain is incapable of self-repair[238–240]. Many studies have focused on preventing or reducing ongoing neurodegeneration and/or secondary neurodegeneration after insult or disease, and there have been attempts using exogenous tissues, cells or cell lines to replace already lost neurons and their function. In spite of these many trials, to date the therapeutic impact has generally been marginal. While stem cell-based therapies provide significant hope for protecting or even replacing neural circuitry[2,3], this approach poses challenges due to the limited therapeutic window following trauma, the necessity for generating standardized, safe, and effective cell products, and the possibility of immunorejection[1,241,242].

Alternatively, by trans-differentiating resident host cells, such as glia, new replacement neurons may be generated in the brain. By forced expression of a neurogenic transgene, we investigated the potential to reprogram reactive astrocytes into neurons. This approach has the additional advantage of reducing the burden of reactive astrocytosis on repair. Our approached is founded on the fact that astrocytes exhibit great proliferative capacity, being utilised by nature to form a protective scar following injury, stroke, and neurodegenerative diseases[10,43]. Reactive astrocytes can have some beneficial effects, for example enhancing local plasticity and angiogenesis[243], and they are also involved in phagocytosis and the formation of a fibrous defence barrier to preserve the integrity of surrounding cells. However, their long-term persistence is detrimental to circuit regeneration and repair. This is largely due to the secretion of inhibitors such as chondroitin sulfate proteoglycans (CSPGs), tenascins, and NogoA[43],[244]. The ongoing presence of reactive astrocytes constitutes an ideal endogenous

therapeutic target, as they potentially provide a rich cell source for generating induced neurons (iNs). Furthermore, *in situ* conversion of reactive astrocytes to neurons via trans-differentiation will extend the treatment time window from hours to even months.

The process of cellular trans-differentiation involves altering gene expression patterns in somatic/mature cells to convert them into another specialized type of cell[245]. Manipulating expression of transcription factors (TFs), proteins that bind to DNA promoter regions, regulates the level of key developmental genes. Ectopic expression of these TFs in somatic cells to change cell fate can be efficiently accomplished through the delivery of viral vectors encoded with the desired TF. Recently, vectors derived from adeno-associated viruses (AAVs) have established themselves as powerful tools for gene delivery in the CNS[246,247]. One obstacle to the systemic use of AAV vectors in CNS diseases is inefficient penetration of the blood-brain-barrier (BBB) and difficulty inducing local overexpression of target genes. To bypass the BBB and temporally and spatially restrict transgene expression, most applications rely on local AAV injections into the brain. Among the single TF-mediated direct reprogramming candidate genes, NeuroD1 is the most efficient and effective at reprograming glial cells into functional neurons[25,27,176,248]. However, questions have recently been raised about the accuracy of AAV-GFAP-mediated delivery of NeuroD1 claiming the leaky expression into endogenous neurons leads to misinterpretation, give false-positive results, and decreases the efficiency of glia-to-neuron conversion because of the cis-regulatory interaction that occurs in close proximity between the GFAP promoter and a transgene[27,157,249,250]. However, others have argued that the reported AAV leakage to endogenous neurons is because of the administration of excessive amounts of AAV, using titers greater than 1×10^{13} vg/ml [157],[177].

On the other hand, for a gene therapy to be effective, an appropriate amount of therapeutic gene must be delivered to target cells to mitigate the disease pathology without substantial

toxicity[190]. Theoretically, one way to achieve this would be to increase the dose of virus until a sufficient level is reached. However, as mentioned, the ability to do this is prevented by dose dependent toxicities which are largely mediated by the immune system[251–253]. When directly transducing neurons the greater the number of cells transduced the better, but higher titers risk greater off-target effects, and minimization of off-target delivery is critical to the safety of vector mediated gene therapy[254]. Thus, the field must develop a multifaceted approach to improve the profile of vector dosage, enhance transduction efficiency, mitigate immunogenicity, and minimize cross-contamination and neutralization[255]. This may be achieved through a model of administering multiple lower doses of vector to achieve a similar therapeutic effect.

To this end, modifying and mutating the AAV capsid, the main determinant of AAV tropism and transduction characteristics, it is possible facilitate the delivery of target genes to the desired cells by AAV vectors[256,257]. Moreover, particular promoter combinations appear to be favourable to deliver gene to target cells with high efficiency and specificity. Here, to further restrict gene expression in astrocytes, an astrocyte-specific promoter, gfaABC1D, was included in the AAV cassette. Recent studies have reported promising data using the gfaABC1D promoter with efficient gene expression in astrocytes *in vivo* using an AAV-based delivery strategy[207,258,259]. Importantly, it has been demonstrated that the safe level of AAV dosage is 10^{10}-10^{12} vg/ml in the rodent brain, a level that reduces the risk of loss of pre-existing neurons caused by toxic dosage[157][260].

Finally, to further limit uncontrolled dissemination and neutralization of AAVs, thereby increasing infection/transduction efficiency, and decrease the potential leakage of AAV to endogenous neurons, we demonstrated sustained delivery of AAV from an optimized self-assembling peptide (SAP) hydrogel delivered to the site of therapeutic need. This fabricated SAP hydrogel was able to retain AAV function when utilised *in vivo* to transduce resident

reactive astrocytes. Furthermore, the spatiotemporal release of the AAV provided by SAP hydrogels may overcome the risk of off-targeted transduction/leakage into neuronal populations as a result of high dosage of AAV. Furthermore, the gels provide structural support for newly generated nerve cells.

In vivo, we incorporated the AAV within the SAP hydrogels to provide a spatially confined reservoir for local and sustained release of AAV, whilst acting as a screen to reduce off-target adverse effects. Using AAV-NeuroD1 based gene therapy, we were able to replenish some of the lost neurons locally at the injury site by 7-fold compared to the control by needle stick injury. Furthermore, reprogramming of reactive astrocytes within and around the needle injury resulted in extensive reduction of glial scar intensity. It should be noted the *in vivo* cell conversion approach indicates the astrocytes are not entirely depleted in the injured area and reprogrammed cells are intermingled with astrocytes within the needle track. This observation suggesting that only a fraction of reactive astrocytes is reprogrammed to neurons leaving the remaining glia to ensure a level of neuron-glia balance which is important for CNS repair.

5.4 Results and discussion

5.4.1 *In vitro* conversion of primary astrocytes to neuronal cells

To confirm targeted reprogramming of glia to neurons-like we initially performed *in* vitro studies on cultured primary postnatal day 1.5-2 murine astrocytes, comprising of 91 ± 6.0% GFAP+ purity **(Figure 5.2).**

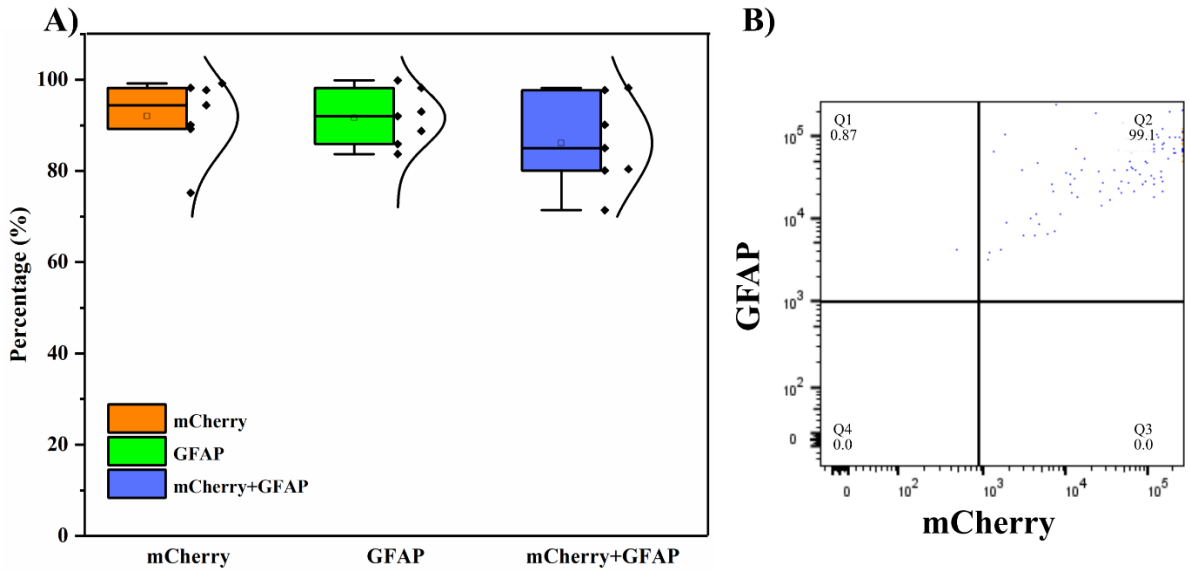

Figure 5.2. Percentage of astrocytes in primary mouse astrocyte culture. (A) Quantification data based on FACS analysis demonstrates 91 ± 6.0% of cells were positive for astrocyte marker (GFAP). (n=7/per group)

To trace the origin of the induced neurons, an mCherry tagged AAV-NeuroD1 was generated under a gfaAB1D promoter, which is active primarily in astrocytes. The resultant vector, DJ gfaABC1D-NeuroD1-mCherry, was used for both *in vitro* and *in vivo* transduction (viral titer=9.44×10^{12} viral genome (vg)/ml). The choice for AAV delivery, over other viral vectors, was based upon the reported observation that the genome of the recombinant AAVs do not undergo site-specific integration in the host DNA and mainly remains episomal in the nucleus of transduced cells, thereby decreasing the risk of insertional mutation.

AAV transduced astrocyte cultures (multiplicity of transduction= 10^5 vg/cell) began to adopt neuronal features, displaying either a unipolar or bipolar morphology, around 7 days post transduction (DPT) (Figure 5.3). At 10 days post transduction (DPT), neuronal fate was confirmed by the expression of β3-tubulin or MAP2 (green) within mCherry-positive (i.e., transduced) cells (Figure 5.3A, B). Fluorescence-activated cell sorting (FACS) analysis of the mCherry transduced cells at 10 DPT revealed 27.4 ± 2.8% and 25.2 ± 3.7% expressed β3-tubulin and MAP2, respectively (Figure 5.3G, H). In contrast, transduction with empty vector, gfaABC1D-mCherry, had no obvious impact on the morphology of cultured astrocytes

(Figure 5.3

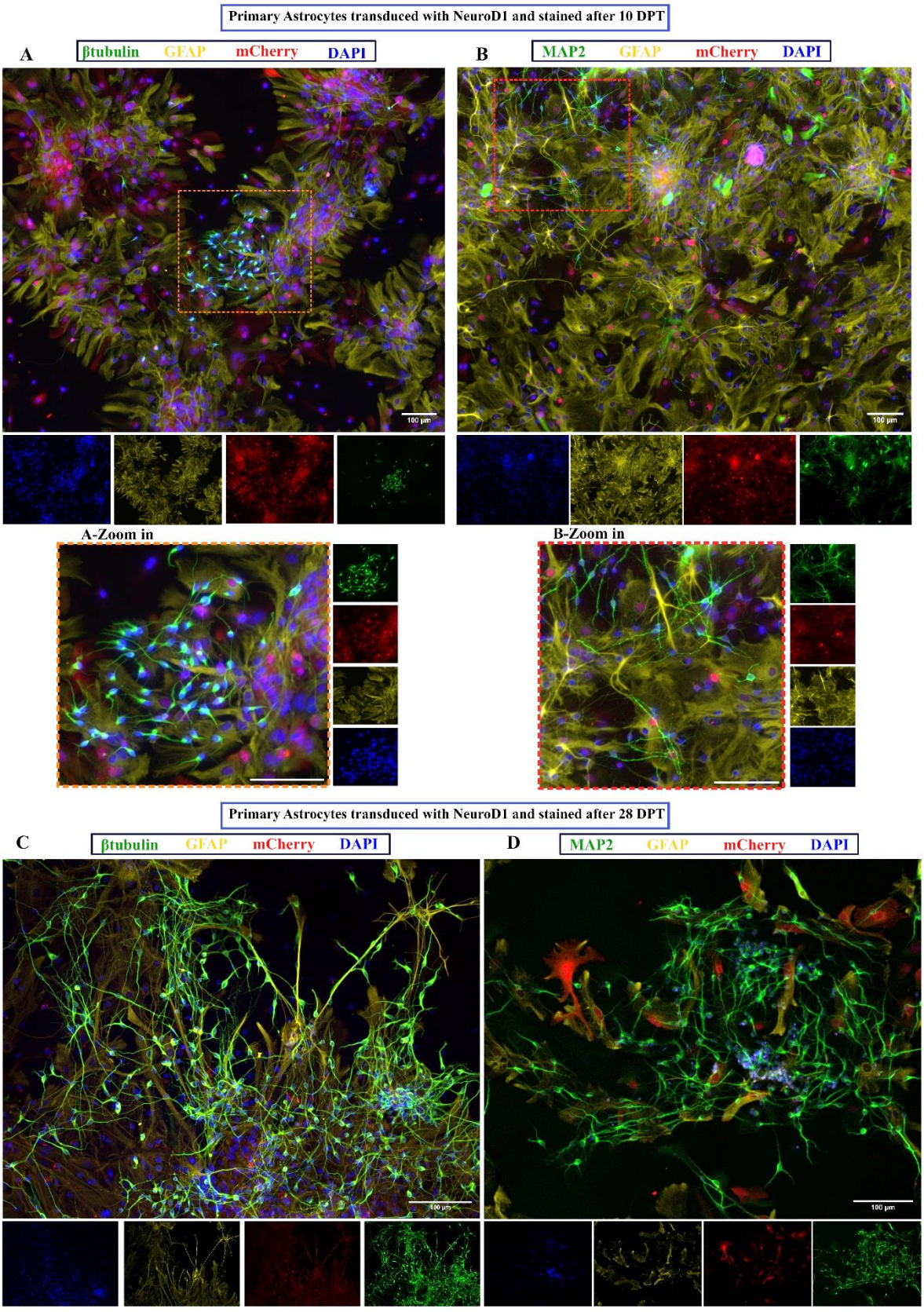
Primary Astrocytes transduced with NeuroD1 and stained after 10 DPT
A
βtubulin GFAP mCherry DAPI
B
MAP2 GFAP mCherry DAPI
100 μm
A-Zoom in
B-Zoom in
Primary Astrocytes transduced with NeuroD1 and stained after 28 DPT
C
βtubulin GFAP mCherry DAPI
D
MAP2 GFAP mCherry DAPI
100 μm

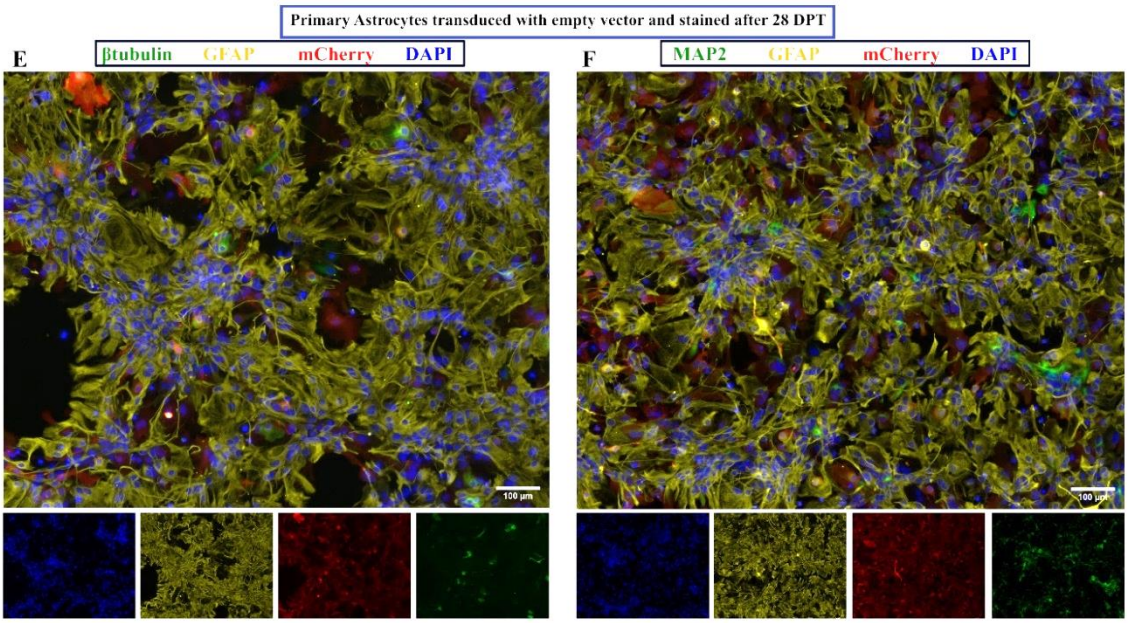
Primary Astrocytes transduced with empty vector and stained after 28 DPT
E
βtubulin GFAP mCherry DAPI
F
MAP2 GFAP mCherry DAPI
100 μm
100 μm

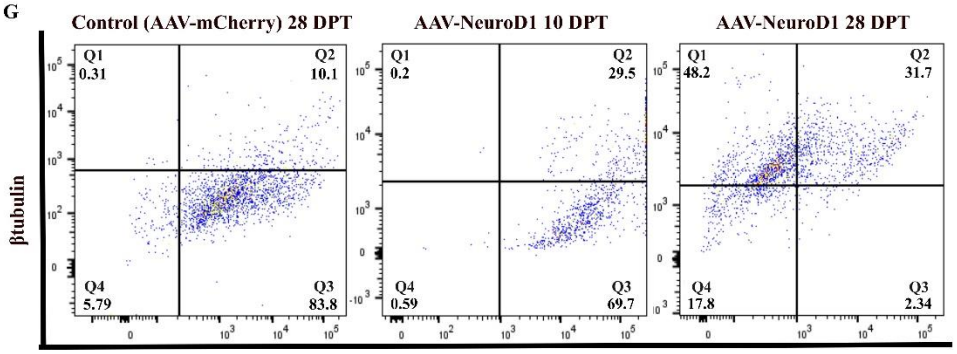
G
Control (AAV-mCherry) 28 DPT
AAV-NeuroD1 10 DPT
AAV-NeuroD1 28 DPT
βtubulin
mCherry
Q1 0.31
Q2 10.1
Q4 5.79
Q3 83.8
Q1 0.2
Q2 29.5
Q4 0.59
Q3 69.7
Q1 48.2
Q2 31.7
Q4 17.8
Q3 2.34

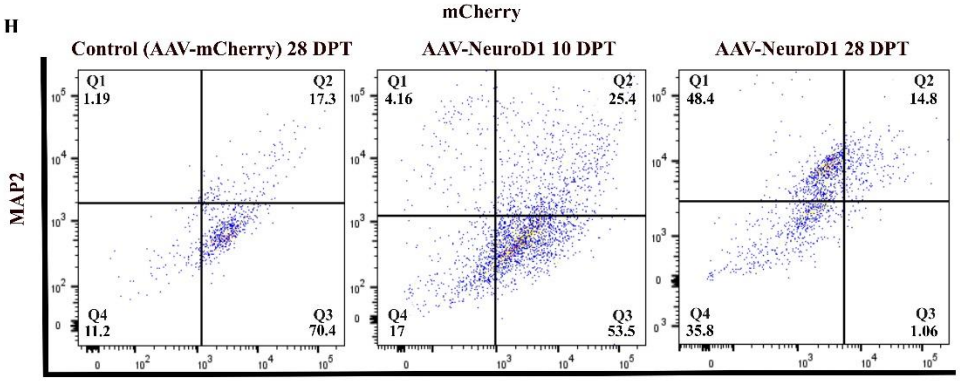
H
Control (AAV-mCherry) 28 DPT
AAV-NeuroD1 10 DPT
AAV-NeuroD1 28 DPT
MAP2
mCherry
Q1 1.19
Q2 17.3
Q4 11.2
Q3 70.4
Q1 4.16
Q2 25.4
Q4 17
Q3 53.5
Q1 48.4
Q2 14.8
Q4 35.8
Q3 1.06

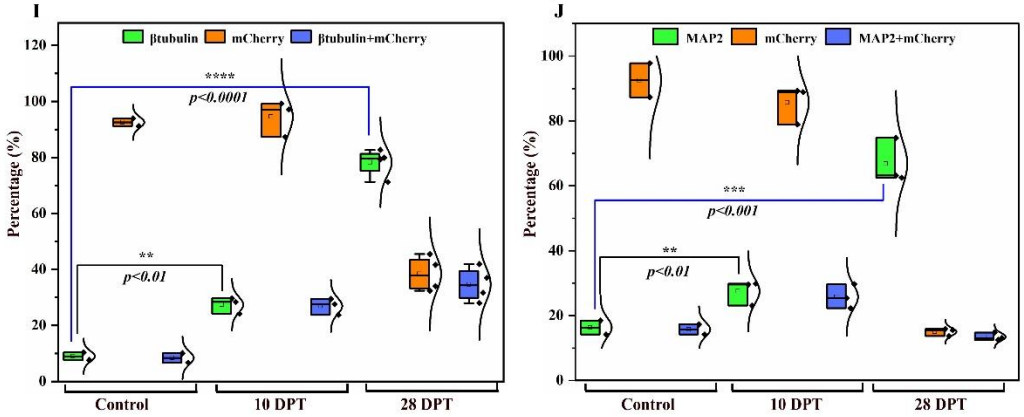
I
βtubulin mCherry βtubulin+mCherry
Percentage (%)
****
p<0.0001
**
p<0.01
Control
10 DPT
28 DPT
J
MAP2 mCherry MAP2+mCherry
Percentage (%)
***
p<0.001
**
p<0.01
Control
10 DPT
28 DPT

Figure 5.3**E, F)**

As lineage trans-differentiation is a time-dependent process, cells were assessed at more protracted periods after AAV-NeuroD1 transduction. By 28 DPT, 78.2 ± 4.9% and 69.4 ± 7.7% of cells were β3-

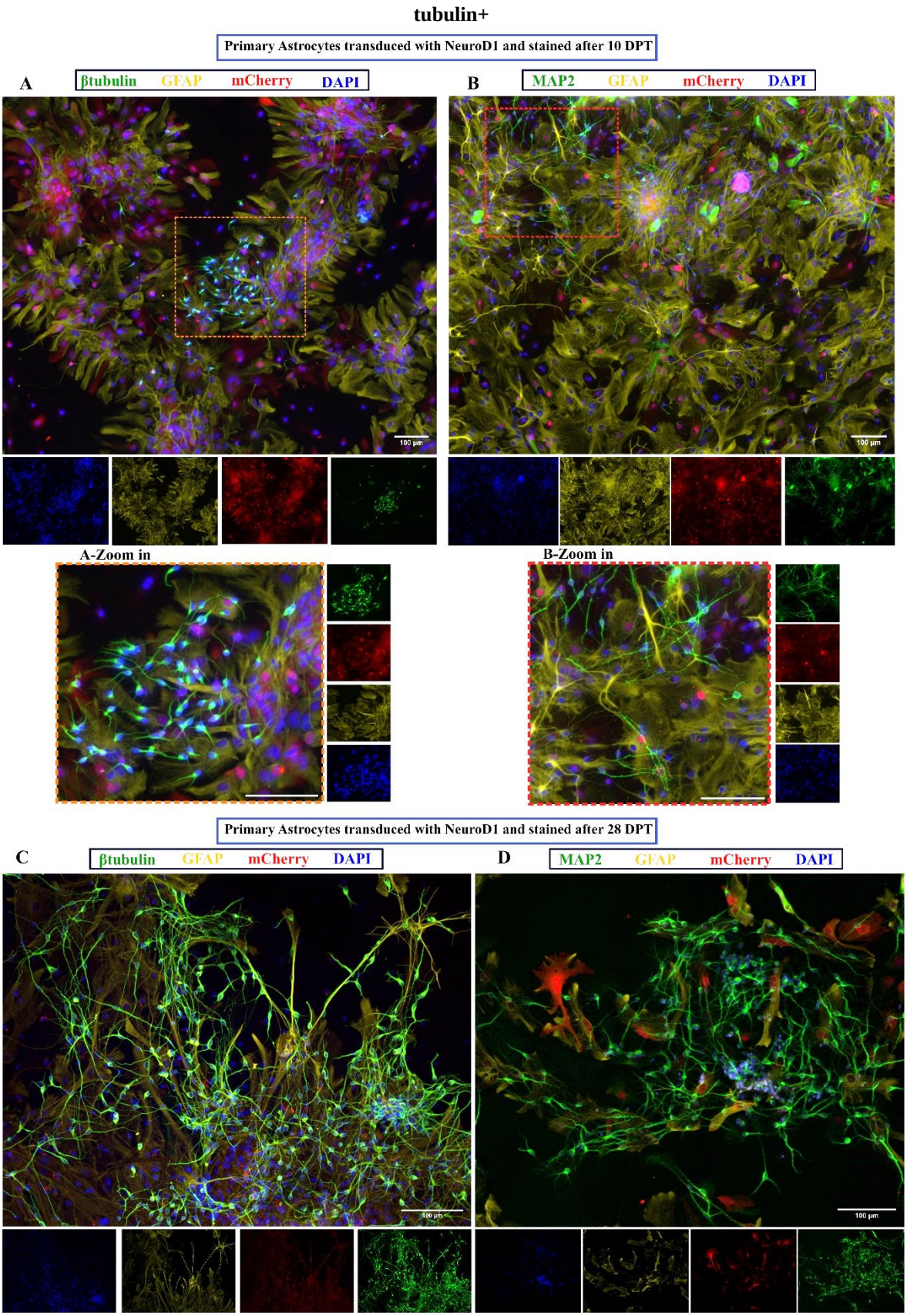
tubulin+
Primary Astrocytes transduced with NeuroD1 and stained after 10 DPT
A
βtubulin GFAP mCherry DAPI
B
MAP2 GFAP mCherry DAPI
100 μm
A-Zoom in
B-Zoom in
Primary Astrocytes transduced with NeuroD1 and stained after 28 DPT
C
βtubulin GFAP mCherry DAPI
D
MAP2 GFAP mCherry DAPI
100 μm

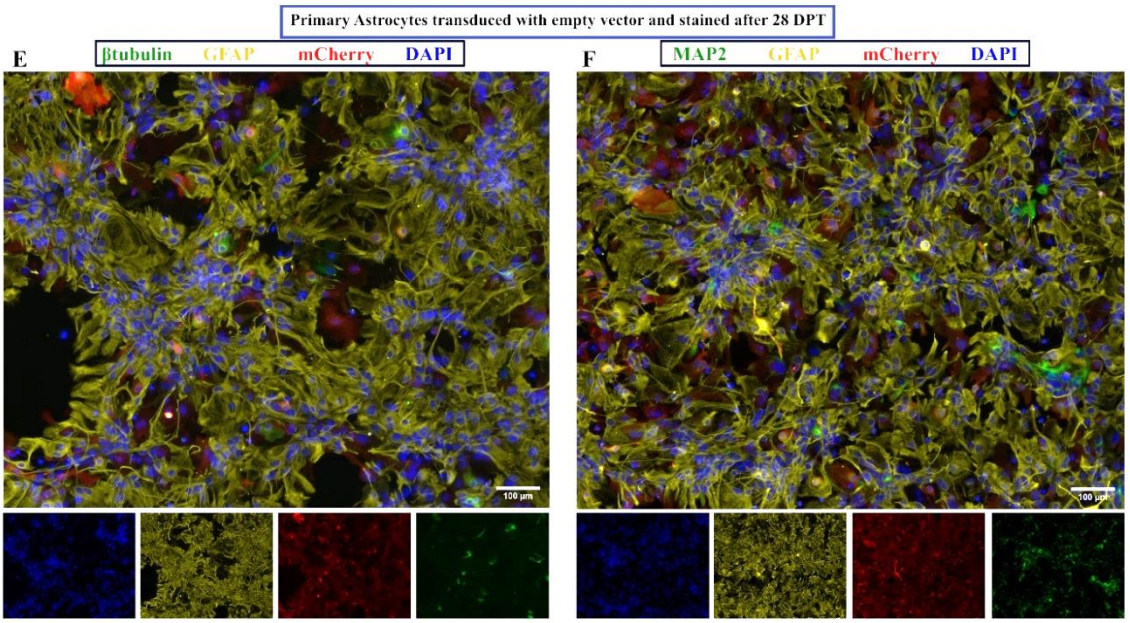
Primary Astrocytes transduced with empty vector and stained after 28 DPT
E
βtubulin GFAP mCherry DAPI
F
MAP2 GFAP mCherry DAPI
100 μm
100 μm

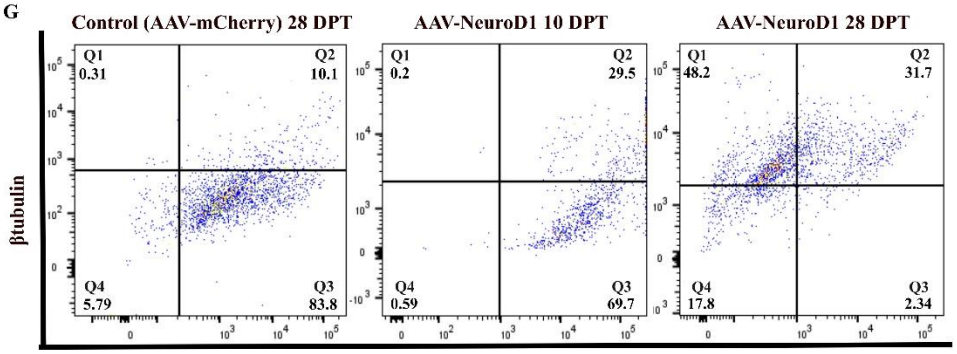
G
Control (AAV-mCherry) 28 DPT
AAV-NeuroD1 10 DPT
AAV-NeuroD1 28 DPT
βtubulin
mCherry
Q1 0.31
Q2 10.1
Q4 5.79
Q3 83.8
Q1 0.2
Q2 29.5
Q4 0.59
Q3 69.7
Q1 48.2
Q2 31.7
Q4 17.8
Q3 2.34

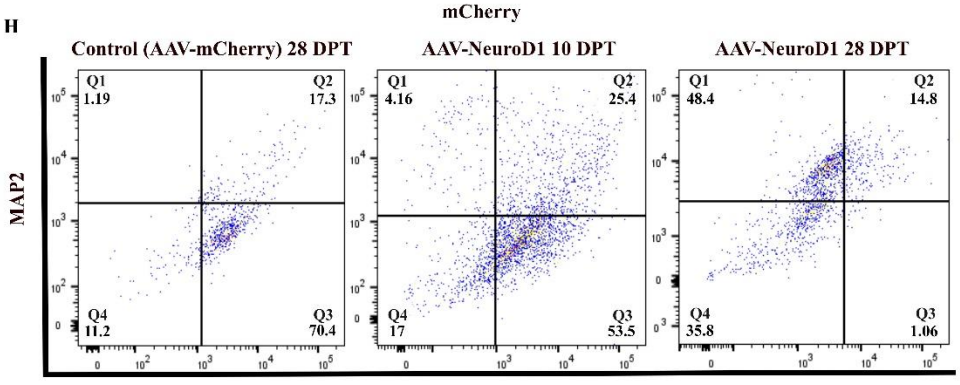
H
Control (AAV-mCherry) 28 DPT
AAV-NeuroD1 10 DPT
AAV-NeuroD1 28 DPT
MAP2
mCherry
Q1 1.19
Q2 17.3
Q4 11.2
Q3 70.4
Q1 4.16
Q2 25.4
Q4 17
Q3 53.5
Q1 48.4
Q2 14.8
Q4 35.8
Q3 1.06

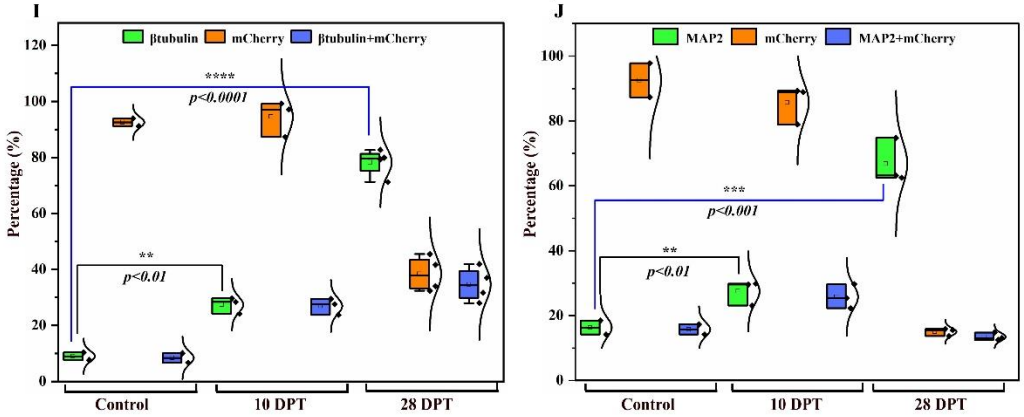
I
βtubulin mCherry βtubulin+mCherry
Percentage (%)
****
p<0.0001
**
p<0.01
Control
10 DPT
28 DPT
J
MAP2 mCherry MAP2+mCherry
Percentage (%)
***
p<0.001
**
p<0.01
Control
10 DPT
28 DPT

Figure 5.3and/or MAP2+, respectively (Figure 5.3G, H). Despite 92.5

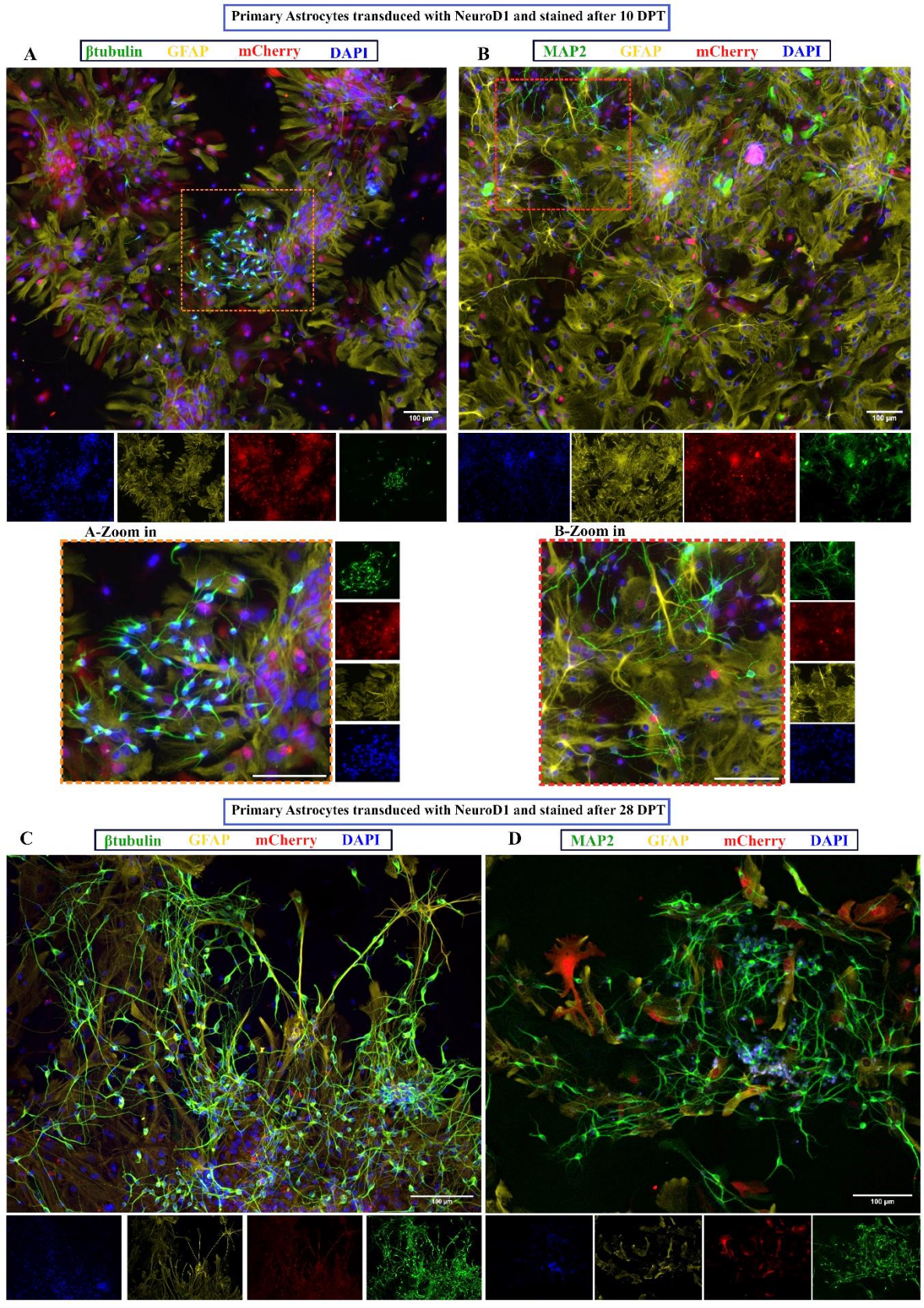

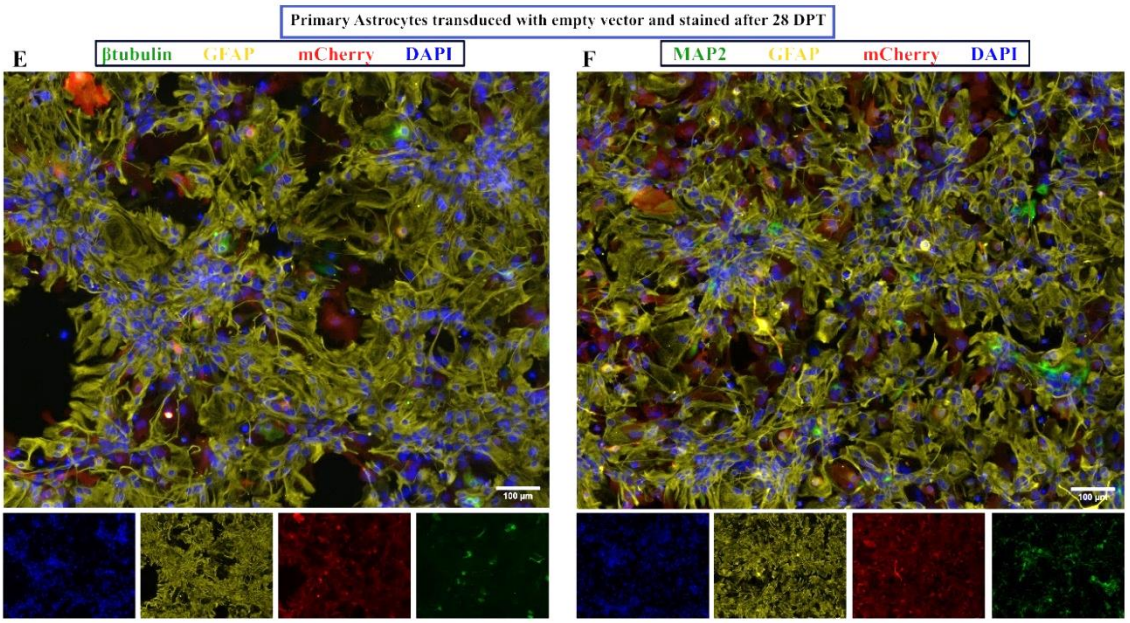
Primary Astrocytes transduced with empty vector and stained after 28 DPT
E
βtubulin GFAP mCherry DAPI
F
MAP2 GFAP mCherry DAPI
100 μm
100 μm

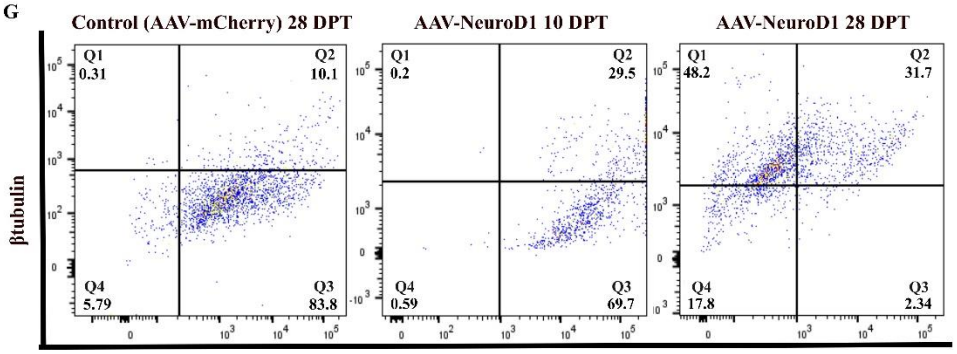
G
Control (AAV-mCherry) 28 DPT
AAV-NeuroD1 10 DPT
AAV-NeuroD1 28 DPT
βtubulin
mCherry
Q1 0.31
Q2 10.1
Q4 5.79
Q3 83.8
Q1 0.2
Q2 29.5
Q4 0.59
Q3 69.7
Q1 48.2
Q2 31.7
Q4 17.8
Q3 2.34

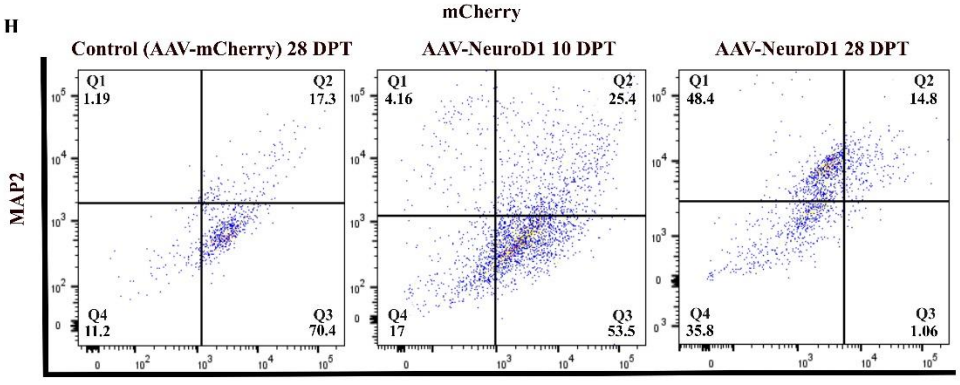
H
Control (AAV-mCherry) 28 DPT
AAV-NeuroD1 10 DPT
AAV-NeuroD1 28 DPT
MAP2
mCherry
Q1 1.19
Q2 17.3
Q4 11.2
Q3 70.4
Q1 4.16
Q2 25.4
Q4 17
Q3 53.5
Q1 48.4
Q2 14.8
Q4 35.8
Q3 1.06

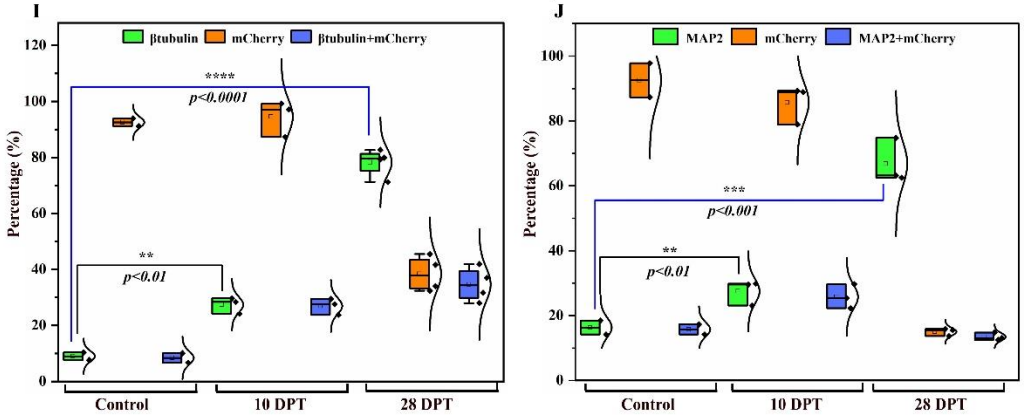
I
βtubulin mCherry βtubulin+mCherry
Percentage (%)
****
p<0.0001
**
p<0.01
Control
10 DPT
28 DPT
J
MAP2 mCherry MAP2+mCherry
Percentage (%)
***
p<0.001
**
p<0.01
Control
10 DPT
28 DPT

Figure 5.3± 1.9% transduction efficiency at 10 DPT, by 28 DPT

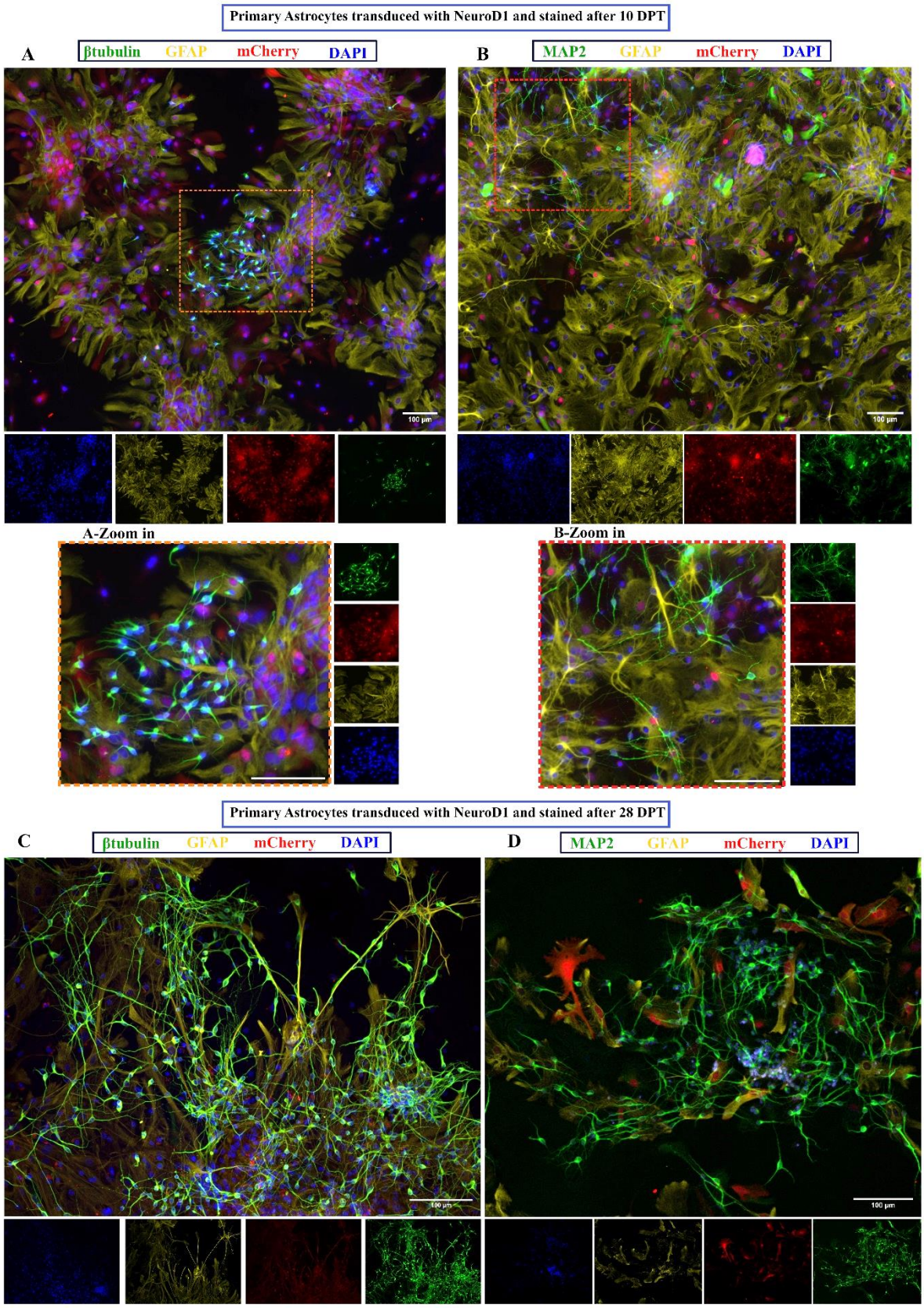

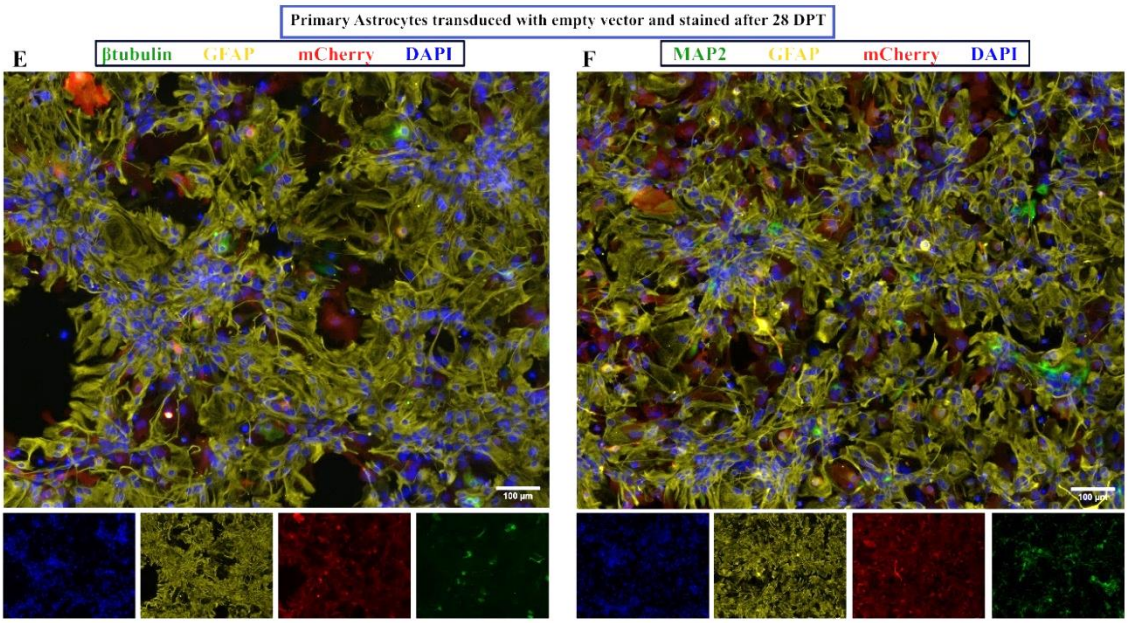
Primary Astrocytes transduced with empty vector and stained after 28 DPT
E
βtubulin GFAP mCherry DAPI
F
MAP2 GFAP mCherry DAPI
100 μm
100 μm

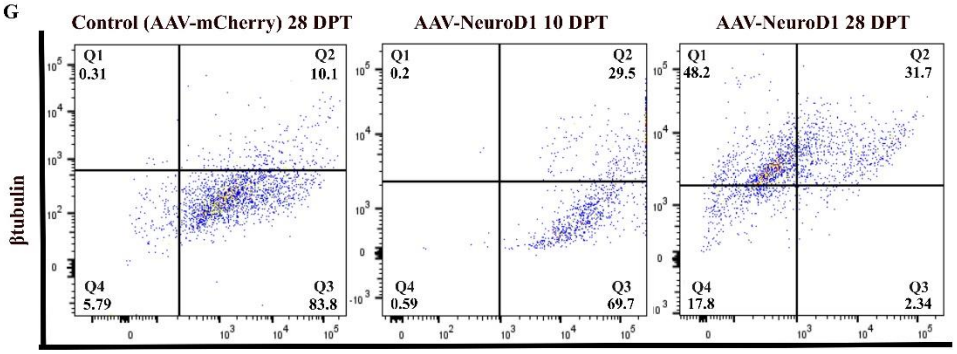
G
Control (AAV-mCherry) 28 DPT
AAV-NeuroD1 10 DPT
AAV-NeuroD1 28 DPT
βtubulin
mCherry
Q1 0.31
Q2 10.1
Q4 5.79
Q3 83.8
Q1 0.2
Q2 29.5
Q4 0.59
Q3 69.7
Q1 48.2
Q2 31.7
Q4 17.8
Q3 2.34

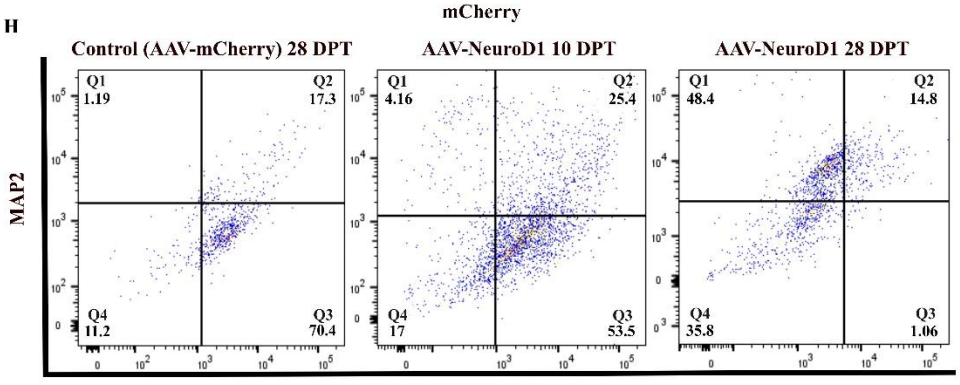
H
Control (AAV-mCherry) 28 DPT
AAV-NeuroD1 10 DPT
AAV-NeuroD1 28 DPT
MAP2
mCherry
Q1 1.19
Q2 17.3
Q4 11.2
Q3 70.4
Q1 4.16
Q2 25.4
Q4 17
Q3 53.5
Q1 48.4
Q2 14.8
Q4 35.8
Q3 1.06

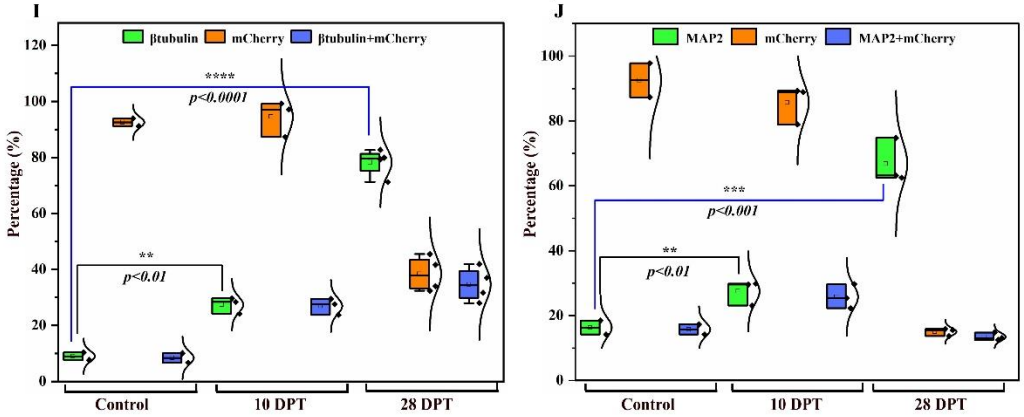
I
βtubulin mCherry βtubulin+mCherry
Percentage (%)
****
p<0.0001
**
p<0.01
Control
10 DPT
28 DPT
J
MAP2 mCherry MAP2+mCherry
Percentage (%)
***
p<0.001
**
p<0.01
Control
10 DPT
28 DPT

Figure 5.3 the transduction efficiency drastically reduced to 38.3

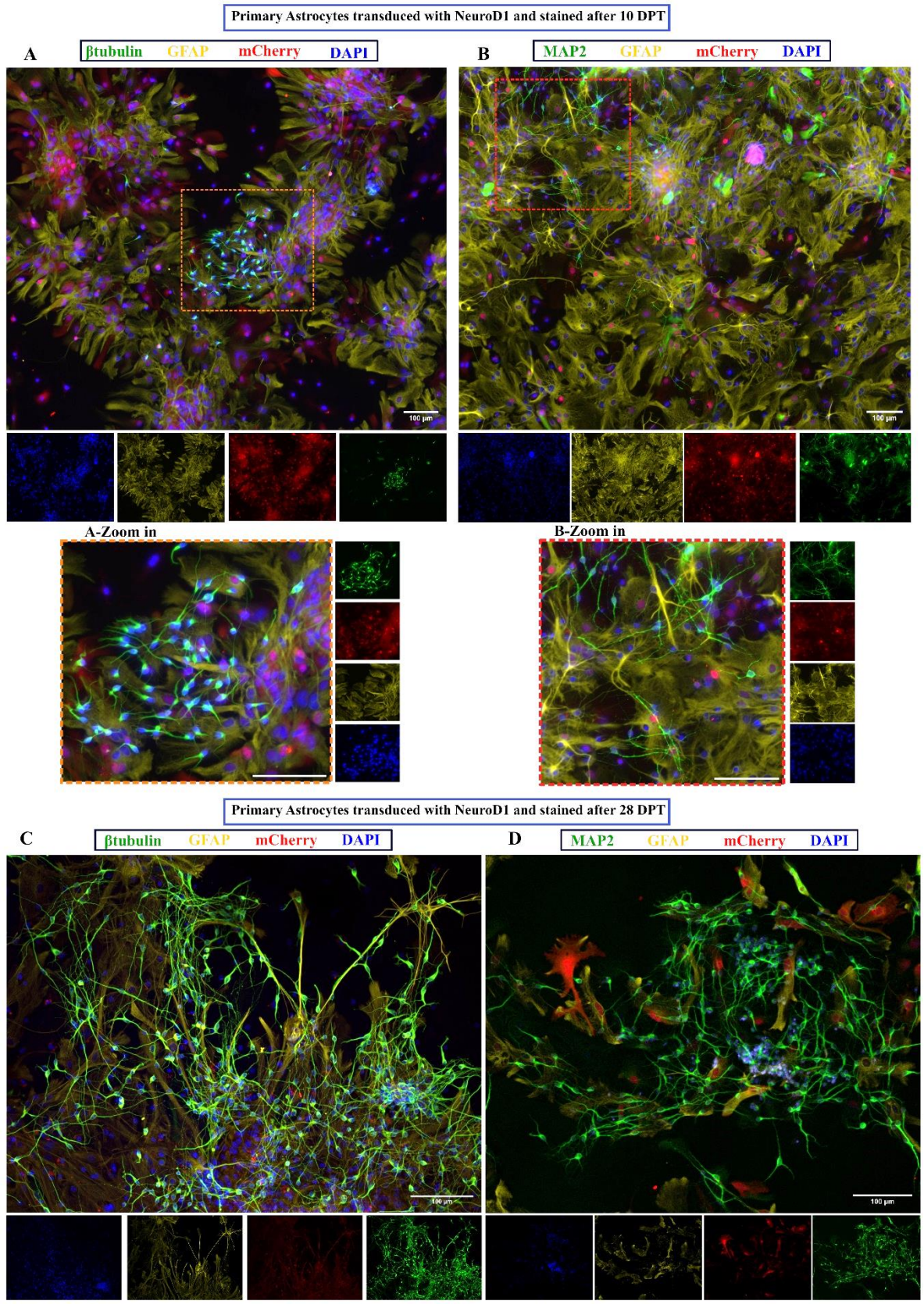

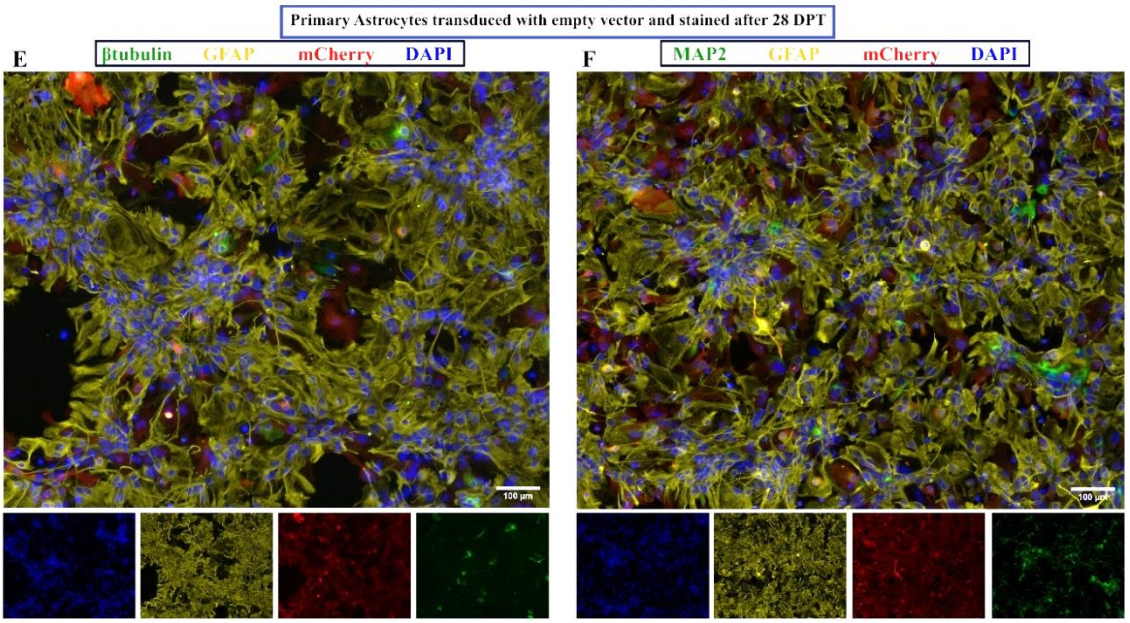
Primary Astrocytes transduced with empty vector and stained after 28 DPT
E
βtubulin GFAP mCherry DAPI
F
MAP2 GFAP mCherry DAPI
100 μm
100 μm

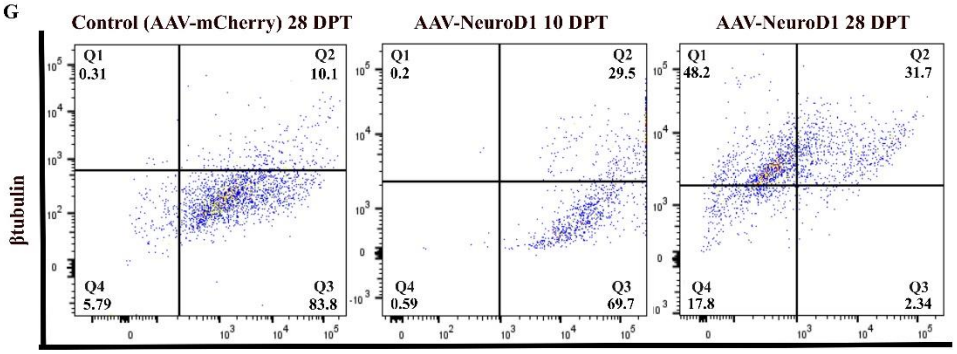
G
Control (AAV-mCherry) 28 DPT
AAV-NeuroD1 10 DPT
AAV-NeuroD1 28 DPT
βtubulin
mCherry
Q1 0.31
Q2 10.1
Q4 5.79
Q3 83.8
Q1 0.2
Q2 29.5
Q4 0.59
Q3 69.7
Q1 48.2
Q2 31.7
Q4 17.8
Q3 2.34

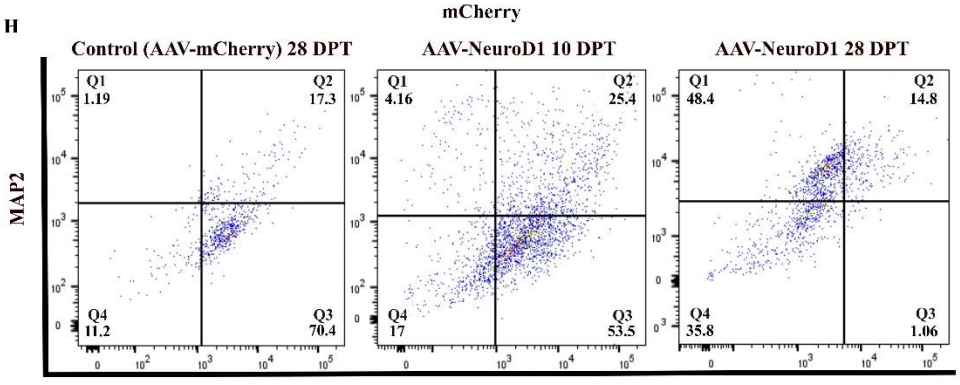
H
Control (AAV-mCherry) 28 DPT
AAV-NeuroD1 10 DPT
AAV-NeuroD1 28 DPT
MAP2
mCherry
Q1 1.19
Q2 17.3
Q4 11.2
Q3 70.4
Q1 4.16
Q2 25.4
Q4 17
Q3 53.5
Q1 48.4
Q2 14.8
Q4 35.8
Q3 1.06

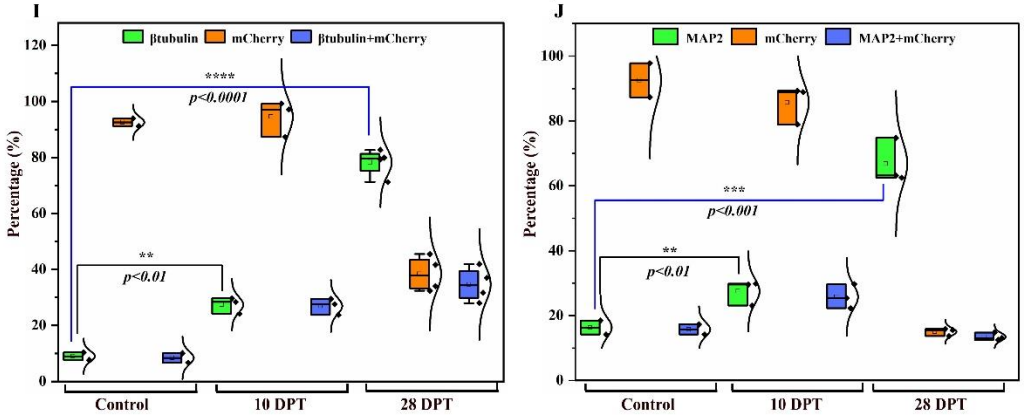
I
βtubulin mCherry βtubulin+mCherry
Percentage (%)
****
p<0.0001
**
p<0.01
Control
10 DPT
28 DPT
J
MAP2 mCherry MAP2+mCherry
Percentage (%)
***
p<0.001
**
p<0.01
Control
10 DPT
28 DPT

Figure 5.3

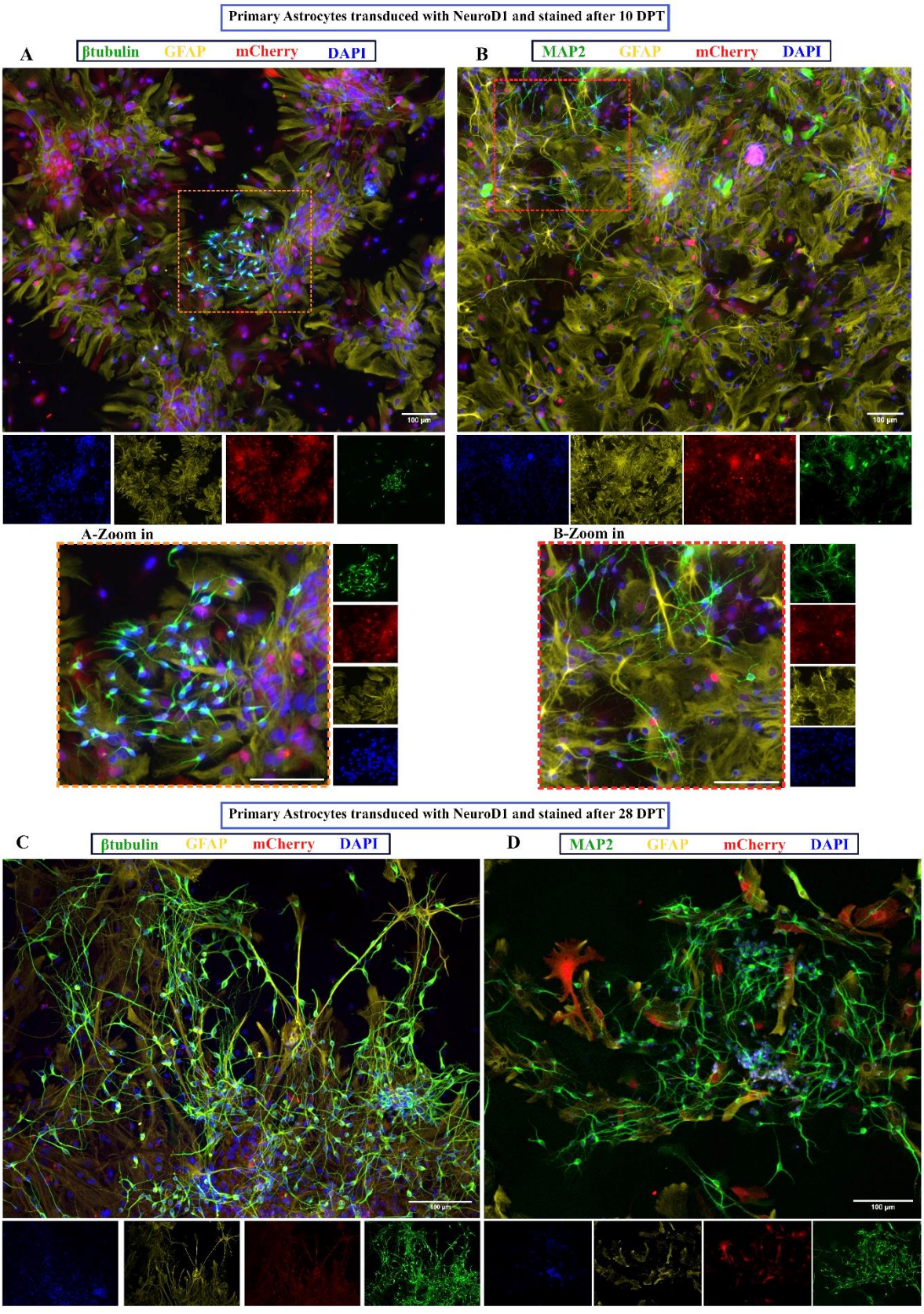
Primary Astrocytes transduced with NeuroD1 and stained after 10 DPT
A
βtubulin GFAP mCherry DAPI
B
MAP2 GFAP mCherry DAPI
100 µm
100 µm
A-Zoom in
B-Zoom in
Primary Astrocytes transduced with NeuroD1 and stained after 28 DPT
C
βtubulin GFAP mCherry DAPI
D
MAP2 GFAP mCherry DAPI
100 µm
100 µm

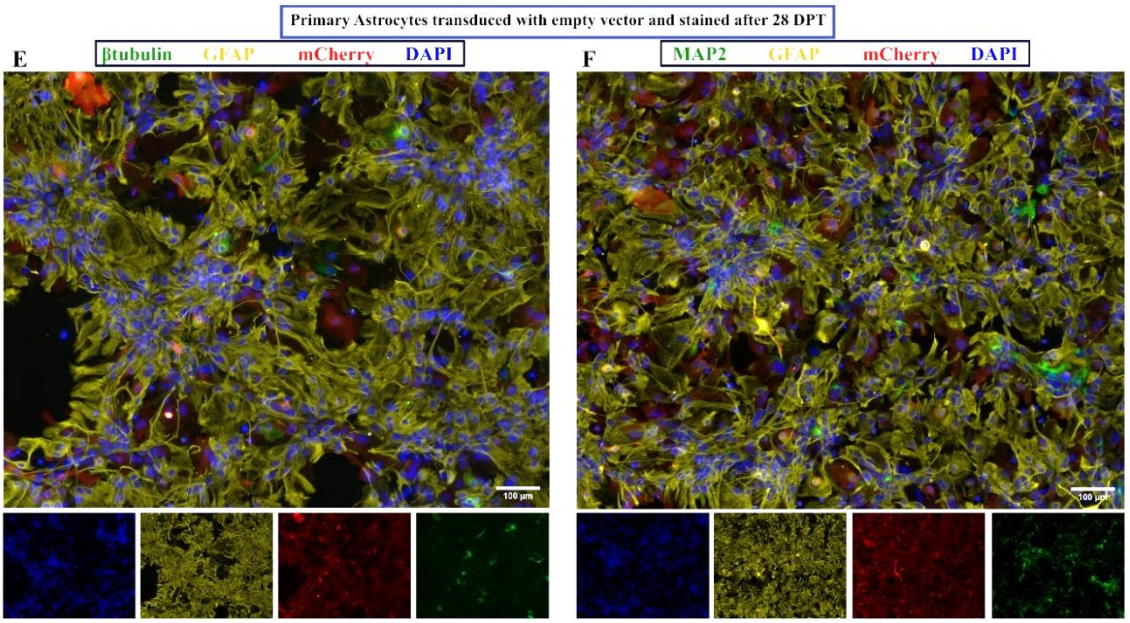
Primary Astrocytes transduced with empty vector and stained after 28 DPT
E
βtubulin GFAP mCherry DAPI
F
MAP2 GFAP mCherry DAPI
100 μm
100 μm

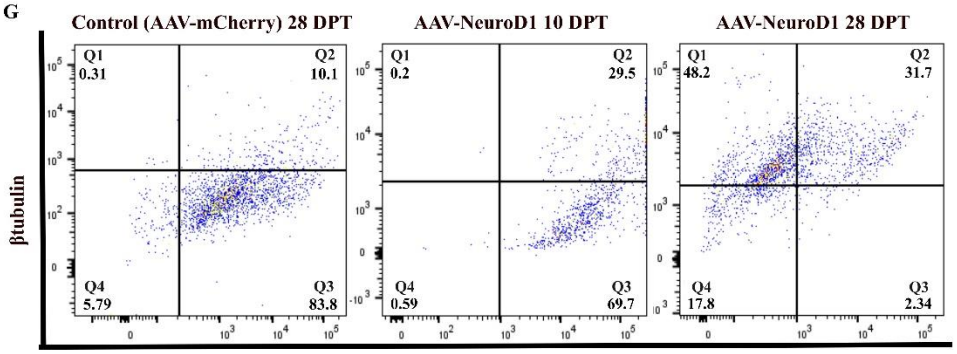
G
Control (AAV-mCherry) 28 DPT
AAV-NeuroD1 10 DPT
AAV-NeuroD1 28 DPT
βtubulin
mCherry
Q1 0.31
Q2 10.1
Q4 5.79
Q3 83.8
Q1 0.2
Q2 29.5
Q4 0.59
Q3 69.7
Q1 48.2
Q2 31.7
Q4 17.8
Q3 2.34

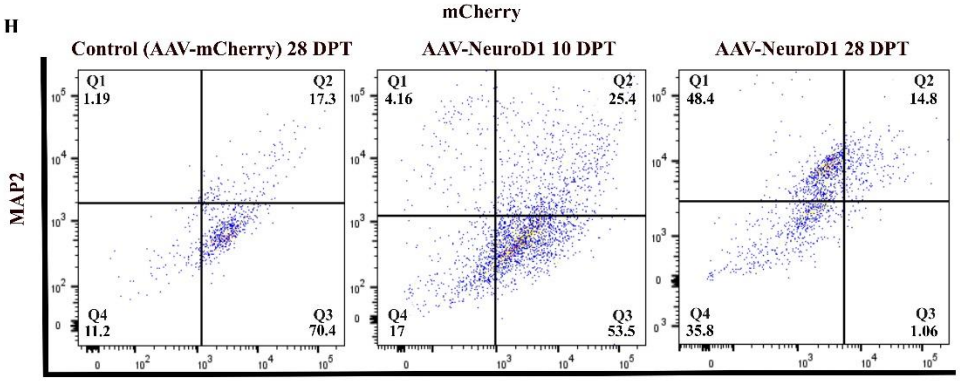
H
Control (AAV-mCherry) 28 DPT
AAV-NeuroD1 10 DPT
AAV-NeuroD1 28 DPT
MAP2
mCherry
Q1 1.19
Q2 17.3
Q4 11.2
Q3 70.4
Q1 4.16
Q2 25.4
Q4 17
Q3 53.5
Q1 48.4
Q2 14.8
Q4 35.8
Q3 1.06

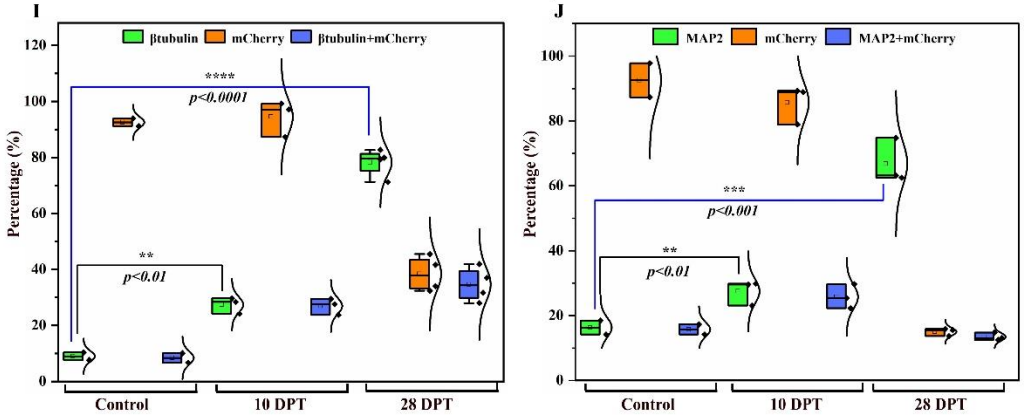
I
βtubulin mCherry βtubulin+mCherry
Percentage (%)
****
p<0.0001
**
p<0.01
Control
10 DPT
28 DPT
J
MAP2 mCherry MAP2+mCherry
Percentage (%)
***
p<0.001
**
p<0.01
Control
10 DPT
28 DPT

Figure 5.3± 6.2% with

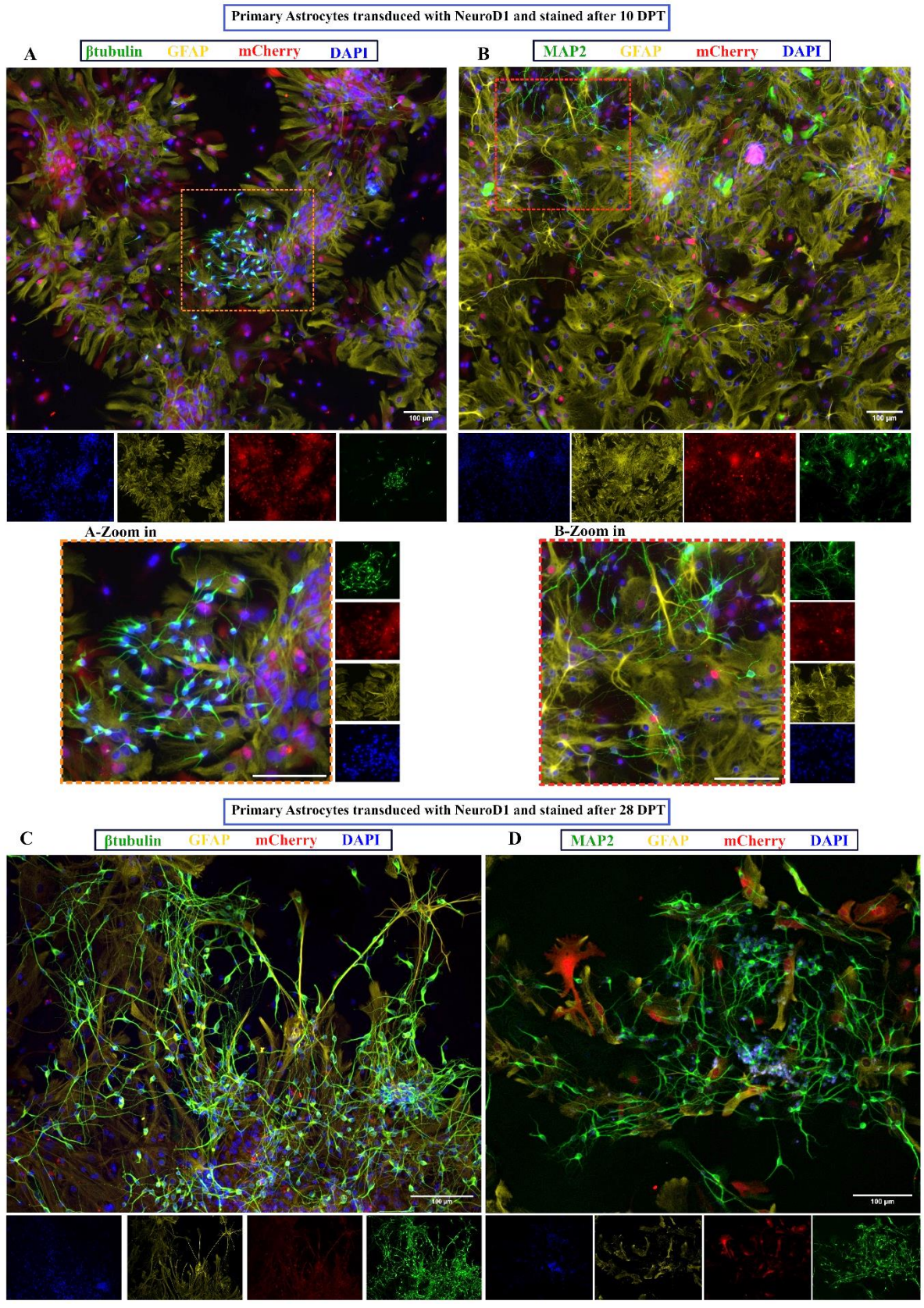

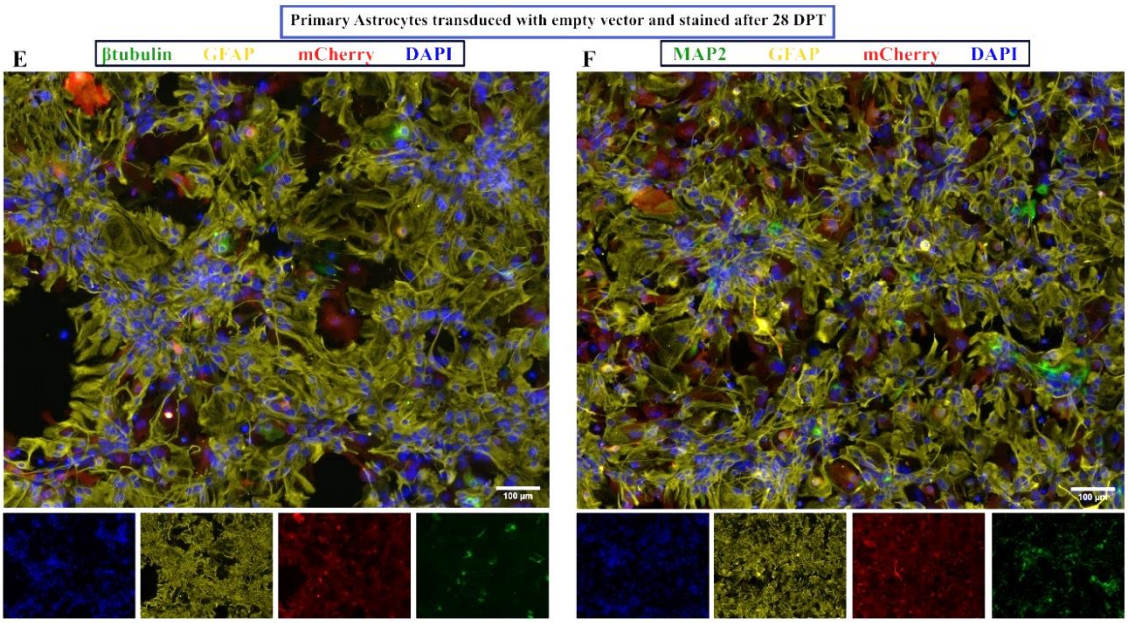
Primary Astrocytes transduced with empty vector and stained after 28 DPT
E
βtubulin GFAP mCherry DAPI
F
MAP2 GFAP mCherry DAPI
100 μm
100 μm

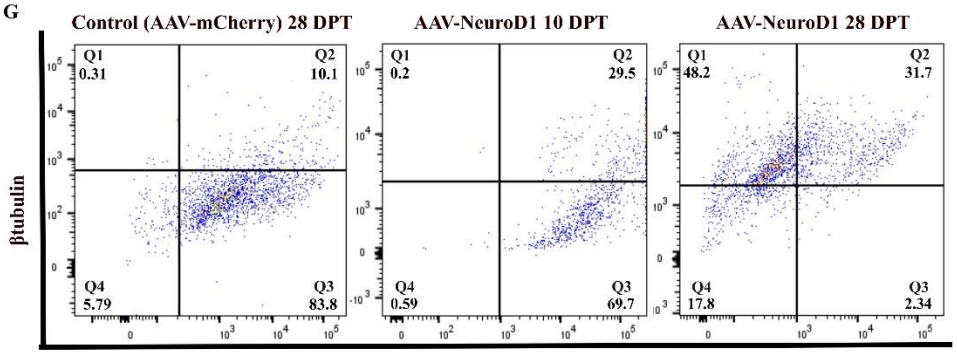
G
Control (AAV-mCherry) 28 DPT
AAV-NeuroD1 10 DPT
AAV-NeuroD1 28 DPT
βtubulin
mCherry
Q1 0.31
Q2 10.1
Q4 5.79
Q3 83.8
Q1 0.2
Q2 29.5
Q4 0.59
Q3 69.7
Q1 48.2
Q2 31.7
Q4 17.8
Q3 2.34

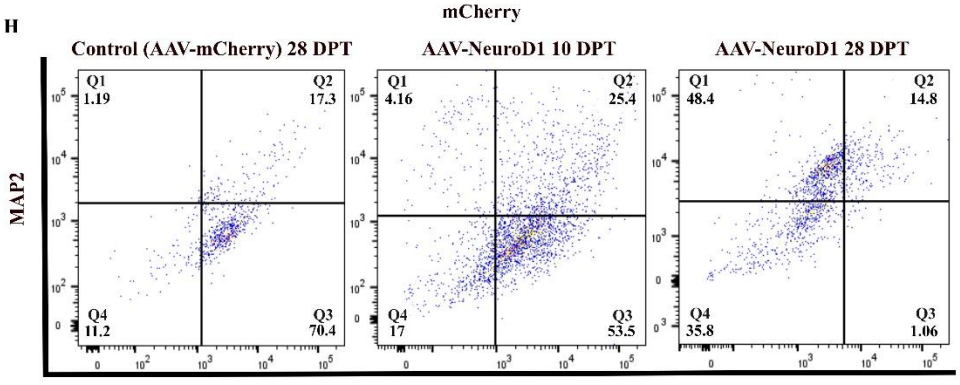
H
Control (AAV-mCherry) 28 DPT
AAV-NeuroD1 10 DPT
AAV-NeuroD1 28 DPT
MAP2
mCherry
Q1 1.19
Q2 17.3
Q4 11.2
Q3 70.4
Q1 4.16
Q2 25.4
Q4 17
Q3 53.5
Q1 48.4
Q2 14.8
Q4 35.8
Q3 1.06

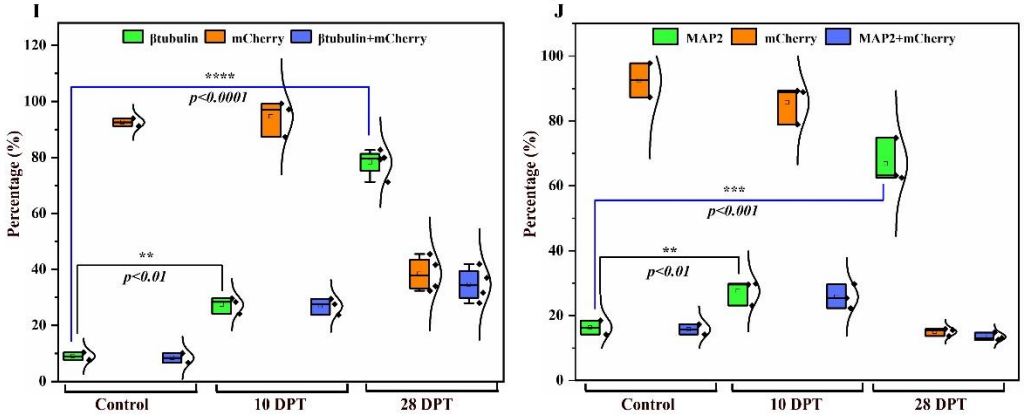
I
βtubulin mCherry βtubulin+mCherry
Percentage (%)
****
p<0.0001
**
p<0.01
Control
10 DPT
28 DPT
J
MAP2 mCherry MAP2+mCherry
Percentage (%)
***
p<0.001
**
p<0.01
Control
10 DPT
28 DPT

Figure 5.3

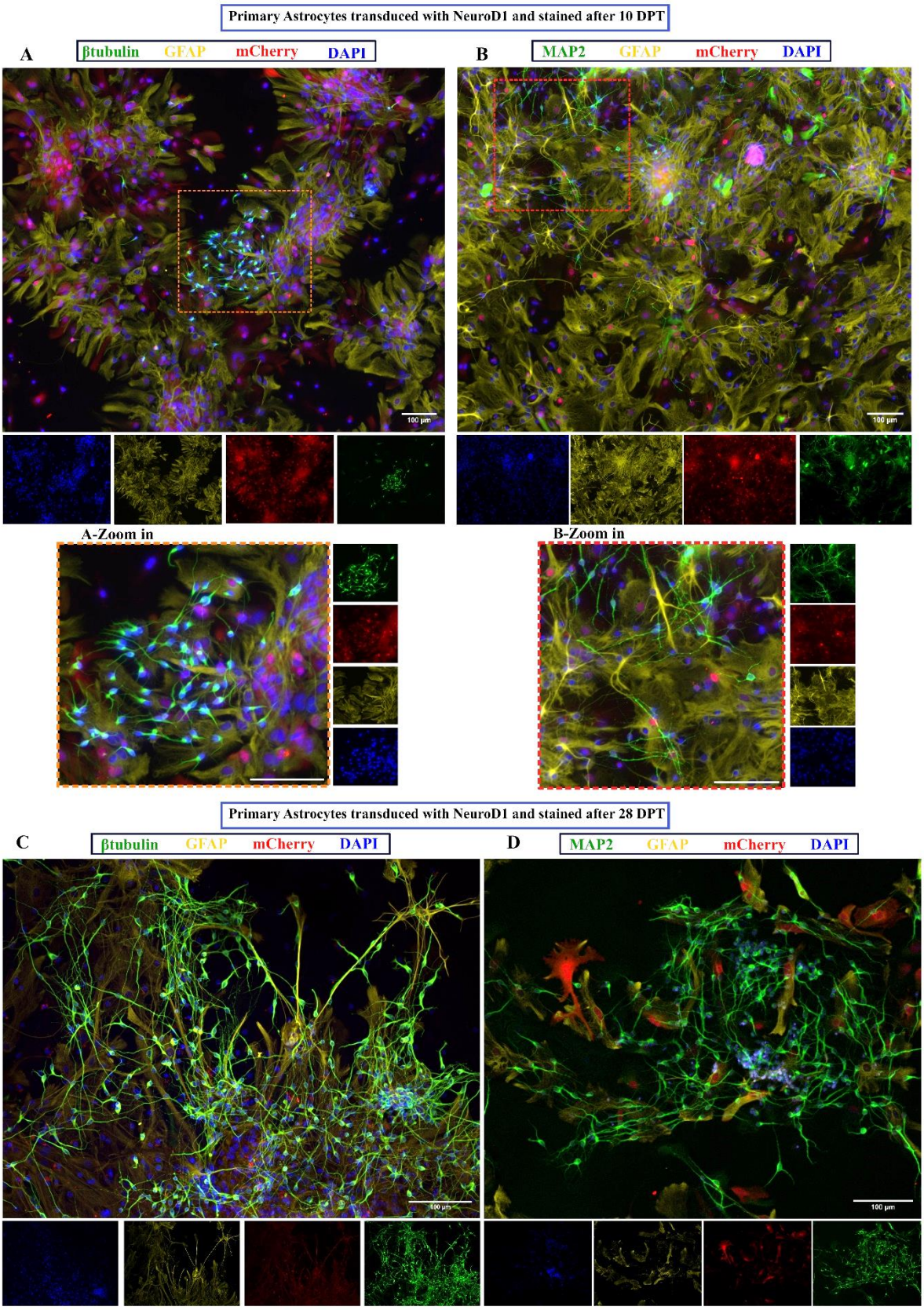
Primary Astrocytes transduced with NeuroD1 and stained after 10 DPT
A
βtubulin GFAP mCherry DAPI
B
MAP2 GFAP mCherry DAPI
100 µm
100 µm
A-Zoom in
B-Zoom in
Primary Astrocytes transduced with NeuroD1 and stained after 28 DPT
C
βtubulin GFAP mCherry DAPI
D
MAP2 GFAP mCherry DAPI
100 µm
100 µm

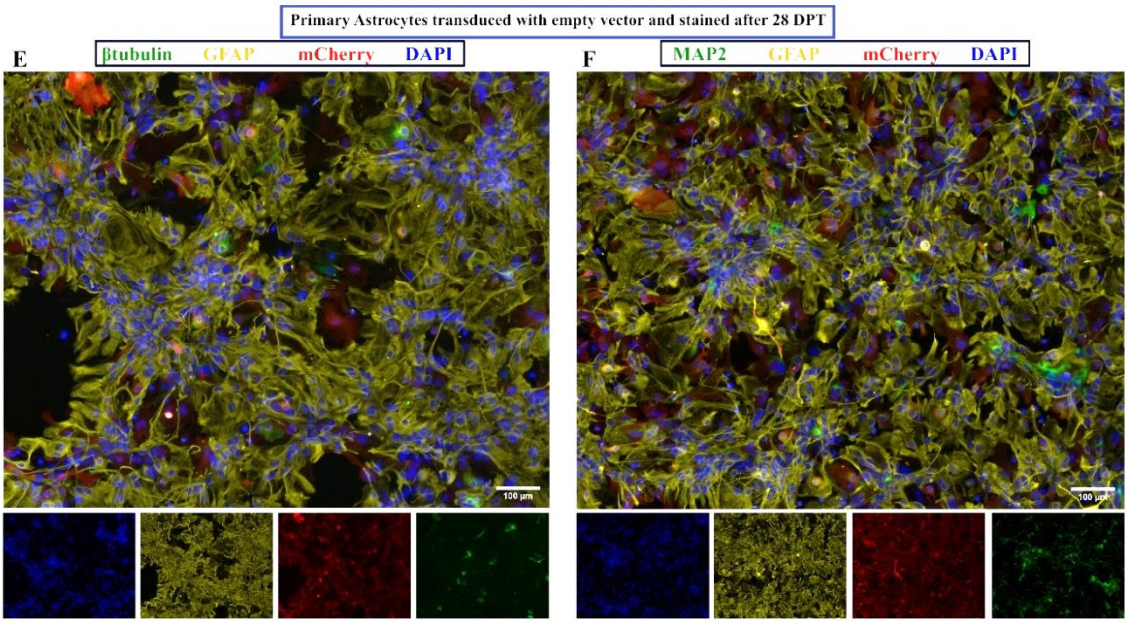
Primary Astrocytes transduced with empty vector and stained after 28 DPT
E
βtubulin GFAP mCherry DAPI
F
MAP2 GFAP mCherry DAPI
100 μm
100 μm

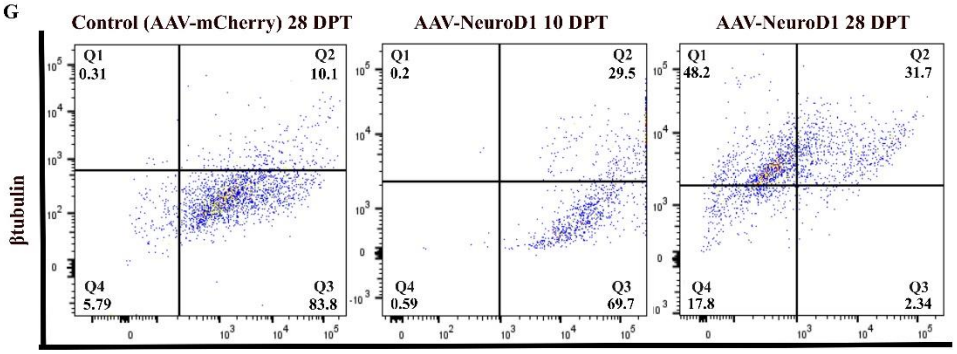
G
Control (AAV-mCherry) 28 DPT
AAV-NeuroD1 10 DPT
AAV-NeuroD1 28 DPT
βtubulin
mCherry
Q1 0.31
Q2 10.1
Q4 5.79
Q3 83.8
Q1 0.2
Q2 29.5
Q4 0.59
Q3 69.7
Q1 48.2
Q2 31.7
Q4 17.8
Q3 2.34

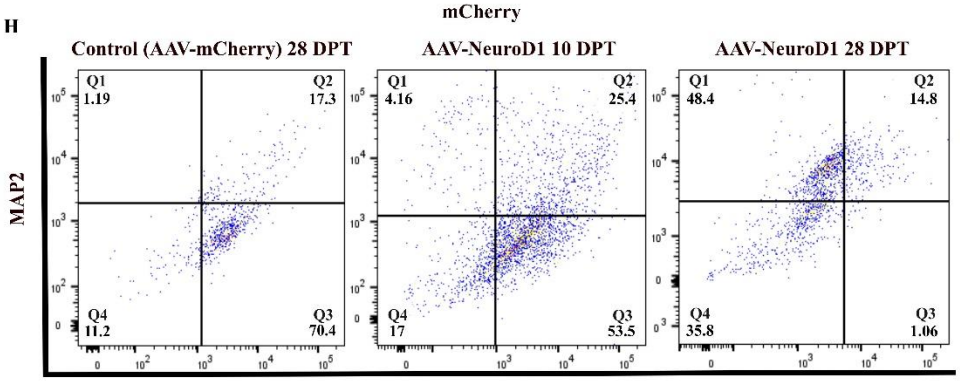
H
Control (AAV-mCherry) 28 DPT
AAV-NeuroD1 10 DPT
AAV-NeuroD1 28 DPT
MAP2
mCherry
Q1 1.19
Q2 17.3
Q4 11.2
Q3 70.4
Q1 4.16
Q2 25.4
Q4 17
Q3 53.5
Q1 48.4
Q2 14.8
Q4 35.8
Q3 1.06

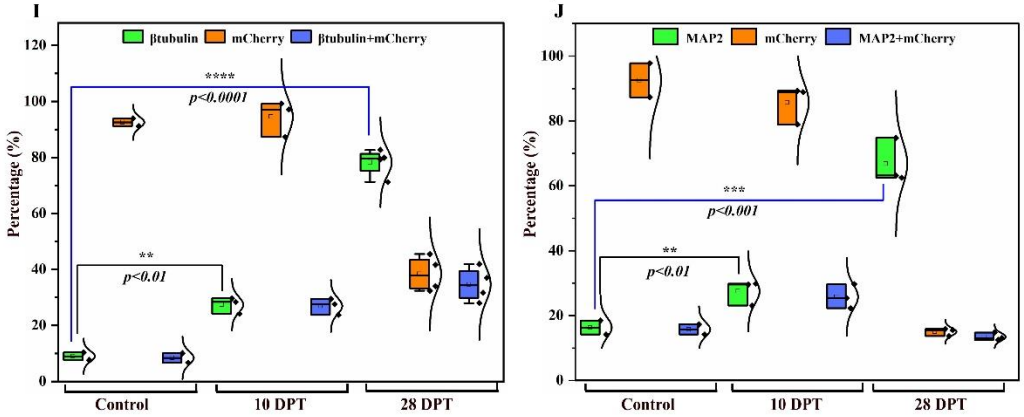
I
βtubulin mCherry βtubulin+mCherry
Percentage (%)
****
p<0.0001
**
p<0.01
Control
10 DPT
28 DPT
J
MAP2 mCherry MAP2+mCherry
Percentage (%)
***
p<0.001
**
p<0.01
Control
10 DPT
28 DPT

Figure 5.3

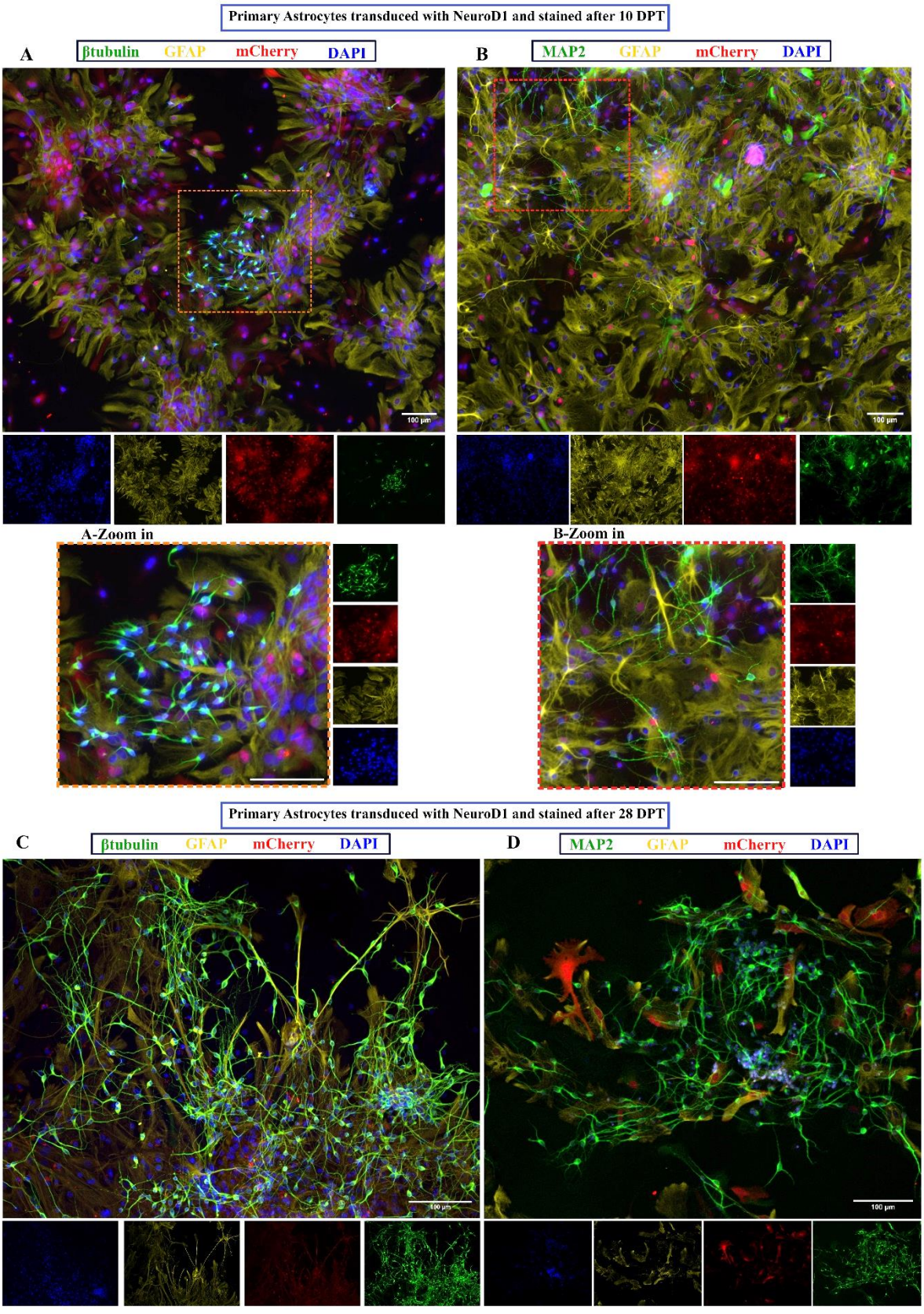
Primary Astrocytes transduced with NeuroD1 and stained after 10 DPT
A
βtubulin GFAP mCherry DAPI
B
MAP2 GFAP mCherry DAPI
100 µm
100 µm
A-Zoom in
B-Zoom in
Primary Astrocytes transduced with NeuroD1 and stained after 28 DPT
C
βtubulin GFAP mCherry DAPI
D
MAP2 GFAP mCherry DAPI
100 µm
100 µm

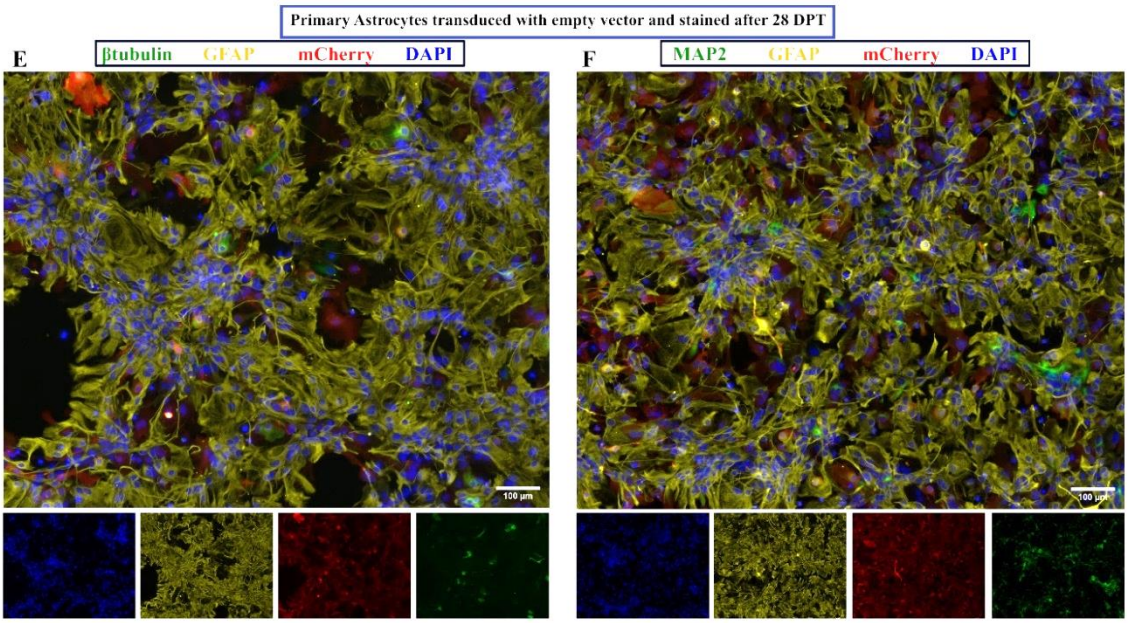
Primary Astrocytes transduced with empty vector and stained after 28 DPT
E
βtubulin GFAP mCherry DAPI
F
MAP2 GFAP mCherry DAPI
100 μm
100 μm

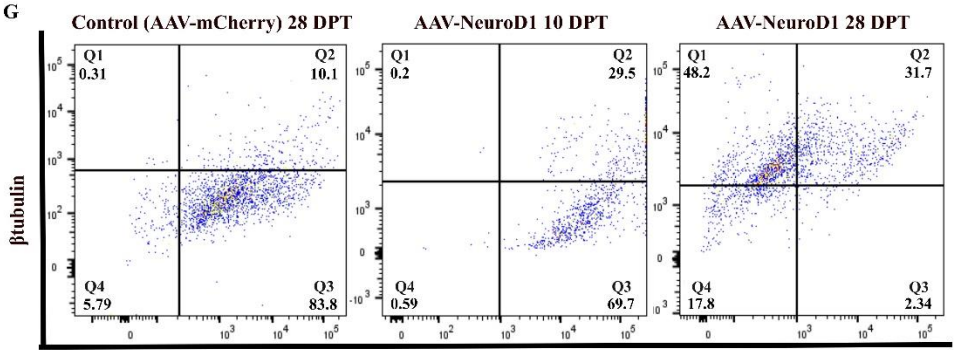
G
Control (AAV-mCherry) 28 DPT
AAV-NeuroD1 10 DPT
AAV-NeuroD1 28 DPT
βtubulin
mCherry
Q1 0.31
Q2 10.1
Q4 5.79
Q3 83.8
Q1 0.2
Q2 29.5
Q4 0.59
Q3 69.7
Q1 48.2
Q2 31.7
Q4 17.8
Q3 2.34

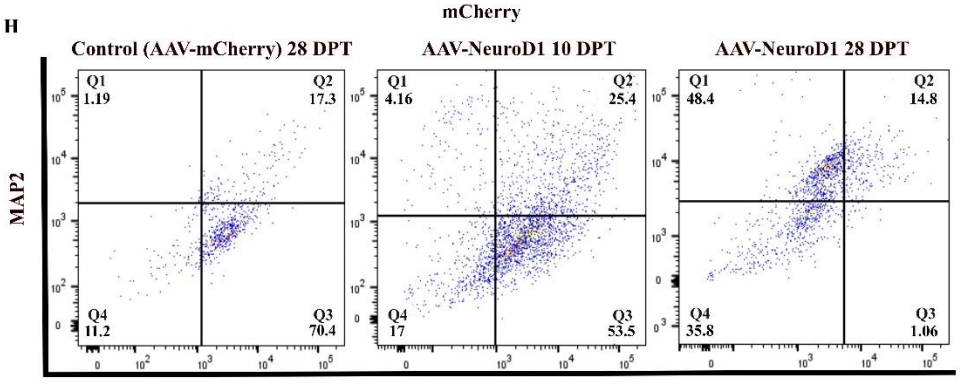
H
Control (AAV-mCherry) 28 DPT
AAV-NeuroD1 10 DPT
AAV-NeuroD1 28 DPT
MAP2
mCherry
Q1 1.19
Q2 17.3
Q4 11.2
Q3 70.4
Q1 4.16
Q2 25.4
Q4 17
Q3 53.5
Q1 48.4
Q2 14.8
Q4 35.8
Q3 1.06

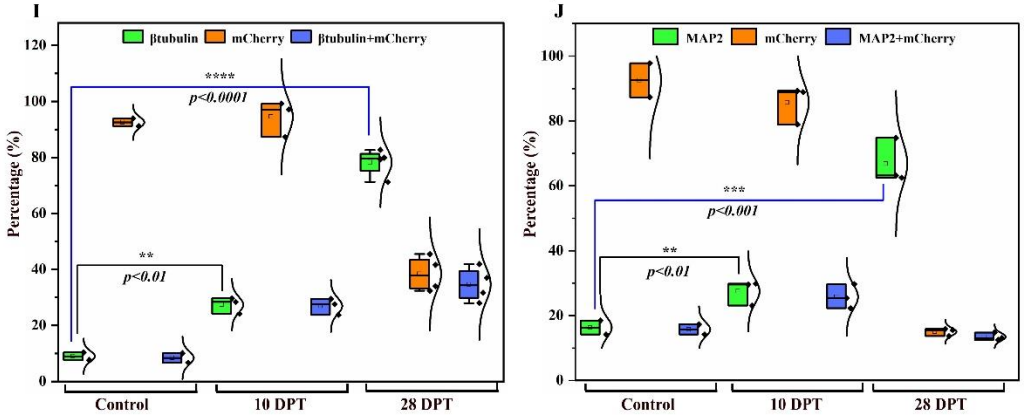
I
βtubulin mCherry βtubulin+mCherry
Percentage (%)
****
p<0.0001
**
p<0.01
Control
10 DPT
28 DPT
J
MAP2 mCherry MAP2+mCherry
Percentage (%)
***
p<0.001
**
p<0.01
Control
10 DPT
28 DPT

Figure 5.3few β-tubulin+ **(Figure 5.3C)** and MAP2+ **(Figure 5.3D)** cells retained mCherry expression, suggesting that the neuron-like cells converted from primary astrocytes gradually lost their mCherry signal, likely due to downregulation of the gfaABC1D promoter. Of relevance, astrocyte to neuron reprogramming using a GFAP promoter has been reported to create a closed-loop feedback system whereby initial translation of ectopic NeuroD1 is high in hypertrophied reactive astrocytes but diminishes/silences as the cell reprograms into more neuronal phenotypes[261].

As illustrated **(Figure 5.3C, D)**, the intensity of GFAP labelling in AAV-NeuroD1 transduced cells significantly decreased compared to control, AAV-mCherry transduction **(Figure 5.3E, F)**.

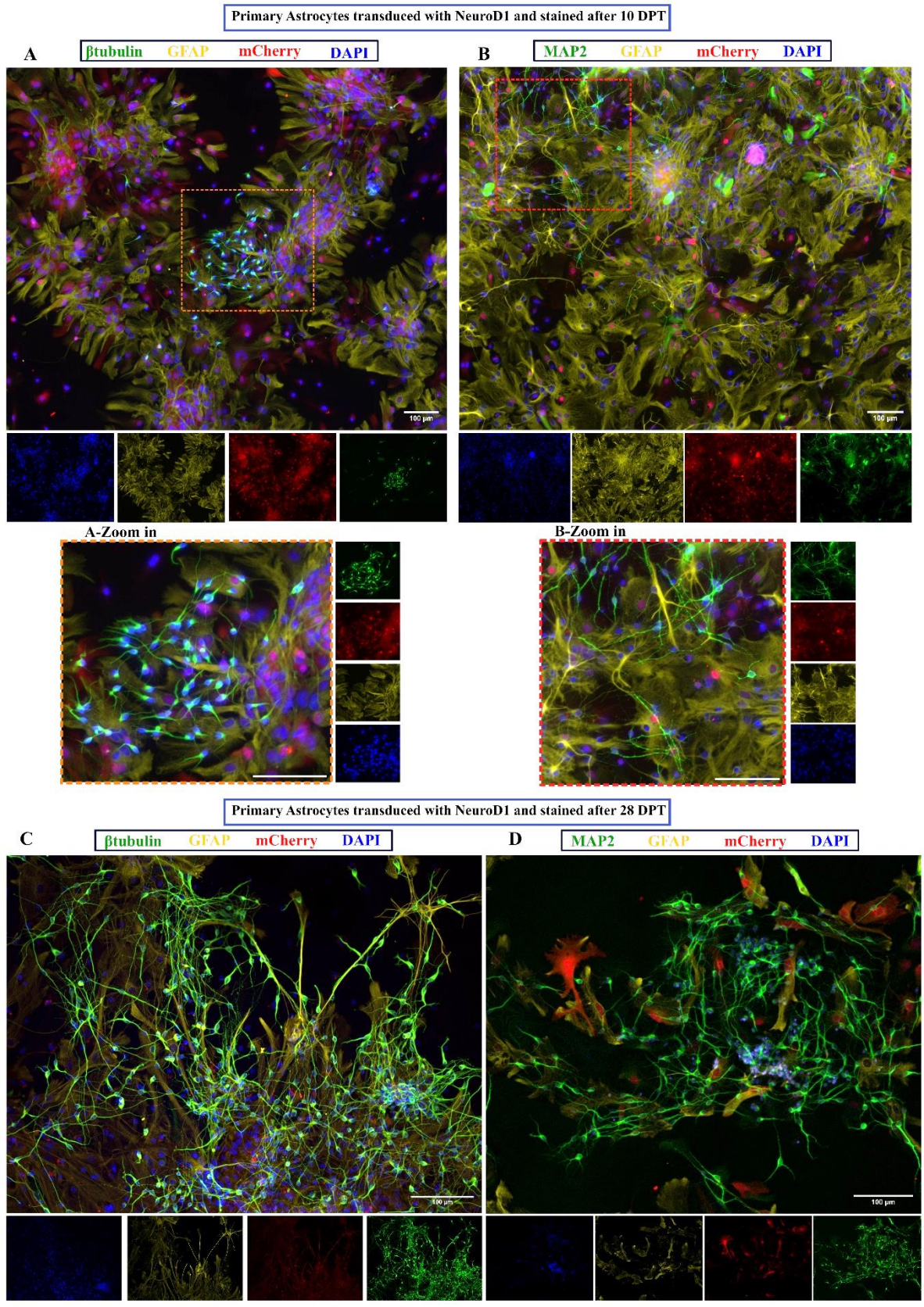
Primary Astrocytes transduced with NeuroD1 and stained after 10 DPT
A
βtubulin GFAP mCherry DAPI
B
MAP2 GFAP mCherry DAPI
100 µm
100 µm
A-Zoom in
B-Zoom in
Primary Astrocytes transduced with NeuroD1 and stained after 28 DPT
C
βtubulin GFAP mCherry DAPI
D
MAP2 GFAP mCherry DAPI
100 µm
100 µm

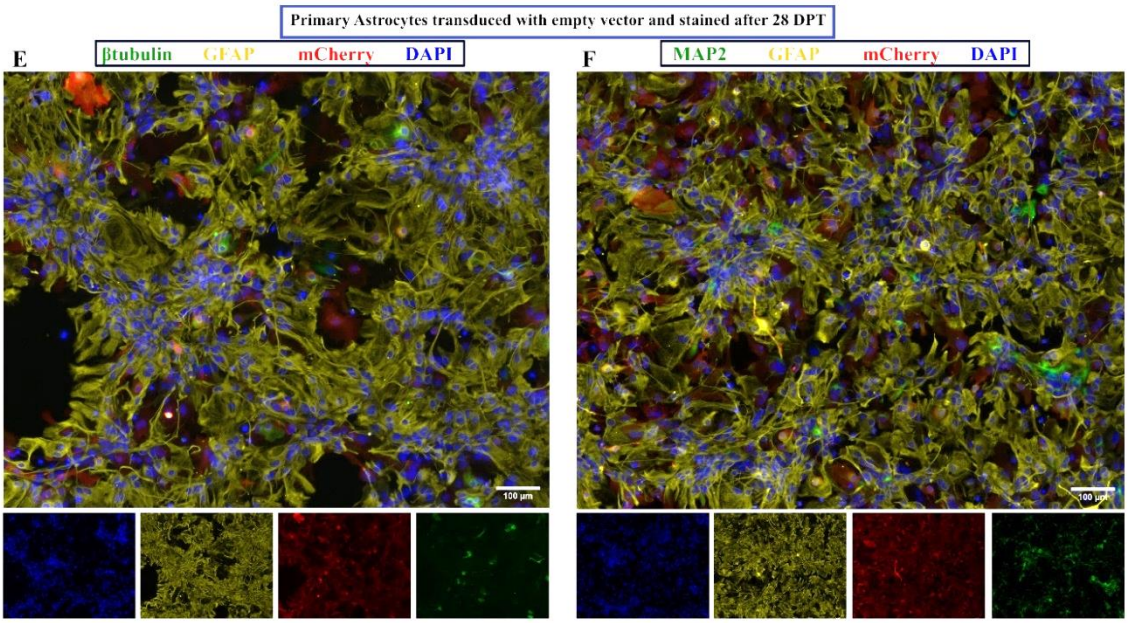
Primary Astrocytes transduced with empty vector and stained after 28 DPT
E
βtubulin GFAP mCherry DAPI
F
MAP2 GFAP mCherry DAPI
100 μm
100 μm

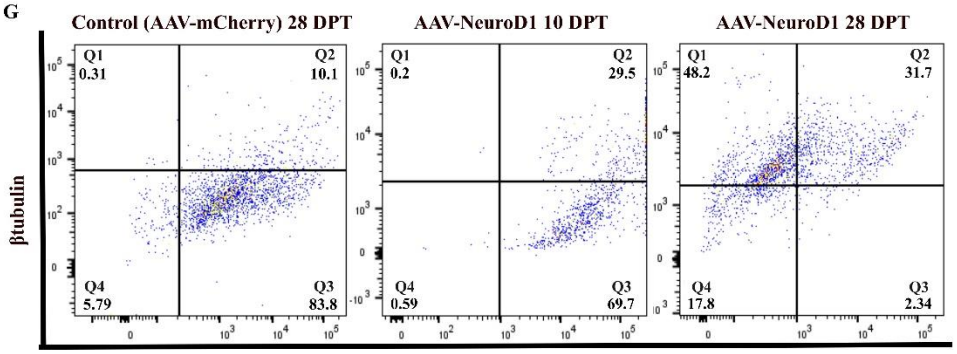
G
Control (AAV-mCherry) 28 DPT
AAV-NeuroD1 10 DPT
AAV-NeuroD1 28 DPT
βtubulin
mCherry
Q1 0.31
Q2 10.1
Q4 5.79
Q3 83.8
Q1 0.2
Q2 29.5
Q4 0.59
Q3 69.7
Q1 48.2
Q2 31.7
Q4 17.8
Q3 2.34

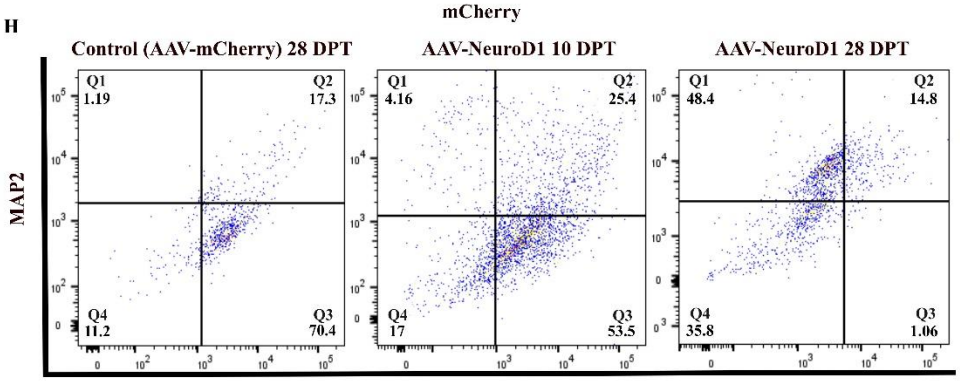
H
Control (AAV-mCherry) 28 DPT
AAV-NeuroD1 10 DPT
AAV-NeuroD1 28 DPT
MAP2
mCherry
Q1 1.19
Q2 17.3
Q4 11.2
Q3 70.4
Q1 4.16
Q2 25.4
Q4 17
Q3 53.5
Q1 48.4
Q2 14.8
Q4 35.8
Q3 1.06

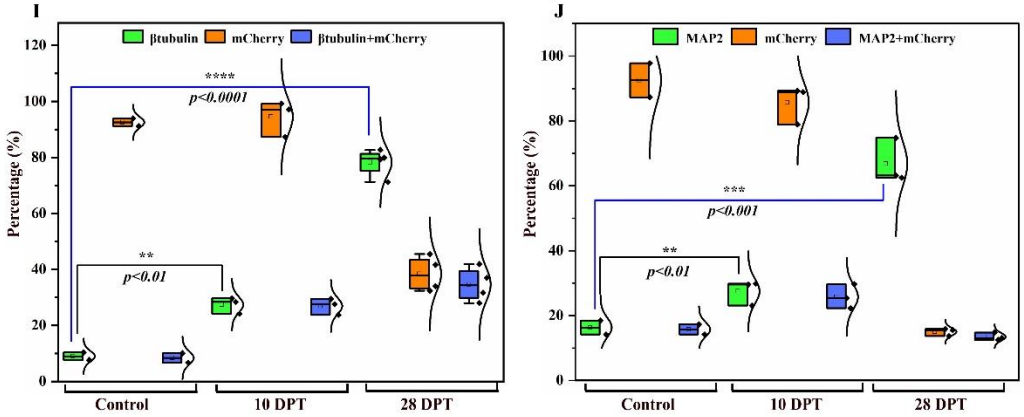
I
βtubulin mCherry βtubulin+mCherry
Percentage (%)
****
p<0.0001
**
p<0.01
Control
10 DPT
28 DPT
J
MAP2 mCherry MAP2+mCherry
Percentage (%)
***
p<0.001
**
p<0.01
Control
10 DPT
28 DPT

Figure 5.3. *In vitro* direct reprogramming of astrocytes to induced neurons (iN) 10- and 28-days post transduction (DPT). (A-D) A representative image of astrocytes transduced with AAV-NeuroD1 or **(E, F)** empty vector control, AAV-mCherry and stained with transduction efficiency marker (red), astrocytic protein GFAP (yellow), neuronal markers β3 tubulin or MAP2 (green), and DAPI (blue). **(A, B)**, After 10 DPT significant increase in the population of cells expressing the neural lineage marker β tubulin and MAP2 (green) was observed, further increasing by 28 DPT. **(E, F)** Representative images of control culture transduced with empty vector showing no altered morphology of the cultured astrocytes. **(G, H)** Representative FACS plots for DJ gfaABC1D-NeuroD1-mCherry and DJ gfaABC1D-mCherry transduced astrocyte cultures showing proportions of mCherry+, β3 tubulin+ or MAP2+ populations. n=3-5 independent cultures/group. **(I, J)** Quantification of mCherry+, β3 tubulin+ and MAP2+ cells in culture. Data represents Mean + SEM, *$p < 0.05$; **$p < 0.01$; ***$p < 0.001$, ****$p < 0.0001$. Scale bar= 100µm.

5.4.2 *In vitro* conversion of human astrocytes to neuronal cells

With confirmation of efficient astrocyte to neuron reprogramming in murine primary astrocytes, we next investigated the capacity of the AAV-NeuroD1 vector to transdifferentiate human astrocytes, human brain progenitor-derived astrocytes, as well. After 7 days in culture, confluent human astrocytes were transduced with DJ gfaABC1D-NeuroD1-mCherry (AAV-NeuroD1) or the control DJ gfaABC1D-mCherry (AAV-mCherry). T 10 DPT, 31.9 ± 2.1% and 34.1 ± 2.9% of mCherry positive cells were positive for β3-tubulin and MAP, respectively **(Figure 5.4A, B)**.

Consistent with the expected reduction in cell proliferation and survival rate of converted cells under culture conditions, the cell numbers in cultures that received NeuroD1 transduction were drastically less than that in control cultures transduced by the empty vector where astrocytes continued to proliferate

(Figure 5.4

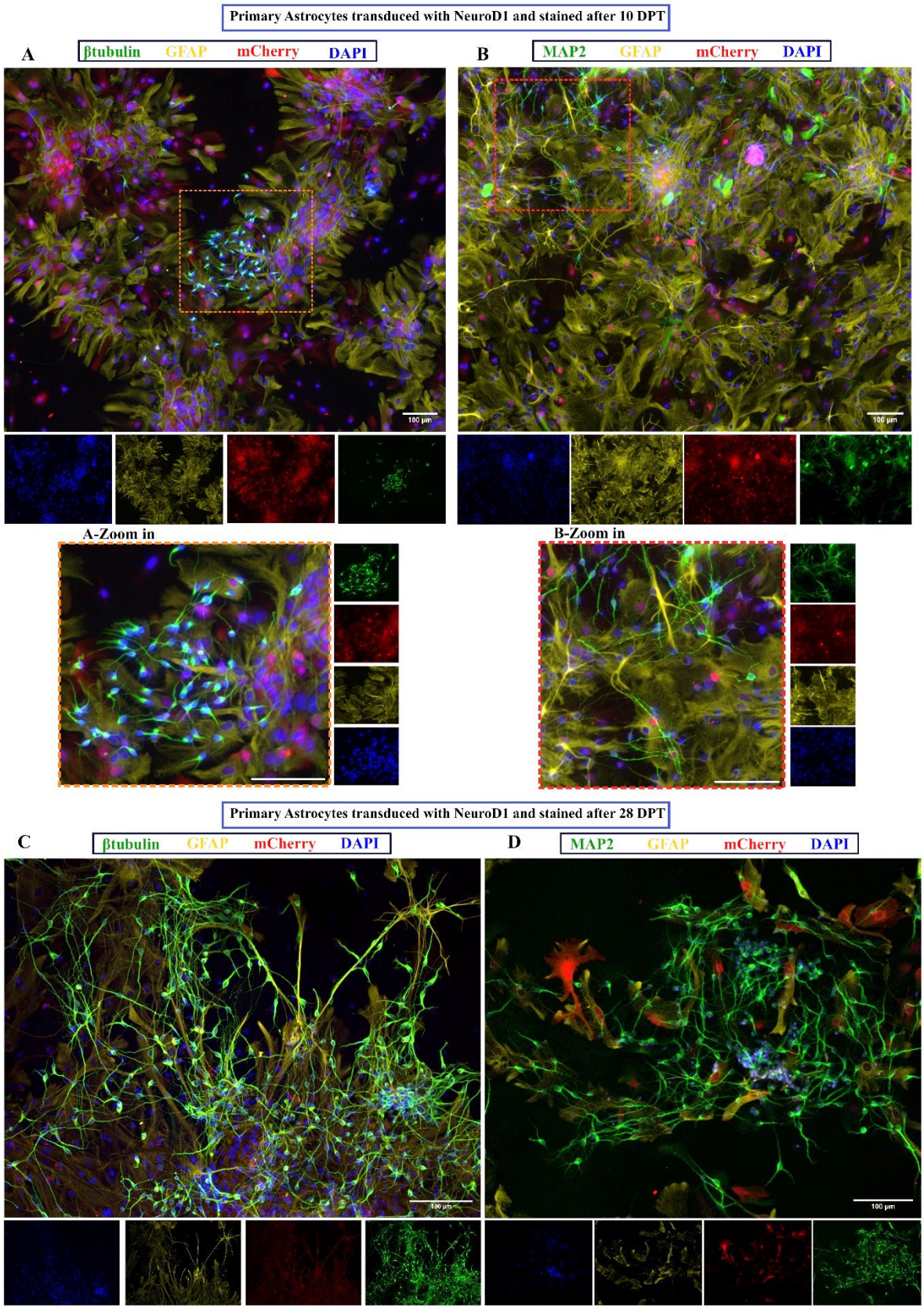
Primary Astrocytes transduced with NeuroD1 and stained after 10 DPT
A
βtubulin GFAP mCherry DAPI
B
MAP2 GFAP mCherry DAPI
100 µm
100 µm
A-Zoom in
B-Zoom in
Primary Astrocytes transduced with NeuroD1 and stained after 28 DPT
C
βtubulin GFAP mCherry DAPI
D
MAP2 GFAP mCherry DAPI
100 µm
100 µm

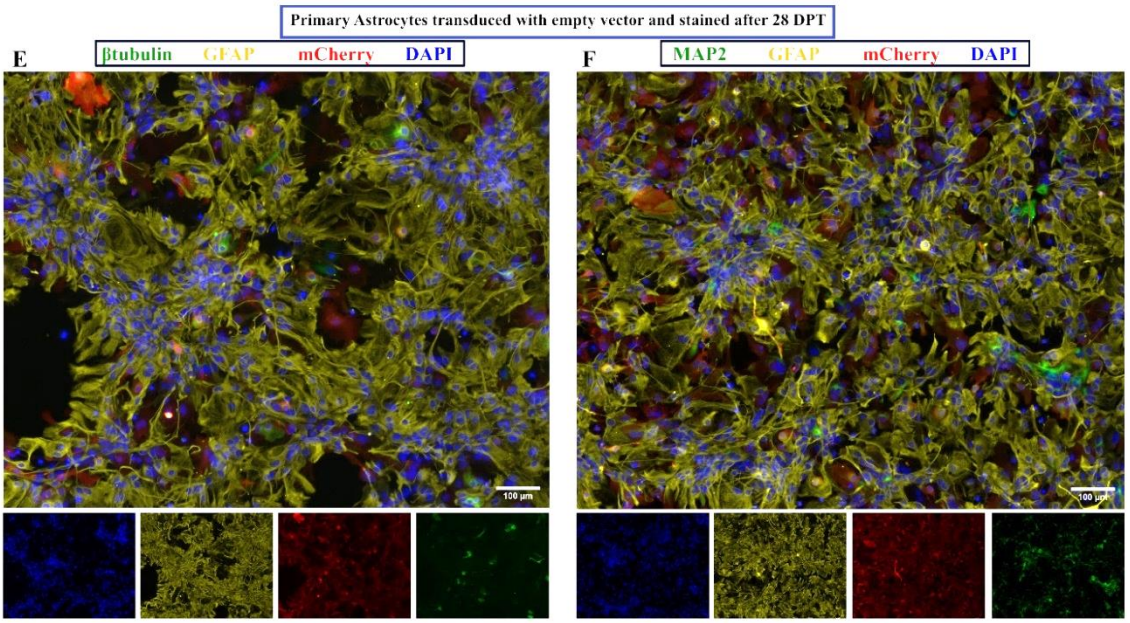
Primary Astrocytes transduced with empty vector and stained after 28 DPT
E
βtubulin GFAP mCherry DAPI
F
MAP2 GFAP mCherry DAPI
100 μm
100 μm

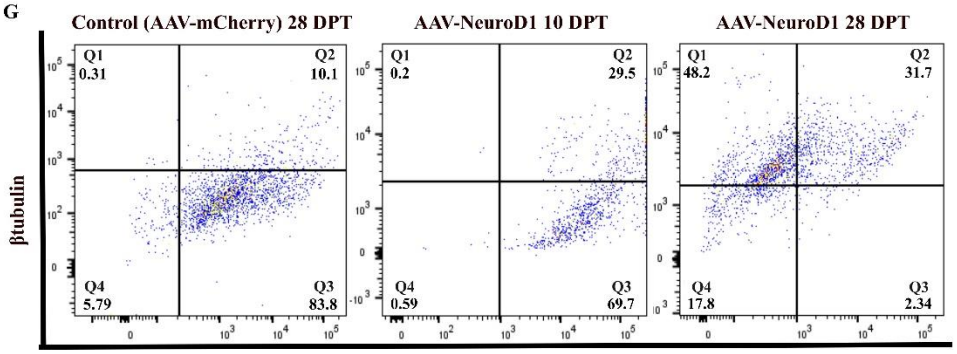
G
Control (AAV-mCherry) 28 DPT
AAV-NeuroD1 10 DPT
AAV-NeuroD1 28 DPT
βtubulin
mCherry
Q1 0.31
Q2 10.1
Q4 5.79
Q3 83.8
Q1 0.2
Q2 29.5
Q4 0.59
Q3 69.7
Q1 48.2
Q2 31.7
Q4 17.8
Q3 2.34

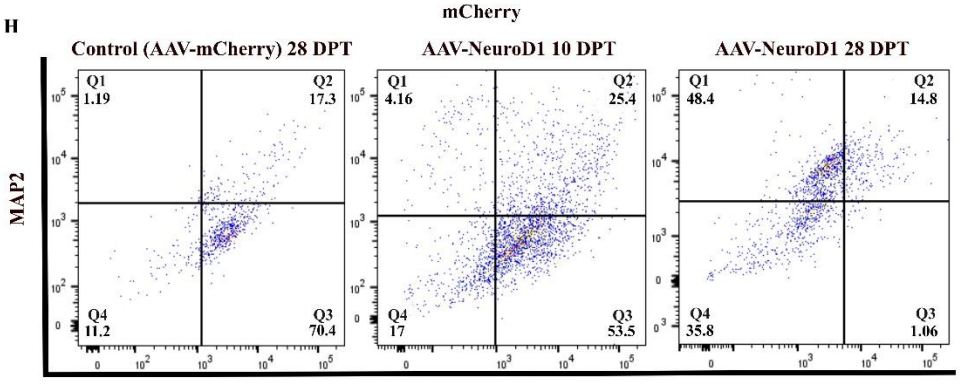
H
Control (AAV-mCherry) 28 DPT
AAV-NeuroD1 10 DPT
AAV-NeuroD1 28 DPT
MAP2
mCherry
Q1 1.19
Q2 17.3
Q4 11.2
Q3 70.4
Q1 4.16
Q2 25.4
Q4 17
Q3 53.5
Q1 48.4
Q2 14.8
Q4 35.8
Q3 1.06

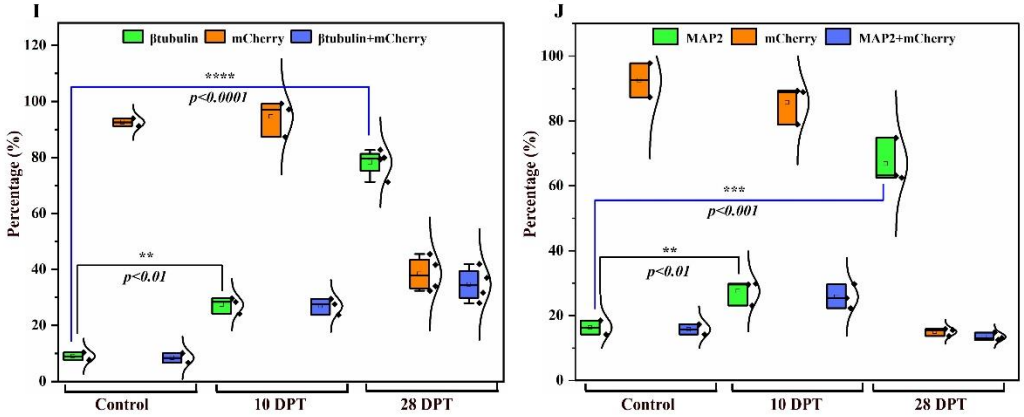
I
βtubulin mCherry βtubulin+mCherry
Percentage (%)
****
p<0.0001
**
p<0.01
Control
10 DPT
28 DPT
J
MAP2 mCherry MAP2+mCherry
Percentage (%)
***
p<0.001
**
p<0.01
Control
10 DPT
28 DPT

Figure 5.3E, F). Furthermore, as before, transduction with empty vector did not exhibit any alterations to astrocytes morphology (Figure 5.4

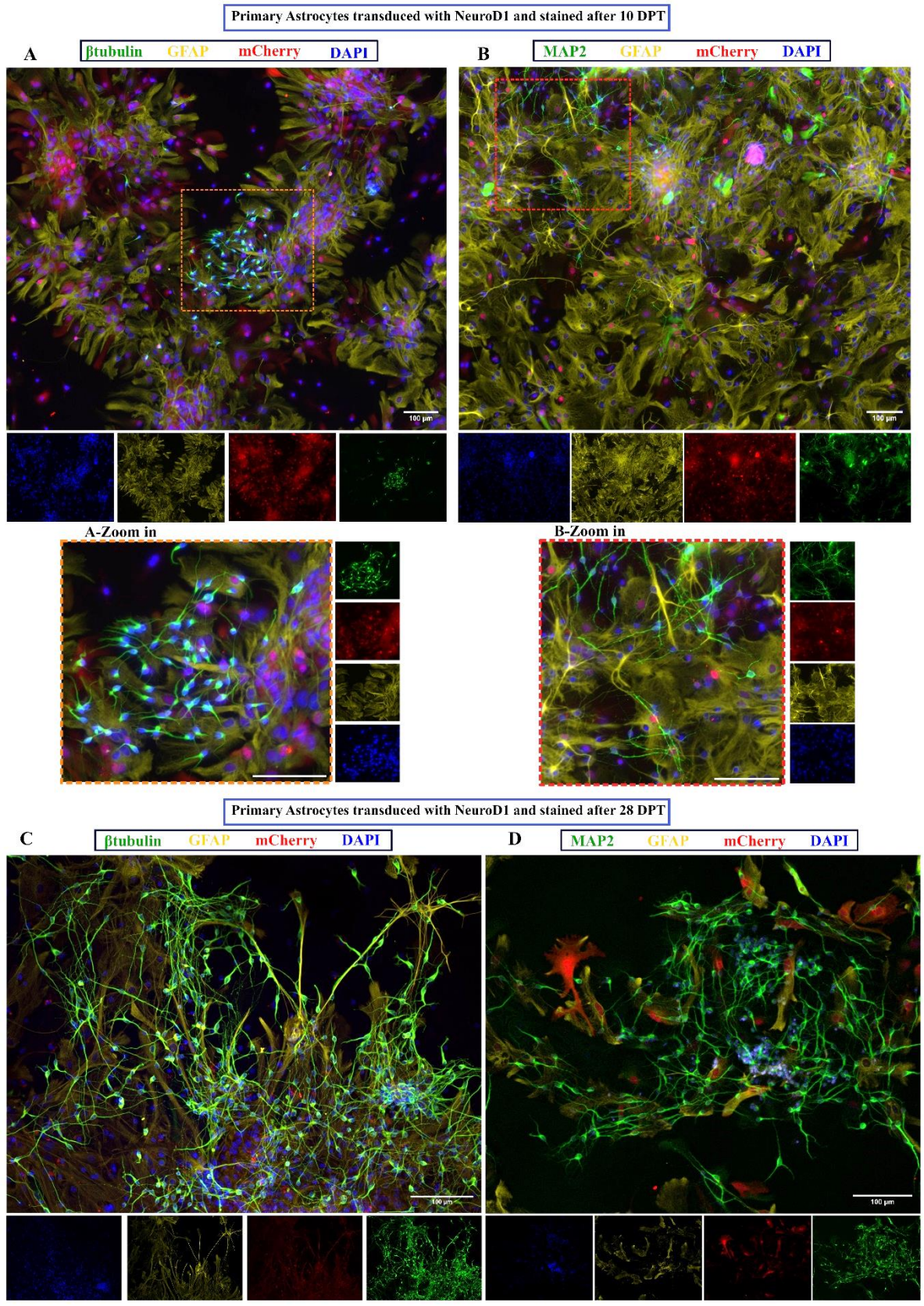

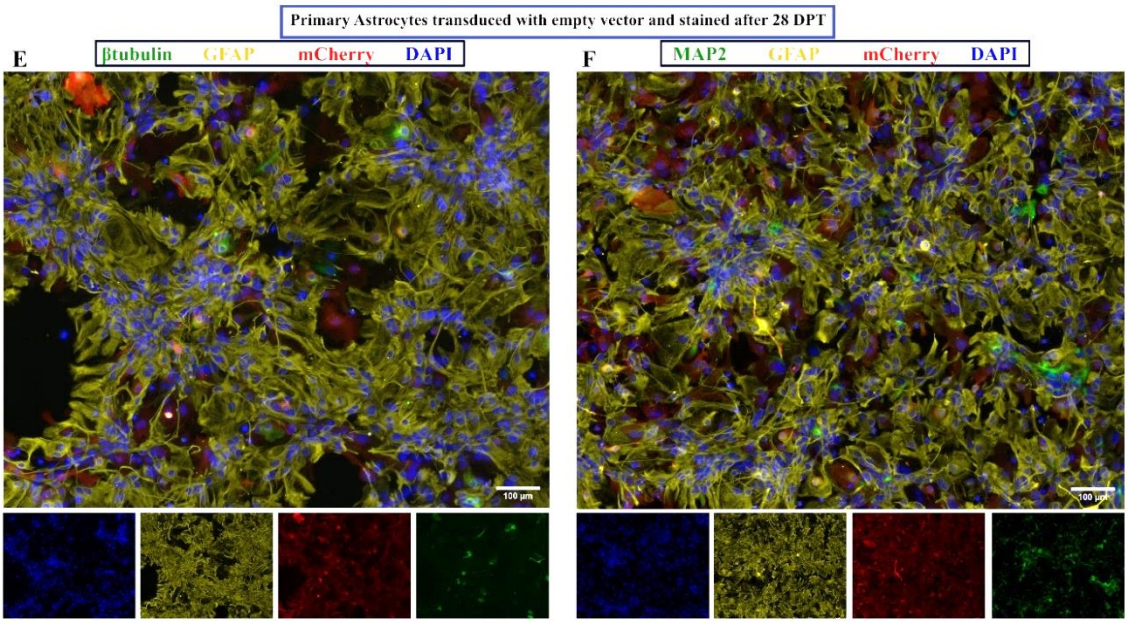
Primary Astrocytes transduced with empty vector and stained after 28 DPT
E
βtubulin GFAP mCherry DAPI
F
MAP2 GFAP mCherry DAPI
100 μm
100 μm

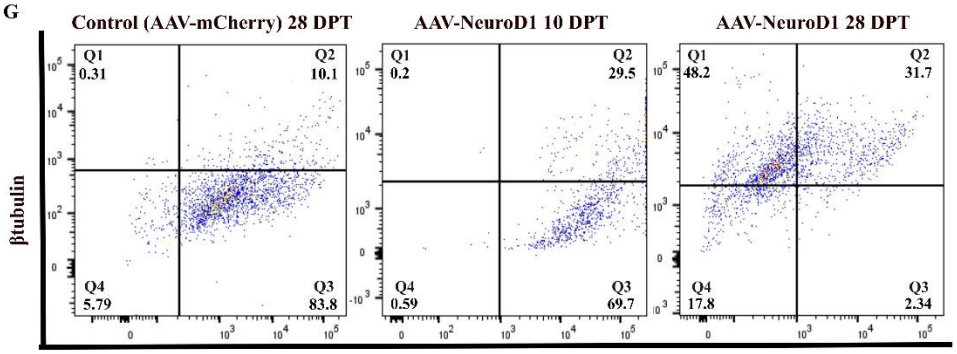
G
Control (AAV-mCherry) 28 DPT
AAV-NeuroD1 10 DPT
AAV-NeuroD1 28 DPT
βtubulin
mCherry
Q1 0.31
Q2 10.1
Q4 5.79
Q3 83.8
Q1 0.2
Q2 29.5
Q4 0.59
Q3 69.7
Q1 48.2
Q2 31.7
Q4 17.8
Q3 2.34

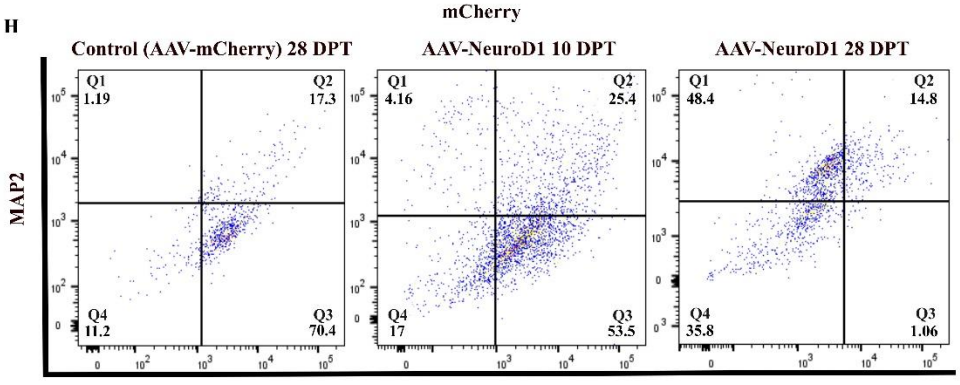
H
Control (AAV-mCherry) 28 DPT
AAV-NeuroD1 10 DPT
AAV-NeuroD1 28 DPT
MAP2
mCherry
Q1 1.19
Q2 17.3
Q4 11.2
Q3 70.4
Q1 4.16
Q2 25.4
Q4 17
Q3 53.5
Q1 48.4
Q2 14.8
Q4 35.8
Q3 1.06

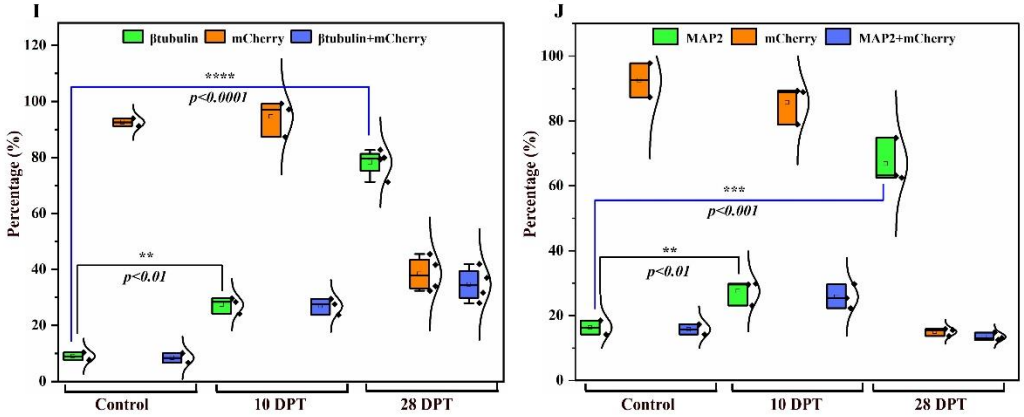
I
βtubulin mCherry βtubulin+mCherry
Percentage (%)
****
p<0.0001
**
p<0.01
Control
10 DPT
28 DPT
J
MAP2 mCherry MAP2+mCherry
Percentage (%)
***
p<0.001
**
p<0.01
Control
10 DPT
28 DPT

Figure 5.3**E, F)**. By 28 DPT, 76.6 ± 3.2% were positive for β3-tubulin and 57.9 ± 8.6% of cells were positive for MAP2 **(Figure 5.4G-H)**.

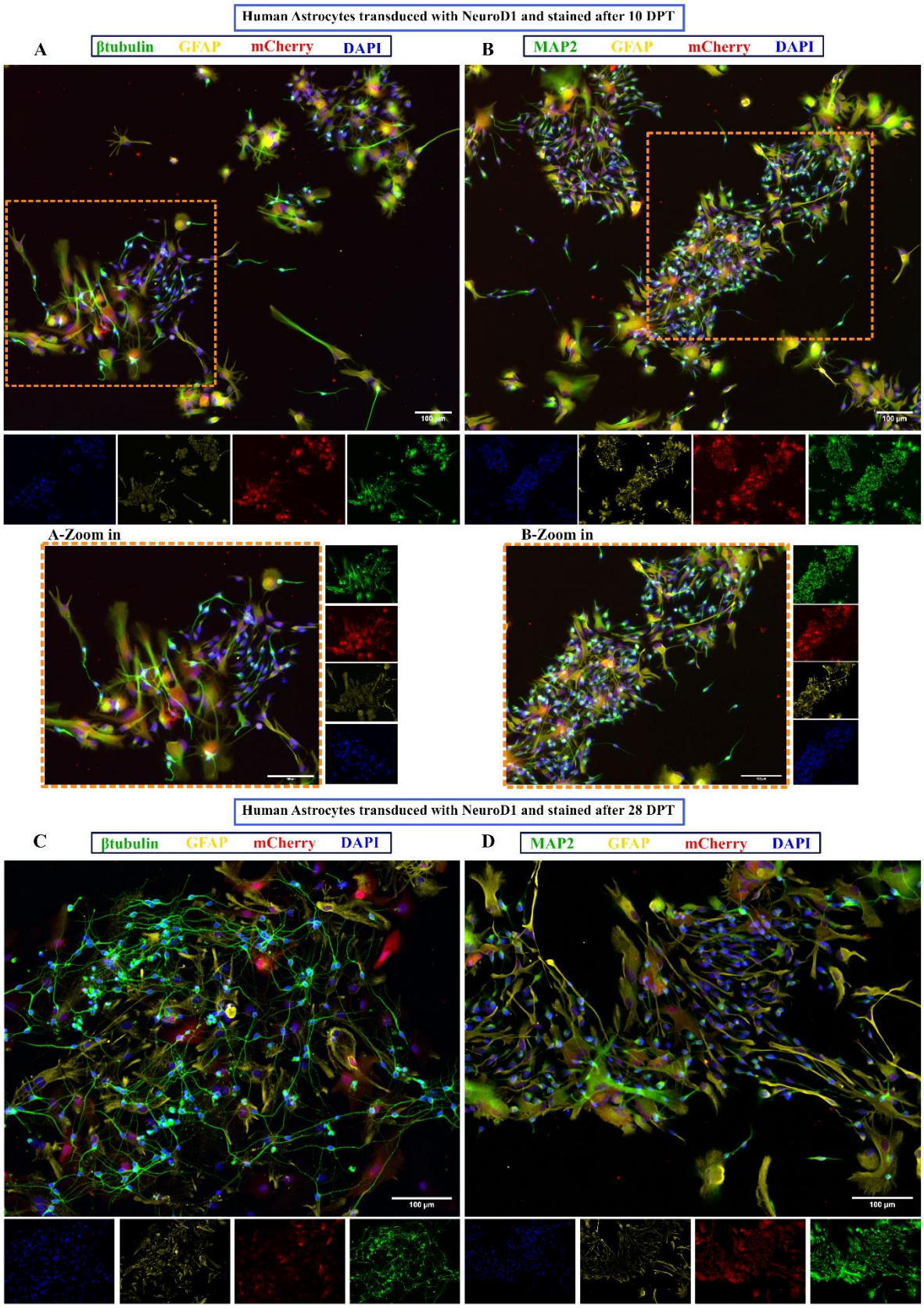
Human Astrocytes transduced with NeuroD1 and stained after 10 DPT
A
βtubulin GFAP mCherry DAPI
B
MAP2 GFAP mCherry DAPI
100 µm
100 µm
A-Zoom in
B-Zoom in
Human Astrocytes transduced with NeuroD1 and stained after 28 DPT
C
βtubulin GFAP mCherry DAPI
D
MAP2 GFAP mCherry DAPI
100 µm
100 µm

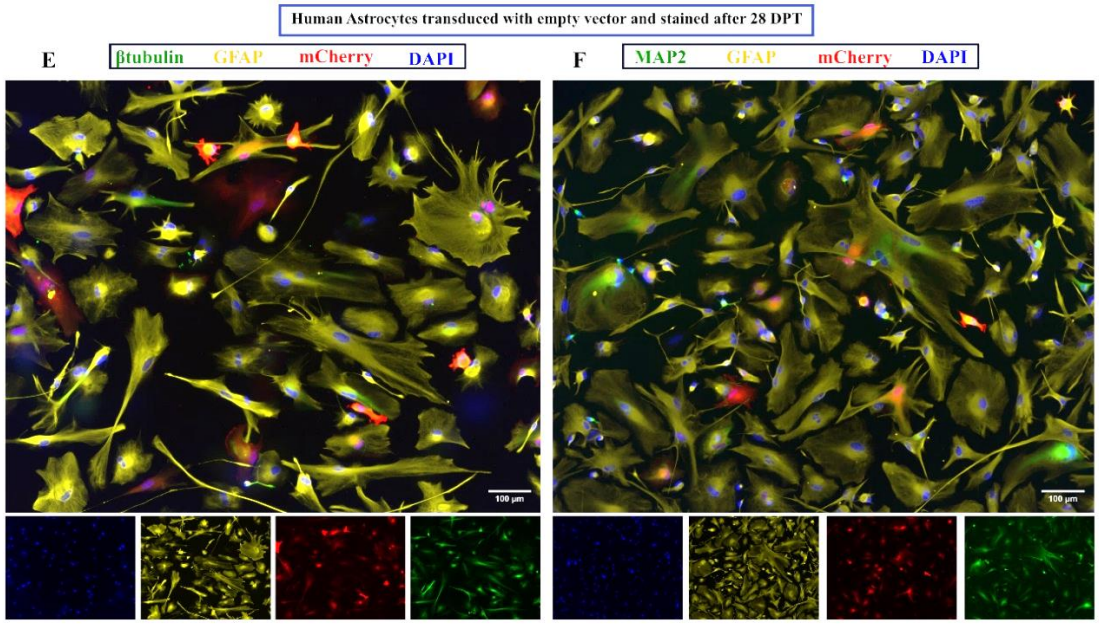
Human Astrocytes transduced with empty vector and stained after 28 DPT
E
βtubulin GFAP mCherry DAPI
F
MAP2 GFAP mCherry DAPI
100 μm
100 μm

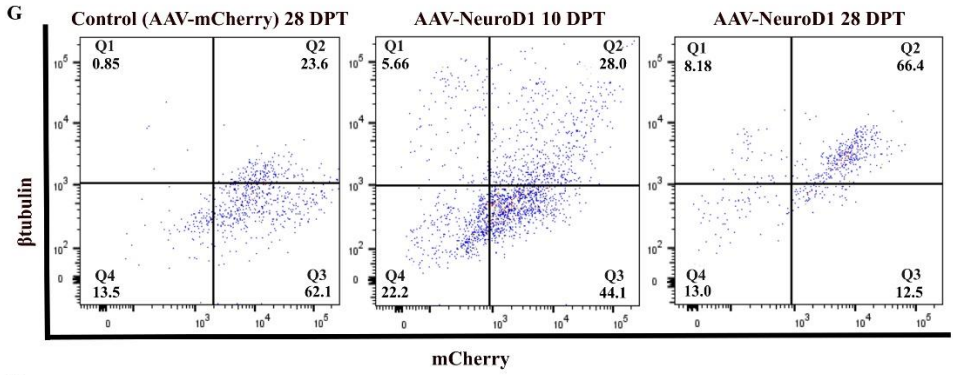
G
Control (AAV-mCherry) 28 DPT
AAV-NeuroD1 10 DPT
AAV-NeuroD1 28 DPT
βtubulin
mCherry
Q1 0.85
Q2 23.6
Q4 13.5
Q3 62.1
Q1 5.66
Q2 28.0
Q4 22.2
Q3 44.1
Q1 8.18
Q2 66.4
Q4 13.0
Q3 12.5

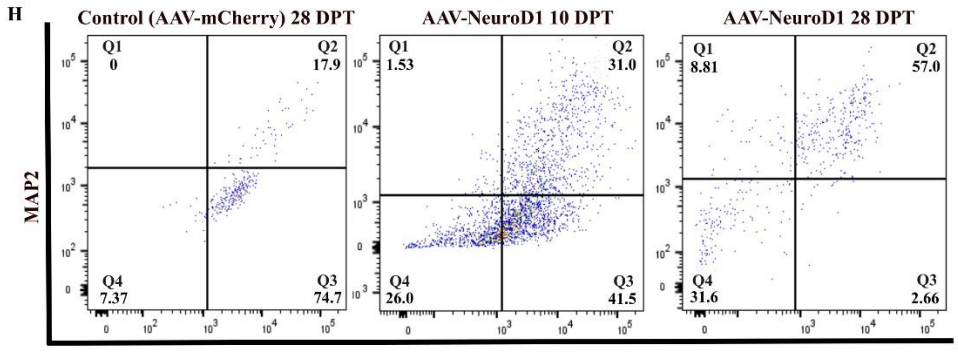
H
Control (AAV-mCherry) 28 DPT
AAV-NeuroD1 10 DPT
AAV-NeuroD1 28 DPT
MAP2
mCherry
Q1 0
Q2 17.9
Q4 7.37
Q3 74.7
Q1 1.53
Q2 31.0
Q4 26.0
Q3 41.5
Q1 8.81
Q2 57.0
Q4 31.6
Q3 2.66

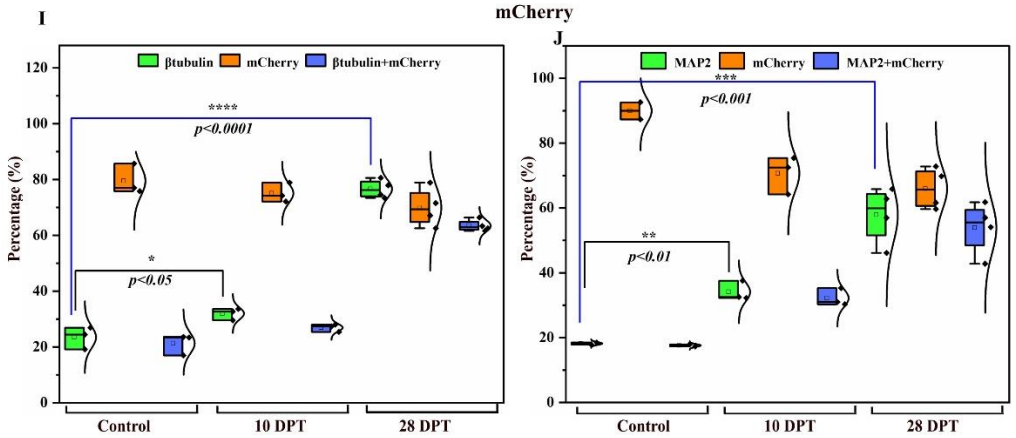
I
βtubulin mCherry βtubulin+mCherry
Percentage (%)
****
p<0.0001
*
p<0.05
Control
10 DPT
28 DPT
J
MAP2 mCherry MAP2+mCherry
Percentage (%)
***
p<0.001
**
p<0.01
Control
10 DPT
28 DPT

Figure 5.4. *In vitro* trans-differentiation of human astrocytes to induced neurons (iN) at 10/ and28 DPT. (A-D) A representative image of human astrocytes transduced with AAV-NeuroD1 or **(E, F)** empty vector control, AAV-mCherry and stained with transduction efficiency marker mCherry (red), astrocytic protein GFAP (yellow), neuronal markers β3 tubulin or MAP2 (green), and DAPI (blue). **(A, B)**, After 10 DPT a significant increase in the proportion of cells expressing β tubulin and MAP2 (green) was observed, further increasing by 28 DPT. **(E, F)** Representative images of control culture transduced with empty vector showing no altered morphology of the cultured astrocytes. **(G, H)** Representative FACS plots for DJ gfaABC1D-NeuroD1-mCherry and DJ gfaABC1D-mCherry transduced astrocyte cultures showing proportions of mCherry+, β3 tubulin+ or MAP2+ populations. n=3-5 independent cultures/group. **(I, J)** Quantification of mCherry+, β3 tubulin+ and MAP2+ cells in culture. Data represents Mean + SEM, *$p < 0.05$; **$p < 0.01$; ***$p < 0.001$, ****$p < 0.0001$. Scale bar=100 μm.

5.4.3 Reprogrammed primary astrocytes and human astrocytes were able to fire action potentials

Astrocytes are considered to be electrically non-excitable cells, as they do not propagate or fire sodium-potassium driven action potentials along their processes[262,263]. To provide evidence that the reprogramming process had generated functional neurons from reactive astrocytes, at 28DPT we performed whole-cell electrophysiological recording to determine if iNs could produce action potentials. Cells were probed for their capacity to generate action potentials when stimulated and spontaneous calcium activity was also recorded. Cells had resting membrane potentials resembling that of typical mature neurons (i.e., approximately between -60 and -80 mV; **Figure 5.5A, G**). At resting membrane potential, spontaneous calcium activity was also observed, indicating intrinsic excitability often observed in immature neurons **(Figure 5.5B, H)**. In current-clamp mode, gradually increasing membrane depolarisation steps triggered the firing of action potentials in cells transduced from primary astrocytes (PA; n=8 cells out of 8 cells recorded) **(Figure 5.5C, D)** and human astrocytes (HA; n=4 cells out of 6 cells recorded) **(Figure 5.5I, J)**. Cells also displayed typical action potential kinetics, including a threshold near -20 to -30 mV **(Figure 5.5E, K)** and an amplitude of 30 mV or larger **(Figure 5.5F, L)**, as well as appropriate rise and decay times (i.e., < 2 ms; data not shown). Recorded cells were visualized by the infusion of Neurobiotin and stained positive for NeuN and mCherry **(Figure 5.5M, N)**, to confirm their neuronal identity.

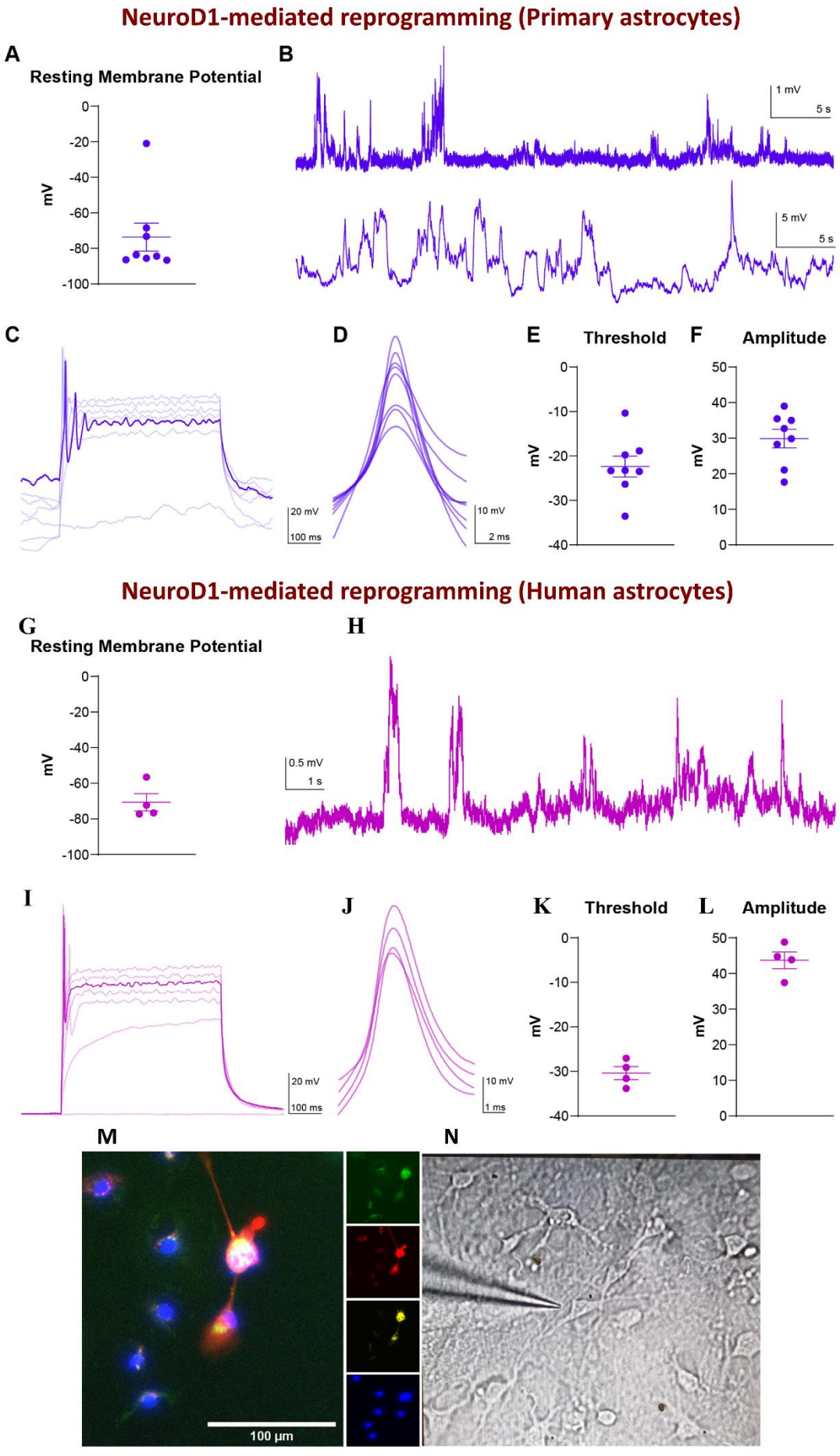
NeuroD1-mediated reprogramming (Primary astrocytes)
A
Resting Membrane Potential
mV
0
-20
-40
-60
-80
-100
B
1 mV
5 s
5 mV
5 s
C
20 mV
100 ms
D
10 mV
2 ms
E
Threshold
mV
0
-10
-20
-30
-40
F
Amplitude
mV
50
40
30
20
10
0
NeuroD1-mediated reprogramming (Human astrocytes)
G
Resting Membrane Potential
mV
0
-20
-40
-60
-80
-100
H
0.5 mV
1 s
I
20 mV
100 ms
J
10 mV
1 ms
K
Threshold
mV
0
-10
-20
-30
-40
L
Amplitude
mV
50
40
30
20
10
0
M
100 µm
N

Figure 5.5. The ND1-mediated Primary astrocytes (PA) and human astrocytes (HA) reprogramming was monitored *in vitro* and functionally characterised. (A, G) Resting membrane potential for PA and HA, respectively. **(B, H)** Representative examples of spontanous calcium activity in recorded cells. **(C, I)** Action potential and spikelet resulting from 25 pA current steps in cell. **(D, J)** Overlaid action potentials from all recorded cells. **(E, K)** Action potential threshold. **(F, L)** Amplitude of action potential (from threshold to peak). **(M, N)** A representative image of recorded cells visualized by the infusion of Neurobiotin (yellow) (positive for mCherry (red) and NeuN (green)).

5.4.4 SAP hydrogels prolongs AAV-NeuroD1 release

To mimic the physical properties of the brain, substrate stiffness/elasticity are critical factors in the development of hydrogels. The fabricated hydrogel demonstrated viscoelastic behaviour (G'>G") and mechanical properties within the range of rodent brain stiffness **(Figure 5.6A)**. Moreover, shear-tinning behaviour of hydrogel was confirmed through continuous step-strain measurement **(Figure 5.6B).** This behavior is indicative of the sol-gel transformation of the Fmoc-DDIKVAV hydrogel in response to the applied shear force. Based on the mesh size calculated using **equation (1)**, the mesh size of Fmoc-DDIKVAV was calculated to be 21.2 ± 2.5 nm **(Figure 5.6C)** which correlates with our previous findings a nanopore size of ~22 nm as measured via Small Angle X-Ray Scattering (SAXS). This measure is important for nutrient diffusion and can be considered in terms of the distance between structures and should not be confused with micropore size which is seen via TEM[264]. It is well known that the AAV is a small non-enveloped virus with a size of 24-26 nm[252],[265]. When the payload size is larger than the mesh size of hydrogel, the payload is physically constrained as it becomes incorporated inside the network during shear thinning and entrapped upon gelation. In this case, the release of the immobilized drug/payload can happen through diffusion, network degradation, swelling, or deformation of the network[266]. Previously we have shown that in the focal ischemia model in rats, within 9 months post Fmoc-DDIKVAV implantation, there was some evidence of fibres within the brain slice, but the majority of the hydrogel had degraded[267]. Moreover, in another study, we have shown that after 9 months post-implantation of SAP hydrogel no detrimental impact was observed on host immune response[268]. However, several factors can dictate their degradation rate such as mechanical properties, molecular weight, implant size, pore density,

and the degree of cross-linking degradability[269]. Therefore, it was anticipated that the SAP hydrogel has multiple physicochemical properties to moderate the sustained release for AAV. To demonstrate the controlled release of AAV, the DJ gfaABC1D-NeuroD1-mCherry release profile was monitored for a period of 5 days using qPCR method. As expected, the results revealed the sustained release of the AAV from SAP hydrogel **(Figure 5.6D)**.

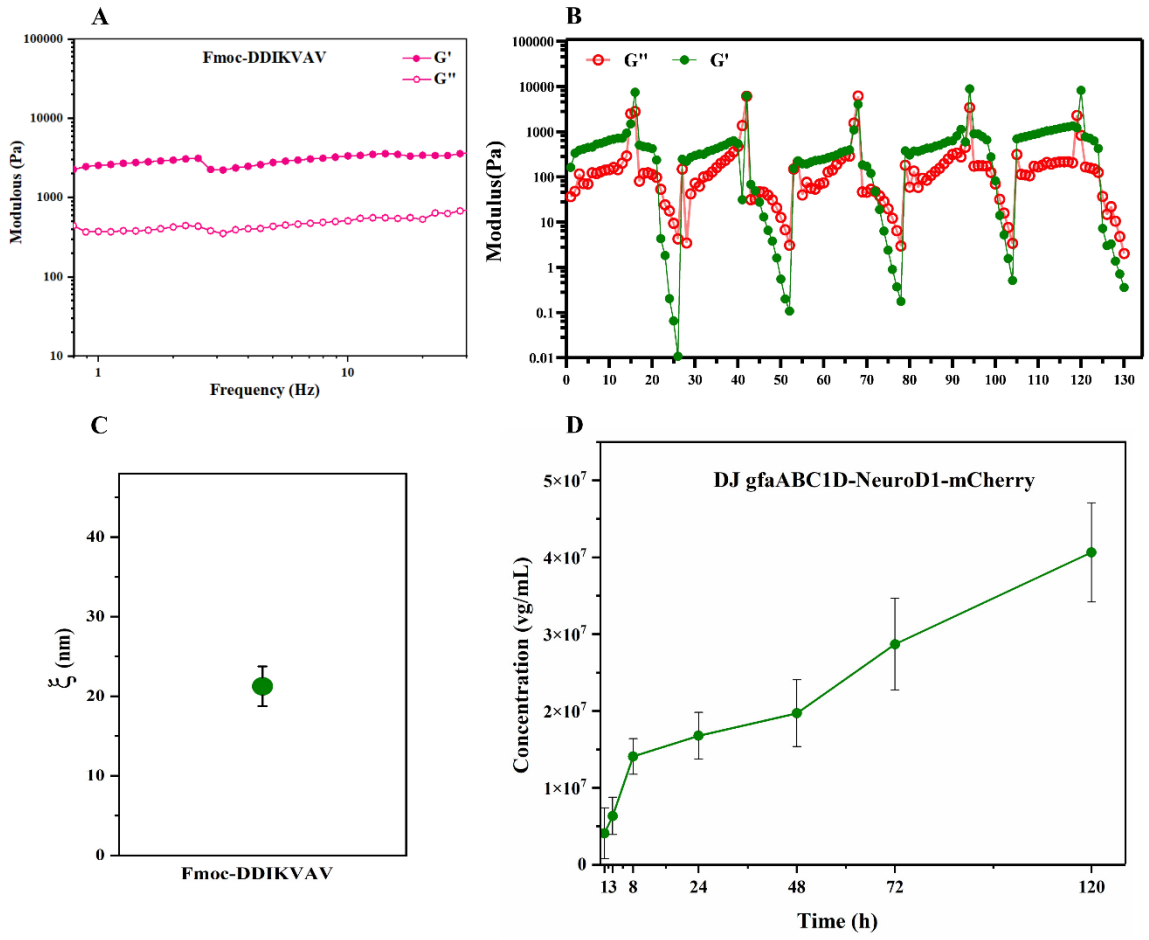

Figure 5.6. Fmoc-DDIKVAV SAP hydrogel show sheat-thinning properties and prolongs AAV-NeuroD1 release. (A) Rheological analysis confirms viscoelastic behaviour of all fabricated hydrogels confirmed with storage modulus (G′) greater than loss modulus (G″). **(B)** shear thinning properties of the DDIKVAV confirms sol-gel transition upon injection and during AAV incorporation. **(C)** Mesh size (ξ) (nm) value of the Fmoc-DDIKVAV calculated based on the equation of the theory of rubber elasticity. **(D)** Release profile of the DJ gfaABC1D-NeuroD1-mCherry from SAP hydrogel showing the concentration of AAV released from hydrogel at any given timepoints.

5.4.5 AAV dosage optimisation in a needle stick injury model

AAVs have shown outstanding potential in various clinical trials due to its relatively low immunogenicity, however, since AAV particles can be produced in very high titre, as high as

10^{13}–10^{14} vg/ml, extra caution should be taken. Evidence has shown that AAV dosing is critical when considering how much AAV should be administered *in vivo*. In the brain it is even more important to use minimal effective dosing to avoid tissue damage. The optimal dosage of AAV delivery can be defined through a series of dose-finding experiments[157] to confirm avoidance of toxicity and associated brain damage.

In addition to examining different AAV dosages, here an SAP hydrogel was additionally adopted to provide a lower and more protracted payload delivery. Mice were injected with different ratio of DJ gfaABC1D-mCherry and Fmoc-DDIKVAV SAP hydrogel. All animals (except virus neat (AAV) 0.5 µL) received a total volume of 1µL/injection. The groups included SAP alone **(Figure 5.7A)**, AAV (AAV-mCherry alone, **Figure 5.7B)**, AAV:SAP high dose (1:1, **Figure 5.7C)**, AAV:SAP medium dose (1:3, **Figure 5.7D)**, and SAP:AAV low dose (1:10, **Figure 5.7E)**.

After 10 days post implantation high levels of GFAP immunoreactivity were observed around the injection site, typical of astrocyte activation after injury. Red fluorescent protein (RFP) viral expression (to visualise mCherry expression) was localized to the injection site, with an obvious concentration/dose effect. The results indicated that the high dose of AAV:SAP was optimal as it provided the maximum transduction without evident toxicity (i.e., non-specific damage to the host tissue or elevated GFAP+ reactive astrocytic response), **Figure 5.7F**. Therefore, the subsequent *in vivo* experiment was performed with 1:1 SAP:AAV ratio. These findings also confirmed the activity of AAV after release from hydrogel, reflected in the capability to transduce the host cells (i.e., mCherry immunolabeling).

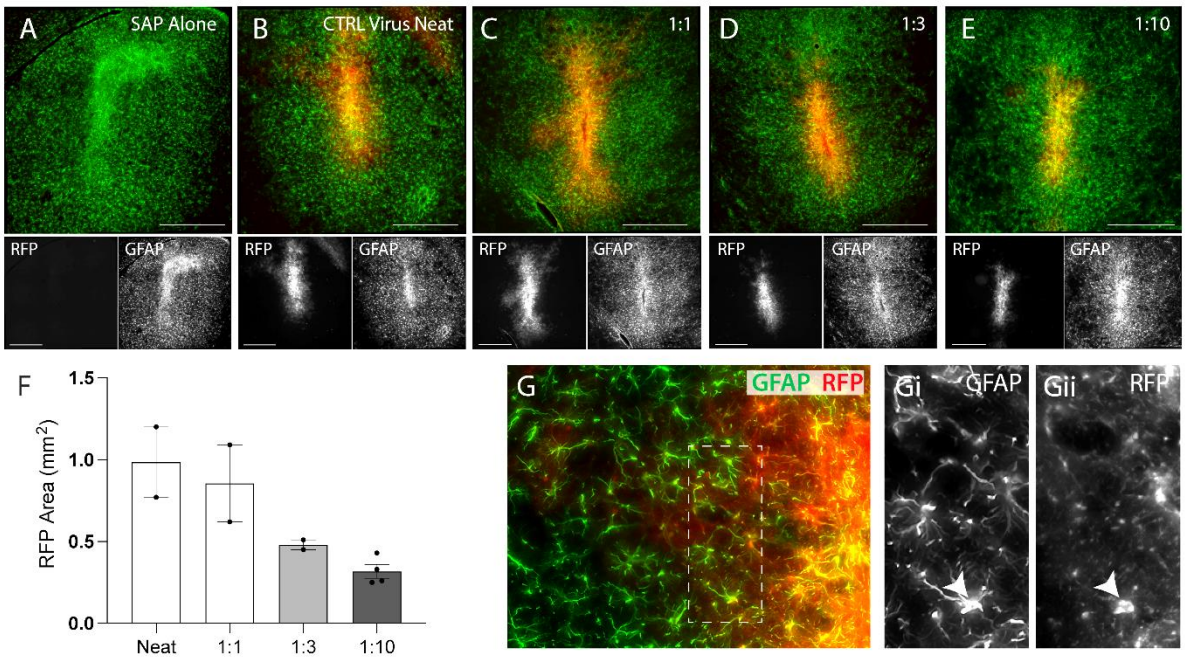

Figure 5.7. Representative images at the AAV-mCherry injection site illustrating transduced cells (red) co-labeled with astrocytic marker GFAP (green) across different ratio of SAP:AAV. Arrowheads indicate double stained cells.

5.4.6 Incorporating AAV-NeuroD1 within a SAP hydrogel sustains and confines viral delivery within the needle track

The timing of AAV injection also influences cell-type transduction[257]. Thus, it was necessary to determine the optimal treatment windows to not only transduce the astrocytes but also reprogram astrocytes at their most reactive stage. We therefore performed AAV injection to reprogram reactive astrocytes within the glial scar at 10 days post-injury for two reasons, i) astrocytes have been shown to be significantly upregulated at 10 days post trauma[27], and ii) to preferentially target astrocytes and not neural stem cells/radial glia that also express GFAP[270–272]. It has been demonstrated that there is a rapid decline in the number of migratory subependymal zone (SEZ)-derived neural stem cells/radial glia present by 7 days post trauma[273].

At 10 days post needle stick injury, mice received one of the following (1 µl) injections at the same intracerebral site: i) Saline + AAV-NeuroD1, ii) SAP + AAV-NeuroD1, iii) Saline + AAV-mCherry, iv) SAP + AAV-mCherry **(Figure 5.8A)**. In all groups the AAVs with SAP

were injected into the left brain hemisphere and AAVs with saline the right **(Figure 5.8B)**. Four weeks post viral injection (wpi), immunohistochemical analyses around the injected needle track regions were performed. AAV transduction efficiency was visualized using mCherry immunolabeling, noting increased containment of the AAV at the injection site **Figure 5.8C**.

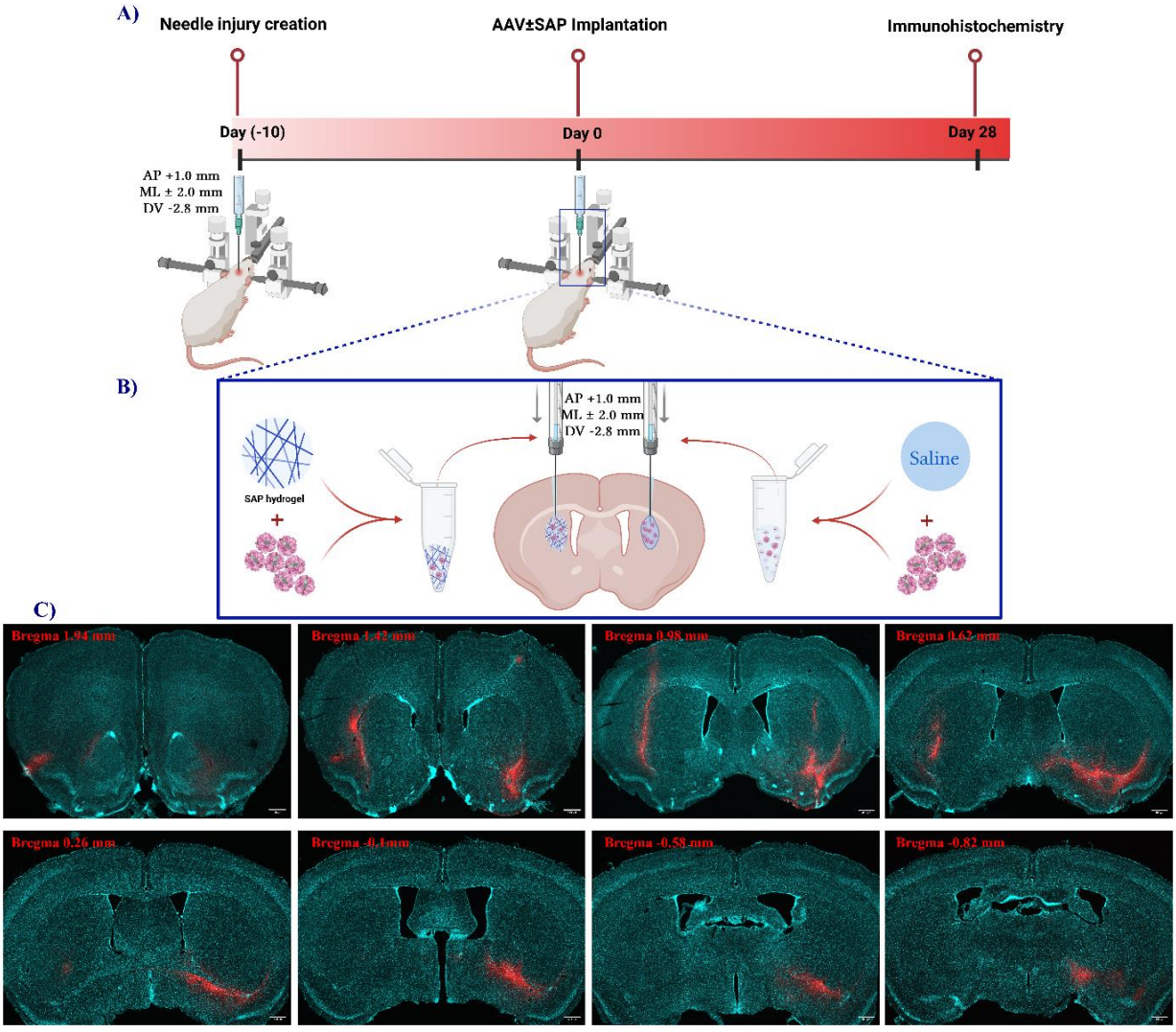

Figure 5.8. AAV distribution in the brain. A) Schematic overview of the designed experiment. **B)** AAV±SAP implantation. **C)** AAV distribution within the brain in AAV±SAP identified with mCherry positive cells (shown as red) in representative overview of different sections of a brain. Left hemisphere (AAV+SAP), Right hemisphere (AAV+Saline). Scale bar= 400 µm

5.4.7 DJ gfaABC1D-mCherry preferentially transduces astrocytes

Then, to further assess the specificity of the constructed AAV to GFAP-expressing cells, brain coronal sections injected with the control AAV-mCherry vector were examined at 28 days post implantation. As seen in **Figure 5.9A, B**, only astrocytes (GFAP+) cells were transduced with AAV (co-stained with mCherry), whereas no NeuN+ cells were stained positive for mCherry, suggesting targeted transduction of astrocytes and no neuronal leakage. In addition, to confirm that insertion of NeuroD1 TF in the AAV construct show the same pattern, cultured primary cortical neurons were transduced with AAV-NeuroD1. At 3 DPT, cells were visualised using mCherry, MAP2, GFAP, and DAPI. As demonstrated in **Figure 5.9C** almost all mCherry+ cells were immunopositive for GFAP+ but not MAP2+, suggesting targeted NeuroD1 transgene delivery in GFAP-expressing cells.

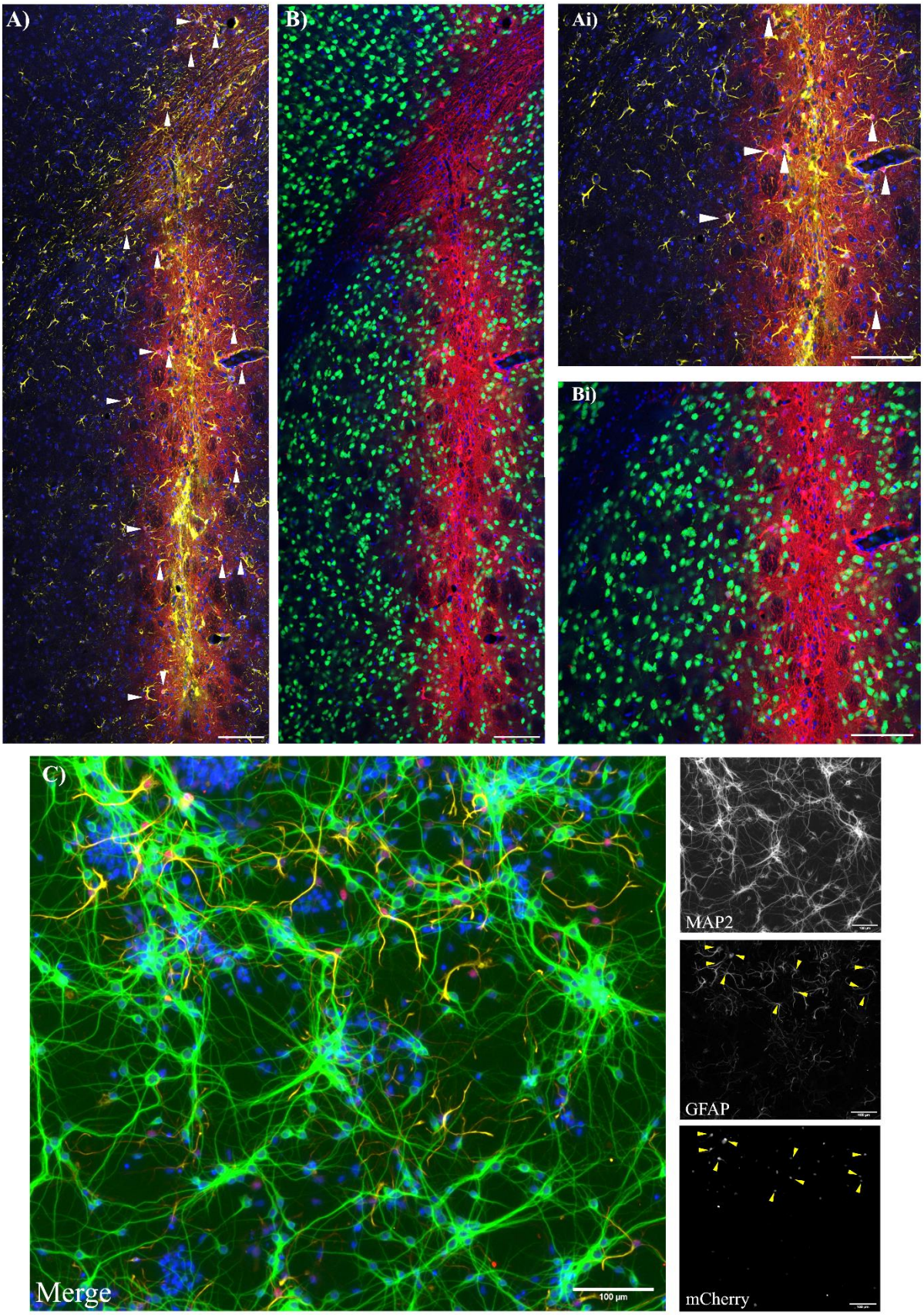

Figure 5.9. AAV-NeuroD1 transduced GFAP-expressing cells preferentially. A representative image of the core section of AAV-mCherry (control empty vector) implantation in left hemisphere. (C) cortical neurons transduced with AAV-NeuroD1 and stained at 3DPT. The coronal sections/ cortical neurons stained with

transduction efficiency marker (mCherry, red), astrocytic protein GFAP (yellow), neuronal marker NeuN (B, Bi)/ or MAP2 (C) (green), and DAPI (blue), scale bar= 400 µm **(A, B)**, 100 µm **(C)**. Some double stained cells with mCherry are indicated with arrowhead.

5.4.8 Reprogramming of reactive astrocytes reduces the glial scar after injury

An additional purpose of reprogramming reactive astrocyte into neurons is to reduce the extent of the glial scar, anticipated to also support residual neuron plasticity through colateral sprouting of axons. Seen in **Figure 5.10A,** the thickness of glial scar around the needle injury track was significantly attenuated, as described in Chapter **3- 3.15**, compared to the scar in empty vector treated groups **(Figure 5.10A, B, E)**. Moreover, the presence of SAP hydrogel did not exacerbate reactive astrogliosis. A possible concern is the adverse effect of significant astrocyte depletion in the converted area. Importantly however, such depletion was not obvious in AAV-NeuroD1injected brains, where neurons were observed to be intermingled with resident astrocytes. These observations are consistent with the notion that astrocytes are dividing cells with proliferative capability and in line with the results reported by others[27,157,260]. Furthermore, the implanted SAP hydrogel did not activate resident Iba1+ microglia **Figure 5.10C, D, F**.

The reduction of Iba-1+ cells in the AAV-NeuroD1 treated group compared to control group may be linked to a reduction in the glial scar and/or reduced size of the lesion[274], both suggestive of enhanced repair processes.

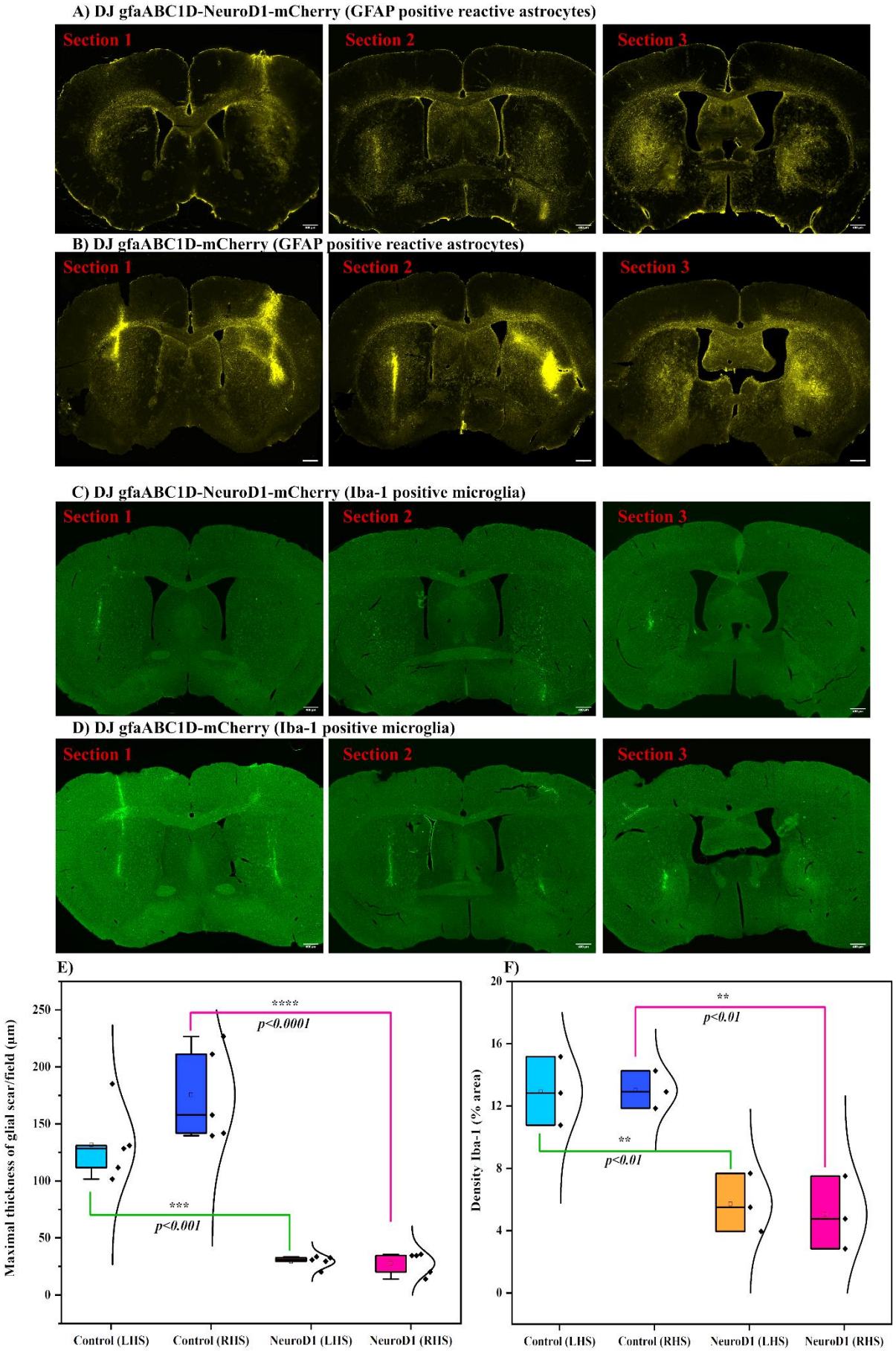
A) DJ gfaABC1D-NeuroD1-mCherry (GFAP positive reactive astrocytes)
Section 1
Section 2
Section 3
B) DJ gfaABC1D-mCherry (GFAP positive reactive astrocytes)
Section 1
Section 2
Section 3
C) DJ gfaABC1D-NeuroD1-mCherry (Iba-1 positive microglia)
Section 1
Section 2
Section 3
D) DJ gfaABC1D-mCherry (Iba-1 positive microglia)
Section 1
Section 2
Section 3
E)
Maximal thickness of glial scar/field (µm)
0
50
100
150
200
250
****
p<0.0001
***
p<0.001
Control (LHS)
Control (RHS)
NeuroD1 (LHS)
NeuroD1 (RHS)
F)
Density Iba-1 (% area)
0
4
8
12
16
20
**
p<0.01
**
p<0.01
Control (LHS)
Control (RHS)
NeuroD1 (LHS)
NeuroD1 (RHS)

Figure 5.10. Direct reprogramming of astrocytes attenuated astrogliosis and microglial activation. Inflammatory activities including astrogliosis and microglia activation were examined within and adjacent to the needle track. (A-D) Representative overview of different sections of a brain. Astrocyte accumulation or glial scar thickness from different brain sections and Iba-1 expression were examined 4 weeks post NeuroD1 and empty vector transduction. GFAP positive astrocytes (yellow) and Iba-1 positive microglia (Green) were significantly less intense within the needle track in the NeuroD1 treated mice compared to control group. The quantification data in **(E)** demonstrates a significant reduction in GFAP positive astrogliosis and **(F)** demonstrates a significant decrease in active microglia after NeuroD1 treatment. Scale bar=400 µm. ***p < 0.01, ****p < 0.001,* *****p < 0.0001*. Data are represented as mean ± SD. (n = 3-5/ per group)

5.4.9 Reprogrammed neurons transition through an immature stage

To confirm AAV-NeuroD1 mediated the conversion of astrocytes into neurons and ensure that mCherry+ neurons were not previously existing endogenous neurons, doublecortin (DCX) expressing cells, an immature stage in neuronal maturation, were examined. DCX is a microtubule associated protein broadly expressed in neuroblasts and immature neurons during development and in neurogenic regions of the adult brain[275,276], and is not associated with reactive gliosis or regenerative axonal growth[277]. Our results showed a significant expression of DCX+ cells surrounding the core of AAV-NeuroD1 injected animals **(Figure 5.11),** at 4 wpi. This observation supported the evidence of AAV-NeuroD1 inducing the reprogramming of endogenous reactive astrocytes to new neurons.

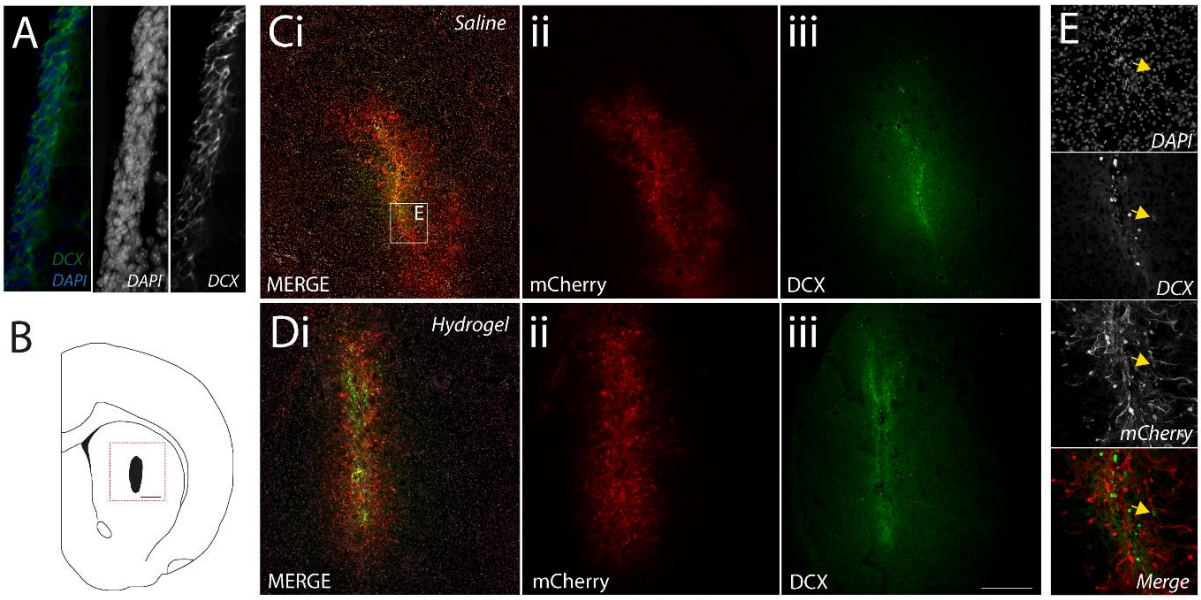

Figure 5.11. **Direct reprogramming of astrocytes give rise to DCX postive cells within the AAV-NeuroD1 injected brain. A)** DCX staining in subventricular zone (SVZ) to confirm the DCX staining. **B)** Schematic brain coronal section showing area imaged relative to injection site. **C)** Representative image of DCX/mCherry, RHS (AAV-NeuroD1+Saline). **D)** Representative image of DCX/mCherry, LHS (AAV-NeuroD1+SAP). **E)** High magnification images showing a DCX+ cell colocalized with mCherry validate that the mCherry expression silences as the cell reprograms to neuronal phenotype. Scale bar=500 µm.

5.4.10 The overall number of neurons increased within the needle track

Furthermore, we expected that the trans-differentiation of reactive astrocytes into neurons would increase the neuronal density within the injection site. Therefore, we investigated whether the overall number of neurons was greater within the NeuroD1-AAV injected regions **(Figure 5.12)**. NeuN immunostaining revealed a significant decrease (7-fold) in the size of the injury (i.e., areas within the striatum depleted of NeuN staining). The results demonstrated 7-fold increase in NeuN+ cells within the needle track in AAV-NeuroD1 treated mice compared to AAV-mCherry (control) treated group as demonstrated in **Figure 5.12E**. Moreover, the goal of this research was to provide similar efficacy at lower doses of AAV facilitated by our rationally designed hydrogel. Interestingly, here we demonstrate that AAV-NeuroD1 spatiotemporal release was aided by SAP hydrogel with the number of NeuN positive cells significantly higher compared to NeuroD1-AAV injected area without SAP hydrogel (RHS) **(Figure 5.12E).**

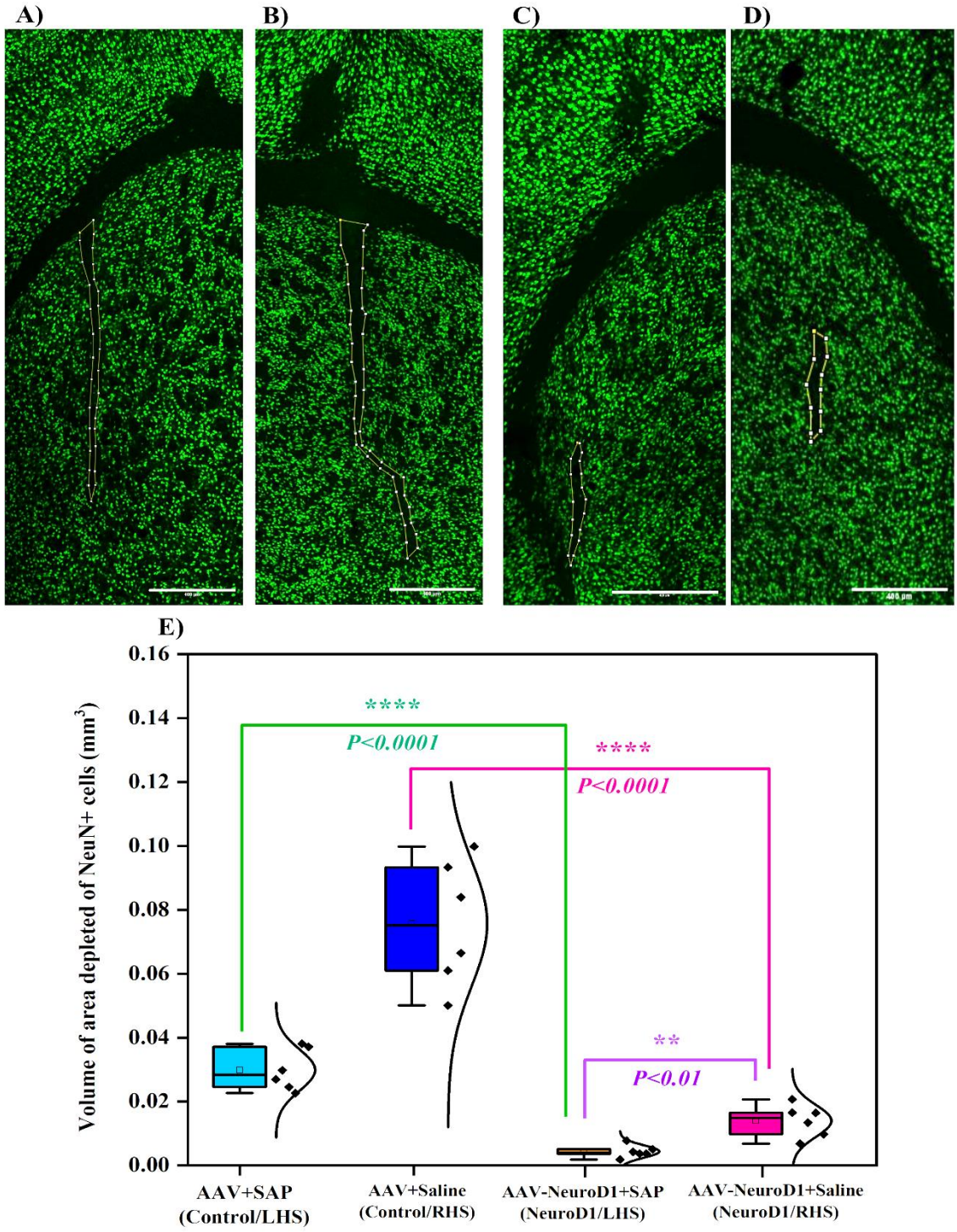

Figure 5.12. Direct reprogramming of astrocytes increases the overal number of NeuN postive cells within the AAV-NeuroD1 injected region. Representative overview of LHS and RHS of the control AAV±SAP **(A and B)** and NeuroD1 ±SAP **(C and D)**. NeuN positive cells (green) were dramatically less in empty vector injected brain sections compared to NeuroD1-AAV injected one. Interestingly, NeuroD1-AAV+SAP treated mice showed significantly higher NeuN replenishment compared to AAV-NeuroD1 without SAP. **E)** Data are represented as mean ± SD. (n = 6/per group). Scale bar= 400 µm. ***p < 0.01*, ****p < 0.001*, *****p < 0.0001*.

Our results, however, do not argue against a potential AAV leakage to pre-existing neurons in reprogramming capability of NeuroD1 under certain conditions specially with the use of high

dose of the Cre-dependent FLEX (flip-excision), DIO (doublefloxed inverse orientation), or LSL (loxP-STOP-loxP) system, which is broadly employed in glia to neuron conversions to induce robust viral reporter expression in neurons[278]. Taken together, it can be concluded that, ectopic expression of NeuroD1 with optimal dosage is able to replenish at least some neurons at the injury site. Moreover, the goal of this research was to provide similar efficacy at lower doses of AAV provided by the SAP hydrogel. This study provides the proof-of-principle that injured adult mammalian brains can be at least partially repaired through *in vivo* cell conversion approach.

Chapter 6. *In vitro* and *in vivo* dedifferentiation of reactive astrocytes

6.1 Preamble

In this chapter, SOX2 transcription factor (TF) is delivered with an adeno-associated viral vector (AAV). DJ gfaABC1D-SOX2-mCherry is used to reprogram reactive astrocytes to functional neuron when supplemented with valproic acid (VPA)/ or BDNF. This conversion occurs through neural progenitor cells (NPCs) also known as neural stem cells (NSCs) intermediate state. The materials and experimental methodology used in this chapter are described in Chapter 3. A paper reporting subsequent *in vitro/in vivo* studies is in preparation and will be entitled “In vivo generation of functional neurons with focally defined hydrogel factories that recruit, reprogram, and release”.

Author contribution: Negar Mahmoudi performed the major experiments, analysed the data, made the figures and original draft. Niamh Moriarty and Clare Parish implanted animals. Nathalie Dehorter, Nathan Reynolds, and Noorya Ahmed performed whole-cell electrophysiological recording and analysis. Leszek Lisowski provided expertise and guidance on viral constructs and packaging. Alan Harvey provided detailed feedback on all areas of the project and reviewed the manuscript. Clare Parish, Richard Williams, and David Nisbet reviewed the data interpretation and manuscript content and supervised the entire project. David Nisbet also supported this study financially.

6.2 Abstract

Generating neural stem cells and neurons through epigenetically reprogramming astrocytes is a potential strategy for neurological repair. Herein, ectopic expression of stem reprogramming factor, SOX2 transcription factor (TF), delivered through adeno-associated viral vector (AAV) exhibits a high astrocyte-to-neuron reprogramming efficiency both in vitro and in vivo. Conversion passes through the generation of induced progenitor neural stem cells (iPNSCs) which bypasses some of the concerns and risks of using induced pluripotent stem cells (iPSCs). More importantly, to address the difficulty of differentiation and maturation in vivo, neuronal maturation is further promoted by treatment with a histone deacetylase inhibitor, valproic acid (VPA), using an efficient hybrid composite biomaterial (consisting of short electrospun nanofibres embedded with valproic acid (VPA) and immobilized in self-assembling peptide (SAP) hydrogel). This fabricated hybrid composite biomaterial can be injected in a minimally invasive manner into a brain region and deliver VPA and AAV-SOX2 in a single dose.

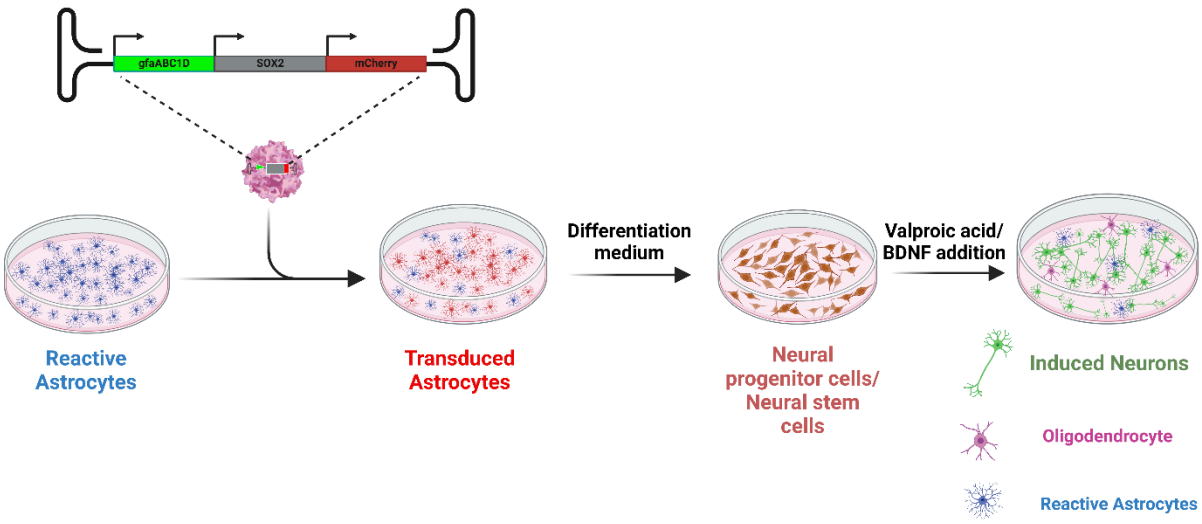

Figure 6.1. Graphical abstract of Chapter 6. Astrocyte culture from 1-2 days postnatal pups reprogramming/de-differentiation to induced neurons (iN) passes through neural progenitor cells (NPCs)/Neural stem cells (NSCs). **Created with BioRender.com**

6.3 Introduction

Neurogenesis, the birth of new neurons, decreases with age but does not disappear completely and persists in the neurogenic regions of the brain including the subventricular zone (SVZ) of the lateral ventricles and the subgranular zone (SGZ) of the dentate gyrus[279–281]. In response to injury, the proliferation of progenitor cells upregulates in these niches. However, SVZ-derived cells migrate toward the area of damage and differentiate into specific neural lineage[223] in the attempts to replace lost cells[282,283] whereas hippocampal cells remain within the granular cell layer. However, the capacity for this self-repair is insufficient because of the unconducive microenvironment, the absence of physical support after insult, and poor survival and integration of newly generated cells[284]. In addition, maximum populations of those endogenously generated cells under specific conditions develop a propensity to differentiate into glial cells such as astrocytes that contribute to astrocyte scar formation[273], therefore further hindering neuronal regeneration[285,286].

Despite neural progenitor cells that are limited to a few neurogenic zones, astrocytes are common cells in almost every brain structure. In response to neural injuries and degeneration, astrocytes turn into an active form called reactive astrocytes, characterised by dramatic morphological, transcriptional, and functional changes[8]. It has been reported that up to 50% of astrocytes re-entered the cell cycle and proliferate between three days and a week after injury to create more astrocytes around the site of injury in a stab wound model[287]. These reactive astrocytes constitute a major cellular component of glial scar formation which serves as a compensatory response modulating tissue damage and recovery[74,75]. Considering the role of reactive astrocytes in response to injury, reprogramming some of these cells potentially provides new means for replenishing damaged or dead neurons [288]. Astrocytes have the potential to generate new neurons if epigenetically reprogrammed by master regulator/pioneer transcription factors (TFs).

Recently, somatic cells have been reprogrammed by the addition of a set of selective TFs including (OCT-3/4, SOX2, KLF4, and C-MYC)[182]. Employing the ectopic expression of these TFs in combination can reprogram somatic cells towards pluripotency[39,289]. However, using these TFs in combination has been subsequently shown to induce tumorigenesis *in vivo*[183,184]. It has been revealed that SOX2, and OCT4 alone are sufficient to epigenetically reprogram astrocytes and successfully generate a pool of induced progenitor neural cells (iPNSCs)/neural stem cells (NSCs)[24,290] which bypass some of the concerns and risks of using iPSCs (e.g., teratoma formation, immature tumorigenesis due to potential iPSCs contamination or incomplete differentiation) [291,292]. This lineage-restricted stem cell reprogramming complements the iPSCs technology and addresses the difficulty of differentiating neural cells from iPSCs. Indeed, no histological signs of tumorigenesis in brains or spinal cords were observed with ectopic SOX2 expression when examined up to 1 year post virus injection[24].

SOX2 overexpression initiates a progressive reprogramming process that transforms astrocytes into neuronal progenitor cells, that can ultimately be differentiated to generate new neurons in the damaged adult CNS[21]. However, *in vivo* it has been shown that the induced neuroblast cells seldomly differentiate into mature neurons without further induction using brain-derived neurotrophic factor (BDNF)/ or VPA, a histone deacetylase (HDAC) inhibitor[293]. This suggests that the microenvironment is also essential for cell reprogramming, or at least the controlled differentiation of reprogrammed cells. Therefore, daily intraperitoneal injection of VPA were carried out the further drive the maturation of newly generated cells[24]. To address some disadvantages of intraperitoneal injection such as pain and infection because of multiple punctures, biomaterial-based drug delivery systems using electrospun nanofibres were used to locally deliver VPA and therefore promote tissue repair. VPA loaded electrospun nanofibres were immobilized in a N-fluorenylmethyloxycarbonyl self-assembling peptide (Fmoc-SAPs)

hydrogel to mimic the extracellular matrix (ECM) of the brain and provide a 3-dimensional (3D) microenvironment for newly generated cells. This ECM-mimicking hydrogel enhanced the ability of newborn neurons to integrate into circuitry, either by affecting the newborn neurons themselves or by affecting the plasticity of the local circuitry. This resulted in improved newborn neuron survival and functional outcome following neural damage. Moreover, this SAP hydrogel acts as a delivery platform for viral vector. To further bypass off-targeting transduction, a cell-specific promoter was utilised to drive the expression of the transgene in target cell and improve cell-specific targeting[207],[208]. Thus, to selectively reinduce pluripotency gene in mature astroglial cells *in vivo/in vitro*, we constructed a promoter gfaABC1D, a truncated version of hGFAP promoter[294,295], to drive the expression of the SOX2 TF selectively in astrocytes.

Results and Discussion

6.3.1 AAV-SOX2 dosage optimisation *in vitro*

AAV have high infection rates and negligible pathogenicity in human and have been approved by the FDA in clinical trials aimed at treating a range of CNS disorders[195],[246]. For successful gene therapy, an appropriate amount of a therapeutic gene must be delivered into the target tissue without substantial toxicity[190]. In the present study, the AAV was tagged with mCherry as a tracing marker to visualize transduced cells. The constructed DJ gfaABC1D-SOX2-mCherry was initially tested *in vitro* on cultured murine/mouse primary astrocytes to examine its transduction and reprogramming efficiency. Two different multiplicities of transduction (MOT), MOT=10^5 and MOT=10^6, were examined. After 3 days post transduction (DPT), transduced astrocytes began to divide and adopt pseudoepithelial morphologies. To determine the transduction efficiency cells were fixed and stained at 10 DPT. Strong mCherry expression visualized using fluorescent microscopy, confirming the successful transduction of astrocytes with DJ gfaABC1D-SOX2-mCherry **(Figure 6.2A, B red)**. Fluorescence-activated

cell sorting (FACS) analysis was used to quantify the number of transduced and converted cells **(Figure 6.2C)**. Some cells were immunopositive for both β3-tubulin and mCherry **(Figure 6.2C**, Q10 and Q2), suggesting a transitional stage from astrocytes to neurons. As illustrated in FACS plots and consequent quantified data **(Figure 6.2C, D)**, the percentage of cells expressing mCherry transduction efficiency marker in MOT=10^6 (93.9± 3.7% mCherry+) was significantly higher than MOT=10^5 (10.9± 3.7% mCherry+). Therefore, MOI=10^6 was selected for subsequent *in vitro* testing.

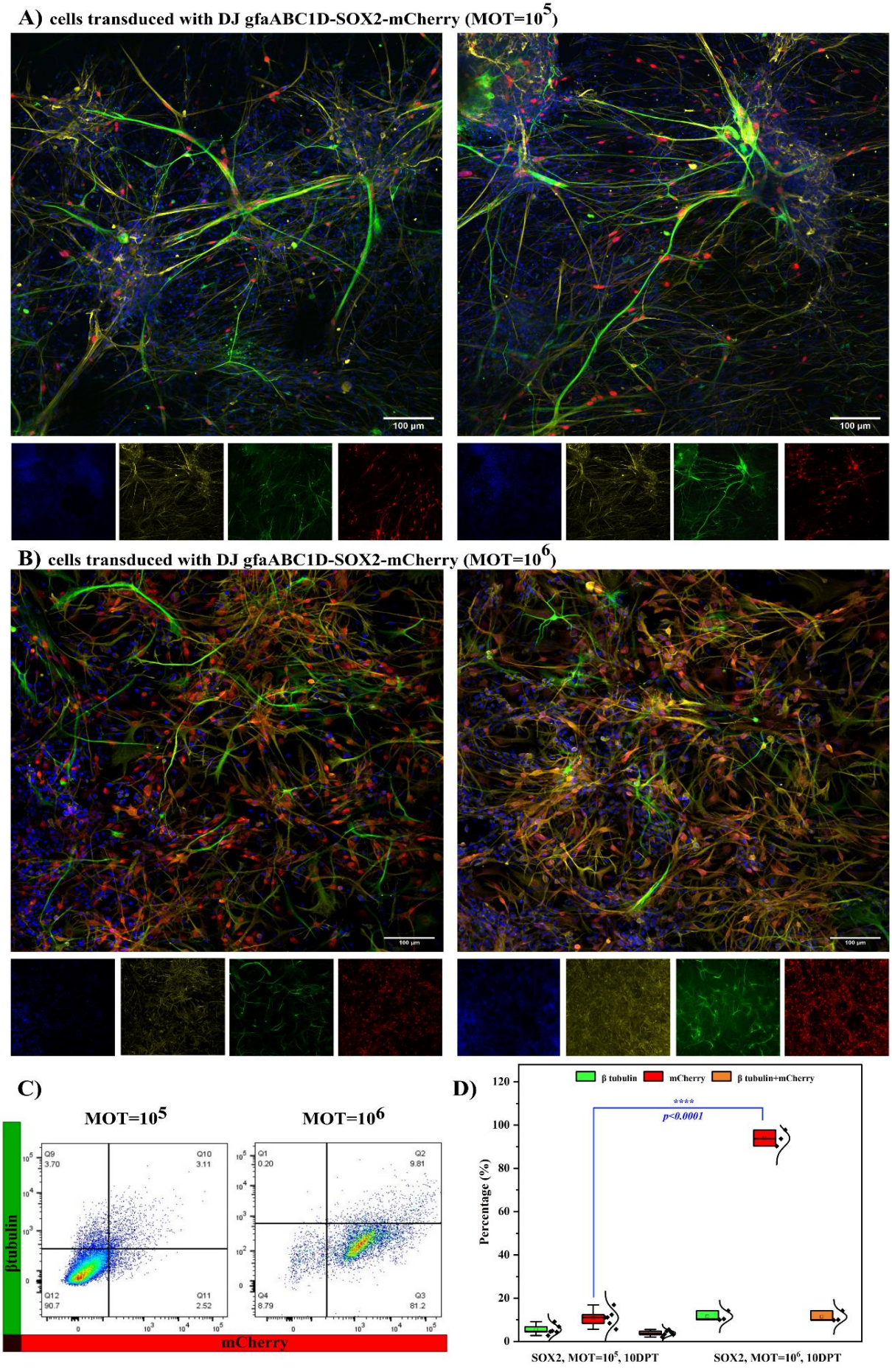
A) cells transduced with DJ gfaABC1D-SOX2-mCherry (MOT=10^5)
100 µm
100 µm
B) cells transduced with DJ gfaABC1D-SOX2-mCherry (MOT=10^6)
100 µm
100 µm
C)
MOT=10^5
MOT=10^6
βtubulin
mCherry
Q9 3.70
Q10 3.11
Q12 90.7
Q11 2.52
Q1 0.20
Q2 9.81
Q4 8.79
Q3 81.2
D)
β tubulin
mCherry
β tubulin+mCherry
****
p<0.0001
Percentage (%)
SOX2, MOT=10^5, 10DPT
SOX2, MOT=10^6, 10DPT

Figure 6.2. Transduction efficiency of DJ gfaABC1D-SOX2-mCherry. Cells were transduced with **A)** MOT=10^5 and **B)** MOT=10^6, fixed and stained with transduction efficiency marker (red), neuronal marker β3 tubulin (green), astrocytic protein GFAP (yellow), and DAPI (blue) at 10 DPT. **C)** Representative data of FACS plots for DJ gfaABC1D-SOX2-mCherry transduced astrocyte with MOT=10^5 and MOT=10^6. **D)** Quantification data for mCherry+, β tubulin+, and double positive cells (both mCherry+ and β tubulin+ cells shown in Q10 and Q2). Data represents Mean ± SEM, **** $p < 0.0001$. Scale bar=100µm.

6.3.2 SOX2 transduced astrocytes pass through a proliferative state.

Reprogramming towards pluripotency involves the expression of master stem cell factors followed by a series of molecular events that include the generation of various intermediate cells. These regenerated progenitor cells are capable of self-renewal and further differentiate into neurons and all macroglial cells *in situ*, filling a tissue cavity and/or replenishing neurons lost due to disease or injury[296]. Here, we confirmed that the majority of SOX2 transduced cells switched to neural progenitor/stem cells and underwent self-renewal. The terms neural stem cell and neural progenitor cell are often used interchangeably, as properties such as self-renewal and the range of progeny are limited. The iPNSCs formation was confirmed through following methods/approaches: i) immunostaining for nestin (as an intermediate filament protein highly enriched in embryonic and adult NSCs), ii) IncuCyte live microscope imaging, and iii) cell cycle using Flow Cytometry.

- **Nestin**

To examine nestin expression[297], astrocytes transduced with either DJ gfaABC1D-SOX2-mCherry (AAV-SOX2) or DJ gfaABC1D-mCherry (AAV-mCherry) as control, were fixed and immunostained for nestin. At 5 DPT, 65.7±7.5% of AAV-SOX2 transduced cells were positive

for nestin marker, while in AAV-mCherry transduced cells only 3.4±1.2% were positive **(**

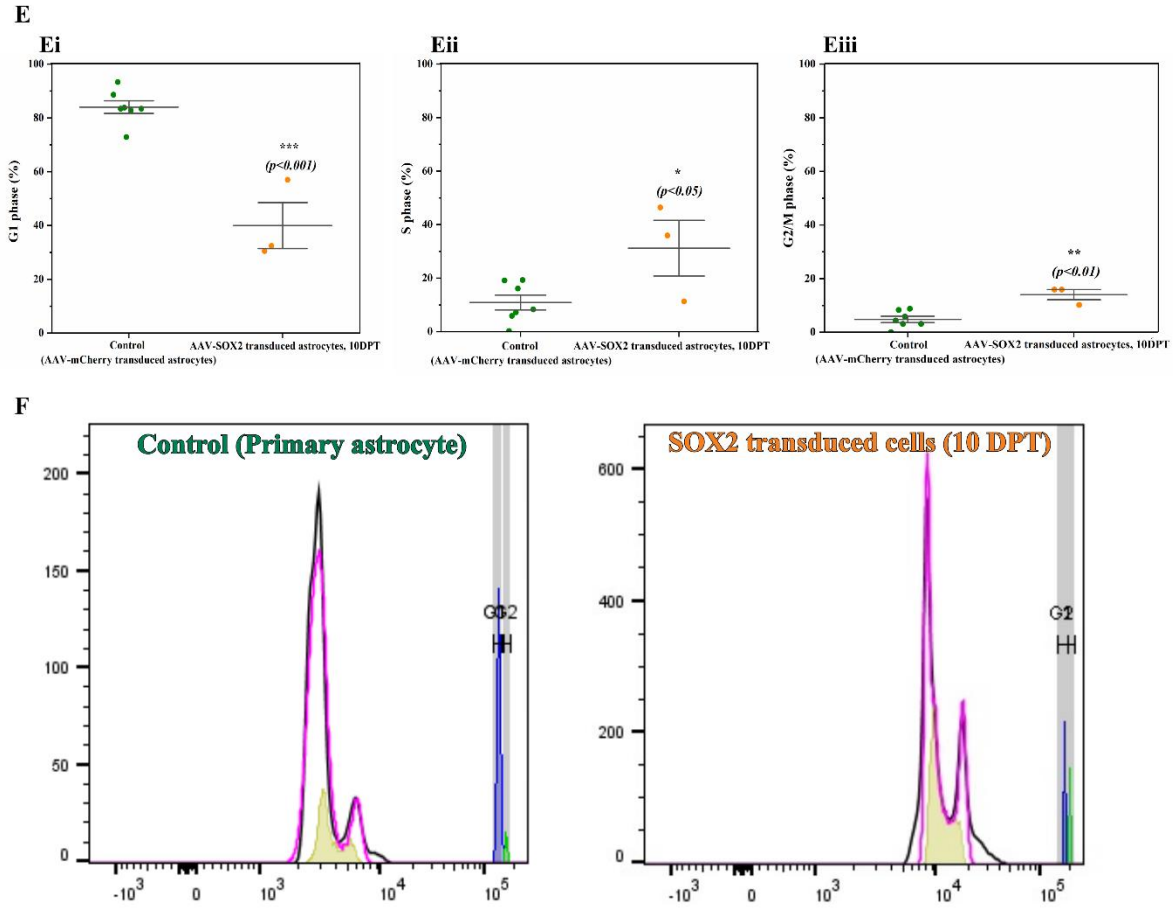

Figure 6.3A-C). While nestin is not exclusively a marker for neuro progenitor cells, the data do suggest that AAV-SOX2 enables astrocytes to dedifferentiate toward iPNSCs.

- **InCucyte live imaging microscope**

After initial transduction of astrocytes with AAV-SOX2 or AAV-mCherry, cells were monitored for 7 days using live microscope IncuCyte by taking images every 4 hours. The

percentage of confluence of cells at any given time point was calculated **(**

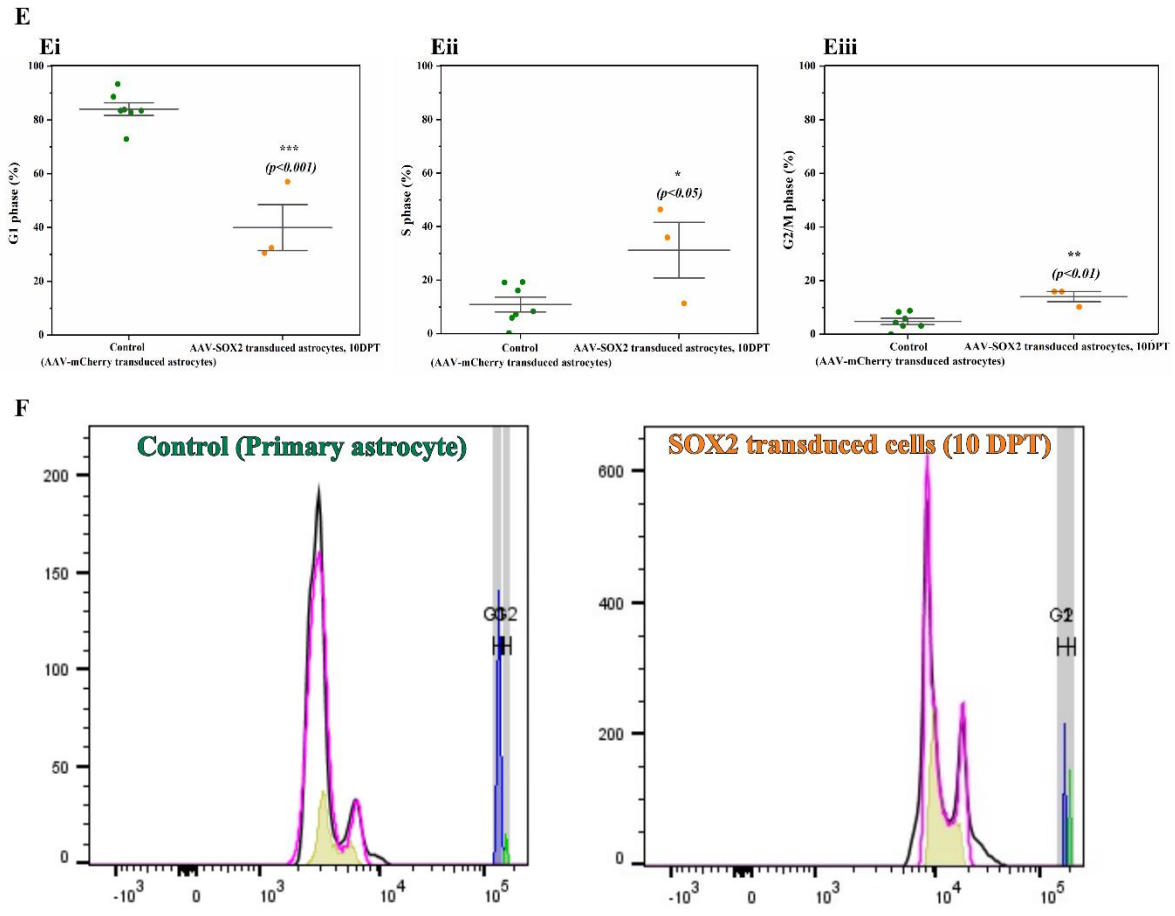

Figure 6.3D). As anticipated, cells received AAV-SOX2 have shown significant cell proliferation rate, in contrast with control cultures that received AAV-mCherry/empty vector. To further characterise these cells molecularly, cell cycle analysis was performed.

- **Cell cycle**

The transduction of astrocytes with episomal DJ gfaABC1D-SOX2-mCherry at the G1 phase and transitioning through the S phase may provide a pool of iNPSCs. Therefore, astrocytes were transduced with either AAV-SOX2 or AAV-mCherry and examined for their cell cycle stages at 10 DPT using Flow Cytometry. The proliferation and division of cells was confirmed through the S phase (the process for the synthesis or replication of DNA) and G2/M phase (indicating the stage that DNA has been duplicated and the cell is almost ready to divide). As

revealed in

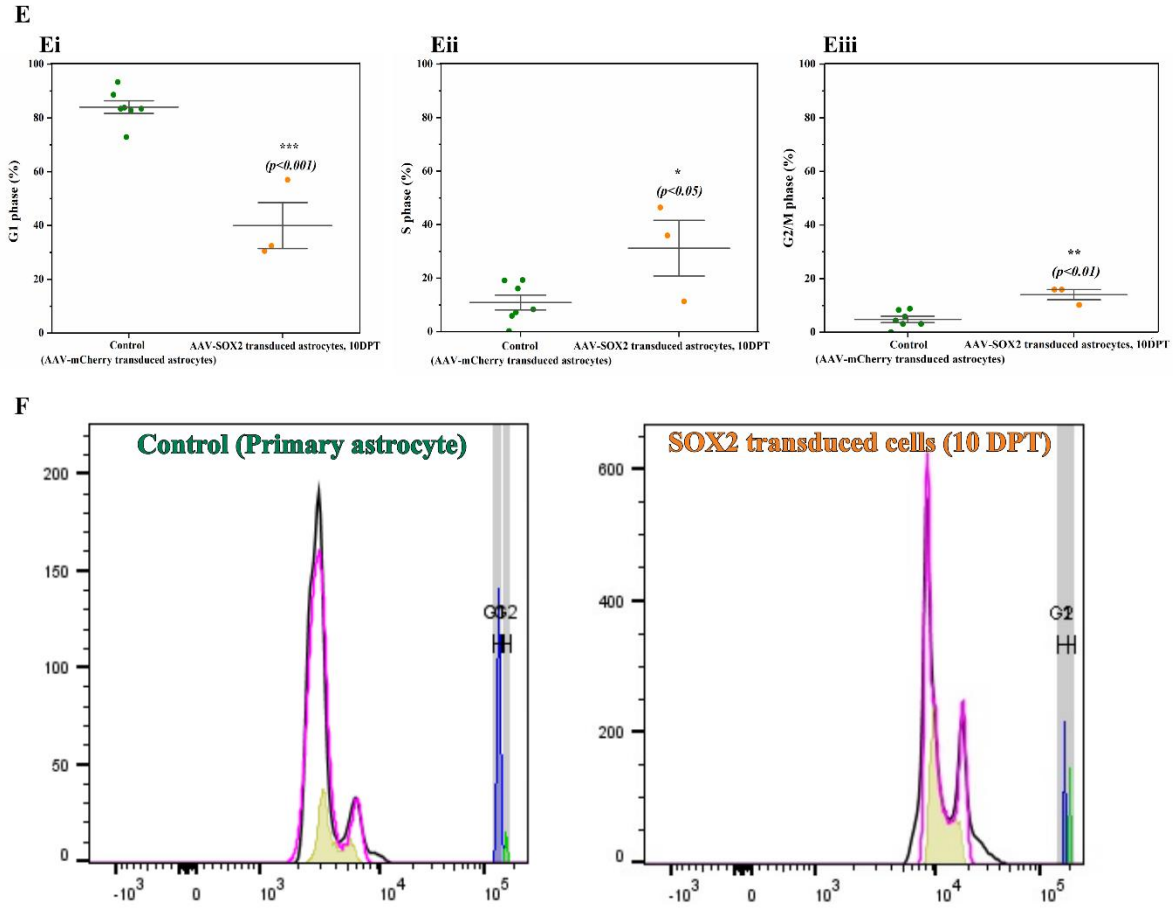

Figure 6.3E, F AAV-SOX2 transduced cells returned to a S phase indicating the up-regulation of cell cycle components is associated with the passage of AAV-SOX2 transduced cells through the proliferative state and division. G0-G1, S, and G2/M phases were significantly different between AAV-SOX2 and AAV-mCherry transduced cells. Taken together, these data from nestin marker, IncuCyte live imaging, and cell cycle analysis appear to confirm that the desired cells (PNSCs) were induced.

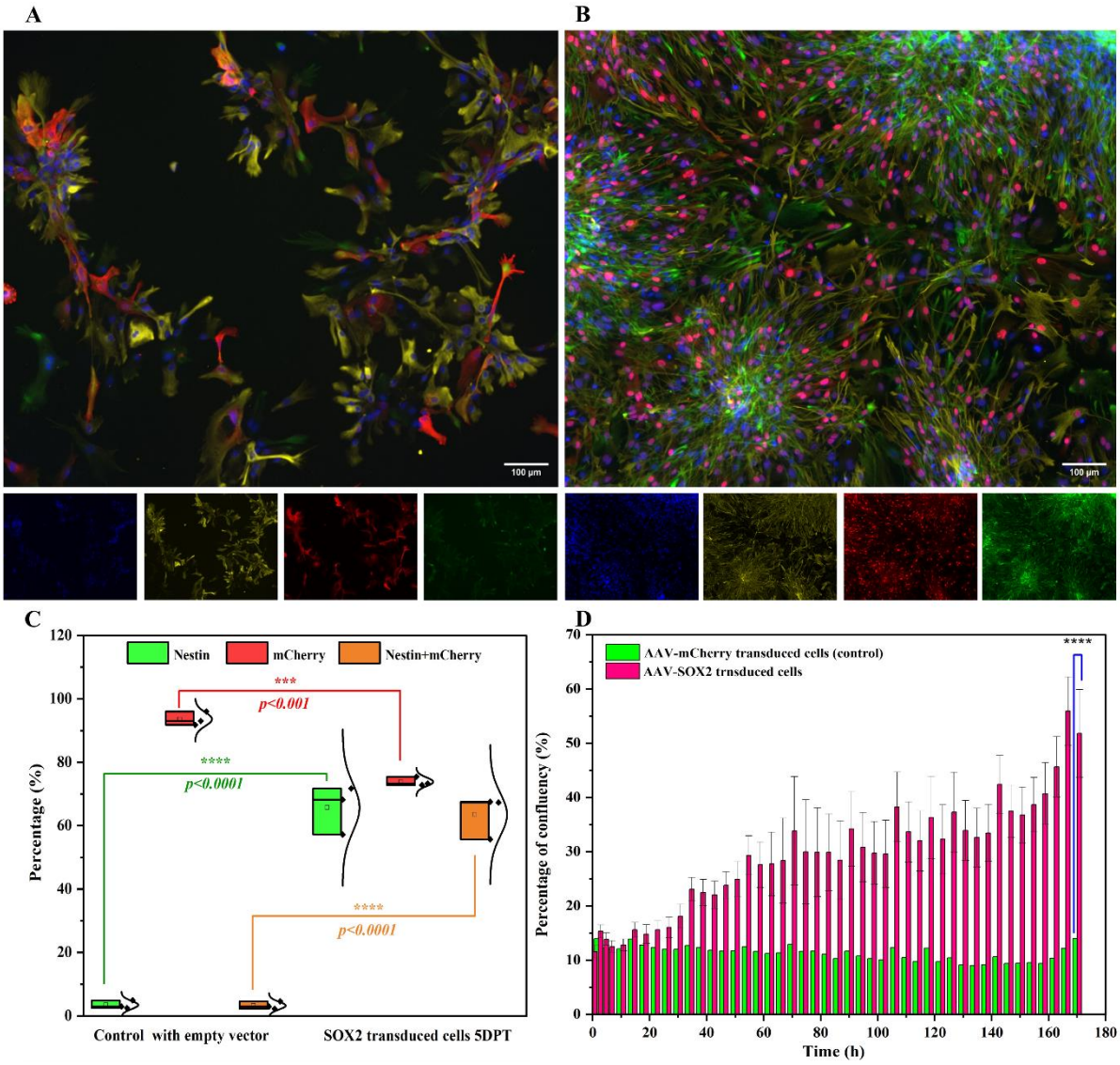
A
B
100 µm
100 µm
C
Nestin
mCherry
Nestin+mCherry
***
p<0.001
****
p<0.0001
****
p<0.0001
Percentage (%)
Control with empty vector
SOX2 transduced cells 5DPT
D
AAV-mCherry transduced cells (control)
AAV-SOX2 trnsduced cells
****
Percentage of confluency (%)
Time (h)

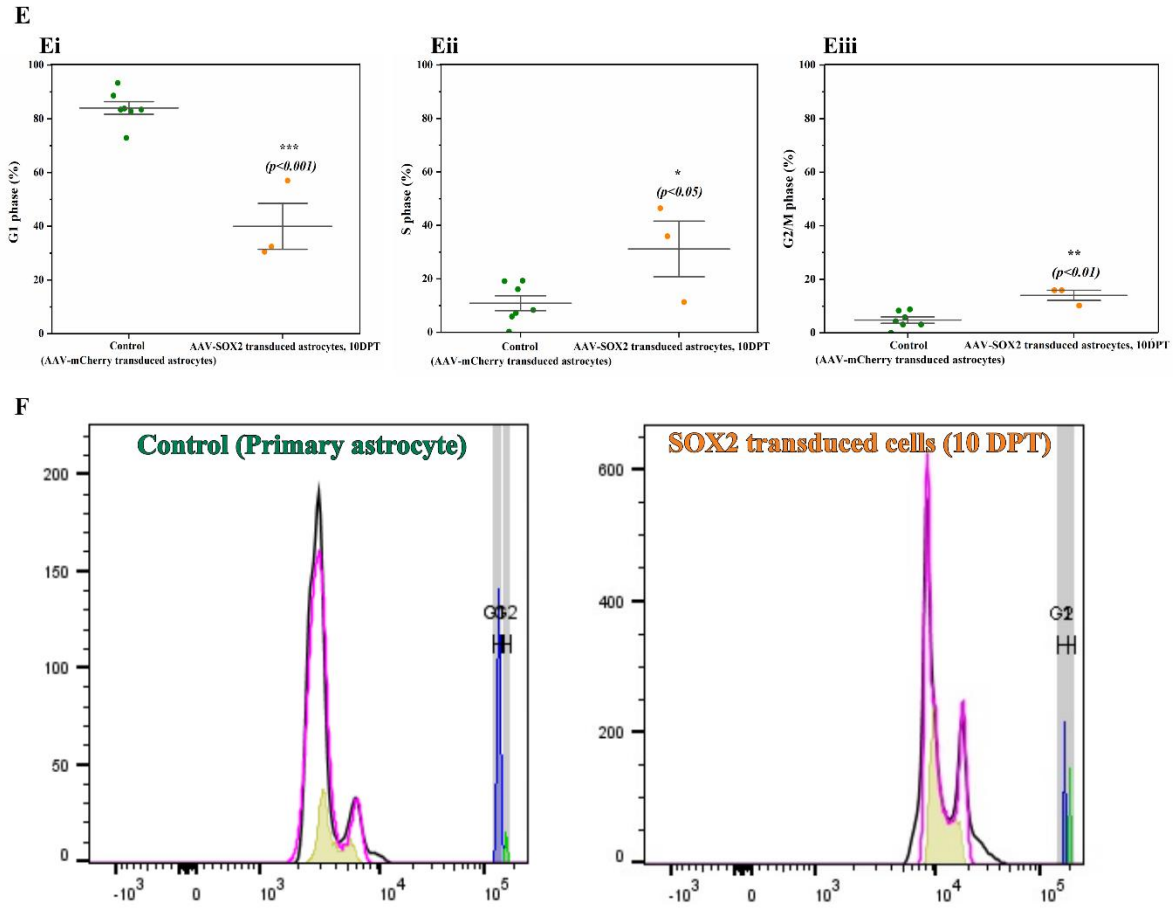

Figure 6.3. Fluorescent/live microscopy and cell cycle analysis for AAV-SOX2 and AAV-mCherry transduced cells. A representative image of astrocytes transduced with **A)** AAV-mCherry and **B)** AAV-SOX2, and stained with nestin marker (green), anti-mCherry (red), anti-GFAP (yellow), and DAPI (blue). **C)** Quantification data showing the population of nestin+, mCherry+, and double positive cells (both nestin+ and mCherry+) in culture. **D)** The percentage of confluence for AAV-SOX2 and AAV-mCherry transduced cells at any given time point acquired using IncuCyte live imaging. **E, F)** Cell cycle analysis on AAV-SOX2 and AAV-mCherry transduced astrocytes showing significant increase in S phase and G2/M phase of SOX2 transduced cells indicating the presence of iPNSCs. Data represents Mean ± SEM, * $p < 0.05$, ** $p < 0.01$, *** $p < 0.001$. n=3-5 independent cultures/group. Scale bar=100µm.

6.3.3 *In vitro* transduction of primary astrocytes with SOX2 leads to astrocyte to neuron conversion.

A necessary goal in reprogramming is to generate enough functional neurons. At 10 DPT as revealed by microscopic images and FACS data **(Figure 6.2B, C, D)**, the percentage of cells expressing β3 tubulin marker was 11.4±2.3%, considered as low reprogramming efficiency (<20%)[42]. Therefore, a longer period was required to achieve higher reprogramming efficiency as the conversion process is time dependent.

As mentioned before, the presence of BDNF or VPA is of paramount importance to further drive the maturation of newly generated cells. Therefore, we initially examined the hypothesis

of using BDNF/or VPA *in vitro* on primary astrocytes by supplementing these two candidate factors to the differentiation medium. Cells were maintained for 28 DPT with medium changed every 3-4 days. Furthermore, control samples were divided into four different groups i) astrocyte transduced with empty vector and treated with VPA, ii) astrocytes treated with VPA (without any vector transduction), iii) astrocytes transduced with empty vector and treated with BDNF, and vi) astrocytes treated with BDNF (without any vector transduction) for 28 days. The controls and AAV-SOX2 transduced cells were fixed and stained for mCherry (AAV), GFAP (astrocytes), and β3 tubulin+/ MAP2+/ NeuN (induced neurons). As seen in **(Figure 6.4A)** control samples, whether transduced or not, BDNF or VPA treatment had no impact on morphology of cultured astrocytes **(Figure 6.4B)**. Moreover, the quantification data **(Figure 6.4G-L)** acquired using FACS did not reveal any significant differences between groups (*ANOVA* statistics at 0.05 level, **Figure 6.4D, E**). These data suggest that either VPA or BDNF alone are not sufficient to induce astrocyte conversion in culture. However, at 28 DPT many AAV-SOX2 transduced cells exhibited neuronal-like phenotypes (small round soma with at least 2 neuritic processes) after both BDNF or VPA treatment **(Figure 6.4C),** a high reprogramming efficiency confirmed by FACS data **(Figure 6.4F, G-L).** As presented in **Figure 6.4G-L**, 68.7±7% and 65.2±5.8% of AAV-SOX2 transduced cells were β3 tubulin+ in BDNF treated and VPA treated groups, respectively. Cells were also MAP2+ with 68.6±1.3% for BDNF treated and 68.4±0.6% for VPA treated. Moreover, 62.4±2.1% and 61.3±2.6% of cells were NeuN+, in BDNF and VPA supplemented medium, respectively. Interestingly, no significant statistical difference was observed between efficiency of reprogramming between BDNF and VPA treated cells (one-way *ANOVA* at 0.05 level).

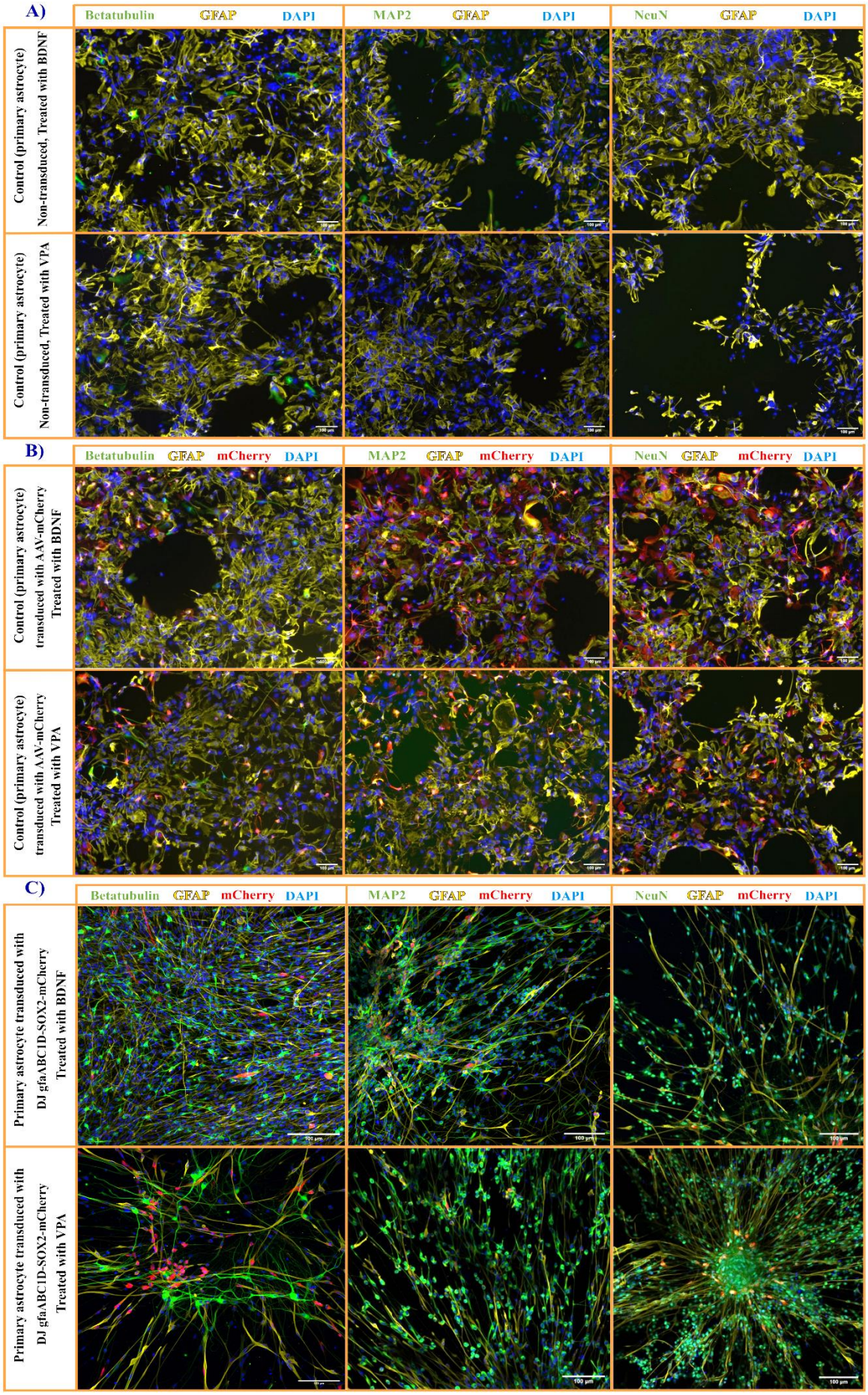
A)
Betatubulin GFAP DAPI
MAP2 GFAP DAPI
NeuN GFAP DAPI
Control (primary astrocyte) Non-transduced, Treated with BDNF
Control (primary astrocyte) Non-transduced, Treated with VPA
B)
Betatubulin GFAP mCherry DAPI
MAP2 GFAP mCherry DAPI
NeuN GFAP mCherry DAPI
Control (primary astrocyte) transduced with AAV-mCherry Treated with BDNF
Control (primary astrocyte) transduced with AAV-mCherry Treated with VPA
C)
Betatubulin GFAP mCherry DAPI
MAP2 GFAP mCherry DAPI
NeuN GFAP mCherry DAPI
Primary astrocyte transduced with DJ gfaABC1D-SOX2-mCherry Treated with BDNF
Primary astrocyte transduced with DJ gfaABC1D-SOX2-mCherry Treated with VPA

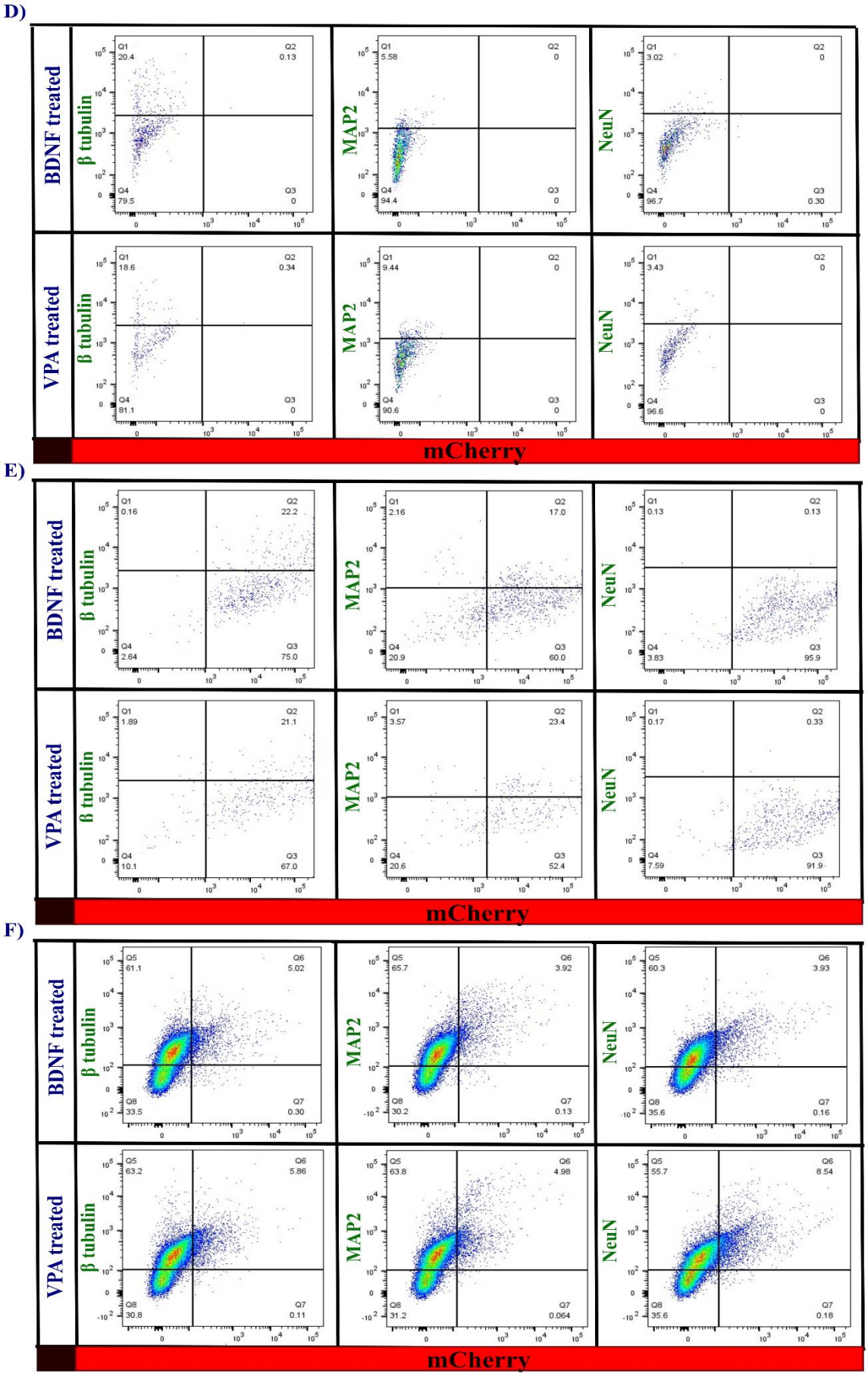
D)
BDNF treated
VPA treated
β tubulin
MAP2
NeuN
Q1 20.4
Q2 0.13
Q4 79.5
Q3 0
Q1 5.58
Q2 0
Q4 94.4
Q3 0
Q1 3.02
Q2 0
Q4 96.7
Q3 0.30
Q1 18.6
Q2 0.34
Q4 81.1
Q3 0
Q1 9.44
Q2 0
Q4 90.6
Q3 0
Q1 3.43
Q2 0
Q4 96.6
Q3 0
mCherry
E)
BDNF treated
VPA treated
β tubulin
MAP2
NeuN
Q1 0.16
Q2 22.2
Q4 2.64
Q3 75.0
Q1 2.16
Q2 17.0
Q4 20.9
Q3 60.0
Q1 0.13
Q2 0.13
Q4 3.83
Q3 95.9
Q1 1.89
Q2 21.1
Q4 10.1
Q3 67.0
Q1 3.57
Q2 23.4
Q4 20.6
Q3 52.4
Q1 0.17
Q2 0.33
Q4 7.59
Q3 91.9
mCherry
F)
BDNF treated
VPA treated
β tubulin
MAP2
NeuN
Q5 61.1
Q6 5.02
Q8 33.5
Q7 0.30
Q5 65.7
Q6 3.92
Q8 30.2
Q7 0.13
Q5 60.3
Q6 3.93
Q8 35.6
Q7 0.16
Q5 63.2
Q6 5.86
Q8 30.8
Q7 0.11
Q5 63.8
Q6 4.98
Q8 31.2
Q7 0.064
Q5 55.7
Q6 8.54
Q8 35.6
Q7 0.18
mCherry

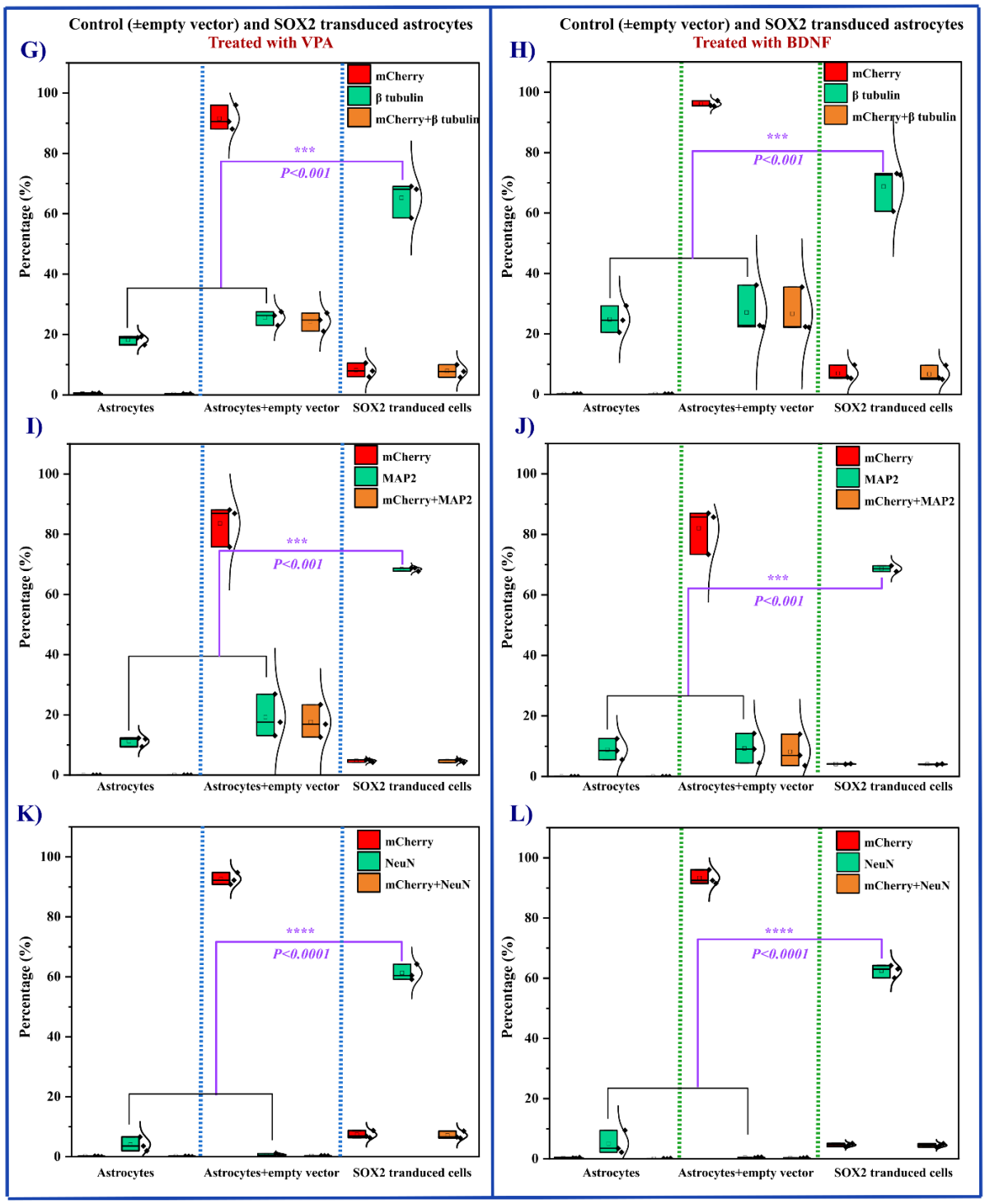

Figure 6.4. Non-transduced/ AAV-mCherry transduced/ or AAV-SOX2 transduced astrocytes supplemented/treated with either BDNF/or VPA *in vitro*. A representative image of **A)** non-transduced primary astrocytes, **(B)** empty vector (AAV-mCherry) transduced astrocytes, and **(C)** AAV-SOX2 transduced astrocytes treated with BDNF/or VPA for 28 days and stained with β3 tubulin/ MAP2/or NeuN (green), anti-mCherry (red), anti-GFAP (yellow), and DAPI (blue). **D-F)** Representative FACS plots for non-transduced/ AAV-mCherry/ and AAV-SOX2 transduced astrocytes reveal different population of positive cells for different markers. **G-I)** Quantified cell counts for different cell markers with different conditions at 28 DPT. Scale bar= 100µm. *** $p < 0.001$, **** $p < 0.0001$. n=3/group.

6.3.4 Cell cycle analysis and GFAP expression at 28 DPT

Using DJ gfaABC1D-SOX2-mCherry we were able to generate cells expressing βtubulin+, MAP2+, or NeuN+ neuronal markers with high reprogramming efficiency *in vitro*. These cells with neuronal fate are expected to be in post-mitotic stages. To investigate this, cell cycle analysis was performed on AAV-SOX2 and AAV-mCherry transduced astrocytes at 28 DPT. As seen in **Figure 6.5A**, S and G1 phase was significantly different between AAV-mCherry and AAV-SOX2 transduced astrocytes after 28 DPT. Since the conversion of astrocytes to neuron-like cells was identified using immunohistochemistry, selecting cortical primary neurons as control would be a better choice to investigate whether cells are in post-mitotic stage or not. As demonstrated in **Figure 6.5B**, the G2/M phase is significantly different between AAV-SOX2 transduced cells at 28 DPT compared to cortical neurons as control. The difference between the G2/M phase in control and AAV-SOX2 transduced cells was attributed to SOX2 transduction giving rise to astrocytes, oligodendrocytes as well as neurons. Thus, to selectively study neuronal-like cells, only the NeuN+ expressing cells were examined for their cell cycle stages. No significant difference was observed between the cell cycle of NeuN+ cells in AAV-SOX2 transduced cells and cortical neurons **(Figure 6.5C)**. These data suggest that the reprogrammed cells are in the post-mitotic state. Being post-mitotic cells, iN are not tumorigenic.

Moreover, the dynamic expression of SOX2 during the reprogramming process was important since at the early stage, high expression of SOX2 is required for initiating endogenous pluripotency/multipotency gene expression[298]. On the other hand, the persistent expression of SOX2 results in the maintenance of progenitor characteristics and hinders neuronal reprogramming[22]. Therefore, the subsequent down regulation of SOX2 was important for cells to exit mitosis and undergo differentiation. The dynamic expression of SOX2 can be

achieved through gene expression under the hGFAP promoter, which is high in astrocytes but rarely expressed in neuronal cells[24].

As illustrated in **Figure 6.5E** reprogramming of astrocyte to neuron using AAV-SOX2 resulted in a significant reduction in mCherry+ cells. This was attributed to the downregulation of SOX2 during the reprogramming process to give rise to neurons. Moreover, during the M phase, many TFs and chromatin binding proteins are ejected from the chromatin; the integrative viruses are gradually silenced, and the non-integrative/episomal viral vectors such as AAVs are gradually removed from host cells. In addition to mCherry downregulation, at 28 DPT the population of cells expressing GFAP+ also drastically decreased in AAV-SOX2 transduced cells compared to control, further reinforcing the fact that the newly generated neurons are the result of the conversion of astrocytes and are not occasional preexisting neurons that may still reside in astrocyte culture.

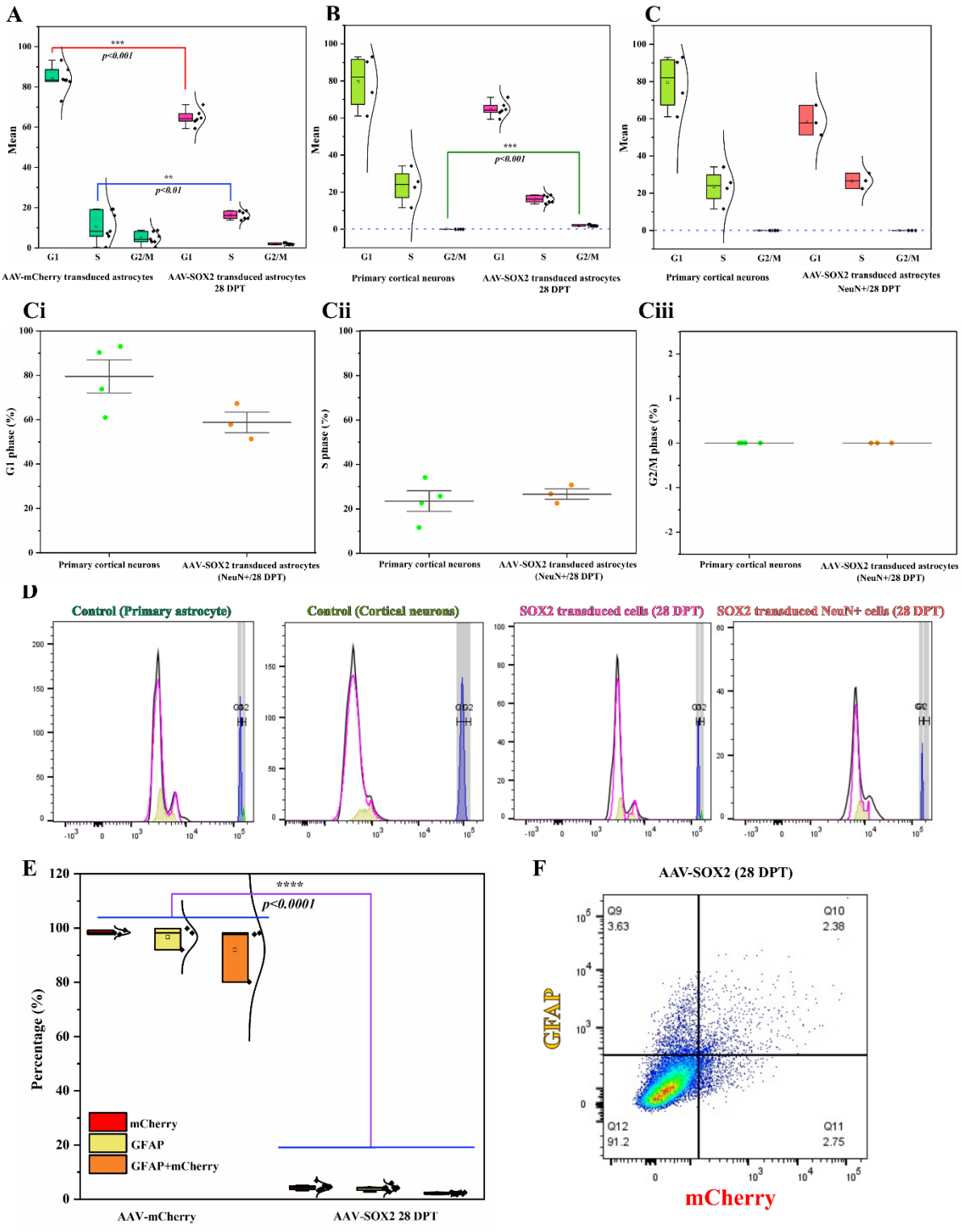

Figure 6.5. Cell cycle analysis on transduced cells at 28 DPT. A-C) Quantification of G1, S, and G2/M phases for primary astrocytes, primary cortical neurons, and AAV-SOX2 transduced astrocytes. **D)** Representative images of cell cycle plots acquired from flow cytometry for different cells. **E)** Quantification of GFAP+, mCherry+, and double positive cells (both GFAP+ and mCherry+), based on FACS data reveals a drastic reduction of mCherry+, GFAP+ and double positive cells after 28 DPT in AAV-SOX2 transduced astrocytes compared to AAV-mCherry transduced astrocytes. **F)** Representative FACS plot for AAV-SOX2 transduced cells indication

different population of GFAP+, mCherry+, and double positive cells. ** $p < 0.01$ *** $p < 0.001$, **** $p < 0.0001$. n=3/group

6.3.5 Reprogrammed primary astrocytes were able to initiate action potentials

To provide additional evidence that the reprogramming process had generated functional neurons from reactive astrocytes, cells (from different wells) were probed for their capacity to generate action potentials using whole-cell electrophysiological recording. Each recorded cell was from different well to make sure the results are representative. Electrophysiology results at 28 DPT showed that AAV-SOX2 transduced neuronal cells rarely become electrophysiologically mature and exhibited spikelet **(Figure 6.6)**. Thus, cells were assessed at more protracted periods after AAV-SOX2 transduction.

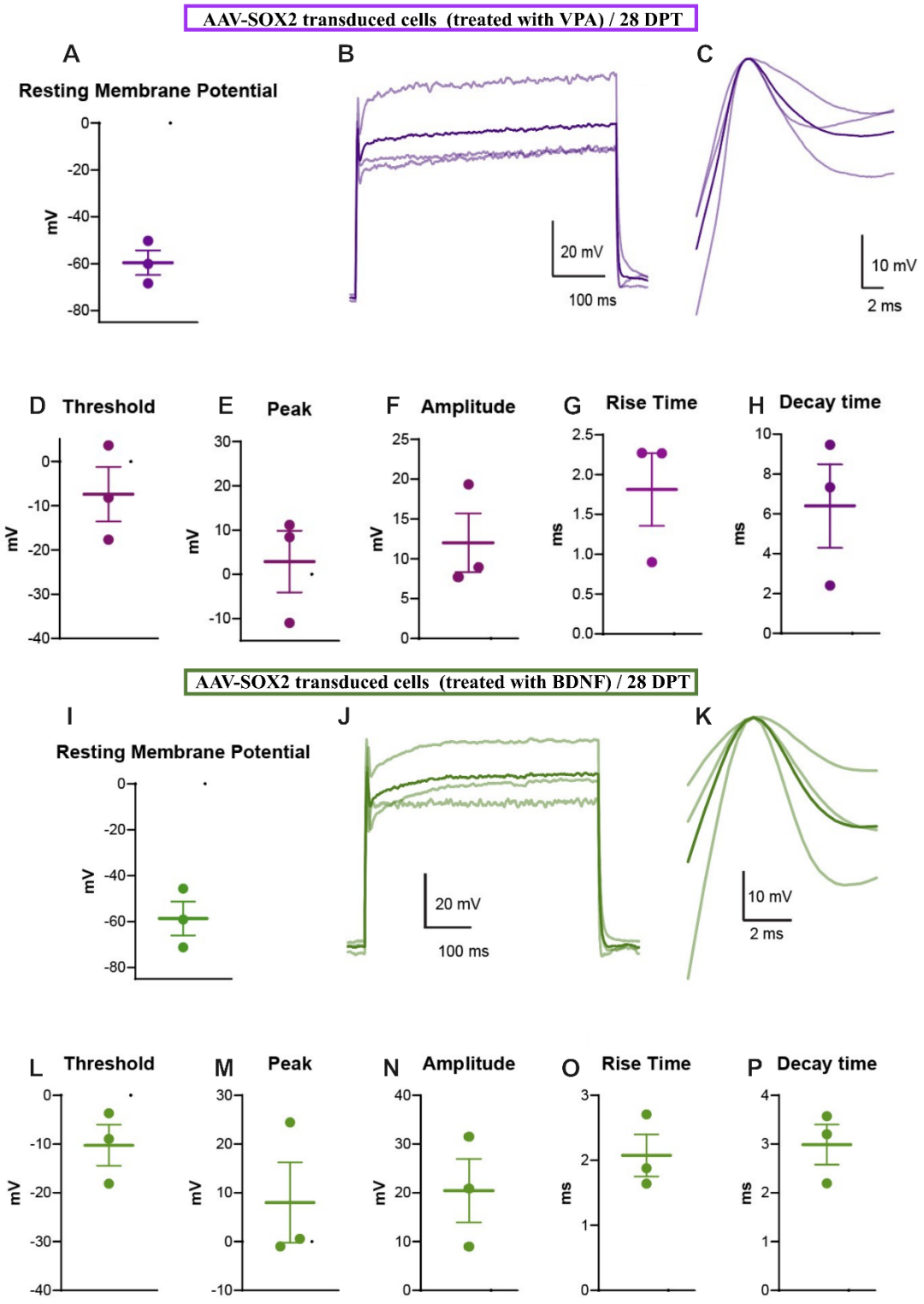

Figure 6.6. The SOX2-mediated reprogramming in both VPA and BDNF supplemented media was monitored *in vitro* and functionally characterised. (A, I) Resting membrane potential for SOX2 transduced cells supplemented with VPA and BDNF, respectively. **(B, J)** Spikelet resulting from 25 pA current steps in cells. **(C, K)** Overlaid spikelet from all recorded cells. **(D, L)** Spikelet threshold. **(E, M)** Peak potential of spikelet. **(F, N)** Amplitude **(G, O)** Rise time of spikelet. **(H, P)** Decay time of spikelet.

By 42 DPT, in current-clamp mode gradually increasing membrane depolarisation steps triggered the firing of action potentials in AAV-SOX2 transduced cells treated with VPA (n=5) **(Figure 6.7C, D)** and BDNF (n=6 cells) **(Figure 6.7L, M).** Recorded cells displayed typical mature neuronal resting membrane potentials (i.e., approximately between -60 and -80 mV; **Figure 6.7A, J**) in which spontaneous calcium activity was also observed, indicating intrinsic excitability **(Figure 6.7B, K)**. Cells also displayed typical action potential kinetics, including a threshold near -20 to -30 mV **(Figure 6.7E, N)** and an amplitude of 30 mV or larger **(Figure 6.7G, P)**, as well as appropriate rise and decay times (i.e., < 2 ms; **Figure 6.7H, I, Q, R**). Slight differences observed in membrane potential and action potential kinetics such as action potential threshold reflected the gradual maturation process of reprogrammed neurons. Together, these data suggested that by 42 DPT, SOX2 TF was capable of reprogramming astrocytes into neurons capable of excitation and the generation of action potentials.

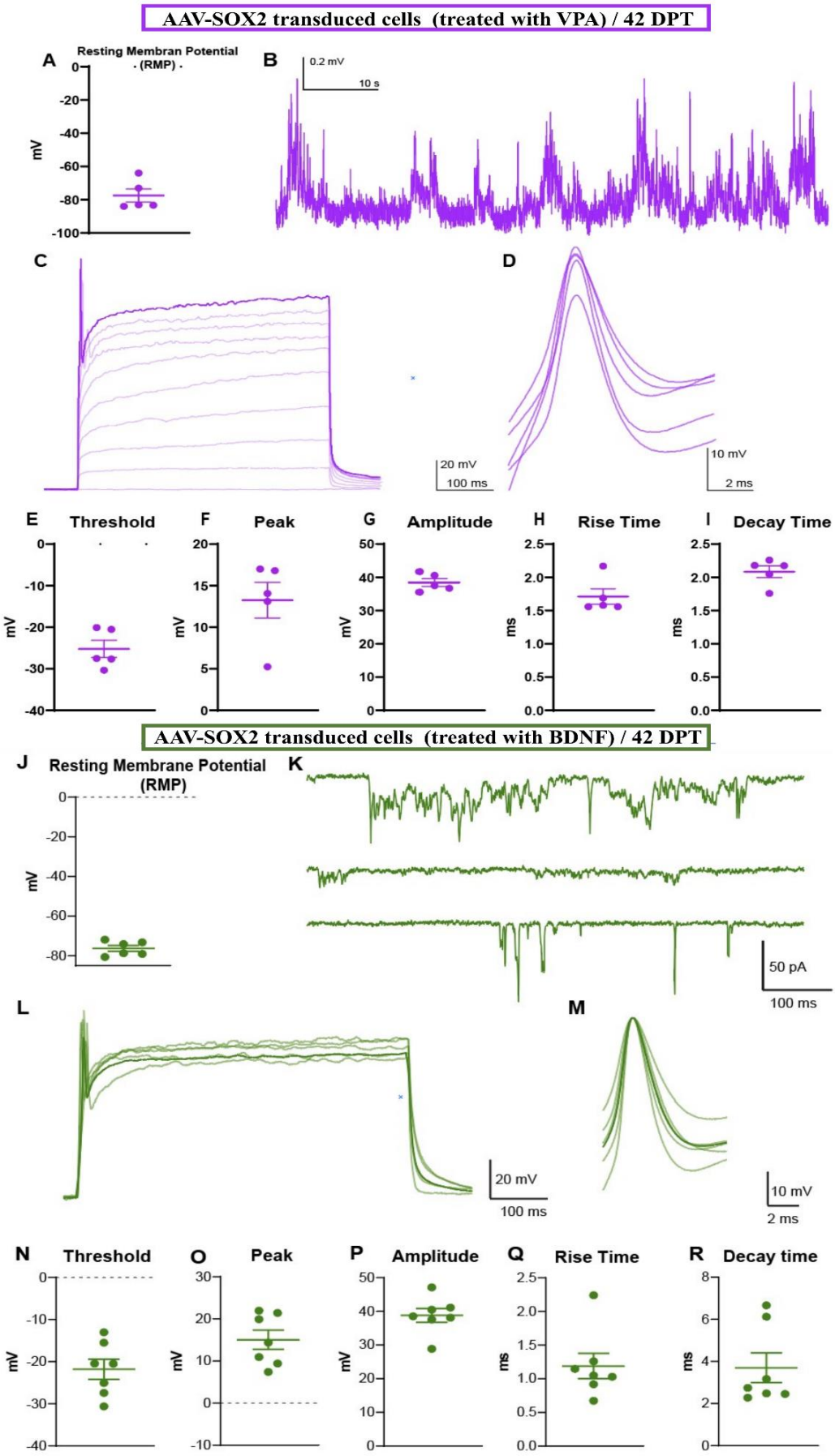
AAV-SOX2 transduced cells (treated with VPA) / 42 DPT
A
Resting Membran Potential
- (RMP) -
mV
B
0.2 mV
10 s
C
20 mV
100 ms
D
10 mV
2 ms
E
Threshold
F
Peak
G
Amplitude
H
Rise Time
I
Decay Time
AAV-SOX2 transduced cells (treated with BDNF) / 42 DPT
J
Resting Membrane Potential
(RMP)
K
50 pA
100 ms
L
20 mV
100 ms
M
10 mV
2 ms
N
Threshold
O
Peak
P
Amplitude
Q
Rise Time
R
Decay time
ms

Figure 6.7. The SOX2-mediated reprogramming in both VPA and BDNF supplemented media was monitored *in vitro* and functionally characterised. (A, J) Resting membrane potential for SOX2 transduced cells supplemented with VPA and BDNF, respectively. **(B, K)** Representative examples of spontanous calcium activity in recorded cells**. (C, L)** Action potential resulting from 25 pA current steps in cells. **(D, M)** Overlaid action potentials from all recorded cells. **(E, N)** Action potential threshold. **(F, O)** Peak potential of action potential. **(G, P)** Amplitude of action potential (from threshold to peak). **(H, Q)** Rise time of action potential (10%-90% of amplitude). **(I, R)** Decay time of action potential.

Although both BDNF and VPA showed similar reprogramming efficiency, due to the difficulty of using BDNF *in vivo* because of its susceptibility to enzyme degradation and short half-life of approximately 45 min, VPA was selected to be embedded in electrospun nanofibres for *in vivo* application. VPA is an ideal candidate due to its clinical stability and minimal cytotoxicity. It has become apparent that chromatin modification plays a critical role in the regulation of cell-type-specific gene expression. Some recent studies on VPA have shown that i) VPA reduces HDAC activity and promotes neuronal differentiation of NSCs[299], ii) upregulates the expression of diverse neurotrophic factors in the rat brain[300], iii) affects the neural differentiation and neurite outgrowth of neural crest progenitors and hippocampal neural stem cells[299], iv) VPA treatment for up to ten days induces profound changes in cell morphology, characterised by less tightly packed cells within the colonies and the generation of long filamentous structures[301], v) increases white matter repair and neurogenesis after a stroke[302], vi) exerts an anti-inflammatory effect[303], vii) reduces cell death of motor neurons and cellular apoptosis[304], viii) attenuates demyelination and axonal loss, preserves oligodendrocytes and neurons[305], ix) increases neurite out growth[306], x) reduces cystic cavitation[307], and increases expression of neuronal progenitor cells in the spinal cord. More importantly, VPA promotes neuronal fate and inhibits glial fate simultaneously through the induction of neurogenic transcription factors including NeuroD1[299]. Therefore, VPA was selected for subsequent *in vivo* testing and embedded in hybrid composite biomaterial as noted in Chapter 3 and Chapter 4.

6.3.6 Hybrid composite biomaterial prolongs delivery of VPA

We examined the release kinetics and stability of the VPA from hybrid composite biomaterial **(section 3.7)** *in vitro* **(Figure 6.8A)**. Upon casting hybrid composite biomaterial PBS was added on top and release profile of VPA was evaluated by analysis of supernatant at defined intervals followed by PBS replenishment. LC-MS analysis indicated that the hybrid composite biomaterial provided prolonged release of VPA over 8 weeks **(Figure 6.8B)**. These findings demonstrate that VPA encapsulated within the hybrid composite biomaterial will provide long-term delivery.

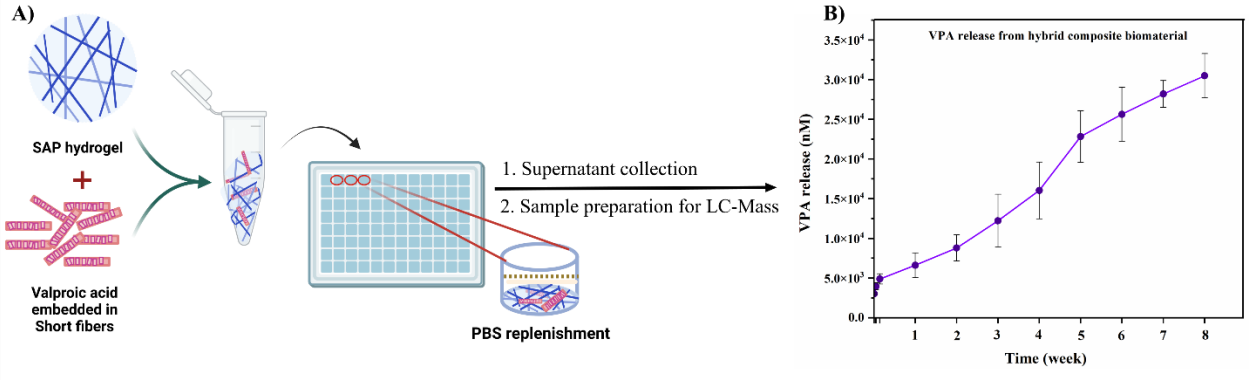

Figure 6.8. In vitro release profile of VPA from hybrid composite biomaterial. A) Schematic diagram of in vitro study design, **B)** Quantification of VPA release from hybrid composite biomaterial over 8 weeks. Data represent mean ± SEM. n=3/time point. Panel A is **Created with BioRender.com.**

6.3.7 Incorporating AAV-SOX2 within a SAP hydrogel sustains viral delivery while retains viral functional activity

To demonstrate the controlled release and functional activity of AAV, the DJ gfaABC1D-SOX2-mCherry was mixed with Fmoc-DDIKVAV SAP hydrogel before gelation (SAP+AAV) then cast in 96/or 24 well plates and equilibrate in incubator overnight.

For release profile assessment, PBS was added on top of the cast SAP+AAV in 96 well plates and PBS was collected at defined time points and replenished with fresh PBS each time. Then the collected PBS was analysed using qPCR **(Figure 6.9A)**. As expected, the results revealed the sustained release of the AAV-SOX2 from SAP hydrogel **(Figure 6.9B)**. The sustain release

of AAVs from hydrogel have several advantages such as: i) minimising rapid clearance of AAV by immune system, ii) avoiding cellular stress, iii) better integration of transgene, and iv) optimal vector exposure, which ultimately guide cell fate.

Moreover, to confirm the functional activity of AAV-SOX2, after casting SAP+AAV in 24 well plates and equilibration overnight, astrocytes were cultured on top of the SAP+AAV, changing the medium every 2-3 days. Cells were monitored for 10 days after transduction. As seen in **(Figure 6.9C)** AAV-SOX2 transduction gave rise to colonies of small cells resembling NSCs confirming cells underwent proliferating states while in mCherry-AAV transduced cells, as control, this pattern was not observed **(Figure 6.9D)**.

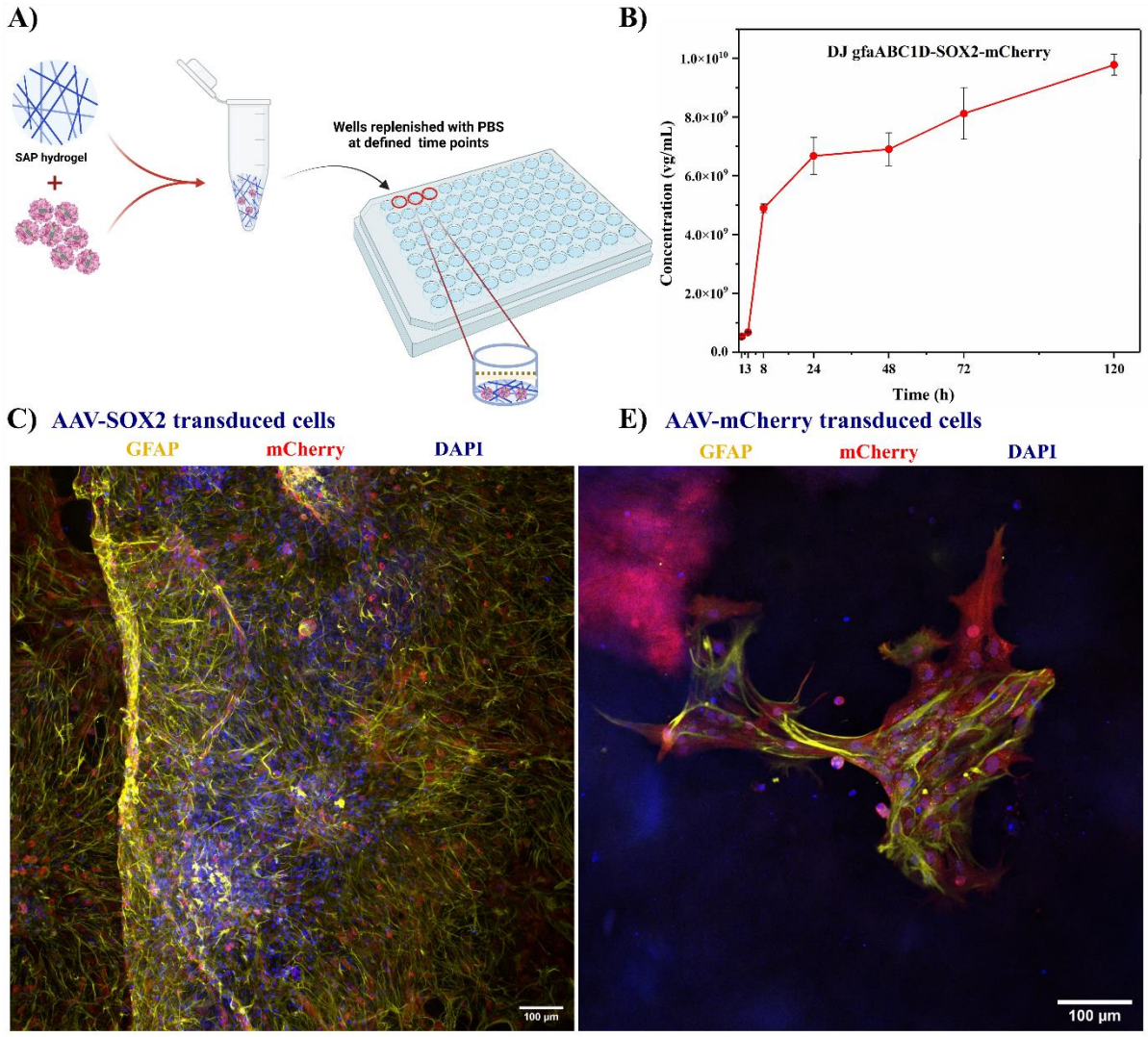

Figure 6.9. Hydrogel encapsulated AAV-SOX2 prolonged viral release and retains its functional activity. A) Schematic diagram of *in vitro* study design, **B)** Quantification of AAV-SOX2 release from SAP hydrogel at defined time points. Representative images of **(C)** AAV-SOX2 and **(D)** empty vector (AAV-mCherry) transduced cells. Scale bar= 100µm. Data represent mean ± SEM. n=3/time point. Panel A is **Created with BioRender.com.**

6.3.8 SOX2 forced expression generates intermediate neuroblast cells *in vivo*

Neurogenesis around the AAV-SOX2 injection site was initially examined by staining for the expression of doublecortin (DCX). It has been reported that neurogenesis through SOX2 ectopic expression is a slow process because DCX+ cells are not readily detectable until 4 weeks post transduction (wpt)[22]. Our observation on 4 wpt confirmed the generation of DCX+ cells mainly surrounding the AAV-SOX2 injection site **(Figure 6.10A)**. While, in sharp contrast DCX+ cells can be sparsely detected along or surrounding the site injected with empty vector (AAV-mCherry), indicating the absence of neuroblast cells **(Figure 6.10B)**. It has also been reported that, continual expression of SOX2 using CAG promoter induced approximately 37-fold fewer DCX+ cells compared to dynamic expression of SOX2 provided by hGFAP promoter[24]. These data indicate that the constitutive expression of SOX2 was not necessary and might even be detrimental to induced adult neuroblast cells (intermediated cells) expansion and survival. Here we observed that the induced DCX+ cells also did not express mCherry marker confirming the dynamic expression of SOX2 and silencing over the process of reprogramming.

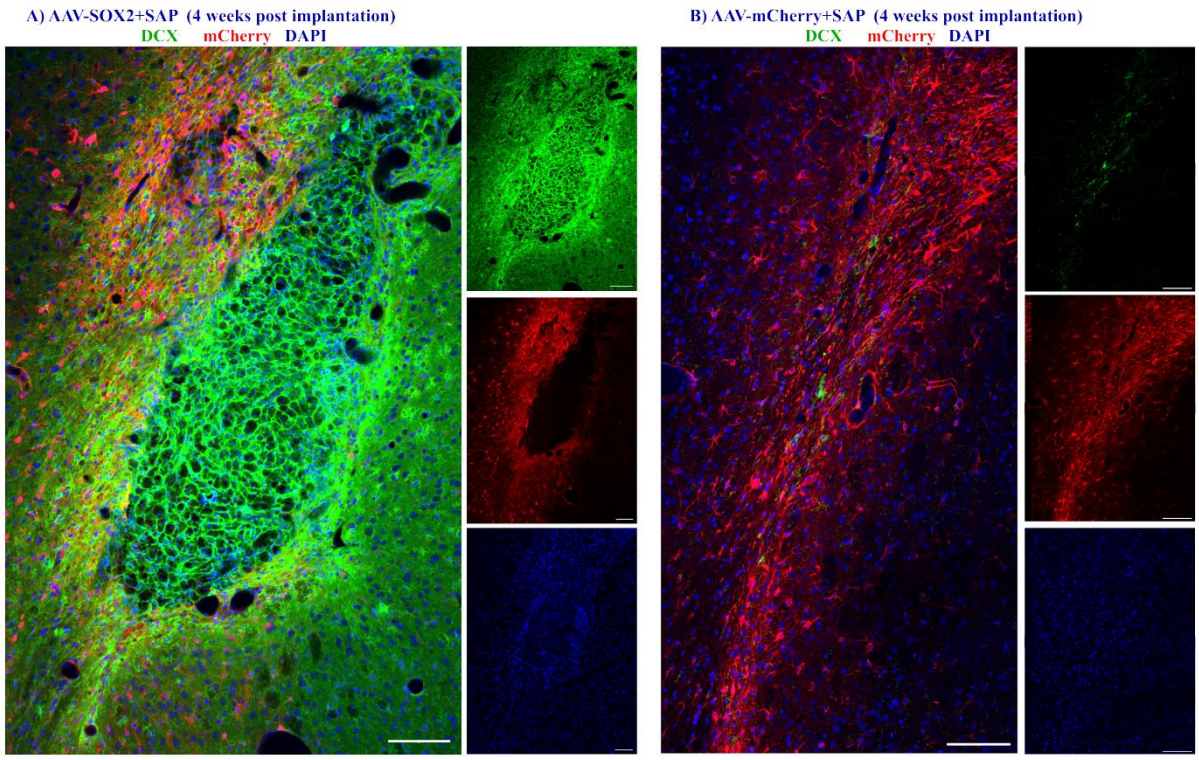

Figure 6.10. SOX2 ectopic expression induces doublecortin (DCX+) neuroblast cells. Representative images at the **A)** AAV-SOX2 and **B)** AAV-mCherry injection site sites illustrating DCX+ cells (green), mCherry transduced cells (red), and DAPI (Blue). Scale bar= 100µm.

These DCX+ neuroblast cells can eventually generate mature neurons when supplied with VPA, which will be the focus of our future works.

The plan for future *in vivo* application is to inject the hybrid composite biomaterial in the injured brain area with VPA concentration in therapeutic window (1 mM). To examine the effect of VPA in neuron maturation, we are planning to use mice in 6 different groups including i) AAV-mCherry + (Saline + VPA), ii) AAV-SOX2 + (Saline + VPA), iii) AAV-mCherry + (SAP + VPA), iv) AAV-SOX2 + (SAP + VPA), v) AAV-mCherry + hybrid composite biomaterial, vi) AAV-SOX2 + hybrid composite biomaterial. The animals will be monitored for 8 weeks and sacrificed.

6.4 Summary

In this chapter, the effect of AAV-SOX2 on the fate of reactive astrocytes was investigated. We have shown that reactive astrocytes transduced with SOX2 transcription factor passed

through the proliferative state (progenitor cells), *in vitro*. Then these progenitor cells adopted neuronal-like phenotype confirmed with immunostaining for neuronal markers. Finally, the generation of functional neurons was confirmed by the patch clamp approach, where the newly generated neurons showed the capacity to fire action potential. We have also shown that the DDIKVAV SAP hydrogel could provide a sustained release to AAV-SOX2 while also maintaining AAV activity after release. Moreover, the *in vivo* result confirmed the generation of DCX+ neuroblast cells as a transient cell in the process of astrocyte-to-neuron transformation.

Chapter 7. Conclusion and future perspectives

7.1 Preamble

In this chapter, the summary of thesis outcome and potential approaches to future investigations are described.

7.2 Conclusion

Traumatic brain injury (TBI) is a debilitating condition with high morbidity and mortality. Many survivors of TBI are left with permanent/long-term functional deficits, cognitive impairment, and they may develop epilepsy, all of which have a significant impact on quality of life. Due to the considerable damage and limited therapeutic approaches available, TBI is a serious public health problem. Thus, a goal of regenerative medicine is to replace lost or degenerate neurons and restore lost functions.

In vivo reprogramming holds great promise for the future of neuroregenerative medicine. This unique approach can generate cells for replacement and repair endogenously from the population of host cells at the injury site, without the need for an exogenous cell source that faces survival, integration, and immunological challenges. In addition to TBI, a wide array of neurodegenerative diseases (e.g., Alzheimer's disease, Parkinson's disease, multiple sclerosis, amyotrophic lateral sclerosis, Huntington's disease) are also associated with astrocyte dysfunction[308]; therefore, i*n vivo* reprogramming of these cells may provide a means to treat these disorders.

In Chapter 3, a solid-phase peptide synthesis (SPPS) method was used to synthesise different libraries of peptide sequences, with the final deprotection step omitted to preserve the aromatic N-fluorenylmethyloxycarbonyl (Fmoc) moiety. These different libraries of peptides were self-assembled into hydrogels under physiological conditions without the addition of any organic solvents. These fabricated self-assembling peptide (SAP) hydrogels were characterised in terms of their molecular arrangement, nanostructure, and mechanical properties. Moreover, a hybrid composite biomaterial was fabricated using incorporation of valproic acid (VPA) in Polylactic acid (PLA) electrospun nanofibres and then the inclusion of short fibres from these electrospun nanofibres in the SAP hydrogel. We have shown that the resultant hybrid composite biomaterial sustained the delivery of VPA over 8 weeks' time, *in vitro*. Moreover,

the inclusion of short fibres in the SAP hydrogel did not cause disruption to self-assembly mechanism.

In Chapter 5, the transduction efficiency and cell fate reprogramming of mouse primary astrocytes and human astrocytes using an adeno-associated virus (AAV) encoded with NeuroD1 single transcription factor (TF) were studied. At 28 days post-transduction (DPT) of primary astrocytes/ and human astrocytes with AAV-NeuroD1, the conversion of astrocyte to neuronal cells was confirmed with a β-tubulin neuronal marker with high reprogramming efficiency, 78.2 ± 4.9%, and 76.6 ± 3.2% respectively. In current-clamp mode, gradually increasing membrane depolarisation steps triggered the firing of action potentials in the cells transduced from primary astrocytes and human astrocytes.

In vivo, in a needle stick injury model, AAV-NeuroD1±SAP implantation redirected the resident reactive astrocytes into neurons in the injection site and reduced the glial scar intensity. More importantly, we have shown that the constructed viral vector preferentially transduces astrocytes, GFAP-positive cells, and not preexisting neurons. Furthermore, with the use of SAP hydrogels to provide spatiotemporal release of AAV-NeuroD1, the population of NeuN-positive cells within the needle track was significantly higher compared to AAV-NeuroD1 implantation alone. This data suggests that higher efficacy of reprogramming was achieved at lower doses (sustained release of AAV from hydrogel provided lower dose at any given time) of AAV-NeuroD1 provided by the SAP hydrogel. Therefore, using this combined approach of delivering NeuroD1-based gene therapy using SAP hydrogels may open a new avenue for brain repair using intrinsic glial cells to generate new functionally active neurons.

In Chapter 6, the transduction efficiency and cell fate reprogramming of mouse primary astrocytes using AAV encoded with SOX2 TF were studied. We have demonstrated several approaches to confirm the intermediate progenitor neural stem cell formation using nestin marker, cell cycle analysis, and IncuCyte live microscope imaging. Then the conversion of

these intermediate cells to neuronal cells was confirmed using neuronal cell markers such as β-tubulin, MAP2, and NeuN. The newly generated neuronal cells were able to fire action potential at 42 DPT. These data suggest that, in vitro, using NeuroD1 ectopic expression, astrocyte-to-neuron conversion can be achieved in 4 weeks' time, whereas with overexpression of SOX2 TF, this conversion occurs in a more protracted time, 42 days post-transduction, as confirmed with electrophysiology recording.

In vivo, the formation of intermediate neuroblast cells was confirmed through the expression of doublecortin (DCX)-positive cells within the needle track. In the end, in the process of reprogramming astrocytes to neurons each of the trans-differentiation and de-differentiation approaches has advantages and disadvantages. For example, to achieve functional neurons using SOX2 transcription factor more protracted time is required. However, using the NeuroD1 transcription factor functional neurons would be generated in a shorter time but much less than the SOX2 transcription factor.

In summary, as discussed inChapter 2, several labs have recently been working on the reprogramming of astrocytes to neurons to restore functional connectivity among neurons and provide neural integration with host tissue. However, concerns around high dosage administration, transgene clearance by the immune system, AAV neural leakage, and lack of physical support for the newly generated cells remained despite significant progress in the field. Our study aimed to advance the field to some extent, by using SAP hydrogels not only as a platform to provide sustained release of AAVs and VPA in the site of therapeutic needs but also to provide physical support for the newly generated cells to revive and survive. Moreover, the engineered AAVDJ preferentially transduced astrocytes which can further address the concerns around AAV neural leakage and its off-target transduction.

Considering the key findings of the present thesis, several future research activities are proposed in this section.

7.3 Future perspectives

Firstly, we are planning to perform an *in vivo* study to implant AAV-SOX2 together with fabricated composite biomaterial (VPA short fibres + SAP hydrogel) after 10 days post-injury and monitor the differentiation to NeuN-positive cells within the needle track at 8 weeks post-implantation. We hypothesised that using the constructed composite biomaterial, the sustained release of VPA *in situ* within the needle track could drive the differentiation of intermediate neuroblast cells (DCX-positive cells) to NeuN-positive cells without the need for daily intraperitoneal injection in mice.

Another avenue for future work would be to determine the exact time point at which TF-encoded AAV should be delivered to minimise the cytotoxic behaviours of reactive astrocytes and encourage growth-supportive/-permissive phenotypes. Currently, researchers agree that it should be sometime after the acute phase of injury (1-2 weeks post-injury), however, this time point would be dependent on the size, severity, and location of the injury. Then, we would need to develop mechanisms to exert temporal control over the delivery of AAV from the biomaterials, achieving such behavioural changes in astrocytes. This might be feasible using the positive residues in the SAP hydrogel to fabricate a positively charged hydrogel without having a detrimental effect on the assembly mechanism. Therefore, the resultant positively charged SAP can interact with AAV with a negative charge which not only can provide delayed delivery of the AAV within the injury site but also might obviate the need for a second needle injection *in vivo* to implant SAP+AAV after 10 days post-injury creation. In this case, all the procedures from injury creation and material implantation can be performed in one injection. Moreover, to provide a greater delayed delivery as well as complex multi-component delivery (e.g., growth factor, VPA, anti-inflammatory drugs) multi-layered short fibres can be prepared by coaxial electrospinning.

It is worth pointing out that during our study, we have noticed a variation among different cell culture plates in terms of neuronal survival *in vitro*. Therefore, in the future working on the survival of the newly generated cells would be an important factor.

Cell fate reprogramming can be also extended to several other fascinating applications such as the reprogramming of inflammatory cells into desired cell types in neurodegenerative disease, spinal cord injuries, stroke, and any traumas to the brain or any other tissues. This approach can also be used in disease modeling using patients' own cells, drug screening, and precision medicine.

The Successful translation of these findings to a larger animal would allow us to develop better treatments and therapies for brain traumas/ and neurodegenerative diseases in humans. The larger animal can provide opportunities to assess the safety profiles of drugs/biomaterials and their potential adverse effects as they offer more similarity to humans compared to murine. However, there are some challenges such as higher maintenance costs and the need for long-term studies because of their lower metabolism rate.

The future work and directions presented in this thesis requires a collaborative approach between tissue engineers and biologists to realise and subsequently harness the reparative potential of astrocytes using novel biomaterial treatment strategies for traumatic brain injury.

References

[1] S.A. Goldman, Stem and Progenitor Cell-Based Therapy of the Central Nervous System: Hopes, Hype, and Wishful Thinking, Cell Stem Cell. 18 (2016) 174–188. https://doi.org/10.1016/j.stem.2016.01.012.

[2] K. Hu, All roads lead to induced pluripotent stem cells: The technologies of iPSC generation, Stem Cells Dev. 23 (2014) 1285–1300. https://doi.org/10.1089/scd.2013.0620.

[3] V.W. Choi, D.M. McCarty, R.J. Samulski, Host Cell DNA Repair Pathways in Adeno-Associated Viral Genome Processing, J. Virol. 80 (2006) 10346–10356. https://doi.org/10.1128/jvi.00841-06.

[4] D.R. Nisbet, A.E. Rodda, M.K. Horne, J.S. Forsythe, D.I. Finkelstein, Neurite infiltration and cellular response to electrospun polycaprolactone scaffolds implanted into the brain, Biomaterials. 30 (2009) 4573–4580. https://doi.org/10.1016/j.biomaterials.2009.05.011.

[5] D. Gustafsson, A. Klang, S. Thams, E. Rostami, The role of bdnf in experimental and clinical traumatic brain injury, Int. J. Mol. Sci. 22 (2021). https://doi.org/10.3390/ijms22073582.

[6] N. Mukherjee, A. Adak, S. Ghosh, Recent trends in the development of peptide and protein-based hydrogel therapeutics for the healing of CNS injury, Soft Matter. 16 (2020) 10046–10064. https://doi.org/10.1039/d0sm00885k.

[7] M. V. Sofroniew, Reactive astrocytes in neural repair and protection, Neuroscientist. 11 (2005) 400–407. https://doi.org/10.1177/1073858405278321.

[8] D.J. Myer, G.G. Gurkoff, S.M. Lee, D.A. Hovda, M. V. Sofroniew, Essential protective roles of reactive astrocytes in traumatic brain injury, Brain. 129 (2006) 2761–2772. https://doi.org/10.1093/brain/awl165.

[9] J. Silver, J.H. Miller, Regeneration beyond the glial scar, Nat. Rev. Neurosci. 5 (2004) 146–156. https://doi.org/10.1038/nrn1326.

[10] M. Pekny, M. Pekna, Astrocyte reactivity and reactive astrogliosis: Costs and benefits, Physiol. Rev. 94 (2014) 1077–1098. https://doi.org/10.1152/physrev.00041.2013.

[11] Y. Chen, J. Lin, W. Yan, A Prosperous Application of Hydrogels With Extracellular Vesicles Release for Traumatic Brain Injury, Front. Neurol. 13 (2022) 1–12. https://doi.org/10.3389/fneur.2022.908468.

[12] Z.G. Zhang, B. Buller, M. Chopp, Exosomes — beyond stem cells for restorative therapy in stroke and neurological injury, Nat. Rev. Neurol. 15 (2019) 193–203. https://doi.org/10.1038/s41582-018-0126-4.

[13] S. Karimi-Abdolrezaee, R. Billakanti, Reactive astrogliosis after spinal cord injury-beneficial and detrimental effects, Mol. Neurobiol. 46 (2012) 251–264. https://doi.org/10.1007/s12035-012-8287-4.

[14] C. Bonnans, J. Chou, Z. Werb, 1. Bonnans, C.; Chou, J.; Werb, Z. No Title. Nat. Rev. Mol. Cell Biol. 2014, 15., Nat. Rev. Mol. Cell Biol. 15 (2014) 786–801. https://doi.org/10.1038/nrm3904.Remodelling.

[15] O.A. Carballo-Molina, I. Velasco, Hydrogels as scaffolds and delivery systems to enhance axonal regeneration after injuries, Front. Cell. Neurosci. 9 (2015). https://doi.org/10.3389/fncel.2015.00013.

[16] F. Berthiaume, P. V. Moghe, M. Toner, M.L. Yarmush, Effect of extracellular matrix

topology on cell structure, function, and physiological responsiveness: hepatocytes cultured in a sandwich configuration, FASEB J. 10 (1996) 1471–1484. https://doi.org/10.1096/fasebj.10.13.8940293.

[17] J.D. Koen, M.D. Rugg, Neural Dedifferentiation in the Aging Brain, Trends Cogn. Sci. 23 (2019) 547–559. https://doi.org/10.1016/j.tics.2019.04.012.

[18] Y. Huang, S. Tan, Direct lineage conversion of astrocytes to induced neural stem cells or neurons, Neurosci. Bull. 31 (2015) 357–367. https://doi.org/10.1007/s12264-014-1517-1.

[19] G. Masserdotti, S. Gascón, M. Götz, Direct neuronal reprogramming: Learning from and for development, Dev. 143 (2016) 2494–2510. https://doi.org/10.1242/dev.092163.

[20] T.I. Lee, R.A. Young, Transcriptional regulation and its misregulation in disease, Cell. 152 (2013) 1237–1251. https://doi.org/10.1016/j.cell.2013.02.014.

[21] W. Niu, T. Zang, D.K. Smith, T.Y. Vue, Y. Zou, R. Bachoo, J.E. Johnson, C.L. Zhang, SOX2 reprograms resident astrocytes into neural progenitors in the adult brain, Stem Cell Reports. 4 (2015) 780–794. https://doi.org/10.1016/j.stemcr.2015.03.006.

[22] Z. Su, W. Niu, M.L. Liu, Y. Zou, C.L. Zhang, In vivo conversion of astrocytes to neurons in the injured adult spinal cord, Nat. Commun. 5 (2014). https://doi.org/10.1038/ncomms4338.

[23] M. Zarei-Kheirabadi, M. Hesaraki, S. Kiani, H. Baharvand, In vivo conversion of rat astrocytes into neuronal cells through neural stem cells in injured spinal cord with a single zinc-finger transcription factor, Stem Cell Res. Ther. 10 (2019) 1–19. https://doi.org/10.1186/s13287-019-1448-x.

[24] W. Niu, T. Zang, Y. Zou, S. Fang, D.K. Smith, R. Bachoo, C.L. Zhang, In vivo reprogramming of astrocytes to neuroblasts in the adult brain, Nat. Cell Biol. 15 (2013) 1164–1175. https://doi.org/10.1038/ncb2843.

[25] M.Q. Jiang, S.P. Yu, Z.Z. Wei, W. Zhong, W. Cao, X. Gu, A. Wu, M.R. McCrary, K. Berglund, L. Wei, Conversion of Reactive Astrocytes to Induced Neurons Enhances Neuronal Repair and Functional Recovery After Ischemic Stroke, Front. Aging Neurosci. 13 (2021) 1–20. https://doi.org/10.3389/fnagi.2021.612856.

[26] G. Chen, M. Wernig, B. Berninger, M. Nakafuku, M. Parmar, C.L. Zhang, In vivo reprogramming for brain and spinal cord repair, ENeuro. 2 (2015). https://doi.org/10.1523/ENEURO.0106-15.2015.

[27] Y.C. Chen, N.X. Ma, Z.F. Pei, Z. Wu, F.H. Do-Monte, S. Keefe, E. Yellin, M.S. Chen, J.C. Yin, G. Lee, A. Minier-Toribio, Y. Hu, Y.T. Bai, K. Lee, G.J. Quirk, G. Chen, A NeuroD1 AAV-Based Gene Therapy for Functional Brain Repair after Ischemic Injury through In Vivo Astrocyte-to-Neuron Conversion, Mol. Ther. 28 (2020) 217–234. https://doi.org/10.1016/j.ymthe.2019.09.003.

[28] C.L. Gooch, E. Pracht, A.R. Borenstein, The burden of neurological disease in the United States: A summary report and call to action, Ann. Neurol. 81 (2017) 479–484. https://doi.org/10.1002/ana.24897.

[29] J.Y. Jiang, G.Y. Gao, J.F. Feng, Q. Mao, L.G. Chen, X.F. Yang, J.F. Liu, Y.H. Wang, B.H. Qiu, X.J. Huang, Traumatic brain injury in China, Lancet Neurol. 18 (2019) 286–295. https://doi.org/10.1016/S1474-4422(18)30469-1.

[30] C. Lazaridis, C.G. Rusin, C.S. Robertson, Secondary brain injury: Predicting and preventing insults, Neuropharmacology. 145 (2019) 145–152.

https://doi.org/10.1016/j.neuropharm.2018.06.005.

[31] H. Wu, J. Zheng, S. Xu, Y. Fang, Y. Wu, J. Zeng, A. Shao, L. Shi, J. Lu, S. Mei, X. Wang, X. Guo, Y. Wang, Z. Zhao, J. Zhang, Mer regulates microglial/macrophage M1/M2 polarization and alleviates neuroinflammation following traumatic brain injury, J. Neuroinflammation. 18 (2021) 1–20. https://doi.org/10.1186/s12974-020-02041-7.

[32] S.Y. Ng, A.Y.W. Lee, Traumatic Brain Injuries: Pathophysiology and Potential Therapeutic Targets, Front. Cell. Neurosci. 13 (2019) 1–23. https://doi.org/10.3389/fncel.2019.00528.

[33] F.M. Chen, X. Liu, Advancing biomaterials of human origin for tissue engineering, Prog. Polym. Sci. 53 (2016) 86–168. https://doi.org/10.1016/j.progpolymsci.2015.02.004.

[34] C. Tsui, K. Koss, M.A. Churchward, K.G. Todd, Biomaterials and glia: Progress on designs to modulate neuroinflammation, Acta Biomater. 83 (2019) 13–28. https://doi.org/10.1016/j.actbio.2018.11.008.

[35] T.E. Murray, C.M. Richards, V.N. Robert-Gostlin, A.K. Bernath, I.A. Lindhout, A. Klegeris, Potential neurotoxic activity of diverse molecules released by astrocytes, Brain Res. Bull. 189 (2022) 80–101. https://doi.org/10.1016/j.brainresbull.2022.08.015.

[36] S. Soleman, M.A. Filippov, A. Dityatev, J.W. Fawcett, Targeting the neural extracellular matrix in neurological disorders, Neuroscience. 253 (2013) 194–213. https://doi.org/10.1016/j.neuroscience.2013.08.050.

[37] A. Trounson, C. McDonald, Stem Cell Therapies in Clinical Trials: Progress and

Challenges, Cell Stem Cell. 17 (2015) 11–22. https://doi.org/10.1016/j.stem.2015.06.007.

[38] M.P. Kahle, G.J. Bix, Neuronal restoration following ischemic stroke: Influences, barriers, and therapeutic potential, Neurorehabil. Neural Repair. 27 (2013) 469–478. https://doi.org/10.1177/1545968312474119.

[39] K. Takahashi, K. Tanabe, M. Ohnuki, M. Narita, T. Ichisaka, K. Tomoda, S. Yamanaka, Induction of Pluripotent Stem Cells from Adult Human Fibroblasts by Defined Factors, Cell. 131 (2007) 861–872. https://doi.org/10.1016/j.cell.2007.11.019.

[40] P.S. Knoepfler, Deconstructing stem cell tumorigenicity: A roadmap to safe regenerative medicine, Stem Cells. 27 (2009) 1050–1056. https://doi.org/10.1002/stem.37.

[41] Y.M. Yuan, C. He, The glial scar in spinal cord injury and repair, Neurosci. Bull. 29 (2013) 421–435. https://doi.org/10.1007/s12264-013-1358-3.

[42] H. Li, G. Chen, In Vivo Reprogramming for CNS Repair: Regenerating Neurons from Endogenous Glial Cells, Neuron. 91 (2016) 728–738. https://doi.org/10.1016/j.neuron.2016.08.004.

[43] M. V. Sofroniew, H. V. Vinters, Astrocytes: Biology and pathology, Acta Neuropathol. 119 (2010) 7–35. https://doi.org/10.1007/s00401-009-0619-8.

[44] D.R. Nisbet, S. Pattanawong, N.E. Ritchie, W. Shen, D.I. Finkelstein, M.K. Horne, J.S. Forsythe, Interaction of embryonic cortical neurons on nanofibrous scaffolds for neural tissue engineering, J. Neural Eng. 4 (2007) 35–41. https://doi.org/10.1088/1741-2560/4/2/004.

[45] P. Kaur, S. Sharma, Recent Advances in Pathophysiology of Traumatic Brain Injury,

Curr. Neuropharmacol. 16 (2017) 1224–1238. https://doi.org/10.2174/1570159x15666170613083606.

[46] K. Zibara, N. Ballout, S. Mondello, N. Karnib, N. Ramadan, S. Omais, A. Nabbouh, D. Caliz, A. Clavijo, Z. Hu, N. Ghanem, S. Gajavelli, F. Kobeissy, Combination of drug and stem cells neurotherapy: Potential interventions in neurotrauma and traumatic brain injury, Neuropharmacology. 145 (2019) 177–198. https://doi.org/10.1016/j.neuropharm.2018.09.032.

[47] J.E. Burda, M. V. Sofroniew, Reactive gliosis and the multicellular response to CNS damage and disease, Neuron. 81 (2014) 229–248. https://doi.org/10.1016/j.neuron.2013.12.034.

[48] V. Bellver-Landete, F. Bretheau, B. Mailhot, N. Vallières, M. Lessard, M.E. Janelle, N. Vernoux, M.È. Tremblay, T. Fuehrmann, M.S. Shoichet, S. Lacroix, Microglia are an essential component of the neuroprotective scar that forms after spinal cord injury, Nat. Commun. 10 (2019). https://doi.org/10.1038/s41467-019-08446-0.

[49] M.A. Anderson, J.E. Burda, Y. Ren, Y. Ao, T.M. O'Shea, R. Kawaguchi, G. Coppola, B.S. Khakh, T.J. Deming, M. V. Sofroniew, Astrocyte scar formation AIDS central nervous system axon regeneration, Nature. 532 (2016) 195–200. https://doi.org/10.1038/nature17623.

[50] D. Davalos, J. Grutzendler, G. Yang, J. V. Kim, Y. Zuo, S. Jung, D.R. Littman, M.L. Dustin, W.B. Gan, ATP mediates rapid microglial response to local brain injury in vivo, Nat. Neurosci. 8 (2005) 752–758. https://doi.org/10.1038/nn1472.

[51] A. Nimmerjahn, F. Kirchhoff, F. Helmchen, Resting microglial cells are highly dynamic surveillants of brain parenchyma in vivo, Neuroforum. 11 (2005) 95–96.

https://doi.org/10.1515/nf-2005-0304.

[52] M. Jun-Ming Zhang, MSc, MD1 and Jianxiong An, MSc, Cytokines, Inflammation and Pain, Int Anesth. Clin. 45 (2007). https://doi.org/10.1097/AIA.0b013e318034194e.

[53] E. Syková, T. Mazel, L. Vargová, I. Voříšek, Š. Prokopová-Kubinová, Extracellular space diffusion and pathological states, Prog. Brain Res. 125 (2000) 155–178. https://doi.org/10.1016/S0079-6123(00)25008-5.

[54] R.M. Adibhatla, J.F. Hatcher, R.J. Dempsey, Lipids and lipidomics in brain injury and diseases, AAPS J. 8 (2006) 314–321. https://doi.org/10.1208/aapsj080236.

[55] M.L. Novak, T.J. Koh, Macrophage phenotypes during tissue repair, J. Leukoc. Biol. 93 (2013) 875–881. https://doi.org/10.1189/jlb.1012512.

[56] J.R. Potas, F. Haque, F.L. Maclean, D.R. Nisbet, Interleukin-10 conjugated electrospun polycaprolactone (PCL) nanofibre scaffolds for promoting alternatively activated (M2) macrophages around the peripheral nerve in vivo, J. Immunol. Methods. 420 (2015) 38–49. https://doi.org/10.1016/j.jim.2015.03.013.

[57] D.M. Mosser, J.P. Edwards, Exploring the full spectrum of macrophage activation, Nat. Rev. Immunol. 8 (2008) 958–969. https://doi.org/10.1038/nri2448.

[58] A. Alam, E.P. Thelin, T. Tajsic, D.Z. Khan, A. Khellaf, R. Patani, A. Helmy, Cellular infiltration in traumatic brain injury, J. Neuroinflammation. 17 (2020) 1–17. https://doi.org/10.1186/s12974-020-02005-x.

[59] M.A. Alam, V.P. Subramanyam Rallabandi, P.K. Roy, Systems biology of immunomodulation for post-stroke neuroplasticity: Multimodal implications of pharmacotherapy and neurorehabilitation, Front. Neurol. 7 (2016) 1–16. https://doi.org/10.3389/fneur.2016.00094.

[60] A. Kumar, D.M. Alvarez-Croda, B.A. Stoica, A.I. Faden, D.J. Loane, Microglial/Macrophage Polarization Dynamics following Traumatic Brain Injury, J. Neurotrauma. 33 (2016) 1732–1750. https://doi.org/10.1089/neu.2015.4268.

[61] L. Ben Haim, M.A. Carrillo-de Sauvage, K. Ceyzériat, C. Escartin, Elusive roles for reactive astrocytes in neurodegenerative diseases, Front. Cell. Neurosci. 9 (2015) 1–27. https://doi.org/10.3389/fncel.2015.00278.

[62] M. Simard, M. Nedergaard, The neurobiology of glia in the context of water and ion homeostasis, Neuroscience. 129 (2004) 877–896. https://doi.org/10.1016/j.neuroscience.2004.09.053.

[63] R.C. Koehler, R.J. Roman, D.R. Harder, Astrocytes and the regulation of cerebral blood flow, Trends Neurosci. 32 (2009) 160–169. https://doi.org/10.1016/j.tins.2008.11.005.

[64] C. Eroglu, B.A. Barres, Regulation of synaptic connectivity by glia, Nature. 468 (2010) 223–231. https://doi.org/10.1038/nature09612.

[65] E.M. Ullian, K.S. Christopherson, B.A. Barres, Role for glia in synaptogenesis, Glia. 47 (2004) 209–216. https://doi.org/10.1002/glia.20082.

[66] K.S. Christopherson, E.M. Ullian, C.C.A. Stokes, C.E. Mullowney, J.W. Hell, A. Agah, J. Lawler, D.F. Mosher, P. Bornstein, B.A. Barres, Thrombospondins are astrocyte-secreted proteins that promote CNS synaptogenesis, Cell. 120 (2005) 421–433. https://doi.org/10.1016/j.cell.2004.12.020.

[67] N. Rouach, A. Koulakoff, V. Abudara, K. Willecke, C. Giaume, Astroglial Metabolic Networks Sustain Hippocampal Synaptic Transmission, Science. 322 (2008) 1551–1555. http://science.sciencemag.org/content/322/5907/1551.abstract.

[68] B.A. Barres, The Mystery and Magic of Glia: A Perspective on Their Roles in Health and Disease, Neuron. 60 (2008) 430–440. https://doi.org/10.1016/j.neuron.2008.10.013.

[69] P. Hasel, W.H. Aisenberg, F.C. Bennett, S.A. Liddelow, Molecular and metabolic heterogeneity of astrocytes and microglia, Cell Metab. 35 (2023) 555–570. https://doi.org/10.1016/j.cmet.2023.03.006.

[70] R. Patani, G.E. Hardingham, S.A. Liddelow, Functional roles of reactive astrocytes in neuroinflammation and neurodegeneration, Nat. Rev. Neurol. 19 (2023) 395–409. https://doi.org/10.1038/s41582-023-00822-1.

[71] X. Han, M. Chen, F. Wang, M. Windrem, S. Wang, S. Shanz, Q. Xu, N.A. Oberheim, L. Bekar, S. Betstadt, A.J. Silva, T. Takano, S.A. Goldman, M. Nedergaard, Forebrain engraftment by human glial progenitor cells enhances synaptic plasticity and learning in adult mice, Cell Stem Cell. 12 (2013) 342–353. https://doi.org/10.1016/j.stem.2012.12.015.

[72] L.E. Clarke, B.A. Barres, Emerging roles of astrocytes in neural circuit development, Nat. Rev. Neurosci. 14 (2013) 311–321. https://doi.org/10.1038/nrn3484.

[73] J.A. Stogsdill, C.C. Harwell, S.A. Goldman, Astrocytes as master modulators of neural networks: Synaptic functions and disease-associated dysfunction of astrocytes, Ann. N. Y. Acad. Sci. (2023) 41–60. https://doi.org/10.1111/nyas.15004.

[74] A. Buffo, C. Rolando, S. Ceruti, Astrocytes in the damaged brain: Molecular and cellular insights into their reactive response and healing potential, Biochem. Pharmacol. 79 (2010) 77–89. https://doi.org/10.1016/j.bcp.2009.09.014.

[75] M. V. Sofroniew, Molecular dissection of reactive astrogliosis and glial scar

formation, Trends Neurosci. 32 (2009) 638–647. https://doi.org/10.1016/j.tins.2009.08.002.

[76] E. Syková, Glial diffusion barriers during aging and pathological states, Prog. Brain Res. 132 (2001) 339–363. https://doi.org/10.1016/S0079-6123(01)32087-3.

[77] T. Roitbak, E. Syková, Diffusion barriers evoked in the rat cortex by reactive astrogliosis, Glia. 28 (1999) 40–48. https://doi.org/10.1002/(SICI)1098-1136(199910)28:1<40::AID-GLIA5>3.0.CO;2-6.

[78] N. Mukherjee, S. Ghosh, Myelin Associated Inhibitory Proteins as a Therapeutic Target for Healing of CNS Injury, ACS Chem. Neurosci. 11 (2020) 1699–1700. https://doi.org/10.1021/acschemneuro.0c00280.

[79] T.S. ARGYRIS, Growth Inhibitors, Science (80-.). 194 (1976) 718–718. https://doi.org/10.1126/science.194.4266.718-a.

[80] F.N. Soria, C. Miguelez, O. Peñagarikano, J. Tønnesen, Current Techniques for Investigating the Brain Extracellular Space, 14 (2020) 1–15. https://doi.org/10.3389/fnins.2020.570750.

[81] S. Budday, G. Sommer, C. Birkl, C. Langkammer, J. Haybaeck, J. Kohnert, M. Bauer, F. Paulsen, P. Steinmann, E. Kuhl, G.A. Holzapfel, Mechanical characterization of human brain tissue, Acta Biomater. 48 (2017) 319–340. https://doi.org/10.1016/j.actbio.2016.10.036.

[82] J.L. Drury, D.J. Mooney, Hydrogels for tissue engineering: Scaffold design variables and applications, Biomaterials. 24 (2003) 4337–4351. https://doi.org/10.1016/S0142-9612(03)00340-5.

[83] J. Zhu, R.E. Marchant, Design properties of hydrogel tissue-engineering scaffolds,

Expert Rev. Med. Devices. 8 (2011) 607–626. https://doi.org/10.1586/erd.11.27.

[84] P.S. Briquez, L.E. Clegg, M.M. Martino, F. Mac Gabhann, J.A. Hubbell, Design principles for therapeutic angiogenic materials, Nat. Rev. Mater. 1 (2016) 1–15. https://doi.org/10.1038/natrevmats.2015.6.

[85] A.M. Akimoto, E. Hasuike, H. Tada, K. Nagase, T. Okano, H. Kanazawa, R. Yoshida, Design of tetra-arm PEG-crosslinked thermoresponsive hydrogel for 3D cell culture, Anal. Sci. 32 (2016) 1203–1206. https://doi.org/10.2116/analsci.32.1203.

[86] E. Ruel-Gariépy, J.C. Leroux, In situ-forming hydrogels - Review of temperature-sensitive systems, Eur. J. Pharm. Biopharm. 58 (2004) 409–426. https://doi.org/10.1016/j.ejpb.2004.03.019.

[87] A. Cembran, K.F. Bruggeman, R.J. Williams, C.L. Parish, D.R. Nisbet, Biomimetic Materials and Their Utility in Modeling the 3-Dimensional Neural Environment, IScience. 23 (2020) 100788. https://doi.org/10.1016/j.isci.2019.100788.

[88] F.L. Maclean, M.K. Horne, R.J. Williams, D.R. Nisbet, Review: Biomaterial systems to resolve brain inflammation after traumatic injury, APL Bioeng. 2 (2018). https://doi.org/10.1063/1.5023709.

[89] F.Y. Hsieh, T.C. Tseng, S.H. Hsu, Self-healing hydrogel for tissue repair in the central nervous system, Neural Regen. Res. 10 (2015) 1922–1923. https://doi.org/10.4103/1673-5374.169624.

[90] V.A. Patil, K.S. Masters, Engineered collagen matrices, Bioengineering. 7 (2020) 1–20. https://doi.org/10.3390/bioengineering7040163.

[91] A.R. Donaldson, C.E. Tanase, D. Awuah, P.V. Bathrinarayanan, L. Hall, M. Nikkhah, A. Khademhosseini, F. Rose, C. Alexander, A.M. Ghaemmaghami, Photocrosslinkable

gelatin hydrogels modulate the production of the major pro-inflammatory cytokine, TNF-α, by human mononuclear cells, Front. Bioeng. Biotechnol. 6 (2018) 1–11. https://doi.org/10.3389/fbioe.2018.00116.

[92] Y.H. Tsou, J. Khoneisser, P.C. Huang, X. Xu, Hydrogel as a bioactive material to regulate stem cell fate, Bioact. Mater. 1 (2016) 39–55. https://doi.org/10.1016/j.bioactmat.2016.05.001.

[93] M. Guvendiren, J.A. Burdick, Engineering synthetic hydrogel microenvironments to instruct stem cells, Curr. Opin. Biotechnol. 24 (2013) 841–846. https://doi.org/10.1016/j.copbio.2013.03.009.

[94] H.K. Lau, K.L. Kiick, Opportunities for multicomponent hybrid hydrogels in biomedical applications, Biomacromolecules. 16 (2015) 28–42. https://doi.org/10.1021/bm501361c.

[95] S. Zhang, Fabrication of novel biomaterials through molecular self-assembly, Nat. Biotechnol. 21 (2003) 1171–1178. https://doi.org/10.1038/nbt874.

[96] G.M. Whitesides, B. Grzybowski, Self-assembly at all scales, Science (80-.). 295 (2002) 2418–2421. https://doi.org/10.1126/science.1070821.

[97] M.J. Mahoney, C. Krewson, J. Miller, W.M. Saltzman, Impact of cell type and density on nerve growth factor distribution and bioactivity in 3-dimensional collagen gel cultures, Tissue Eng. 12 (2006) 1915–1927. https://doi.org/10.1089/ten.2006.12.1915.

[98] J. Jiang, C. Dai, X. Liu, L. Dai, R. Li, K. Ma, H. Xu, F. Zhao, Z. Zhang, T. He, X. Niu, X. Chen, S. Zhang, Implantation of regenerative complexes in traumatic brain injury canine models enhances the reconstruction of neural networks and motor function recovery, Theranostics. 11 (2020) 768–788. https://doi.org/10.7150/thno.50540.

[99] S. Ma, J. Zhou, T. Huang, Z. Zhang, Q. Xing, X. Zhou, K. Zhang, M. Yao, T. Cheng, X. Wang, X. Wen, F. Guan, Sodium alginate/collagen/stromal cell-derived factor-1 neural scaffold loaded with BMSCs promotes neurological function recovery after traumatic brain injury, Acta Biomater. 131 (2021) 185–197. https://doi.org/10.1016/j.actbio.2021.06.038.

[100] S.H. Bhang, T.J. Lee, J.M. Lim, J.S. Lim, A.M. Han, C.Y. Choi, Y.H. Kim Kwon, B.S. Kim, The effect of the controlled release of nerve growth factor from collagen gel on the efficiency of neural cell culture, Biomaterials. 30 (2009) 126–132. https://doi.org/10.1016/j.biomaterials.2008.09.021.

[101] D. Zhang, Y. Ren, Y. He, R. Chang, S. Guo, S. Ma, F. Guan, M. Yao, In situ forming and biocompatible hyaluronic acid hydrogel with reactive oxygen species-scavenging activity to improve traumatic brain injury repair by suppressing oxidative stress and neuroinflammation, Mater. Today Bio. 15 (2022) 100278. https://doi.org/10.1016/j.mtbio.2022.100278.

[102] L. Wang, D. Zhang, Y. Ren, S. Guo, J. Li, S. Ma, M. Yao, F. Guan, Injectable hyaluronic acid hydrogel loaded with BMSC and NGF for traumatic brain injury treatment, Mater. Today Bio. 13 (2022) 100201. https://doi.org/10.1016/j.mtbio.2021.100201.

[103] Y.J. Ren, Z.Y. Zhou, F.Z. Cui, Y. Wang, J.P. Zhao, Q.Y. Xu, Hyaluronic acid/polylysine hydrogel as a transfer system for transplantation of neural stem cells, J. Bioact. Compat. Polym. 24 (2009) 56–62. https://doi.org/10.1177/0883911508099472.

[104] M. Mori, M. Yamaguchi, S. Sumitomo, Y. Takai, Hyaluronan-based Biomaterials in Tissue Engineering, Acta Histochem. Cytochem. 37 (2004) 1–5. https://doi.org/10.1267/ahc.37.1.

[105] L. Pan, Y. Ren, F. Cui, Q. Xu, Viability and differentiation of neural precursors on hyaluronic acid hydrogel scaffold, J. Neurosci. Res. 87 (2009) 3207–3220. https://doi.org/10.1002/jnr.22142.

[106] H. Kumar, Commentary on "The Role of Alginate Hydrogels as a Potential Treatment Modality for Spinal Cord Injury: A Comprehensive Review of the Literature," Neurospine. 19 (2022) 281–282. https://doi.org/10.14245/ns.2244490.245.

[107] N. Siti-Ismail, A.E. Bishop, J.M. Polak, A. Mantalaris, The benefit of human embryonic stem cell encapsulation for prolonged feeder-free maintenance, Biomaterials. 29 (2008) 3946–3952. https://doi.org/10.1016/j.biomaterials.2008.04.027.

[108] B. Singh, A. Kumar, Rohit, Gamma radiation formation of sterculia gum-alginate-carbopol hydrogel dressing by grafting method for use in brain drug delivery, Chem. Phys. Lett. 779 (2021) 138875. https://doi.org/10.1016/j.cplett.2021.138875.

[109] H. Itosaka, S. Kuroda, H. Shichinohe, H. Yasuda, S. Yano, S. Kamei, R. Kawamura, K. Hida, Y. Iwasaki, Fibrin matrix provides a suitable scaffold for bone marrow stromal cells transplanted into injured spinal cord: A novel material for CNS tissue engineering, Neuropathology. 29 (2009) 248–257. https://doi.org/10.1111/j.1440-1789.2008.00971.x.

[110] T.G. do Carmo Oliveira, A.C.M. dos Santos, A.D. Assis, R.T. Borges, J.R. da Costa Silva, C. Ueira-Vieira, G.F. Simões, R.G. Zanon, TNF-mimetic peptide mixed with fibrin glue improves peripheral nerve regeneration, Brain Res. Bull. 174 (2021) 53–62. https://doi.org/10.1016/j.brainresbull.2021.06.001.

[111] D.D. Ojeda-Hernández, U. Gomez-Pinedo, M.A. Hernández-Sapiéns, A.A. Canales-

Aguirre, H. Espinosa-Andrews, J. Matias-Guiu, Y. González-García, J.C. Mateos-Díaz, Biocompatibility of ferulic/succinic acid-grafted chitosan hydrogels for implantation after brain injury: A preliminary study, Mater. Sci. Eng. C. 121 (2021). https://doi.org/10.1016/j.msec.2020.111806.

[112] K.E. Crompton, J.D. Goud, R. V. Bellamkonda, T.R. Gengenbach, D.I. Finkelstein, M.K. Horne, J.S. Forsythe, Polylysine-functionalised thermoresponsive chitosan hydrogel for neural tissue engineering, Biomaterials. 28 (2007) 441–449. https://doi.org/10.1016/j.biomaterials.2006.08.044.

[113] S. Cai, T. Lei, W. Bi, S. Sun, S. Deng, X. Zhang, Y. Yang, Z. Xiao, H. Du, Chitosan Hydrogel Supplemented with Metformin Promotes Neuron–like Cell Differentiation of Gingival Mesenchymal Stem Cells, Int. J. Mol. Sci. 23 (2022). https://doi.org/10.3390/ijms23063276.

[114] D.R. Nisbet, D. Moses, T.R. Gengenbach, J.S. Forsythe, D.I. Finkelstein, M.K. Horne, Enhancing neurite outgrowth from primary neurones and neural stem cells using thermoresponsive hydrogel scaffolds for the repair of spinal cord injury, J. Biomed. Mater. Res. - Part A. 89 (2009) 24–35. https://doi.org/10.1002/jbm.a.31962.

[115] S.E. Stabenfeldt, M.C. Laplaca, Variations in rigidity and ligand density influence neuronal response in methylcellulose-laminin hydrogels, Acta Biomater. 7 (2011) 4102–4108. https://doi.org/10.1016/j.actbio.2011.07.026.

[116] M. Li, M.J. Mondrinos, X. Chen, M.R. Gandhi, F.K. Ko, P.I. Lelkes, Elastin Blends for Tissue Engineering Scaffolds, J. Biomed. Mater. Res. Part A. 79 (2006) 963–73. https://doi.org/10.1002/jbm.a.

[117] S. Woerly, S. Fort, I. Pignot-Paintrand, C. Cottet, C. Carcenac, M. Savasta,

Development of a sialic acid-containing hydrogel of poly[N-(2-hydroxypropyl) methacrylamide]: Characterization and implantation study, Biomacromolecules. 9 (2008) 2329–2337. https://doi.org/10.1021/bm800234r.

[118] H. Containing, S. Cells, I. The, L. Rat, O. Tract, Lesioned Rat Optic Tract, 7 (1998) 381–391.

[119] N.K. Loh, S. Woerly, S.M. Bunt, S.D. Wilton, A.R. Harvey, The regrowth of axons within tissue defects in the cns is promoted by implanted hydrogel matrices that contain BDNF and CNTF producing fibroblasts, Exp. Neurol. 170 (2001) 72–84. https://doi.org/10.1006/exnr.2001.7692.

[120] P.D. Dalton, L. Flynn, M.S. Shoichet, Manufacture of poly(2-hydroxyethyl methacrylate-co-methyl methacrylate) hydrogel tubes for use as nerve guidance channels, Biomaterials. 23 (2002) 3843–3851. https://doi.org/10.1016/S0142-9612(02)00120-5.

[121] G.W. Plant, S. Woerly, A.R. Harvey, Hydrogels containing peptide or aminosugar sequences implanted into the rat brain: Influence on cellular migration and axonal growth, Exp. Neurol. 143 (1997) 287–299. https://doi.org/10.1006/exnr.1997.6407.

[122] P. Lesný, J. De Croos, M. Přádný, J. Vacík, J. Michálek, S. Woerly, E. Syková, Polymer hydrogels usable for nervous tissue repair, J. Chem. Neuroanat. 23 (2002) 243–247. https://doi.org/10.1016/S0891-0618(02)00011-X.

[123] M.V. Wanjale, V.S. Jaikumar, K.C. Sivakumar, R.A. Paul, J. James, G.S.V. Kumar, Supramolecular Hydrogel Based Post-Surgical Implant System for Hydrophobic Drug Delivery Against Glioma Recurrence, Int. J. Nanomedicine. 17 (2022) 2203–2224. https://doi.org/10.2147/IJN.S348559.

[124] S.R. Hynes, M.F. Rauch, J.P. Bertram, E.B. Lavik, A library of tunable poly(ethylene glycol)/poly(L-lysine) hydrogels to investigate the material cues that influence neural stem cell differentiation, J. Biomed. Mater. Res. - Part A. 89 (2009) 499–509. https://doi.org/10.1002/jbm.a.31987.

[125] U. Freudenberg, A. Hermann, P.B. Welzel, K. Stirl, S.C. Schwarz, M. Grimmer, A. Zieris, W. Panyanuwat, S. Zschoche, D. Meinhold, A. Storch, C. Werner, A star-PEG-heparin hydrogel platform to aid cell replacement therapies for neurodegenerative diseases, Biomaterials. 30 (2009) 5049–5060. https://doi.org/10.1016/j.biomaterials.2009.06.002.

[126] L. Wang, D. Zhang, Y. Ren, S. Guo, J. Li, S. Ma, M. Yao, F. Guan, Injectable hyaluronic acid hydrogel loaded with BMSC and NGF for traumatic brain injury treatment, Mater. Today Bio. 13 (2022) 100201. https://doi.org/10.1016/j.mtbio.2021.100201.

[127] R.G. Ellis-Behnke, Y.X. Liang, S.W. You, D.K.C. Tay, S. Zhang, K.F. So, G.E. Schneider, Nano neuro knitting: Peptide nanofiber scaffold for brain repair and axon regeneration with functional return of vision, Proc. Natl. Acad. Sci. U. S. A. 103 (2006) 5054–5059. https://doi.org/10.1073/pnas.0600559103.

[128] G.A. Silva, C. Czeisler, K.L. Niece, E. Beniash, D.A. Harrington, J.A. Kessler, S.I. Stupp, Selective Differentiation of Neural Progenitor Cells by High-Epitope Density Nanofibers, Science (80-.). 303 (2004) 1352–1355. https://doi.org/10.1126/science.1093783.

[129] T.C. Holmes, Pii: S0167-7799(01)01840-6, TRENDS Biotechnol. 20 (2002) 16–21. http://tibtech.trends.com0167-7799/02/$-seefrontmatter.

[130] S. Zhang, F. Gelain, X. Zhao, Designer self-assembling peptide nanofiber scaffolds for 3D tissue cell cultures, Semin. Cancer Biol. 15 (2005) 413–420. https://doi.org/10.1016/j.semcancer.2005.05.007.

[131] D.R. Nisbet, R.J. Williams, Self-assembled peptides: Characterisation and in vivo response, Biointerphases. 7 (2012) 1–14. https://doi.org/10.1007/s13758-011-0002-x.

[132] M.E. Davis, P.C.H. Hsieh, T. Takahashi, Q. Song, S. Zhang, R.D. Kamm, A.J. Grodzinsky, P. Anversa, R.T. Lee, Local myocardial insulin-like growth factor 1 (IGF-1) delivery with biotinylated peptide nanofibers improves cell therapy for myocardial infarction, Proc. Natl. Acad. Sci. U. S. A. 103 (2006) 8155–8160. https://doi.org/10.1073/pnas.0602877103.

[133] H. Xiong, B.L. Buckwalter, H.M. Shieh, M.H. Hecht, Periodicity of polar and nonpolar amino acids is the major determinant of secondary structure in self-assembling oligomeric peptides, Proc. Natl. Acad. Sci. U. S. A. 92 (1995) 6349–6353. https://doi.org/10.1073/pnas.92.14.6349.

[134] J.B. Matson, S.I. Stupp, Drug release from hydrazone-containing peptide amphiphiles, Chem. Commun. 47 (2011) 7962–7964. https://doi.org/10.1039/c1cc12570b.

[135] S. Mura, J. Nicolas, P. Couvreur, Stimuli-responsive nanocarriers for drug delivery, Nat. Mater. 12 (2013) 991–1003. https://doi.org/10.1038/nmat3776.

[136] N.C. Wickremasinghe, V.A. Kumar, J.D. Hartgerink, Two-step self-assembly of liposome-multidomain peptide nanofiber hydrogel for time-controlled release, Biomacromolecules. 15 (2014) 3587–3595. https://doi.org/10.1021/bm500856c.

[137] Y. Geng, P. Dalhaimer, S. Cai, R. Tsai, M. Tewari, T. Minko, D.E. Discher, Shape effects of filaments versus spherical particles in flow and drug delivery, Nat.

Nanotechnol. 2 (2007) 249–255. https://doi.org/10.1038/nnano.2007.70.

[138] S. Zhang, M. Altman, Peptide self-assembly in functional polymer science and engineering, React. Funct. Polym. 41 (1999) 91–102. https://doi.org/10.1016/S1381-5148(99)00031-0.

[139] S. Kyle, A. Aggeli, E. Ingham, M.J. McPherson, Production of self-assembling biomaterials for tissue engineering, Trends Biotechnol. 27 (2009) 423–433. https://doi.org/10.1016/j.tibtech.2009.04.002.

[140] R. Vasita, D.S. Katti, Nanofibers and their applications in tissue engineering, Int. J. Nanomedicine. 1 (2006) 15–30. https://doi.org/10.2147/nano.2006.1.1.15.

[141] G.A. Silva, Nanotechnology approaches for the regeneration and neuroprotection of the central nervous system, Surg. Neurol. 63 (2005) 301–306. https://doi.org/10.1016/j.surneu.2004.06.008.

[142] X. Du, J. Zhou, J. Shi, B. Xu, Supramolecular Hydrogelators and Hydrogels: From Soft Matter to Molecular Biomaterials, Chem. Rev. 115 (2015) 13165–13307. https://doi.org/10.1021/acs.chemrev.5b00299.

[143] R.J. Williams, A.M. Smith, R. Collins, N. Hodson, A.K. Das, R. V. Ulijn, Enzyme-assisted self-assembly under thermodynamic control, Nat. Nanotechnol. 4 (2009) 19–24. https://doi.org/10.1038/nnano.2008.378.

[144] N. Habibi, N. Kamaly, A. Memic, H. Shafiee, Self-assembled peptide-based nanostructures: Smart nanomaterials toward targeted drug delivery, Nano Today. 11 (2016) 41–60. https://doi.org/10.1016/j.nantod.2016.02.004.

[145] K.C.L. Law, N. Mahmoudi, Z.E. Zadeh, R.J. Williams, C.P.J. Hunt, A. Nagy, L.H. Thompson, D.R. Nisbet, C.L. Parish, A Selective , Hydrogel-Based Prodrug Delivery

System Efficiently Activates a Suicide Gene to Remove Undifferentiated Human Stem Cells Within Neural Grafts, 2305771 (2023). https://doi.org/10.1002/adfm.202305771.

[146] A.L. Rodriguez, C.L. Parish, D.R. Nisbet, R.J. Williams, Tuning the amino acid sequence of minimalist peptides to present biological signals via charge neutralised self assembly, Soft Matter. 9 (2013) 3915–3919. https://doi.org/10.1039/c3sm27758e.

[147] F.L. Maclean, M.K. Horne, R.J. Williams, D.R. Nisbet, Review: Biomaterial systems to resolve brain inflammation after traumatic injury, APL Bioeng. 2 (2018). https://doi.org/10.1063/1.5023709.

[148] M.S. Shoichet, Polymer scaffolds for biomaterials applications, Macromolecules. 43 (2010) 581–591. https://doi.org/10.1021/ma901530r.

[149] M.D. Pierschbacher, E. Ruoslahti, Can Be Duplicated By Small Synthetic Fragments of the Molecule, Nature. (1984) 3–6.

[150] K. Tashiro, G.C. Sephel, B. Weeks, M. Sasaki, G.R. Martin, H.K. Kleinman, Y. Yamada, A synthetic peptide containing the IKVAV sequence from the A chain of laminin mediates cell attachment, migration, and neurite outgrowth, J. Biol. Chem. 264 (1989) 16174–16182. https://doi.org/10.1016/s0021-9258(18)71604-9.

[151] N. Huettner, T.R. Dargaville, A. Forget, Discovering Cell-Adhesion Peptides in Tissue Engineering: Beyond RGD, Trends Biotechnol. 36 (2018) 372–383. https://doi.org/10.1016/j.tibtech.2018.01.008.

[152] J. Graf, R.C. Ogle, F.A. Robey, M. Sasaki, G.R. Martin, Y. Yamada, H.K. Kleinman, A Pentapeptide from the Laminin B1 Chain Mediates Cell Adhesion and Binds the 67 000 Laminin Receptor, Biochemistry. 26 (1987) 6896–6900. https://doi.org/10.1021/bi00396a004.

[153] M. Jucker, H.K. Kleinman, D.K. Ingram, Fetal rat septal cells adhere to and extend processes on basement membrane, laminin, and a synthetic peptide from the laminin A chain sequence, J. Neurosci. Res. 28 (1991) 507–517. https://doi.org/10.1002/jnr.490280407.

[154] J.E. Frith, R.J. Mills, J.E. Hudson, J.J. Cooper-White, Tailored integrin-extracellular matrix interactions to direct human mesenchymal stem cell differentiation, Stem Cells Dev. 21 (2012) 2442–2456. https://doi.org/10.1089/scd.2011.0615.

[155] L. Pan, H.A. North, V. Sahni, S.J. Jeong, T.L. Mcguire, E.J. Berns, S.I. Stupp, J.A. Kessler, B1-Integrin and Integrin Linked Kinase Regulate Astrocytic Differentiation of Neural Stem Cells, PLoS One. 9 (2014). https://doi.org/10.1371/journal.pone.0104335.

[156] H. Li, G. Chen, In Vivo Reprogramming for CNS Repair: Regenerating Neurons from Endogenous Glial Cells, Neuron. 91 (2016) 728–738. https://doi.org/10.1016/j.neuron.2016.08.004.

[157] Z. Xiang, L. Xu, M. Liu, Q. Wang, W. Li, W. Lei, G. Chen, Lineage tracing of direct astrocyte-to-neuron conversion in the mouse cortex, Neural Regen. Res. 16 (2021) 750–756. https://doi.org/10.4103/1673-5374.295925.

[158] X. Gao, X. Wang, W. Xiong, J. Chen, In vivo reprogramming reactive glia into iPSCs to produce new neurons in the cortex following traumatic brain injury, Sci. Rep. 6 (2016) 1–13. https://doi.org/10.1038/srep22490.

[159] R. Vignoles, C. Lentini, D. Marie, C. Heinrich, R. Vignoles, C. Lentini, D. Marie, C. Heinrich, D. Lineage, Direct Lineage Reprogramming for Brain Repair : Breakthroughs and Challenges To cite this version : HAL Id : hal-02388277, (2020).

[160] Y. Wang, V.L. Sheen, J.D. Macklis, Cortical interneurons upregulate neurotrophins in

vivo in response to targeted apoptotic degeneration of neighboring pyramidal neurons, Exp. Neurol. 154 (1998) 389–402. https://doi.org/10.1006/exnr.1998.6965.

[161] C. Jopling, S. Boue, J.C.I. Belmonte, Dedifferentiation, transdifferentiation and reprogramming: Three routes to regeneration, Nat. Rev. Mol. Cell Biol. 12 (2011) 79–89. https://doi.org/10.1038/nrm3043.

[162] L.F.R.C.I.F.D.J.M.Z.K.S. Cirillo L.A., L.A. Cirillo, F.R. Lin, I. Cuesta, D. Friedman, M. Jarnik, K.S. Zaret, Opening of compacted chromatin by early developmental transcription factors HNF3 (FoxA) and GATA-4., Mol. Cell. 9 (2002) 279–89. http://www.ncbi.nlm.nih.gov/pubmed/11864602.

[163] A. Mayran, J. Drouin, Pioneer transcription factors shape the epigenetic landscape, J. Biol. Chem. 293 (2018) 13795–13804. https://doi.org/10.1074/jbc.R117.001232.

[164] M. Iwafuchi-Doi, K.S. Zaret, Cell fate control by pioneer transcription factors, Dev. 143 (2016) 1833–1837. https://doi.org/10.1242/dev.133900.

[165] E.D. Larson, A.J. Marsh, M.M. Harrison, Pioneering the developmental frontier, Mol. Cell. 81 (2021) 1640–1650. https://doi.org/10.1016/j.molcel.2021.02.020.

[166] K.S. Zaret, Pioneer Transcription Factors Initiating Gene Network Changes, Annu. Rev. Genet. 54 (2020) 367–385. https://doi.org/10.1146/annurev-genet-030220-015007.

[167] Q.Y. Lee, M. Mall, S. Chanda, B. Zhou, K.S. Sharma, K. Schaukowitch, J.M. Adrian-Segarra, S.D. Grieder, M.S. Kareta, O.L. Wapinski, C.E. Ang, R. Li, T.C. Südhof, H.Y. Chang, M. Wernig, Pro-neuronal activity of Myod1 due to promiscuous binding to neuronal genes, Nat. Cell Biol. 22 (2020) 401–411. https://doi.org/10.1038/s41556-020-0490-3.

[168] S. Tutukova, V. Tarabykin, L.R. Hernandez-Miranda, The Role of Neurod Genes in Brain Development, Function, and Disease, Front. Mol. Neurosci. 14 (2021) 1–13. https://doi.org/10.3389/fnmol.2021.662774.

[169] D.G. Lee, Y.K. Kim, K.H. Baek, The bHLH Transcription Factors in Neural Development and Therapeutic Applications for Neurodegenerative Diseases, Int. J. Mol. Sci. 23 (2022). https://doi.org/10.3390/ijms232213936.

[170] N. Bertrand, D.S. Castro, F. Guillemot, Proneural genes and the specification of neural cell types, Nat. Rev. Neurosci. 3 (2002) 517–530. https://doi.org/10.1038/nrn874.

[171] L. Sommer, Q. Ma, D.J. Anderson, neurogenins, a novel family of atonal-related bHLH transcription factors, are putative mammalian neuronal determination genes that reveal progenitor cell heterogeneity in the developing CNS and PNS, Mol. Cell. Neurosci. 8 (1996) 221–241. https://doi.org/10.1006/mcne.1996.0060.

[172] N.L. Jorstad, M.S. Wilken, W.N. Grimes, S.G. Wohl, L.S. Vandenbosch, T. Yoshimatsu, R.O. Wong, F. Rieke, T.A. Reh, Stimulation of functional neuronal regeneration from Müller glia in adult mice, Nature. 548 (2017) 103–107. https://doi.org/10.1038/nature23283.

[173] P. Rivetti Di Val Cervo, R.A. Romanov, G. Spigolon, D. Masini, E. Martín-Montañez, E.M. Toledo, G. La Manno, M. Feyder, C. Pifl, Y.H. Ng, S.P. Sánchez, S. Linnarsson, M. Wernig, T. Harkany, G. Fisone, E. Arenas, Induction of functional dopamine neurons from human astrocytes in vitro and mouse astrocytes in a Parkinson's disease model, Nat. Biotechnol. 35 (2017) 444–452. https://doi.org/10.1038/nbt.3835.

[174] Z.P. Pang, N. Yang, T. Vierbuchen, A. Ostermeier, D.R. Fuentes, T.Q. Yang, A. Citri, V. Sebastiano, S. Marro, T.C. Südhof, M. Wernig, Induction of human neuronal cells

by defined transcription factors, Nature. 476 (2011) 220–223. https://doi.org/10.1038/nature10202.

[175] G. Ziyuan, Z. Lei, W. Zheng, C. Yuchen, W. Fan, C. Gong, In vivo direct reprogramming of reactive glial cells into functional neurons after brain injury and in an Alzheimer's disease model, Cell Stem Cell. 14 (2014) 188–202. https://doi.org/10.1016/j.stem.2013.12.001.In.

[176] Z. Guo, L. Zhang, Z. Wu, Y. Chen, F. Wang, G. Chen, In vivo direct reprogramming of reactive glial cells into functional neurons after brain injury and in an Alzheimer's disease model, Cell Stem Cell. 14 (2014) 188–202. https://doi.org/10.1016/j.stem.2013.12.001.

[177] B. Puls, Y. Ding, F. Zhang, M. Pan, Z. Lei, Z. Pei, M. Jiang, Y. Bai, C. Forsyth, M. Metzger, T. Rana, L. Zhang, X. Ding, M. Keefe, A. Cai, A. Redilla, M. Lai, K. He, H. Li, G. Chen, Regeneration of Functional Neurons After Spinal Cord Injury via in situ NeuroD1-Mediated Astrocyte-to-Neuron Conversion, Front. Cell Dev. Biol. 8 (2020) 1–18. https://doi.org/10.3389/fcell.2020.591883.

[178] R.F. Hevner, R.D. Hodge, R.A.M. Daza, C. Englund, Transcription factors in glutamatergic neurogenesis: Conserved programs in neocortex, cerebellum, and adult hippocampus, Neurosci. Res. 55 (2006) 223–233. https://doi.org/10.1016/j.neures.2006.03.004.

[179] L. Roybon, T.L. Mastracci, J. Li, S.R.W. Stott, A.B. Leiter, L. Sussel, P. Brundin, J.Y. Li, The origin, development and molecular diversity of rodent olfactory bulb glutamatergic neurons distinguished by expression of transcription factor NeuroD1, PLoS One. 10 (2015) 1–21. https://doi.org/10.1371/journal.pone.0128035.

[180] Z. Wu, M. Parry, X.Y. Hou, M.H. Liu, H. Wang, R. Cain, Z.F. Pei, Y.C. Chen, Z.Y. Guo, S. Abhijeet, G. Chen, Gene therapy conversion of striatal astrocytes into GABAergic neurons in mouse models of Huntington's disease, Nat. Commun. 11 (2020) 1–18. https://doi.org/10.1038/s41467-020-14855-3.

[181] L. Zhang, Z. Lei, Z. Guo, Z. Pei, Y. Chen, F. Zhang, A. Cai, G. Mok, G. Lee, V. Swaminathan, F. Wang, Y. Bai, G. Chen, Development of Neuroregenerative Gene Therapy to Reverse Glial Scar Tissue Back to Neuron-Enriched Tissue, Front. Cell. Neurosci. 14 (2020) 1–19. https://doi.org/10.3389/fncel.2020.594170.

[182] S. Ruiz, K. Brennand, A.D. Panopoulos, A. Herrerías, F.H. Gage, J.C. Izpisua-Belmonte, High-efficient generation of induced pluripotent stem cells from human astrocytes, PLoS One. 5 (2010) 1–9. https://doi.org/10.1371/journal.pone.0015526.

[183] M. Abad, L. Mosteiro, C. Pantoja, M. Cañamero, T. Rayon, I. Ors, O. Graña, D. Megías, O. Domínguez, D. Martínez, M. Manzanares, S. Ortega, M. Serrano, Reprogramming in vivo produces teratomas and iPS cells with totipotency features, Nature. 502 (2013) 340–345. https://doi.org/10.1038/nature12586.

[184] K. Ohnishi, K. Semi, T. Yamamoto, M. Shimizu, A. Tanaka, K. Mitsunaga, K. Okita, K. Osafune, Y. Arioka, T. Maeda, H. Soejima, H. Moriwaki, S. Yamanaka, K. Woltjen, Y. Yamada, Premature termination of reprogramming in vivo leads to cancer development through altered epigenetic regulation, Cell. 156 (2014) 663–677. https://doi.org/10.1016/j.cell.2014.01.005.

[185] L.H. Pevny, S.K. Nicolis, Sox2 roles in neural stem cells, Int. J. Biochem. Cell Biol. 42 (2010) 421–424. https://doi.org/10.1016/j.biocel.2009.08.018.

[186] K. Arnold, A. Sarkar, M.A. Yram, J.M. Polo, R. Bronson, S. Sengupta, M. Seandel, N.

Geijsen, K. Hochedlinger, Sox2 + adult stem and progenitor cells are important for tissue regeneration and survival of mice, Cell Stem Cell. 9 (2011) 317–329. https://doi.org/10.1016/j.stem.2011.09.001.

[187] D.E. Cohen, D. Melton, Turning straw into gold: Directing cell fate for regenerative medicine, Nat. Rev. Genet. 12 (2011) 243–252. https://doi.org/10.1038/nrg2938.

[188] L.L. Wang, Z. Su, W. Tai, Y. Zou, X.M. Xu, C.L. Zhang, The p53 Pathway Controls SOX2-Mediated Reprogramming in the Adult Mouse Spinal Cord, Cell Rep. 17 (2016) 891–903. https://doi.org/10.1016/j.celrep.2016.09.038.

[189] M.A. Kotterman, D. V. Schaffer, Engineering adeno-associated viruses for clinical gene therapy, Nat. Rev. Genet. 15 (2014) 445–451. https://doi.org/10.1038/nrg3742.

[190] M.A. Kay, J.C. Glorioso, L. Naldini, Viral vectors for gene therapy: The art of turning infectious agents into vehicles of therapeutics, Nat. Med. 7 (2001) 33–40. https://doi.org/10.1038/83324.

[191] S. Soltani Dehnavi, Z. Eivazi Zadeh, A.R. Harvey, N.H. Voelcker, C.L. Parish, R.J. Williams, R. Elnathan, D.R. Nisbet, Changing Fate: Reprogramming Cells via Engineered Nanoscale Delivery Materials, Adv. Mater. 34 (2022). https://doi.org/10.1002/adma.202108757.

[192] J. Yan, M. Ran, X. Shen, H. Zhang, Therapeutic DNAzymes: From Structure Design to Clinical Applications, Adv. Mater. 35 (2023) 1–34. https://doi.org/10.1002/adma.202300374.

[193] B. Dhungel, C.A. Ramlogan-Steel, J.C. Steel, Microrna-regulated gene delivery systems for research and therapeutic purposes, Molecules. 23 (2018) 1–14. https://doi.org/10.3390/molecules23071500.

[194] Y. Fu, J. Chen, Z. Huang, Recent progress in microrna-based delivery systems for the treatment of human disease, ExRNA. 1 (2019) 1–14. https://doi.org/10.1186/s41544-019-0024-y.

[195] D.S. Ojala, D.P. Amara, D. V. Schaffer, Adeno-associated virus vectors and neurological gene therapy, Neuroscientist. 21 (2015) 84–98. https://doi.org/10.1177/1073858414521870.

[196] M.A. Kotterman, T.W. Chalberg, D. V Schaffer, Viral Vectors for Gene Therapy : Translational and Clinical Outlook, (2015). https://doi.org/10.1146/annurev-bioeng-071813-104938.

[197] K.E. Brown, The expanding range of parvoviruses which infect humans, (2010) 231–244. https://doi.org/10.1002/rmv.

[198] D. Wang, P.W.L. Tai, G. Gao, Adeno-associated virus vector as a platform for gene therapy delivery, Nat. Rev. Drug Discov. 18 (2019) 358–378. https://doi.org/10.1038/s41573-019-0012-9.

[199] E. Lusby, K.H. Fife, K.I. Berns, Nucleotide sequence of the inverted terminal repetition in adeno-associated virus DNA., J. Virol. 34 (1980) 402–409. https://doi.org/10.1128/jvi.34.2.402-409.1980.

[200] T.R. Flotte, Gene therapy progress and prospects: Recombinant adeno-associated virus (rAAV) vectors, Gene Ther. 11 (2004) 805–810. https://doi.org/10.1038/sj.gt.3302233.

[201] P. Colella, G. Ronzitti, F. Mingozzi, Emerging Issues in AAV-Mediated In Vivo Gene Therapy, Mol. Ther. - Methods Clin. Dev. 8 (2018) 87–104. https://doi.org/10.1016/j.omtm.2017.11.007.

[202] Z. Wu, A. Asokan, R.J. Samulski, Adeno-associated Virus Serotypes: Vector Toolkit

for Human Gene Therapy, Mol. Ther. 14 (2006) 316–327. https://doi.org/10.1016/j.ymthe.2006.05.009.

[203] S.S. Issa, A.A. Shaimardanova, V. V. Solovyeva, A.A. Rizvanov, Various AAV Serotypes and Their Applications in Gene Therapy: An Overview, Cells. 12 (2023) 1–41. https://doi.org/10.3390/cells12050785.

[204] F. Mingozzi, K.A. High, Immune responses to AAV vectors: Overcoming barriers to successful gene therapy, Blood. 122 (2013) 23–36. https://doi.org/10.1182/blood-2013-01-306647.

[205] F. Sonntag, K. Schmidt, J.A. Kleinschmidt, A viral assembly factor promotes AAV2 capsid formation in the nucleolus, Proc. Natl. Acad. Sci. U. S. A. 107 (2010) 10220–10225. https://doi.org/10.1073/pnas.1001673107.

[206] J.J. Siu, N.J. Queen, W. Huang, F.Q. Yin, X. Liu, C. Wang, D.M. McTigue, L. Cao, Improved gene delivery to adult mouse spinal cord through the use of engineered hybrid adeno-associated viral serotypes, Gene Ther. 24 (2017) 361–369. https://doi.org/10.1038/gt.2017.27.

[207] J.M. Griffin, B. Fackelmeier, D.M. Fong, A. Mouravlev, D. Young, S.J. O'Carroll, Astrocyte-selective AAV gene therapy through the endogenous GFAP promoter results in robust transduction in the rat spinal cord following injury, Gene Ther. 26 (2019) 198–210. https://doi.org/10.1038/s41434-019-0075-6.

[208] D.L. Puhl, A.R. D'Amato, R.J. Gilbert, Challenges of gene delivery to the central nervous system and the growing use of biomaterial vectors, Brain Res. Bull. 150 (2019) 216–230. https://doi.org/10.1016/j.brainresbull.2019.05.024.

[209] Y. Lee, A. Messing, M. Su, M. Brenner, GFAP promoter elements required for region-

specific and astrocyte-specific expression, Glia. 56 (2008) 481–493. https://doi.org/10.1002/glia.20622.

[210] S. Daya, K.I. Berns, Gene therapy using adeno-associated virus vectors, Clin. Microbiol. Rev. 21 (2008) 583–593. https://doi.org/10.1128/CMR.00008-08.

[211] Z. Wu, A. Asokan, J.C. Grieger, L. Govindasamy, M. Agbandje-McKenna, R.J. Samulski, Single Amino Acid Changes Can Influence Titer, Heparin Binding, and Tissue Tropism in Different Adeno-Associated Virus Serotypes, J. Virol. 80 (2006) 11393–11397. https://doi.org/10.1128/jvi.01288-06.

[212] Y. Mao, X. Wang, R. Yan, W. Hu, A. Li, S. Wang, H. Li, Single point mutation in adeno-associated viral vectors -DJ capsid leads to improvement for gene delivery in vivo, BMC Biotechnol. 16 (2016) 1–8. https://doi.org/10.1186/s12896-015-0230-0.

[213] S.E. Beck, L.A. Jones, K. Chesnut, S.M. Walsh, T.C. Reynolds, B.J. Carter, F.B. Askin, T.R. Flotte, W.B. Guggino, Repeated Delivery of Adeno-Associated Virus Vectors to the Rabbit Airway, J. Virol. 73 (1999) 9446–9455. https://doi.org/10.1128/jvi.73.11.9446-9455.1999.

[214] W. Shen, S. Liu, L. Ou, rAAV immunogenicity, toxicity, and durability in 255 clinical trials: A meta-analysis, Front. Immunol. 13 (2022) 1–13. https://doi.org/10.3389/fimmu.2022.1001263.

[215] C.S. Manno, V.R. Arruda, G.F. Pierce, B. Glader, M. Ragni, J. Rasko, M.C. Ozelo, K. Hoots, P. Blatt, B. Konkle, M. Dake, R. Kaye, M. Razavi, A. Zajko, J. Zehnder, H. Nakai, A. Chew, D. Leonard, J.F. Wright, R.R. Lessard, J.M. Sommer, M. Tigges, D. Sabatino, A. Luk, H. Jiang, F. Mingozzi, L. Couto, H.C. Ertl, K.A. High, M.A. Kay, Successful transduction of liver in hemophilia by AAV-Factor IX and limitations

imposed by the host immune response, Nat. Med. 12 (2006) 342–347. https://doi.org/10.1038/nm1358.

[216] A.L. Rodriguez, T.Y. Wang, K.F. Bruggeman, R. Li, R.J. Williams, C.L. Parish, D.R. Nisbet, Tailoring minimalist self-assembling peptides for localized viral vector gene delivery, Nano Res. 9 (2016) 674–684. https://doi.org/10.1007/s12274-015-0946-0.

[217] and L.D.S. Jaclyn A. Sheparda, Paul J. Wessona, Christine E. Wangb, Alyson C. Stevansa, Samantha J. Hollanda, Ariella Shikanova, Bartosz A. Grzybowskia,c, Gene Therapy Vectors with Enhanced Transfection Based on Hydrogels Modified with Affinity Peptides, Biomaterials. (2011) 5092–5099. https://doi.org/10.1016/j.biomaterials.2011.03.083. Gene.

[218] S.S. Dehnavi, A. Cembran, N. Mahmoudi, M. Lilith, C. Aguilar, Y. Wang, S. Cheeseman, N. Malagutti, S. Franks, B. Long, L. Lisowski, A.R. Harvey, L. Clare, R.J. Williams, D.R. Nisbet, Molecular Camouflage by a context-specific hydrogel as the key to unlock the potential of viral vector gene therapy, Chem. Eng. J. (2023) 146857. https://doi.org/10.1016/j.cej.2023.146857.

[219] I. Jun, H.S. Han, J.R. Edwards, H. Jeon, Electrospun fibrous scaffolds for tissue engineering: Viewpoints on architecture and fabrication, Int. J. Mol. Sci. 19 (2018). https://doi.org/10.3390/ijms19030745.

[220] A. Luraghi, F. Peri, L. Moroni, Electrospinning for drug delivery applications: A review, J. Control. Release. 334 (2021) 463–484. https://doi.org/10.1016/j.jconrel.2021.03.033.

[221] C. Wang, J. Wang, L. Zeng, Z. Qiao, X. Liu, H. Liu, J. Zhang, J. Ding, Fabrication of electrospun polymer nanofibers with diverse morphologies, Molecules. 24 (2019).

https://doi.org/10.3390/molecules24050834.

[222] P.B. Welzel, S. Prokoph, A. Zieris, M. Grimmer, S. Zschoche, U. Freudenberg, C. Werner, Modulating Biofunctional starPEG Heparin Hydrogels by Varying Size and Ratio of the Constituents, Polymers (Basel). 3 (2011) 602–620. https://doi.org/10.3390/polym3010602.

[223] G. li Ming, H. Song, Adult Neurogenesis in the Mammalian Brain: Significant Answers and Significant Questions, Neuron. 70 (2011) 687–702. https://doi.org/10.1016/j.neuron.2011.05.001.

[224] Z. Tian, F. Guo, S. Biswas, W. Deng, Rationale and methodology of reprogramming for generation of induced pluripotent stem cells and induced neural progenitor cells, Int. J. Mol. Sci. 17 (2016) 1–22. https://doi.org/10.3390/ijms17040594.

[225] H. Khabou, C. Cordeau, L. Pacot, S. Fisson, D. Dalkara, Dosage Thresholds and Influence of Transgene Cassette in Adeno-Associated Virus-Related Toxicity, Hum. Gene Ther. 29 (2018) 1235–1241. https://doi.org/10.1089/hum.2018.144.

[226] W. Xiong, D.M. Wu, Y. Xue, S.K. Wang, M.J. Chung, X. Ji, P. Rana, S.R. Zhao, S. Mai, C.L. Cepko, AAV cis-regulatory sequences are correlated with ocular toxicity, Proc. Natl. Acad. Sci. U. S. A. 116 (2019) 5785–5794. https://doi.org/10.1073/pnas.1821000116.

[227] C.C. Lin, A.T. Metters, Hydrogels in controlled release formulations: Network design and mathematical modeling, Adv. Drug Deliv. Rev. 58 (2006) 1379–1408. https://doi.org/10.1016/j.addr.2006.09.004.

[228] Y.F. Goh, I. Shakir, R. Hussain, Electrospun fibers for tissue engineering, drug delivery, and wound dressing, J. Mater. Sci. 48 (2013) 3027–3054.

https://doi.org/10.1007/s10853-013-7145-8.

[229] S. Agarwal, A. Greimer, J.H. Wendorff, Electrospinning of manmade and biopolymer nanofibers - Progress in techniques, materials, and applications, Adv. Funct. Mater. 19 (2009) 2863–2879. https://doi.org/10.1002/adfm.200900591.

[230] D.Y. Ko, U.P. Shinde, B. Yeon, B. Jeong, Recent progress of in situ formed gels for biomedical applications, Prog. Polym. Sci. 38 (2013) 672–701. https://doi.org/10.1016/j.progpolymsci.2012.08.002.

[231] N.A. Peppas, J.Z. Hilt, A. Khademhosseini, R. Langer, Hydrogels in biology and medicine: From molecular principles to bionanotechnology, Adv. Mater. 18 (2006) 1345–1360. https://doi.org/10.1002/adma.200501612.

[232] S.Y. Chew, J. Wen, E.K.F. Yim, K.W. Leong, Sustained release of proteins from electrospun biodegradable fibers, Biomacromolecules. 6 (2005) 2017–2024. https://doi.org/10.1021/bm0501149.

[233] J. Hu, L. Tian, M.P. Prabhakaran, X. Ding, S. Ramakrishna, Fabrication of nerve growth factor encapsulated aligned poly(ε-caprolactone) nanofibers and their assessment as a potential neural tissue engineering scaffold, Polymers (Basel). 8 (2016). https://doi.org/10.3390/polym8020054.

[234] K.F. Bruggeman, Y. Wang, F.L. Maclean, C.L. Parish, R.J. Williams, D.R. Nisbet, Temporally controlled growth factor delivery from a self-assembling peptide hydrogel and electrospun nanofibre composite scaffold, Nanoscale. 9 (2017) 13661–13669. https://doi.org/10.1039/c7nr05004f.

[235] N. Ain, N. Asri, M.M. Mahat, A. Zakaria, M. Fauzi, Fabrication Methods of Electroactive Scaffold-Based Conducting Polymers for Tissue Engineering

Application : A Review, 10 (2022) 1–13. https://doi.org/10.3389/fbioe.2022.876696.

[236] S. Xu, L. Deng, J. Zhang, L. Yin, A. Dong, Composites of electrospun-fibers and hydrogels: A potential solution to current challenges in biological and biomedical field, J. Biomed. Mater. Res. - Part B Appl. Biomater. 104 (2016) 640–656. https://doi.org/10.1002/jbm.b.33420.

[237] A.J. Engler, S. Sen, H.L. Sweeney, D.E. Discher, Matrix Elasticity Directs Stem Cell Lineage Specification, Cell. 126 (2006) 677–689. https://doi.org/10.1016/j.cell.2006.06.044.

[238] L.R. Nih, S. Gojgini, S.T. Carmichael, T. Segura, Dual-function injectable angiogenic biomaterial for the repair of brain tissue following stroke, Nat. Mater. 17 (2018) 642–651. https://doi.org/10.1038/s41563-018-0083-8.

[239] J. Houlton, N. Abumaria, S.F.R. Hinkley, A.N. Clarkson, Therapeutic potential of neurotrophins for repair after brain injury: A helping hand from biomaterials, Front. Genet. 10 (2019). https://doi.org/10.3389/fnins.2019.00790.

[240] R. Boni, A. Ali, A. Shavandi, A.N. Clarkson, Current and novel polymeric biomaterials for neural tissue engineering, J. Biomed. Sci. 25 (2018) 1–21. https://doi.org/10.1186/s12929-018-0491-8.

[241] E.Y. Snyder, C. Yoon, J.D. Flax, J.D. Macklis, Multipotent neural precursors can differentiate toward replacement of neurons undergoing targeted apoptotic degeneration in adult mouse neocortex, Proc. Natl. Acad. Sci. U. S. A. 94 (1997) 11663–11668. https://doi.org/10.1073/pnas.94.21.11663.

[242] A.R. Harvey, Differentiation and functional connectivity of fetal tectal transplants, Neural Regen. Res. 18 (2023) 2325–2331. https://doi.org/10.4103/1673-5374.371348.

[243] Q.M. Alhadidi, G.A. Bahader, O. Arvola, P. Kitchen, Z.A. Shah, M.M. Salman, Astrocytes in functional recovery following central nervous system injuries, J. Physiol. 0 (2023) 1–28. https://doi.org/10.1113/JP284197.

[244] A.G. Boghdadi, J. Spurrier, L. Teo, M. Li, M. Skarica, B. Cao, W.C. Kwan, T.D. Merson, S.K. Nilsson, N. Sestan, S.M. Strittmatter, J.A. Bourne, NogoA-expressing astrocytes limit peripheral macrophage infiltration after ischemic brain injury in primates, Nat. Commun. 12 (2021) 1–16. https://doi.org/10.1038/s41467-021-27245-0.

[245] C. Mollinari, J. Zhao, L. Lupacchini, E. Garaci, D. Merlo, G. Pei, Transdifferentiation: a new promise for neurodegenerative diseases, Cell Death Dis. 9 (2018). https://doi.org/10.1038/s41419-018-0891-4.

[246] S.T.C. Amy J. Gleichman1, Riki Kawaguchi1, 2, Michael V. Sofroniew3, A toolbox of astrocyte-specific, serotype-independent adeno-associated viral vectors using microRNA targeting sequences., BioRxiv. 43 (2023) 245–250. https://doi.org/https://doi.org/10.1101/2023.02.21.529451.

[247] R.J. Samulski, L.S. Chang, T. Shenk, Helper-free stocks of recombinant adeno-associated viruses: normal integration does not require viral gene expression, J. Virol. 63 (1989) 3822–3828. https://doi.org/10.1128/jvi.63.9.3822-3828.1989.

[248] M.H. Liu, W. Li, J.J. Zheng, Y.G. Xu, Q. He, G. Chen, Differential neuronal reprogramming induced by NeuroD1 from astrocytes in grey matter versus white matter, Neural Regen. Res. 15 (2020) 342–351. https://doi.org/10.4103/1673-5374.265185.

[249] Y. Xie, J. Zhou, L.L. Wang, C.L. Zhang, B. Chen, New AAV tools fail to detect Neurod1-mediated neuronal conversion of Müller glia and astrocytes in vivo,

EBioMedicine. 90 (2023) 104531. https://doi.org/10.1016/j.ebiom.2023.104531.

[250] Z. Wu, M. Parry, X.Y. Hou, M.H. Liu, H. Wang, R. Cain, Z.F. Pei, Y.C. Chen, Z.Y. Guo, S. Abhijeet, G. Chen, Gene therapy conversion of striatal astrocytes into GABAergic neurons in mouse models of Huntington's disease, Nat. Commun. 11 (2020) 1–18. https://doi.org/10.1038/s41467-020-14855-3.

[251] H.C. Verdera, K. Kuranda, F. Mingozzi, AAV Vector Immunogenicity in Humans : A Long Journey to Successful Gene Transfer, Mol. Ther. 28 (2020) 723–746. https://doi.org/10.1016/j.ymthe.2019.12.010.

[252] R.J. Rabinowitz, J., Chan, Y. K., and Samulski, Adeno-associated Virus (AAV) versus immune response., Viruses. 11 (2019) 1–11. https://doi.org/10.3390/v11020102.

[253] B.A. Perez, A. Shutterly, Y.K. Chan, B.J. Byrne, M. Corti, Management of Neuroinflammatory Responses to AAV-Mediated Gene Therapies for Neurodegenerative Diseases, Brain Sci. (2020). https://doi.org/10.3390/brainsci10020119.

[254] J.M. Fischell, P.S. Fishman, C.I.D.N.A. C, A Multifaceted Approach to Optimizing AAV Delivery to the Brain for the Treatment of Neurodegenerative Diseases, Front. Neurosci. 15 (2021) 1–20. https://doi.org/10.3389/fnins.2021.747726.

[255] T.K. Kishimoto, R.J. Samulski, Addressing high dose AAV toxicity–'one and done' or 'slower and lower'?, Expert Opin. Biol. Ther. 22 (2022) 1067–1071. https://doi.org/10.1080/14712598.2022.2060737.

[256] Z. Peng, H. Lu, Q. Yang, Q. Xie, Astrocyte Reprogramming in Stroke: Opportunities and Challenges, Front. Aging Neurosci. 14 (2022) 1–11. https://doi.org/10.3389/fnagi.2022.885707.

[257] P. Chakrabarty, A. Rosario, P. Cruz, Z. Siemienski, C. Ceballos-Diaz, K. Crosby, K. Jansen, D.R. Borchelt, J.Y. Kim, J.L. Jankowsky, T.E. Golde, Y. Levites, Capsid Serotype and Timing of Injection Determines AAV Transduction in the Neonatal Mice Brain, PLoS One. 8 (2013) 0–8. https://doi.org/10.1371/journal.pone.0067680.

[258] Y. Xie, T. Wang, G.Y. Sun, S. Ding, Specific disruption of astrocytic Ca2+ signaling pathway in vivo by adeno-associated viral transduction, Neuroscience. 170 (2010) 992–1003. https://doi.org/10.1016/j.neuroscience.2010.08.034.

[259] A. Adamsky, A. Kol, T. Kreisel, A. Doron, N. Ozeri-Engelhard, T. Melcer, R. Refaeli, H. Horn, L. Regev, M. Groysman, M. London, I. Goshen, Astrocytic Activation Generates De Novo Neuronal Potentiation and Memory Enhancement, Cell. 174 (2018) 59-71.e14. https://doi.org/10.1016/j.cell.2018.05.002.

[260] Z.C. Wang LL, Garcia CS, Zhong X, Ma S, Rapid and efficient in vivo astrocyte-to-neuron conversion with regional identity and connectivity?, BioRxiv. (2020). https://doi.org/10.1101/2020.08.16.253195.

[261] G.R. Choudhury, S. Ding, Reactive astrocytes and therapeutic potential in focal ischemic stroke, Neurobiol. Dis. 85 (2016) 234–244. https://doi.org/10.1016/j.nbd.2015.05.003.

[262] G. Seifert, K. Schilling, C. Steinhäuser, Astrocyte dysfunction in neurological disorders: A molecular perspective, Nat. Rev. Neurosci. 7 (2006) 194–206. https://doi.org/10.1038/nrn1870.

[263] M. Nedergaard, B. Ransom, S.A. Goldman, New roles for astrocytes: Redefining the functional architecture of the brain, Trends Neurosci. 26 (2003) 523–530. https://doi.org/10.1016/j.tins.2003.08.008.

[264] K. Firipis, M. Boyd-moss, B. Long, C. Dekiwadia, W. Hoskin, E. Pirogova, D.R. Nisbet, R.M.I. Kapsa, A.F. Quigley, R.J. Williams, Tuneable Hybrid Hydrogels via Complementary Self-Assembly of a Bioactive Peptide with a Robust Polysaccharide, (2021). https://doi.org/10.1021/acsbiomaterials.1c00675.

[265] E.D. Horowitz, K.S. Rahman, B.D. Bower, D.J. Dismuke, M.R. Falvo, J.D. Griffith, S.C. Harvey, A. Asokan, Biophysical and Ultrastructural Characterization of Adeno-Associated Virus Capsid Uncoating and Genome Release, J. Virol. 87 (2013) 2994–3002. https://doi.org/10.1128/jvi.03017-12.

[266] J. Li, D.J. Mooney, Designing hydrogels for controlled drug delivery, Nat. Rev. Mater. 1 (2016). https://doi.org/10.1038/natrevmats.2016.71.

[267] F.A. Somaa, T.Y. Wang, J.C. Niclis, K.F. Bruggeman, J.A. Kauhausen, H. Guo, S. McDougall, R.J. Williams, D.R. Nisbet, L.H. Thompson, C.L. Parish, Peptide-Based Scaffolds Support Human Cortical Progenitor Graft Integration to Reduce Atrophy and Promote Functional Repair in a Model of Stroke, Cell Rep. 20 (2017) 1964–1977. https://doi.org/10.1016/j.celrep.2017.07.069.

[268] D.R. Nisbet, T.Y. Wang, K.F. Bruggeman, J.C. Niclis, F.A. Somaa, V. Penna, C.P.J. Hunt, Y. Wang, J.A. Kauhausen, R.J. Williams, L.H. Thompson, C.L. Parish, Shear Containment of BDNF within Molecular Hydrogels Promotes Human Stem Cell Engraftment and Postinfarction Remodeling in Stroke, Adv. Biosyst. 2 (2018) 1–13. https://doi.org/10.1002/adbi.201800113.

[269] N. Mahmoudi, E. Mohamed, S.S. Dehnavi, L.M.C. Aguilar, A.R. Harvey, C.L. Parish, R.J. Williams, D.R. Nisbet, Calming the Nerves via the Immune Instructive Physiochemical Properties of Self-Assembling Peptide Hydrogels, Adv. Sci. 2303707 (2023) 1–23. https://doi.org/10.1002/advs.202303707.

[270] T. Imura, H.I. Kornblum, M. V. Sofroniew, The predominant neural stem cell isolated from postnatal and adult forebrain but not early embryonic forebrain expresses GFAP, J. Neurosci. 23 (2003) 2824–2832. https://doi.org/10.1523/jneurosci.23-07-02824.2003.

[271] C.M. Morshead, A.D. Garcia, M. V. Sofroniew, D. Van Der Kooy, The ablation of glial fibrillary acidic protein-positive cells from the adult central nervous system results in the loss of forebrain neural stem cells but not retinal stem cells, Eur. J. Neurosci. 18 (2003) 76–84. https://doi.org/10.1046/j.1460-9568.2003.02727.x.

[272] F. Doetsch, J.M. García-Verdugo, A. Alvarez-Buylla, Regeneration of a germinal layer in the adult mammalian brain, Proc. Natl. Acad. Sci. U. S. A. 96 (1999) 11619–11624. https://doi.org/10.1073/pnas.96.20.11619.

[273] M. Faiz, N. Sachewsky, S. Gascón, K.W.A. Bang, C.M. Morshead, A. Nagy, Adult Neural Stem Cells from the Subventricular Zone Give Rise to Reactive Astrocytes in the Cortex after Stroke, Cell Stem Cell. 17 (2015) 624–634. https://doi.org/10.1016/j.stem.2015.08.002.

[274] H.C.S. Abeysinghe, L. Bokhari, G.J. Dusting, C.L. Roulston, Brain Remodelling following Endothelin-1 Induced Stroke in Conscious Rats, PLoS One. 9 (2014) 1–14. https://doi.org/10.1371/journal.pone.0097007.

[275] J.P. Brown, S. Couillard-Després, C.M. Cooper-Kuhn, J. Winkler, L. Aigner, H.G. Kuhn, Transient Expression of Doublecortin during Adult Neurogenesis, J. Comp. Neurol. 467 (2003) 1–10. https://doi.org/10.1002/cne.10874.

[276] J.G. Gleeson, P.T. Lin, L.A. Flanagan, C.A. Walsh, Doublecortin Is a Microtubule-Associated Protein and Is Expressed Widely by Migrating Neurons Neurons migrating

either along radial glia or indepen-dent of radial glia demonstrate a variety of cytoskeletal changes within the soma and processes that may un, Neuron. 23 (1999) 257–271.

[277] S. Couillard-Despres, B. Winner, S. Schaubeck, R. Aigner, M. Vroemen, N. Weidner, U. Bogdahn, J. Winkler, H.G. Kuhn, L. Aigner, Doublecortin expression levels in adult brain reflect neurogenesis, Eur. J. Neurosci. 21 (2005) 1–14. https://doi.org/10.1111/j.1460-9568.2004.03813.x.

[278] K.B. Fischer, H.K. Collins, E.M. Callaway, Sources of off-target expression from recombinasedependent AAV vectors and mitigation with cross-over insensitive ATG-out vectors, Proc. Natl. Acad. Sci. U. S. A. 116 (2019) 27001–27010. https://doi.org/10.1073/pnas.1915974116.

[279] M. Bylund, E. Andersson, B.G. Novitch, J. Muhr, Vertebrate neurogenesis is counteracted by Sox1-3 activity, Nat. Neurosci. 6 (2003) 1162–1168. https://doi.org/10.1038/nn1131.

[280] H. Hirase, A multi-photon window onto neuronal-glial-vascular communication, Trends Neurosci. 28 (2005) 217–219. https://doi.org/10.1016/j.tins.2005.03.002.

[281] A.L.M. Ferri, M. Cavallaro, D. Braida, A. Di Cristofano, A. Canta, A. Vezzani, S. Ottolenghi, P.P. Pandolfi, M. Sala, S. DeBiasi, S.K. Nicolis, Sox2 deficiency causes neurodegeneration and impaired neurogenesis in the adult mouse brain, Development. 131 (2004) 3805–3819. https://doi.org/10.1242/dev.01204.

[282] T. Yamashita, M. Ninomiya, P.H. Acosta, J.M. García-Verdugo, T. Sunabori, M. Sakaguchi, K. Adachi, T. Kojima, Y. Hirota, T. Kawase, N. Araki, K. Abe, H. Okano, K. Sawamoto, Subventricular zone-derived neuroblasts migrate and differentiate into

mature neurons in the post-stroke adult striatum, J. Neurosci. 26 (2006) 6627–6636. https://doi.org/10.1523/JNEUROSCI.0149-06.2006.

[283] B.J. Chiasson, V. Tropepe, C.M. Morshead, D. Van Der Kooy, Adult mammalian forebrain ependymal and subependymal cells demonstrate proliferative potential, but only subependymal cells have neural stem cell characteristics, J. Neurosci. 19 (1999) 4462–4471. https://doi.org/10.1523/jneurosci.19-11-04462.1999.

[284] O. Lindvall, Z. Kokaia, Neurogenesis following stroke affecting the adult brain, Cold Spring Harb. Perspect. Biol. 7 (2015) 1–20. https://doi.org/10.1101/cshperspect.a019034.

[285] A.I. Ahmed, A.B. Shtaya, M.J. Zaben, E. V. Owens, C. Kiecker, W.P. Gray, Endogenous GFAP-positive neural stem/progenitor cells in the postnatal mouse cortex are activated following traumatic brain injury, J. Neurotrauma. 29 (2012) 828–842. https://doi.org/10.1089/neu.2011.1923.

[286] C. Lois, A. Alvarez-Buylla, Long-distance neuronal migration in the adult mammalian brain, Science (80-.). 264 (1994) 1145–1148. https://doi.org/10.1126/science.8178174.

[287] C. Simon, M. Götz, L. Dimou, Progenitors in the adult cerebral cortex: Cell cycle properties and regulation by physiological stimuli and injury, Glia. 59 (2011) 869–881. https://doi.org/10.1002/glia.21156.

[288] A.B.C. Cherry, G.Q. Daley, Reprogramming cellular identity for regenerative medicine, Cell. 148 (2012) 1110–1122. https://doi.org/10.1016/j.cell.2012.02.031.

[289] K. Takahashi, S. Yamanaka, Induction of Pluripotent Stem Cells from Mouse Embryonic and Adult Fibroblast Cultures by Defined Factors, Cell. 126 (2006) 663–

676. https://doi.org/10.1016/j.cell.2006.07.024.

[290] W. Tai, W. Wu, L.L. Wang, H. Ni, C. Chen, J. Yang, T. Zang, Y. Zou, X.M. Xu, C.L. Zhang, In vivo reprogramming of NG2 glia enables adult neurogenesis and functional recovery following spinal cord injury, Cell Stem Cell. 28 (2021) 923-937.e4. https://doi.org/10.1016/j.stem.2021.02.009.

[291] C.Y. Fong, K. Gauthaman, A. Bongso, Teratomas from pluripotent stem cells: A clinical hurdle, J. Cell. Biochem. 111 (2010) 769–781. https://doi.org/10.1002/jcb.22775.

[292] S. Yamanaka, A Fresh Look at iPS Cells, Cell. 137 (2009) 13–17. https://doi.org/10.1016/j.cell.2009.03.034.

[293] T. Eckschlager, J. Plch, M. Stiborova, J. Hrabeta, Histone deacetylase inhibitors as anticancer drugs, Int. J. Mol. Sci. 18 (2017) 1–25. https://doi.org/10.3390/ijms18071414.

[294] J.I. Ayers, S. Fromholt, O. Sinyavskaya, Z. Siemienski, A.M. Rosario, A. Li, K.W. Crosby, P.E. Cruz, N.M. Dinunno, C. Janus, C. Ceballos-diaz, D.R. Borchelt, T.E. Golde, P. Chakrabarty, Y. Levites, Widespread and Efficient Transduction of Spinal Cord and Brain Following Neonatal AAV Injection and Potential Disease Modifying Effect in ALS Mice, Mol. Ther. 23 (2015) 53–62. https://doi.org/10.1038/mt.2014.180.

[295] P.I. Ortinski, J. Dong, A. Mungenast, C. Yue, H. Takano, D.J. Watson, P.G. Haydon, D.A. Coulter, Selective induction of astrocytic gliosis generates deficits in neuronal inhibition, Nat. Publ. Gr. 13 (2010). https://doi.org/10.1038/nn.2535.

[296] S. Robel, B. Berninger, M. Götz, The stem cell potential of glia: Lessons from reactive gliosis, Nat. Rev. Neurosci. 12 (2011) 88–104. https://doi.org/10.1038/nrn2978.

[297] D.C. Lagace, M.C. Whitman, M.A. Noonan, J.L. Ables, N.A. Decarolis, A.A. Arguello, M.H. Donovan, S.J. Fischer, L.A. Farnbauch, R.D. Beech, R.J. Dileone, C.A. Greer, C.D. Mandyam, A.J. Eisch, Dynamic Contribution of Nestin-Expressing Stem Cells to Adult Neurogenesis, 27 (2007) 12623–12629. https://doi.org/10.1523/JNEUROSCI.3812-07.2007.

[298] V. Graham, J. Khudyakov, P. Ellis, L. Pevny, SOX2 functions to maintain neural progenitor identity, Neuron. 39 (2003) 749–765. https://doi.org/10.1016/S0896-6273(03)00497-5.

[299] J. Hsieh, K. Nakashima, T. Kuwabara, E. Mejia, F.H. Gage, Histone deacetylase inhibition-mediated neuronal differentiation of multipotent adult neural progenitor cells, Proc. Natl. Acad. Sci. U. S. A. 101 (2004) 16659–16664. https://doi.org/10.1073/pnas.0407643101.

[300] L.P. Niles, A. Sathiyapalan, S. Bahna, N.H. Kang, Y. Pan, Valproic acid up-regulates melatonin MT1 and MT2 receptors and neurotrophic factors CDNF and MANF in the rat brain, Int. J. Neuropsychopharmacol. 15 (2012) 1343–1350. https://doi.org/10.1017/S1461145711001969.

[301] M. Talwadekar, S. Fernandes, V. Kale, L. Limaye, Valproic acid enhances the neural differentiation of human placenta derived-mesenchymal stem cells in vitro, J. Tissue Eng. Regen. Med. 11 (2017) 3111–3123. https://doi.org/10.1002/term.2219.

[302] X.S. Liu, M. Chopp, H. Kassis, L.F. Jia, A. Hozeska-Solgot, R.L. Zhang, C. Chen, Y.S. Cui, Z.G. Zhang, Valproic acid increases white matter repair and neurogenesis after stroke, Neuroscience. 220 (2012) 313–321. https://doi.org/10.1016/j.neuroscience.2012.06.012.

[303] S. Chen, J. Ye, X. Chen, J. Shi, W. Wu, W. Lin, W. Lin, Y. Li, H. Fu, S. Li, Valproic acid attenuates traumatic spinal cord injury-induced inflammation via STAT1 and NF-KB pathway dependent of HDAC3, J. Neuroinflammation. 15 (2018) 1–14. https://doi.org/10.1186/s12974-018-1193-6.

[304] L. Lv, Y. Sun, X. Han, C.C. Xu, Y.P. Tang, Q. Dong, Valproic acid improves outcome after rodent spinal cord injury: Potential roles of histone deacetylase inhibition, Brain Res. 1396 (2011) 60–68. https://doi.org/10.1016/j.brainres.2011.03.040.

[305] C. Penas, E. Verdú, E. Asensio-Pinilla, M.S. Guzmán-Lenis, M. Herrando-Grabulosa, X. Navarro, C. Casas, Valproate reduces CHOP levels and preserves oligodendrocytes and axons after spinal cord injury, Neuroscience. 178 (2011) 33–44. https://doi.org/10.1016/j.neuroscience.2011.01.012.

[306] A. Abdanipour, H.J. Schluesener, T. Tiraihi, Effects of valproic acid, a histone deacetylase inhibitor, on improvement of locomotor function in rat spinal cord injury based on epigenetic science, Iran. Biomed. J. 16 (2012) 90–100. https://doi.org/10.6091/ibj.1060.2012.

[307] M. Darvishi, T. Tiraihi, S.A. Mesbah-Namin, A.R. Delshad, T. Taheri, Decreased GFAP Expression and Improved Functional Recovery in Contused Spinal Cord of Rats Following Valproic Acid Therapy, Neurochem. Res. 39 (2014) 2319–2333. https://doi.org/10.1007/s11064-014-1429-5.

[308] S.-A. Ahadiat, Z. Hosseinian, Astrocytes' innate role in neurodegenerative disorders, Bull. Natl. Res. Cent. 47 (2023). https://doi.org/10.1186/s42269-023-01083-0.

Appendix A

RESEARCH ARTICLE

ADVANCED FUNCTIONAL MATERIALS
www.afm-journal.de

A Selective, Hydrogel-Based Prodrug Delivery System Efficiently Activates a Suicide Gene to Remove Undifferentiated Human Stem Cells Within Neural Grafts

Kevin C. L. Law, Negar Mahmoudi, Zahra E. Zadeh, Richard. J. Williams, Cameron P. J. Hunt, Andras Nagy, Lachlan H. Thompson, David R. Nisbet, and Clare L. Parish**

The directed differentiation of human pluripotent stem cells (hPSCs) into defined populations has advanced regenerative medicine, especially for Parkinson's disease where clinical trials are underway. Despite this, tumorigenic risks associated with incompletely patterned and/or quiescent proliferative cells within grafts remain. Addressing this, donor stem cells carrying the suicide gene, thymidine kinase (activated by the prodrug ganciclovir, GCV), are employed to enable the programmed ablation of proliferative cells within neural grafts. However, coinciding the short half-life of GCV with the short S-phase of neural progenitors is a key challenge. To overcome this, a smart hydrogel delivery matrix is fabricatedto prolong GCV presentation. Following matrix embedment, GCV retains its functionality, demonstrated by ablation of hPSCs and proliferating neural progenitors in vitro. A prolonged GCV release is measured by mass spectrometry following the injection of a GCV-functionalized hydrogel into mouse brains. Compared to suboptimal, daily systemic GCV injections, the intracerebral delivery of the functionalized hydrogel, as a "one-off treatment", reduce proliferative cells in both hPSC-derived teratomas and neural grafts, without affecting the graft's functional unit (i.e., neurons). It is demonstrated that a functionalized biomaterial can enhance prodrug delivery and address safety concerns associated with the use of hPSCs for brain repair.

1. Introduction

In both preclinical and clinical studies, the transplantation of neural progenitors has been shown to effectively replace neural circuitry lost to disease or injury. Among the most advanced of these are for Parkinson's disease (PD), where fetal-derived dopaminergic (DA) progenitors have shown structural integration in the brain and alleviation of motor deficits.[1] More recently, research has shifted to human pluripotent stem cells (hPSCs) as the superior donor source – providing control over standardization and greater availability. However, even though differentiation protocols are increasingly refined, there are still technical challenges. Additionally, while the process yields large volumes of donor cells with high proportions of the correctly specified progenitors, the pluripotent/proliferative origin of the cells (responsible for neural overgrowth and generation of unwanted cell types and functions) continues to raise concerns for regulatory groups.

While cell sorting strategies have been heavily investigated to improve the purity of

K. C. L. Law, C. P. J. Hunt, L. H. Thompson, C. L. Parish
The Florey Institute of Neuroscience and Mental Health
The University of Melbourne
Parkville, VIC 3052, Australia
E-mail: clare.parish@unimelb.edu.au

N. Mahmoudi, D. R. Nisbet
Laboratory of Advanced Biomaterials
Research School of Chemistry and the John Curtin School of Medical Research
Australian National University
Canberra, ACT 2601, Australia
E-mail: david.nisbet@unimelb.edu.au

N. Mahmoudi
ANU College of Engineering & Computer Science
Canberra, ACT 2601, Australia

Z. E. Zadeh, D. R. Nisbet
The Graeme Clark Institute
The University of Melbourne
Parkville, VIC 3010, Australia

Z. E. Zadeh, D. R. Nisbet
Department of Biomedical Engineering
Faculty of Engineering and Information Technology
The University of Melbourne
Parkville, VIC 3010, Australia

The ORCID identification number(s) for the author(s) of this article can be found under https://doi.org/10.1002/adfm.202305771

DOI: 10.1002/adfm.202305771